THE BOULDER LOW-LEVEL INTERCOMPARISON EXPERIMENT

Preprint of WMO Report

Editors:
J. C. Kaimal
H. W. Baynton
J. E. Gaynor

Report Number Two
June 1980

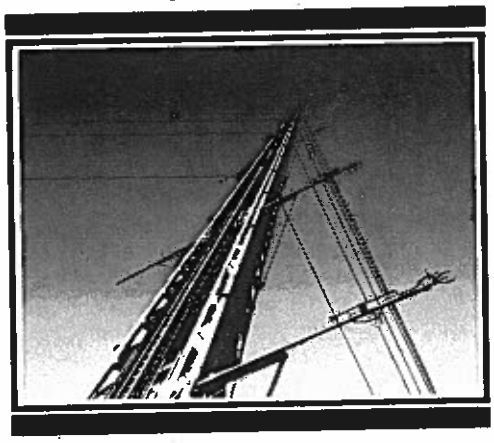

NOAA/NCAR
Boulder Atmospheric Observatory

A joint publication of NCAR and NOAA available from NOAA/ERL, Boulder, CO 80303, and from the NCAR Publications Office, P.O. Box 3000, Boulder, CO 80307.

NOTICE

Mention of a commercial company or product does not constitute an endorsement by NOAA Environmental Research Laboratories. Use for publicity or advertising purposes of information from this publication concerning proprietary products or the tests of such products is not authorized.

This report is to be published in a series of the World Meteorological Organization.

For sale by the Superintendent of Documents, U.S. Government Printing Office, Washington, D.C. 20402
(Order by SD Stock No. 003-017-00480-5)

FOREWORD

(to be added by WMO)

PREFACE

In preparing this report for the WMO Commission for Instruments and Methods of Observation (CIMO), the editors have aimed at providing adequate coverage of all three aspects of the Boulder Low-Level Intercomparison Experiment (BLIE): the workshop preceding the experiment, the experiment itself, and the results of the intercomparison. Papers presented at the workshop form the first part of the report, Chapters 1-23. The description of the experiment in Chapter 24 reflects the perspective of the three members of the organizing committee who planned and directed the experiment. Chapter 25, prepared by the same three authors, describes the results and includes comments from participants on the performance of their sensors and explanations for possible discrepancies in their results. Here we have tried to remain faithful to the spirit of the discussion session held at the end of the experiment, when preliminary results from the experiment were first examined and discussed. Our objective is to improve the present understanding of low-level sounding techniques, not to rank sensors according to performance.

The experiment was conducted in August and September 1979 at the Boulder Atmospheric Observatory (BAO), located 25 km east of Boulder, Colorado. It was divided into the following phases:

(1) Checkout and preparation, 20-22 August.
(2) Workshop, 23-24 August.
(3) Comparison tests, 27 August-5 September.
(4) Discussion session, 6 September.

Scientists from the National Oceanic and Atmospheric Administration (NOAA) of the U.S. Department of Commerce and from the National Center for Atmospheric Research (NCAR) collaborated in the planning and direction of all phases of the experiment. The BLIE organizing committee consisted of the following members: J. C. Kaimal, Chairman (NOAA), H. W. Baynton (NCAR), J. E. Gaynor (NOAA), F. G. Finger (NOAA), W. U. Weimann (WMO/CIMO), and H. P. Treussart (WMO/CIMO).

Readers of this report will note that three of the measuring techniques described at the workshop were not tested during the experiment. The descriptions of those techniques contain data from an experiment conducted at the same site a year earlier under very similar conditions (Project PHOENIX, September 1978). The instrumented aircraft, dual-Doppler radar, and passive radiometry techniques required such extensive data processing that guidelines imposed on other participants for data submission could not be applied to them. Nevertheless, those techniques were considered important enough to be included in the workshop.

Participation in BLIE required that processed data be submitted within 24 hours of any operating period or that analog voltages be made available for real-time sampling and processing on the BAO data-acquisition systems. Without these restrictions the discussion session held after the experiment to evaluate the results would not have been possible. Years of delay, disagreements, and frustrations over the outcome can be expected when participants do their processing after returning home from the experiment.

Eleven member nations of WMO participated in the experiment with equipment or as observers. Both the visitors and the resident staff of NOAA and NCAR cooperated to make this complex operation a success. Many of them put in long hard hours in the field. We take this opportunity to express our

gratitude to all the participants. We are happy to acknowledge the financial and moral support provided by NOAA management: Dr. Wilmot N. Hess, Director, Environmental Research Laboratories, and Dr. C. Gordon Little, Director, Wave Propagation Laboratory. Facilities for holding the workshop and discussion sessions were generously provided by NCAR management: Dr. Francis P. Bretherton, President, UCAR, and Dr. John W. Firor, Executive Director, NCAR. We are also grateful to WMO for financial assistance extended to participants who would otherwise have been unable to attend, and to the participating organizations and member nations for their strong endorsement of this comparison. An experiment of this magnitude would not have been possible without the full support and commitment of resources that accompany such endorsement.

J. C. Kaimal
H. W. Baynton
J. E. Gaynor

Editors

CONTENTS

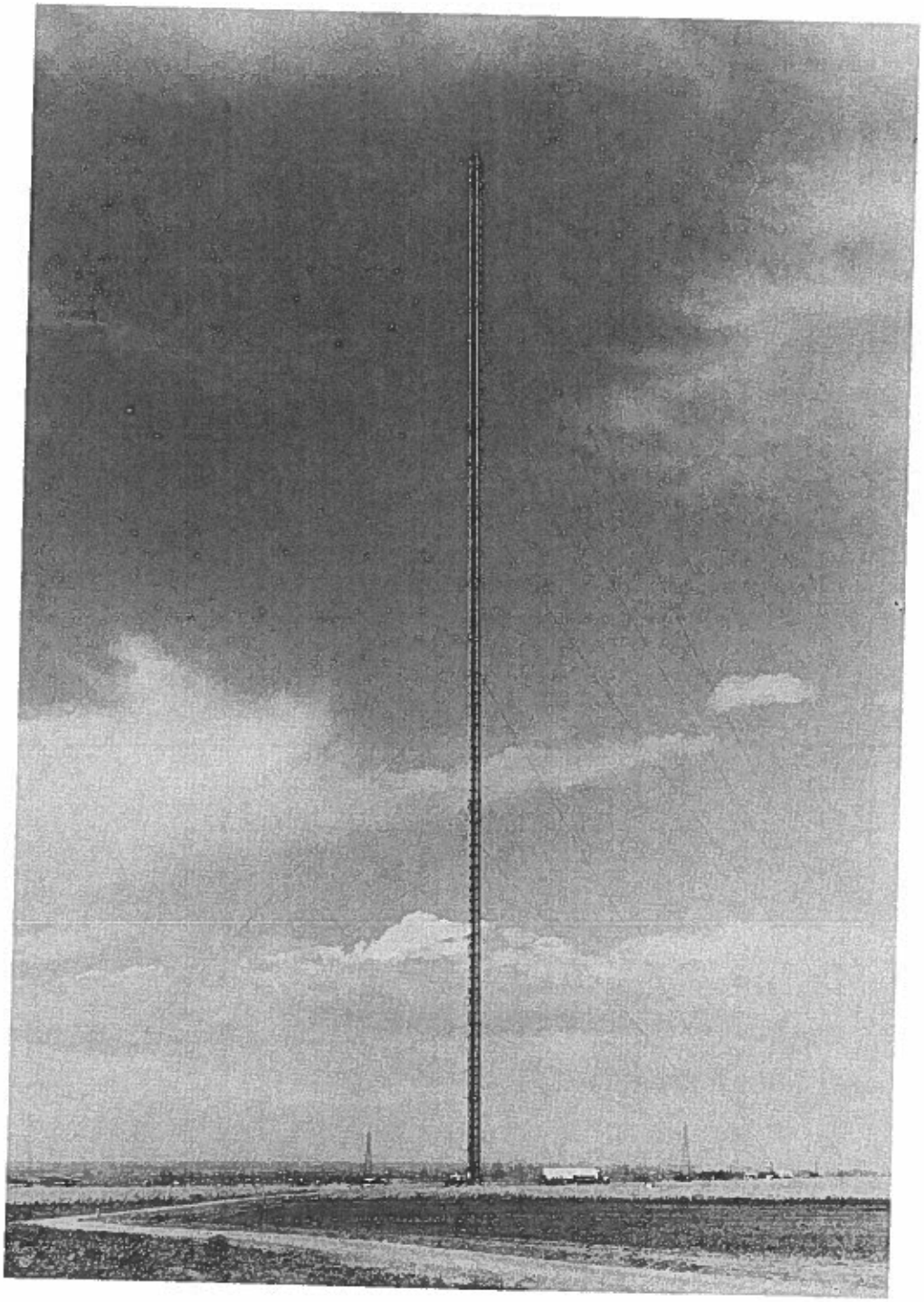

Figure 1.1. Instrumented 300-m tower at the BAO site.

1. BAO SENSORS FOR WIND, TEMPERATURE, AND HUMIDITY PROFILING

J. C. Kaimal
NOAA/ERL/Wave Propagation Laboratory
Boulder, Colorado, U.S.A.

1.1 INTRODUCTION

The Boulder Atmospheric Observatory (BAO) is a research facility operated jointly by NOAA's Wave Propagation Laboratory and the National Center for Atmospheric Research (NCAR). It is designed to provide high-quality measurements for use in boundary layer studies and instrument calibration. Located on gently rolling terrain 25 km east of Boulder, its main feature is a 300-m tower (Fig. 1.1) instrumented at eight levels to measure the mean and turbulent properties of atmospheric parameters such as wind speed, wind direction, temperature, and humidity. In-situ and remote sensors deployed around the tower provide additional information on the structure of the flow (e.g., pressure fluctuations at several stations, temperature structure from acoustic sounders, acoustic Doppler winds and wind convergence from a triangular configuration of optical crosswind sensors). A computer at the site processes information from these sensors for real-time printout of data summaries and archiving of raw data. Mean profiles of wind, temperature, and humidity for successive 20-min periods are available routinely. This real-time processing capability was an important factor in the choice of a site for the Boulder Low-Level Intercomparison Experiment (BLIE). A brief description of the tower sensors, the handling of data, and the parameters listed on the summary sheets can be found in the sections to follow. For more details of the site, instrumentation, and data processing see Kaimal (1978).

1.2 TOWER INSTRUMENTATION

For BLIE, data from the eight instrumented levels on the tower (10, 22, 50, 100, 150, 200, 250, and 300 m) will be used as reference for comparing results obtained from the various sounding techniques. At each level, the sensors are distributed between two booms, one of which points approximately SSE (154°) and the other approximately NNW (334°) (Fig. 1.2). The three-axis sonic anemometer and the fast- and slow-response temperature sensors are mounted on the SSE boom (Fig. 1.3). In the absence of strong downslope winds from the Rocky Mountains, the winds blow generally from the southeast during the day, but from the west or northwest during the night. The orientation of the SSE boom is therefore optimum for daytime observations. A propeller-vane anemometer and a cooled-mirror dew point hygrometer are mounted on the NNW boom (Fig. 1.4).

1.2.1 Three-Axis Sonic Anemometer

The sonic anemometer used on the BAO tower uses a fixed orthogonal array; the two horizontal axes are oriented along and perpendicular to the boom, while the vertical axis is mounted at the end of the boom directed away from the tower (Fig. 1.3). The acceptable azimuth range for vertical velocity measurement is much larger in this array than in the non-orthogonal arrays described by Mitsuta (1974) and Kaimal et al. (1974). However, the horizontal wind measurements fare less well in this arrangement. Distortions in the flow within the acoustic path due to the presence of transducers cause the velocity readings to be underestimated when the wind direction is close to one of the anemometer axes. An approximate form for the velocity underestimation as a function of θ (angle between the wind direction and the acoustic path) has been obtained from wind tunnel and atmospheric tests. The measured velocity component u_m approaches the true velocity component u_t in the range $75° > \theta > 90°$ but drops off linearly with θ for angles less than 75° (Fig. 1.5). For a path length-to-diameter ratio of 25, appropriate to the BAO array,

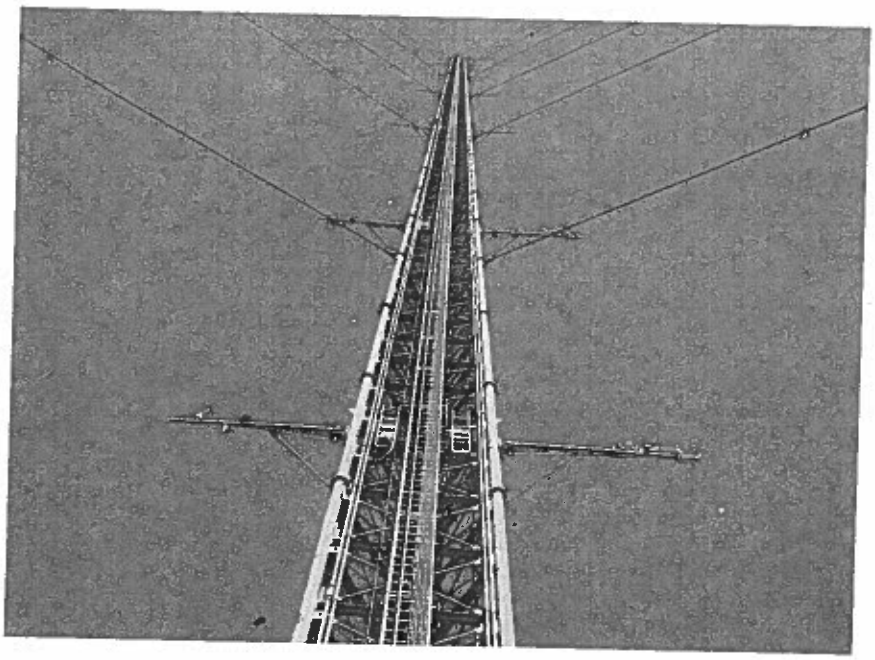

Figure 1.2. Details of the tower structure and booms.

For a path length-to-diameter ratio of 25, appropriate to the BAO array,

$$\left.\begin{aligned} u_m &= u_t(0.87 + 0.13\ \theta/75) \quad ; \quad 0 \le \theta \le 75 \\ &= u_t \quad ; \quad 75 \le \theta \le 90. \end{aligned}\right\} \tag{1.1}$$

The correction is made on each data point sampled. While an arc tangent routine can be used for a first order approximation of θ (with wind components measured along the two horizontal axes), it is more efficient to compute u_t and v_t using analytic expressions given below that very nearly approximate (1.1). Defining u_t as the component more closely aligned with the wind and v_t as the component normal to it,

$$\left.\begin{aligned} u_t &= C\ u_m \\ v_t &= D\ v_m \end{aligned}\right\} \tag{1.2a, 1.2b}$$

where

$$C = 0.926 + 0.31/(R + 1.38) \tag{1.3a}$$

$$\left.\begin{aligned} D &= 2.112 - C \quad ; \quad D > 1 \\ &= 1.0 \quad ; \quad D \le 1 \end{aligned}\right\} \tag{1.3b}$$

and

$$R = |v_m|/|u_m| \quad . \tag{1.3c}$$

No such correction is needed for the vertical velocity measurements. A detailed discussion of these and other aspects of sonic anemometer performance can be found in Kaimal (1979).

The sonic anemometer probes used on the tower include a mix of EG&G (Model 198-2) two-axis probes, Ball Brothers (Model 125-198) two-axis probes, and Ball Brothers (Model

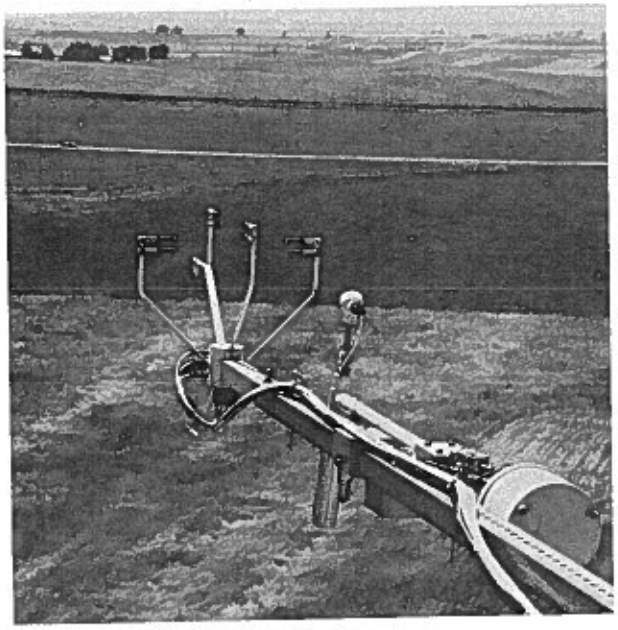

Figure 1.3. Three-axis sonic anemometer and slow-response quartz thermometer in aspirated shield on SSE boom.

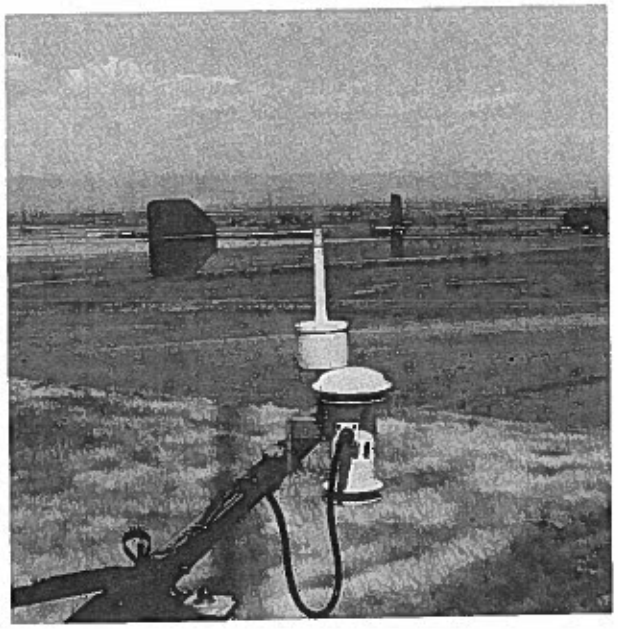

Figure 1.4. Propvane and dew point hygrometer on NNW boom.

125-197) single-axis probes. Driver and receiver circuits associated with the probe are located in waterproof boxes at each level on the tower; coaxial cables connect these circuits to the computer interface circuits located in the van at the base of the tower. To insure proper synchronization in data-sampling the transmitters at all levels are fired simultaneously. The firing proceeds at 200 Hz, exactly 20 times the sampling rate (10 Hz) for all the fast-response channels. The interface circuit automatically accumulates the readings from 20 successive transmissions before transferring the data to computer memory. This block-averaging is provided to minimize aliasing in the spectral computations.

1.2.2 Propeller-Vane Anemometer

A ruggedized version of R. M. Young Co.'s propeller-vane anemometer, Propvane Model 8002, is used. The polystyrene propeller in this model has a distance constant of 2.4 m and a working range from 1 to 54 m/s. Calibration of the wind speed output is accomplished by driving the propeller shaft at a known rate of rotation (1800 rpm) and adjusting the voltage level to the corresponding wind speed indication (15 m/s).

The vane position is indicated by a precision conductive plastic potentiometer connected to the vane shaft. The potentiometer has a deadband of 18°. This deadband is pointed in the direction of the tower so that the active range of the potentiometer coincides with the azimuth range of best exposure for the NNW boom. Data for azimuth wind directions between 110° and 180° are often degraded by a combination of the tower interference and the voltage jump produced by passage of the potentiometer brush across the deadband.

1.2.3 Fluctuating Temperature Sensor

A platinum wire thermometer (AIR Inc. Model DTIA), mounted within the frame of the sonic anemometer's vertical axis probe, measures fluctuations in the temperature with a

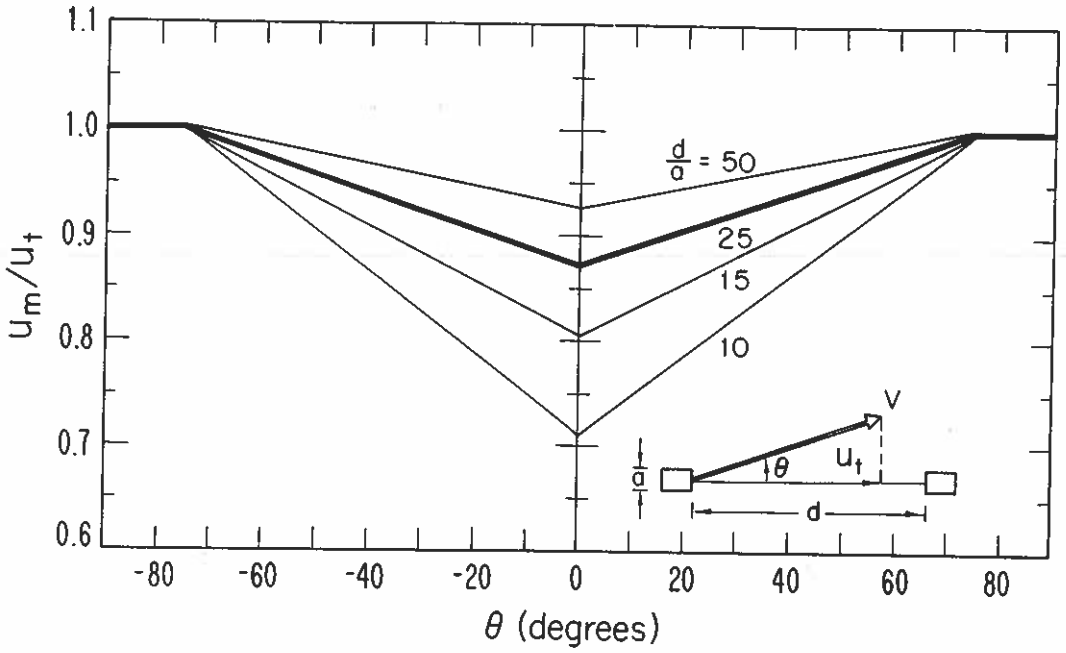

Figure 1.5. Attenuation in measured sonic wind velocity component from flow distortions along the acoustic path caused by the transducers. The heavy line corresponding to d/a = 25 is the response curve for the BAO sonic anemometer.

frequency response comparable with the path-averaged response of the sonic anemometer. The sensor consists of a length of 12-μ platinum wire (nominal resistance of 150 Ω) wound around a helical bobbin. This wire is part of a simple bridge circuit the output of which is amplified by a low-noise, low-drift circuit to provide an output voltage of ± 10 V corresponding to a temperature range of ± 50°C.

1.2.4 Slow-Response Temperature Sensor

Absolute measurements of air temperature are made with a Hewlett Packard quartz thermometer (Model 2850A) housed in an R. M. Young aspirated shield (Model 43404). The sensor is accurate to within 0.005°C, but has a long time constant, about 1 min. Calibration checks performed over the years in the same precision temperature bath show no significant variation in the thermometers' calibration constants with time.

1.2.5 Dew Point Sensor

A Cambridge Systems aspirated cooled mirror hygrometer (Model 110-SM), calibrated as recommended by the manufacturer, measures the dew point at each level. The temperature of a mirror, made to track the dew point (or frost point) temperature, is measured. The cycling time for temperature control is approximately 1 s.

1.3 DATA ACQUISITION AND DISPLAY

Acquisition of data from the sensors is controlled by a PDP 11/34 computer at the BAO site. The data acquisition system samples the fast-response sensors at the rate of 10

BOULDER ATMOSPHERIC OBSERVATORY DATA SUMMARY

AVERAGING PERIOD= 20.00 MIN

5 SEP 79 10 20 MST

Z[M]	VWES	VSOU	U	V	W	VH	AZ	PVS	PVD	T	TD	L
10	-3.22	-3.46	-1.69	4.41	-0.18	4.73	43.	4.42	55.	28.19	1.30	-25.77
22	-3.37	-3.95	-2.07	4.76	-0.10	5.19	41.	4.88	54.	27.64	0.63	-30.21
50	-3.44	-4.00	-2.16	4.88	-0.18	5.33	40.	4.98	51.	27.12	0.43	-63.04
100	-3.82	-4.07	-1.98	5.22	-0.08	5.58	43.	5.05	54.	26.59	0.40	-80.50
150	-3.96	-3.76	-1.64	5.20	-0.16	5.46	46.	5.24	54.	26.06	-0.20	999.99
200	-3.94	-3.33	-1.27	5.00	-0.05	5.15	50.	5.23	56.	25.48	-0.49	999.99
250	-4.11	-3.65	-1.48	5.30	-0.11	5.50	48.	5.24	53.	25.06	-0.99	999.99
300	-4.00	-3.88	-1.73	5.29	-0.11	5.57	46.	5.50	53.	24.56	-1.34	999.99

Z[M]	UU	VV	WW	TT	UV	VW	UT	VT	UW	WT
10	1.4315	0.9045	0.2380	0.3675	-0.4158	-0.0337	-0.2360	-0.0999	-0.1314	0.1623
22	1.2687	0.7045	0.3757	0.1783	-0.3042	-0.0682	-0.1432	-0.0811	-0.1500	0.1685
50	1.0214	0.5257	0.6504	0.0778	-0.2346	-0.0809	-0.0946	-0.0239	-0.2118	0.1352
100	0.7430	0.6420	0.7717	0.0548	-0.0233	-0.0877	-0.0856	-0.0195	-0.2118	0.1057
150	0.8567	0.7280	0.7761	0.0285	0.0889	-0.0716	-0.0697	-0.0186	-0.1297	0.0727
200	0.9299	0.7570	0.6753	0.0211	-0.0354	-0.0859	-0.0658	-0.0391	-0.1253	0.0454
250	1.1671	0.8311	0.7471	0.0284	0.0294	-0.0433	-0.0650	-0.0707	-0.2243	0.0325
300	0.8392	0.8532	0.5918	0.0264	-0.1268	0.0473	-0.0126	-0.0631	-0.0995	-0.0086

OPTICAL TRIANGLE

V [M/SEC]	AZ [DEG]	CONV [1/SEC]	LOG10(CN2)
1.25	13.	0.01118	-13.14339161

RMS PRESSURE VALUES [MICROBARS]

STN 1	STN 2	STN 3	STN 4	STN 5
6.461	7.832	6.597	19.247	8.690

PRESSURE[MB]

842.25

SOLAR RADCLY/MIN]

1.07

Figure 1.6. Sample listing of summary data for a 20-min averaging period. The time indicated at top right refers to the beginning of the averaging period. Column heads are explained in Table 1.1.

Hz and the slow-response sensors at 1 Hz. Real-time computations of means, variances, covariances, and Obukhov lengths are made for consecutive 20-min periods (starting on the hour) and are listed on the line printer at the end of each averaging period. The summaries are recorded on magnetic tape along with a compressed form of the time series.

To minimize tape storage requirements, only 10-s averages and 10-s grab samples (last sample in each 10-s averaging period) of the fast-response time series are stored. On the slow-response channels no attempt is made to save the 10-s grab samples. High-frequency information in the form of smoothed spectral estimates (approximately 10 estimates per decade) is stored for later use in extending spectra computed from the 10-s averaged data points. For this intercomparison experiment only the results from the summary sheets will be used. A sample listing for one period is shown in Fig. 1.6; Table 1.1 explains the symbols.

The parameters relevant to this experiment (VWES, VSOU, W, VH, AZ, T, and T_d) will be listed separately for comparison with data from systems operated by other participants. To minimize possible tower influence on the wind data, sonic anemometer readings will be used only for azimuth wind directions 64° - ~~154°~~ 224° (CW). For wind directions ~~154°~~ 224° - 64° (CW) the Propvane readings will be used instead.

Table 1.1. Explanation of terms used on BAO data summary sheet (Fig. 1.6)

Z(M)	Height (meters)	
AVERAGED PARAMETERS (SI units)		
VWES	Horizontal wind component from west (sonic)	
VSOU	Horizontal wind component from south (sonic)	
U	Horizontal wind component along the x axis, from 154° (sonic)	
V	Horizontal wind component along the y axis, from 64° (sonic)	
W	Vertical wind component (sonic)	
VH	Horizontal wind speed (sonic)	
AZ	Horizontal wind direction (sonic)	
PVS	Horizontal wind speed (propvane)	
PVD	Horizontal true wind direction (propvane)	
T	Temperature (quartz thermometer)	
TD	Dew point (dew point hygrometer)	
L	Obukhov length	
2nd MOMENTS (SI units)		
UU, VV, WW, TT, UV, UW, UT, VT, UW, and WT		
U	(=u) Longitudinal wind component (sonic)	Referenced to 10 m mean wind direction
V	(=v) Lateral wind component (sonic)	
W	(=w) Vertical wind component (sonic)	
T	(=θ) Temperature (platinum wire)	
OPTICAL TRIANGLE (SI units)		
V	Wind speed	From measurements along legs of an equilateral triangle, 450 m on each side, centered on tower
AZ	Wind direction (CW)	
CONV	Convergence	
LOG10(CN2)	Structure parameter for refractive index x 10^{12}	
RMS PRESSURE VALUES (microbars) (STN 1 ... STN 5)		From pressure fluctuation stations around the tower
PRESSURE (mb)		Mean surface pressure
SOLAR RAD (Langleys/min)		Mean solar radiation (direct and diffuse)

1.4 REFERENCES

Kaimal, J. C. (1978): NOAA instrumentation at the Boulder Atmospheric Observatory. Prepr. Vol. 4th Symp. on Meteorol. Obs. and Instrum., 1978, Denver, Colo., American Meteorological Society, Boston, Mass., pp. 35-40.

Kaimal, J. C. (1979): Sonic anemometer measurement of atmospheric turbulence. Proc. Dynamic Flow Conf., 1978, Baltimore, Md., DISA, P.O. Box 121, Skovlunde, Denmark, pp. 551-565.

Kaimal, J. C., J. T. Newman, A. Bisberg, and K. Cole (1974): An improved three-component sonic anemometer for investigation of atmospheric turbulence. In Flow: Its Measurement and Control in Science and Industry, Vol. 1, Proc. of a Symp., 10-14 May 1971, Pittsburgh, Pa., Rodger B. Dowdell (ed.), Instrument Society of America, Pittsburgh, pp. 349-359.

Mitsuta, Y. (1974): Sonic anemometer-thermometer for atmospheric turbulence measurements. In Flow: Its Measurement and Control in Science and Industry, Vol. 1, Proc. of a Symp., 10-14 May 1971, Pittsburgh, Pa., Rodger B. Dowdell (ed.), Instrument Society of America, Pittsburgh, pp. 341-348.

2. SINGLE-HEAD SONIC ANEMOMETER-THERMOMETER

Tatsuo Hanafusa
Meteorological Research Institute
Japan Meteorological Agency
Tsukuba, Japan

Yasuhiro Kobori
Kaijo Electric Co.
Tokyo, Japan

Yasushi Mitsuta
Disaster Prevention Research Institute
Kyoto University
Kyoto, Japan

2.1 INTRODUCTION

A sonic anemometer-thermometer detects by sonic means the wind velocity component and the air density or temperature along the sound path. The first successful sonic anemometer-thermometer for use in the atmospheric turbulence studies was developed by Suomi (1957). In his instrument, velocity and temperature fluctuations were obtained by the difference and sum of transit times for two series of sound pulses traveling in opposite directions along the same sound path.

Amplitude variations in the received pulse signal of Suomi's instrument caused errors in transit time detection. To avoid such errors, Kaimal and Businger (1963) of the University of Washington developed a continuous-wave sonic anemometer-thermometer which measured phase shifts between the two signals received at either end of the sound path. Their instrument gave satisfactory performance in field observations.

Improvement of the pulse-type instrument continued at Kyoto University, and a practical instrument was completed by Mitsuta (1966). The instruments, developed independently by the University of Washington and Kyoto University, when compared in the United States in 1965 showed excellent agreement in the measured wind velocity component (Businger et al., 1969).

After discussions of the merits of the instruments, the two groups decided to develop a new three-dimensional sonic anemometer-thermometer of pulse type as a joint effort. The pulse-type instrument appeared more promising for absolute measurement of pulse transit times and for attaining wide observation range and stable zero point, if only a reliable means of transit-time detection could be developed. Subsequent development of a new technique to determine the time of reception of the signal pulse (by making the trigger pulse from the third wave of received signal pulse instead of the wave envelope) enabled the Japanese group to produce a new solid state three-dimensional sonic anemometer-thermometer (Mitsuta et al., 1967). After several improvements a more refined version with three 20-cm sound paths and using 100-kHz acoustic pulses was completed (Mitsuta, 1974). It was widely and successfully applied in various field experiments as reported by Japan-U.S. Joint Study Group (1971) and has been produced commercially in Japan.

Through almost a decade of practical application of this instrument, we have identified major sources of unreliability. One important source was zero-point drift caused by small variations in the geometrical length of sound paths. Small differences in length between two opposite sound paths cause large zero offsets in the two-head type anemometer. The other source of unreliability arose from the temperature and cross wind approximations in the derived wind and temperature. The new single-head sonic anemometer-thermometer described by the present authors achieves more reliable measurement by removing

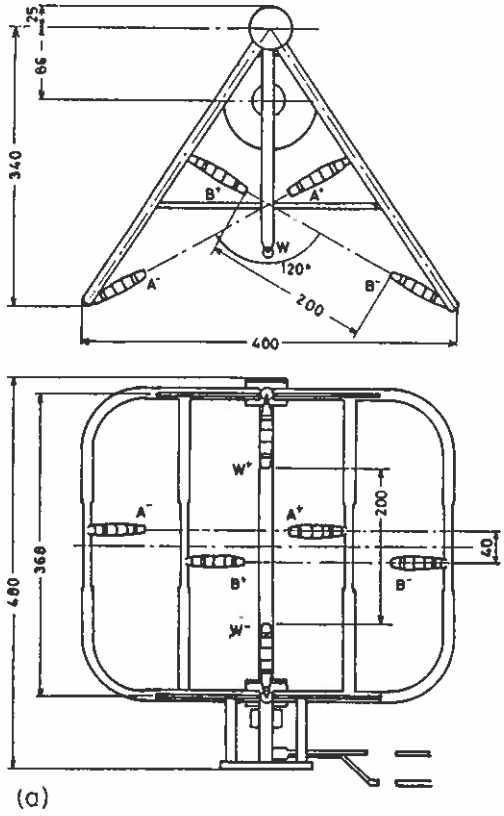

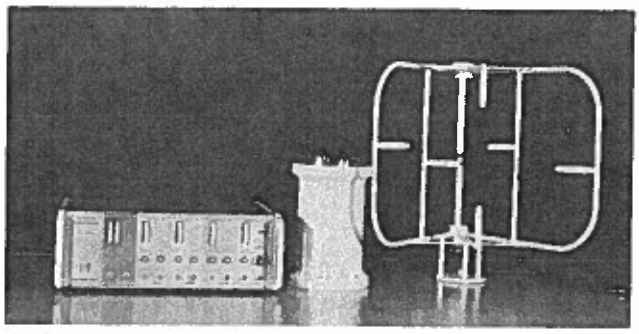

Figure 2.1. The new single-head anemometer-thermometer: a) wind antenna specifications; b) main chassis, junction box, and wind antenna (from left to right).

the difficulties mentioned above. The basic points of improvement from the 1971 model are adoption of a more precise formula for processing, a single-head two-way sound path, and a more effective noise-gate circuit.

2.2 BASIC PRINCIPLES

The transit time of a sound signal traveling from one end of the sound path to the other separated by distance d can be written as follows (Schotland, 1955):

$$t = \frac{(C^2 - V_n^2)^{1/2} \pm V_d}{C^2 - V^2} \cdot d \qquad (2.1)$$

where V is total wind velocity, V_d and V_n are wind velocity components in the directions parallel and normal to the sound path, and C is the velocity of sound in still air. The sign, $\pm$, before V_d should be chosen according to the direction of sound transmission.

If two transit times t_1 and t_2 in opposite directions on the same sound path are detected, V_d can be obtained independent from V and V_n as follows:

$$V_d = \frac{d}{2} \left(\frac{1}{t_1} - \frac{1}{t_2}\right) . \qquad (2.2)$$

C can be obtained by assuming $C^2 >> V_n^2$ as follows:

$$C = \frac{d}{2}\left(\frac{1}{t_1} + \frac{1}{t_2}\right) \quad . \tag{2.3}$$

The velocity of sound in still air, C, can be expressed as follows (Barret and Suomi, 1949):

$$C = 20.067 T_{sv}^{1/2} \quad , \tag{2.4}$$

where T_{sv} is sound virtual temperature of the air and is equal to air temperature if the atmosphere is dry. In moist air T_{sv} can be correlated with air temperature, T, by water vapor pressure, e, as follows:

$$T_{sv} = T(1 + 0.3192e/p) \tag{2.5}$$

where p is atmospheric pressure.

Then T_{sv} can be obtained from two transit times t_1 and t_2 by the following equation:

$$T_{sv} = \frac{d^2}{(2 \times 20.067)^2}\left(\frac{1}{t_1} + \frac{1}{t_2}\right)^2 \quad . \tag{2.6}$$

In the present instrument, the pulse transit times are processed electronically following (2.2) and (2.6) to obtain the wind velocity and virtual temperature outputs.

The wind velocity component obtained by equation (2.2) is the line-averaged wind velocity component over the sound path of length d in the direction parallel to it; air temperature obtained by (2.6) is also sound virtual temperature averaged over the sound path, d. Those are apparently smoother than the point-detected entities. The attenuation characteristics of this line averaging were studied by Mitsuta (1966) and in more detail by Silverman (1968).

2.3 DESCRIPTION OF THE INSTRUMENT

The new three-dimensional sonic anemometer-thermometer is shown in Fig. 2.1, and a block diagram of its functions is shown in Fig. 2.2. The sensor (wind antenna) has two horizontal sound paths (A,B) crossing at 120° and a vertical sound path (W); at both ends of each path are two-way sound transducers which perform alternately as transmitter and receiver. The switching circuit, transmitter, and pre-amplifiers are built in the junction box located near the sensor. The main chassis consists of a main oscillator, a main controller, transit time detection circuits, wind velocity converters, a temperature converter and a power supply. All components are solid state, many of them being integrated circuits.

The main oscillator is a crystal oscillator of 5.5556 MHz. It supplies the clock signals for wind calculation (5.5556 MHz), and for temperature calculation (2.7778 MHz), and the timing signal to the main controller which generates timing signals (110 Hz, six times the observation cycle) to switch transducers and to trigger noise gates and converting circuits. The lead-zirconate transducers at both ends of the three sound paths (A,B,W) are triggered alternatively in the sequence of A^+, A^-, B^+, B^-, W^+ and W^- at equal

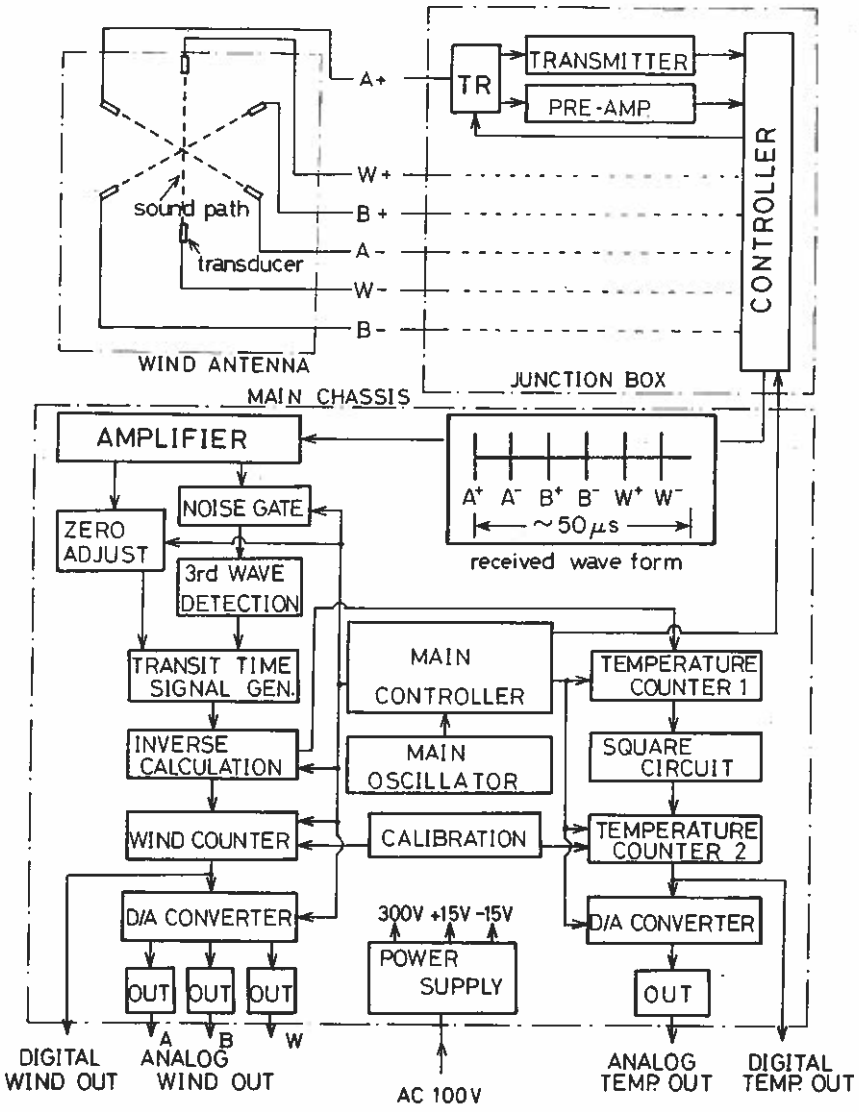

Figure 2.2. Block diagram of the new single-head anemometer-thermometer.

intervals, clocked by the timing signal. The transducers, when triggered, send out burst signals at resonant frequency of 100 kHz. When the transducer at one end of the sound path is triggered, the transducer at the opposite end of the path switches to its receiving mode.

The received signals sent to the receiver amplifier are first separated from the noise by noise gates, then shaped and triggered at the zero crossing point of the third wave to generate the receipt time signal pulse. The transmitting pulse delayed to adjust for the zero point and the receipt time signal pulse are supplied to the inverse calculation circuit which produces the signal pulse whose width is proportional to the inverse of the pulse transit time of each sounding.

The counter for the wind velocity component is an up-down counter clocked by 5.5556 MHz to make the difference of width of the signal pulses corresponding to the

Table 2.1. Specifications of the new sonic anemometer-thermometer

	Anemometer	Thermometer
Measuring mode	Time-sharing multiplex transmission/reception switchover type ultrasonic pulse emission, ~ 20 Hz per channel.	
Measuring range	0 ~ ±30 m/s	Central temperature: -10° ~ 40°C Temperature deviation: 0 ~ ±5°C
Accuracy	1%	1%
Minimum resolution	0.5 cm/s	0.025°C
Frequency resolution	10 Hz	10 Hz
Analog output	OUT 1: 0 to ±1 V/10m/s 8 V max OUT 2: 0 to ±1 V/full scale Full scale *U:±5, ±10, ±25, ±50 m/s **W:±1, ±2, ±5, ±10 m/s	OUT 1: 0 to ±1 V/±50°C OUT 2: 0 to ±1 V/±5°C
Digital output***	15 bit binary code	12 bit binary code
Operating temperature	Main unit: -10° to 40°C,	Probe and junction box: -20° to 50°C
Power supply	AC 100/115/220 V ±10%	50/60Hz

*U: Horizontal component.
**W: Vertical component.
***Not used in the present intercomparison.

successive two soundings in the opposite directions on the same sound path, such as A^+ and A^-, B^+ and B^-, and W^+ and W^-. One bit in this counter corresponds to 0.005 m/s. The digital signal corresponding to the difference is converted into a voltage analog signal in a D-A converter and then distributed to each wind component output circuit.

The first counter in the temperature circuit produces a voltage analog signal proportional to the sum of the two successive soundings in opposite directions on the vertical sound path ($W^+ + W^-$). This voltage is squared, producing a temperature signal pulse whose width is proportional to sound virtual temperature. The width of the temperature signal pulse is converted into a temperature digital signal by the second counter clocked by a 2.778 MHz signal from the main oscillator. One bit in the temperature corresponds to 0.025°C. The digital signal is converted to an analog temperature output through a D-A converter.

Digital techniques were adopted in the pulse-width detecting circuit to attain high accuracy and stability of measurement. Hybrid systems of digital and analog circuits have been replaced by pure digital processing systems.

2.4 PERFORMANCE

All of the circuit parameters can be tested and adjusted electronically within their limits of tolerance, except the aeroacoustic characteristics of the wind antenna. The specifications of the new sonic anemometer-thermometer are as shown in Table 2.1.

The aeroacoustic characteristics of the wind antenna were tested in the wind tunnel of MRI. The length of the sound path is 20 cm, and the diameter of the transducer is about 1.5 cm. Therefore the wake to the lee of the transducer produces some errors in measurement even though streamline shape of the transducer is improved. The horizontal wind speed component detected by each leg of horizontal sound path for various wind direction to the wind antenna is as shown in Fig. 2.3. The crossing angle of the leg is 120°,

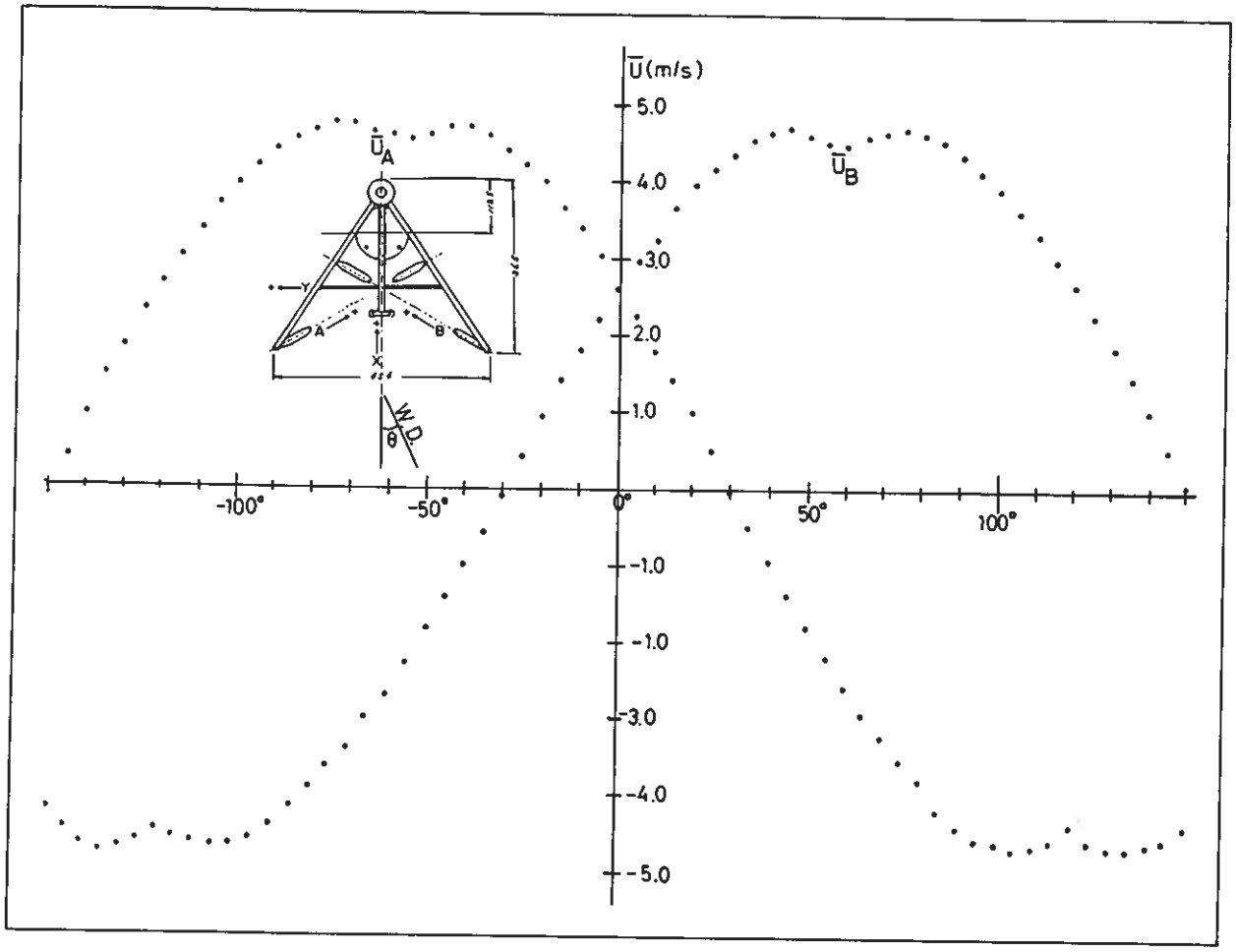

Figure 2.3. Directional characteristics of the two horizontal legs of the wind antenna.

and wind is just along the direction of each leg when wind direction is ±60°. A small dip of the output can be seen at this angle as seen in this figure, which is caused by the wake effect of the transducer. Therefore this antenna should be used in the wind direction range of ±45° from the central axis.

2.5 CONCLUDING REMARKS

The first device of the present type was completed in 1976 and first used in the field observation of International Turbulence Comparison Experiment (ITCE) in Australia. The improved version is now under commercial production. Six sets of them were installed on the Meteorological Research Tower at Tsukuba and performed well for about one year.

The variation of this sonic anemometer-thermometer is a two-dimensional wind sensor with a coordinate converter to compute wind speed and direction. It will be valuable for air pollution study in light wind conditions, because it can measure wind down to 0.005 m/s without restrictions by mechanical inertia and friction under any weather conditions.

2.6 REFERENCES

Barrett, E. W., and V. E. Suomi (1949): Preliminary report on temperature measurement by sonic means. J. Meteorol. 6:273-276.

Businger, J. A., M. Miyake, E. Inoue, Y. Mitsuta, and T. Hanafusa (1969): Sonic anemometer comparison and measurements in the atmospheric surface layer. J. Meteorol. Soc. Japan 47:1-12.

Japan-U.S. Joint Study Group (1971): Development of sonic anemometer-thermometer and its applications to the study of atmospheric surface layer. WDD Technical Note No. 6, Kyoto Univ., Kyoto, Japan, 250 pp.

Kaimal, J. C., and J. A. Businger (1963): A continuous wave sonic anemometer-thermometer. J. Appl. Meteorol. 2:156-164.

Mitsuta, Y. (1966): Sonic anemometer-thermometer for general use. J. Meteorol. Soc. Japan 44:12-24.

Mitsuta, Y., M. Miyake, and Y. Kobori (1967): Three dimensional sonic anemometer-thermometer for atmospheric turbulence measurement. WDD Technical Note, Disaster Prevention Res. Inst., Occasional Report, Kyoto Univ., Kyoto, Japan, 20 pp.

Mitsuta, Y., 1(1974): Sonic anemometer-thermometer for atmospheric turbulence measurements. Flow: Its Measurement and Control in Science and Industry, Vol. 1, Proc. of a Symp., 10-14 May 1971, Pittsburgh, Pa., Rodger B. Dowdell (ed.), Instrument Society of America, Pittsburgh, pp. 341-348.

Schotland, R. M. (1955): The measurement of wind velocity by sonic waves. J. Meteorol. 12:386-390.

Silverman, B. A. (1968): The effect of spatial averaging on spectrum estimation. J. Appl. Meteorol. 7:168-172.

Suomi, V. E. (1957): Sonic anemometer. In Exploring the Atmosphere's First Mile, Vol. 1, H. H. Lettau and B. Davidson (eds.), Pergamon, N.Y., pp. 256-266.

3. VAISALA EIGHT-LEVEL INSTRUMENTED TOWER SYSTEM

Ilkka Ikonen
Vaisala Oy
Helsinki, Finland

3.1 INTRODUCTION

The tower-based wind-shear and temperature-inversion observing and warning system, Vaisala MIDAS 200, gives real-time data on low-altitude atmospheric conditions near an airport.

3.2 GENERAL SYSTEM DESCRIPTION

The main components of the MIDAS 200 system are described below:

(1) Sensors. Sensors are provided for measuring temperature at eight levels, wind speed and direction at four levels, and humidity also at four levels of the instrumentation tower. The number of sensor levels in the system is designed to adequately cover the first 300 meters of the atmosphere, which is considered high enough to provide sufficient information for air traffic, especially during landing and take-off. The sensor types and installation levels are specified in Tables 3.1 and 3.2. Figures 3.1 and 3.2 show the sensors as installed on the BAO tower during BLIE.

(2) Data processing unit. The heart of the system is a microprocessor-based processing unit. It measures the sensor output signals; computes and stores the corresponding average, minimum, and maximum values; and finally provides the weather data to the printer terminals and the cassette unit in a format specified by the operator. The processing system runs on a 5-kilobyte program memory and 4-kilobyte buffer storage memory. It is able to support two independent data terminals and a cassette drive.

(3) Data output and operator terminals. Two 30-char/s printer terminals and a C-cassette drive are provided for data output, system control by operator, and data storage.

Table 3.1. Sensors in the instrumentation tower

Parameter	Sensor type	Quantity	Signal type	Wires/sensor
Temperature	Vaisala DTS 12, Pt 100	8	analog	3
Humidity	Vaisala HMP 14 U, Humicap	4	analog	4
Wind speed	Vaisala WAA 12, anemometer	4	analog	3
Wind direction	Vaisala WAV 12, wind vane	4	analog	9

Table 3.2. Sensor installation

Level	Sensor*				Signal wires required	
	T	H	WS	WD	Analog (T, H)	Digital (WS, WD)
300 m	X	X	X	X	7	12
250 m	X				7	
200 m	X	X	X	X	7	12
150 m	X				7	
100 m	X	X	X	X	7	12
50 m	X				7	
22 m	X	X	X	X	7	12
10 m	X				7	

*The analog sensor and the digital sensor must not be connected to the same cable. Thus two cables are needed from the data processing unit to installation levels 22 m, 100 m, 200 m, and 300 m. All the cables should be shielded. Cross section of 0.75 mm^2 per wire is required.

3.3 MEASURING AND COMPUTING THE PARAMETERS

All the analog sensor signals (temperature and humidity) are measured at intervals of 30 s, and all the digital sensor signals (wind speed and direction) are measured at intervals of 2 s.

At the end of each 2-min period the following values are computed and presented as new data:

(1) Temperature, 2-min average values (°C) for each sensor level.

(2) Relative humidity, 2-min average values (%) for each sensor level.

(3) Wind speed, both 2- and 10-min average, minimum, and maximum values (knots) for each sensor level.

(4) Wind direction, both 2- and 10-min average, minimum, and maximum values (degrees) for each sensor level.

(5) Vertical wind shear values are determined by calculating the wind vector relative differences between each two successive wind sensor levels and between the highest and lowest levels. The shear values are computed on the basis of the 2-min average wind values (ICAO recommendation). Only shear vector magnitudes are available (knots/ 30 m).

(6) To detect temperature inversions the temperature differences between each two successive sensor levels and between the lowest level and all the other levels are computed. (These together make 13 comparisons.)

The wind shear and temperature data are automatically given as an appropriate alarm message, if one or more of the shear values or temperature differences exceeds the alarm limits selected by the operator. All the other data are printed on request or at certain time intervals determined by the operator.

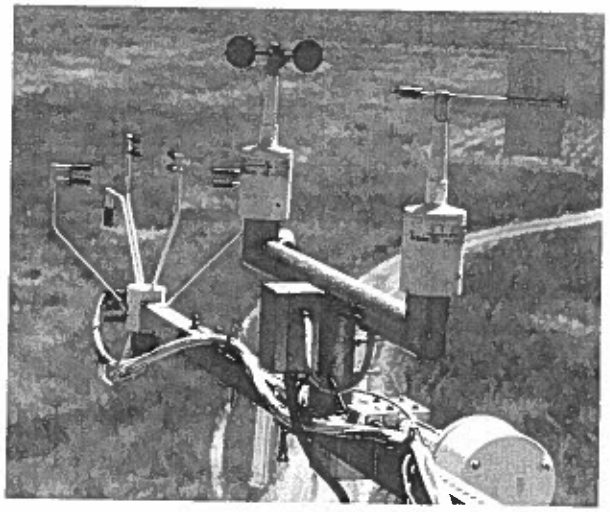

Figure 3.1. Vaisala cup and vane system mounted on SSE boom of BAO tower.

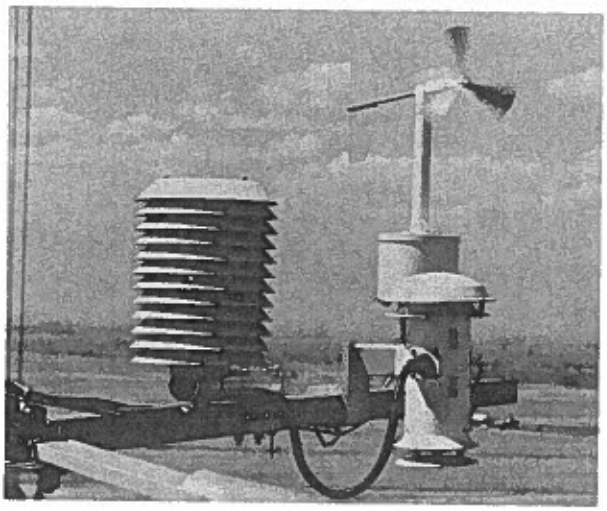

Figure 3.2. Vaisala radiation shield (housing temperature and humidity sensors) mounted on NNW boom of BAO tower.

3.4 DATA OUTPUT AND STORAGE

The MIDAS-200 system supports two independent data terminals. The basic system includes two 300-bits/s (30 char/s) printer terminals and a pair of 300-bits/s data modems for use if the other terminal is installed more than 200 meters away from the processing unit.

The following types of data messages are sent to the printer terminals by simple commands:

(1) Wind data, direction/speed average values from each level (degrees/knots).

(2) Wind data, direction/speed maximum-minimum values from each level (degrees/knots).

(3) Vertical wind shear vector magnitudes between the highest and lowest levels and between each two successive levels, five values together (knots/30 m).

(4) Temperature data from each level (°C).

(5) Humidity data from each level (% RH).

(6) Messages (4) and (5) together.

(7) Messages (1) and (2) together.

(8) Messages (1), (2), and (3) all together.

(9) Messages (1)...(5) all together.

(10) Graphic profile of wind data: direction average and variation, speed average and variation (every level).

(11) Like message (1), but for only one selected level.

(12) Graphic profile of humidity data (every level).

(13) Like message (12), but for only one selected level.

(14) Graphic profile of temperature data (every level).

(15) Like message (14), but for only one selected level.

All the message types above are available either on request or repeatedly at intervals. These intervals can be any number of 2-min increments from 1 to 255. All the messages are provided with current date and time of the day.

If the wind shear or temperature difference values exceed the corresponding alarm limits set by the operator, the message type (3) or (4) is automatically printed together with the alarm signal. Also an "alarm-over" message is sent as conditions come back to normal again.

The system stores in the memory the measured data at selectable time intervals, thus making it possible to compare the previous meteorological condition with the present one. Like the reporting interval, the storing interval can be set in 2-min increments. Memory space for up to 33 separate data stores is provided.

The MIDAS-200 system also contains cassette recording equipment (C-cassette). All the data are recorded at selectable intervals on the cassette. A cassette will hold data for 50 days if the recording interval is 30 minutes. A separate cassette reader is needed for transfer of data to other systems.

3.5 SUMMARY

This tower-based wind-shear and temperature-inversion observing and warning system, designed primarily for aviation services, can be used as an autonomous system giving data directly to users or as a subsystem of a larger data-processing and distribution system. The relevant ICAO recommendations are taken into account in the design.

4. REMOTELY PILOTED AIRCRAFT FOR ATMOSPHERIC SOUNDINGS (SAM)

Daniel Martin
Etablissement d'Etudes et de Recherches Météorologiques (EERM)
Centre de Recherches de Magny les Hameaux
78470 Saint Rémy les Chevreuse, France

4.1 INTRODUCTION

During the last three years the French Meteorological Research Department (EERM) has developed small remotely piloted aircraft for atmospheric soundings. They are particularly suited for boundary layer explorations. As atmospheric probes, the remotely piloted aircraft have the advantage of high resolution, high repetition rate, low cost, the ability to make horizontal and vertical measurements and accessibility over difficult and high risk areas. Its limitations are those imposed by cruising range, ceiling, and visibility flight rules.

The EERM program that uses these devices is called Sondes Aérologiques Motorisées (SAM). The aircraft devices are designed for various applications. SAM-B provides aerological soundings in the layer 0-500 m, with real-time measurements of pressure, temperature, and humidity. SAM-C has an operational ceiling of >4000 m with better capabilities (payload, ceiling, flight duration, aerodynamic self-stability) than the SAM-B. It allows for simultaneous pressure, temperature, and humidity measurements and gas samplings.

4.2 SYSTEM DESCRIPTION

4.2.1 SAM-B

SAM-B has a circular wing of polystyrene covered with kraft paper; the body (moulded fiber) contains the instruments. Its "critical aerodynamics" permit a parachute-like descent, providing an easy and safe approach and landing, as well as good aerodynamic stability at low speed (10 m/s). The simplicity of the design provides low cost and easy maintenance. Figure 4.1 shows SAM-B taking off. Limitations of this aircraft are as follows:

(1) It has a small visual range between pilot and aircraft (800 m) because of its size and geometry.

(2) Maximum wind it can be used in is 10 m/s.

(3) Operational ceiling is about 2000 m.

To overcome these limitations, a SAM-D (Fig. 4.2) with a delta wing that has a front stabilizer is currently being developed, allowing a wider speed range, a vertical speed of about 7 m/s, an operational ceiling of 5000 m, and the ability to be used in winds up to 15 m/s.

Characteristics of SAM-B and SAM-D are given in Table 4.1.

4.2.2 SAM-C

SAM-C is a self-stabilizing motorized glider with modular design, made of polystyrene and fiberglass. A special feature of the aircraft (Fig. 4.3) is its inverted "V"

Figure 4.1. SAM-B taking off.

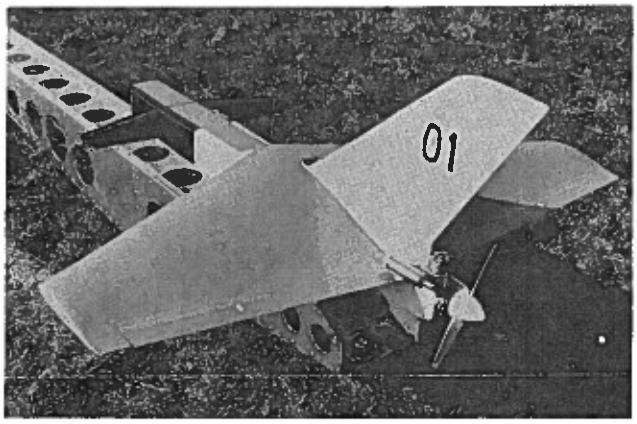

Figure 4.2. SAM-D, a new vehicle being developed.

tail, giving low drag (two wings instead of three) and especially easy control during high-altitude flights. Tail retraction at landing is achieved by use of a semi-rigid hinge. The weight of SAM-C and the need for operation on rough ground dictate the use of a catapult and recovery nets. Because of a fineness ratio of 10, SAM-C can be operated in strong winds (15 m/s). Technical specifications are given in Table 4.1.

Table 4.1. Technical characteristics of SAM aircraft

	SAM-B (Circular wing)	SAM-C (Classic airplane: reversed dihedral)	SAM-D (Stabilizer in front of delta wing)
Payload	0.6 kg	1.8 kg	0.8 kg
Total weight	3.5 kg	7.5 kg	5.2 kg
Minimum speed	5 m/s	10 m/s	9 m/s
Cruise speed	15 m/s	25 m/s	30 m/s
Initial climb rate	4 m/s	5 m/s	7 m/s
Operational ceiling	2000 m	4000 m	5000 m
Endurance at sea level	15 min	1 h	20 min
Wing span	1.20 m	3.15 m	1.40 m
Wing area	0.95 m^2	1 m^2	1.75 m^2
Air foil		NACA 4415	NACA 4415
Engine (diesel)	10 cm^3 1.5 HP at 12000 rpm		
Propeller	28 cm x 18 cm		
Fuel	Methanol + nitromethane + oil		

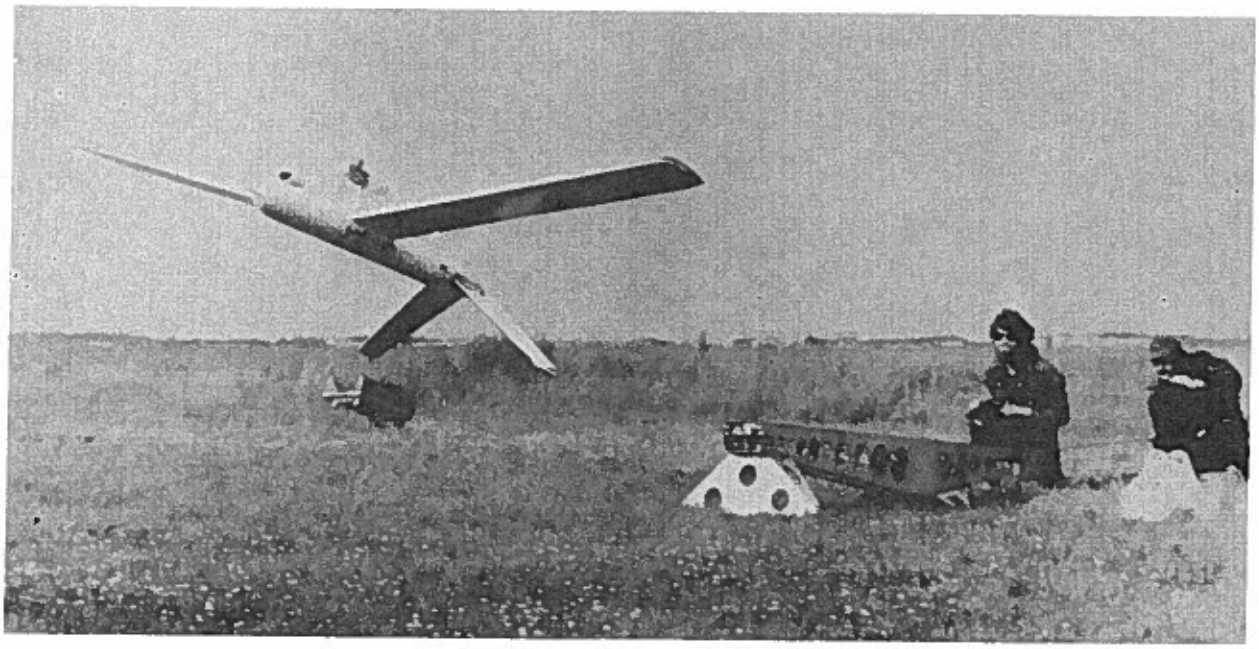

Figure 4.3. SAM-C taking off. Its weight (8 kg) dictates the use of a catapult.

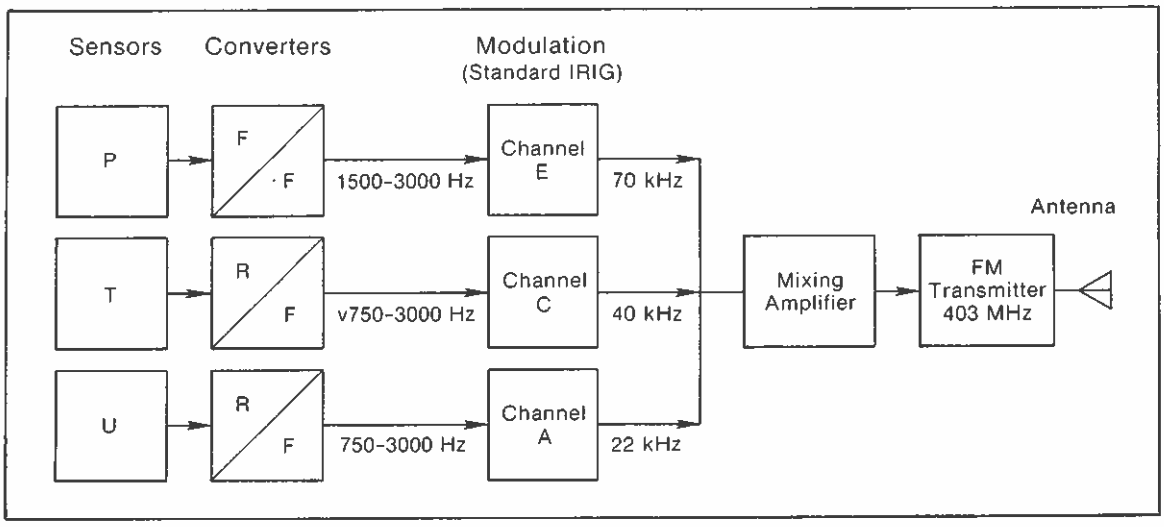

Figure 4.4. Block diagram of telemetry.

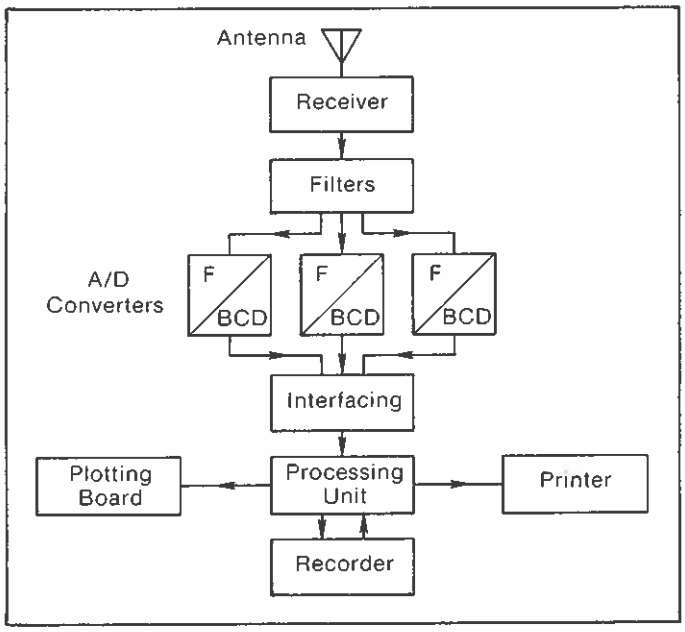

Figure 4.5. Block diagram of data acquisition.

4.2.3 Remote Control

Digital remote control uses a 250-mW transmitter with a center frequency at 436 MHz and a bandwidth of 50 kHz. This device controls the engine, the airbrakes, the ailerons, and the gas-sampling system.

4.2.4 Telemetry

Figures 4.4 and 4.5 are block diagrams of the telemetry and data acquisition. Pressure, temperature, and humidity are measured with a vibrating wire sensor, thermistor, and hygristor (Fig. 4.6). Their characteristics are given in Table 4.2. Temperature and

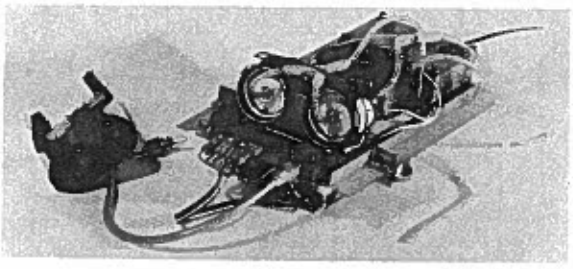

Figure 4.6. Aircraft instrumentation. The picture shows the pressure sensor, the micropump, two filters for gas sampling, and the telemetry equipment.

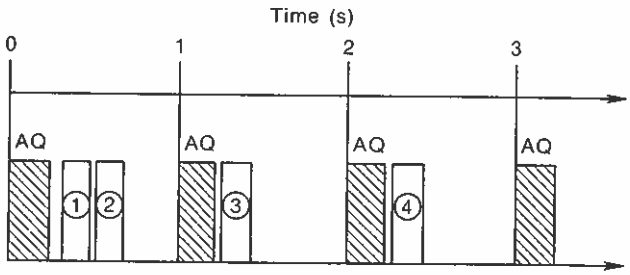

Figure 4.7. Data processing sequence: AQ) data acquisition, 1) median computation, 2) transfer function (frequency/parameter), 3) recording of median value, 4) plotting on 9872 A.

Table 4.2. Characteristics of PTU sensors

Sensors	Measurement Range	Resolution	Precision
Pressure (vibrating wire)	150 mb between 1050 and 500 mb	7 Hz/mb	±0.1 mb
Temperature (thermistor -- ML 419)	-15°C to + 40°C	20 Hz/°C	±0.2°C
Humidity (hygristor -- ML 476)	20% to 100%	20 Hz/%	±5%

humidity sensors are protected against solar radiation, and the shielding device offers appropriate ventilation during the flights.

The transmitter has a carrier frequency of 403 MHz, an HF power of 60 mW, a bandwidth of 100 kHz, and IRIG subcarriers of 22 kHz (humidity), 40 kHz (temperature), and 70 kHz (pressure). It is thus possible to get real-time profiles of temperature and humidity versus pressure or approximate altitude, assuming that the pressure gradient is constant within the flight range.

4.2.5 Data-Processing

The data-processing system consists of a Hewlett Packard HP 9825 minicomputer (24 K memories), a plotter, and a 9866B thermal line printer (Fig. 4.5). The system allows for plotting one value every 3 s, corresponding to three measurements (acquisition rate = 1 Hz). The computer eliminates extreme values, retains the center value, converts into meteorological data, plots temperature versus pressure, and stores the data on a cassette unit. (Figure 4.7 is a time diagram of the computer operations.)

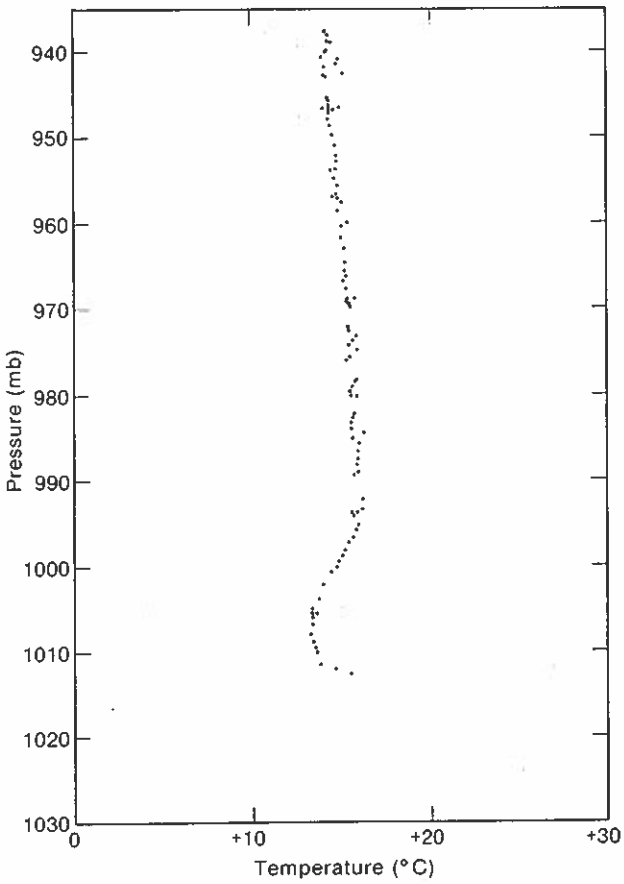

Figure 4.8. Example of temperature-versus-pressure plot on new emagram '900' designed for the boundary layer. (Plot shown is redrawn from original real-time plot.) Taken at Porcheville 6 July 1979 at 0600 by SAM C06.

4.2.5.1 Real-time processing

Real-time plotting of temperature versus pressure is possible on any emagram. A specially designed one (Fig. 4.8) for low atmosphere is characterized by a linear pressure scale between 1050 and 900 mb and isotherms perpendicular to isobars.

4.2.5.2 Delayed data processing (20 min)

Stored data can be further processed. The raw data extraction program prints time, pressure, temperature, humidity, height (through Laplace equation), and altitude. The correction program eliminates the wrong values from the first shorter set. The final processing program prints time, pressure, temperature, humidity, height, altitude, dew point, adiabatic wet-bulb temperature. Final data are also recorded on cassettes.

4.2.5.3 Plottings

Processed data can be plotted on emagrams as temperature, dew-point temperature, and adiabatic wet-bulb temperature versus pressure (Figs. 4.9 and 4.10). Certain flight parameters, such as pressure or vertical speed versus time or height (Fig. 4.11), can also be plotted.

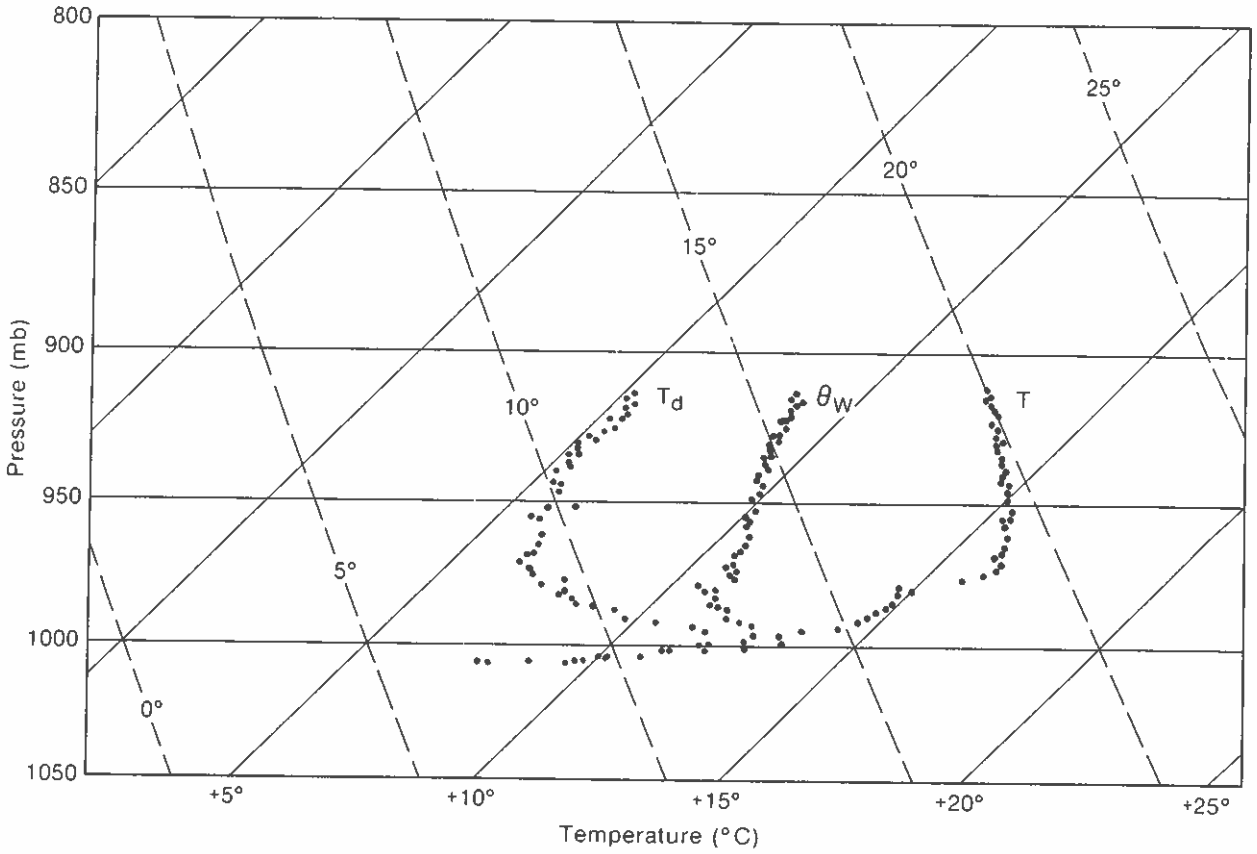

Figure 4.9. Example of T, T_d and θ_W plots during ascent. (Plot is redrawn from real-time plot, which shows points for both ascent and descent.) Data were taken at Chateauroux 23 July 1979 at 0500 by SAM B11.

4.3 SUMMARY OF PREVIOUS USES

4.3.1 Mount Etna

A remotely piloted SAM-C was successfully used in June 1978 on Mount Etna, a volcano in Sicily, in cooperation with H. Tazieff's team of volcanologists. The experiment had two objectives:

(1) To study the thermal environment of the volcano to assess the modification of the vertical profile of temperature by the mountain (and the volcano).

(2) To sample the gases in the plume of the volcano to determine chemical properties and prove the feasibility of the SAM method for physical and chemical research of volcano plumes.

4.3.2 Chateauroux

SAM-B was employed at Chateauroux during July 1978 to monitor the inversion layer early in the morning and give accurate knowledge of the time of thermal plume formation, so that take-off schedules for the Glider World Championship held there could be

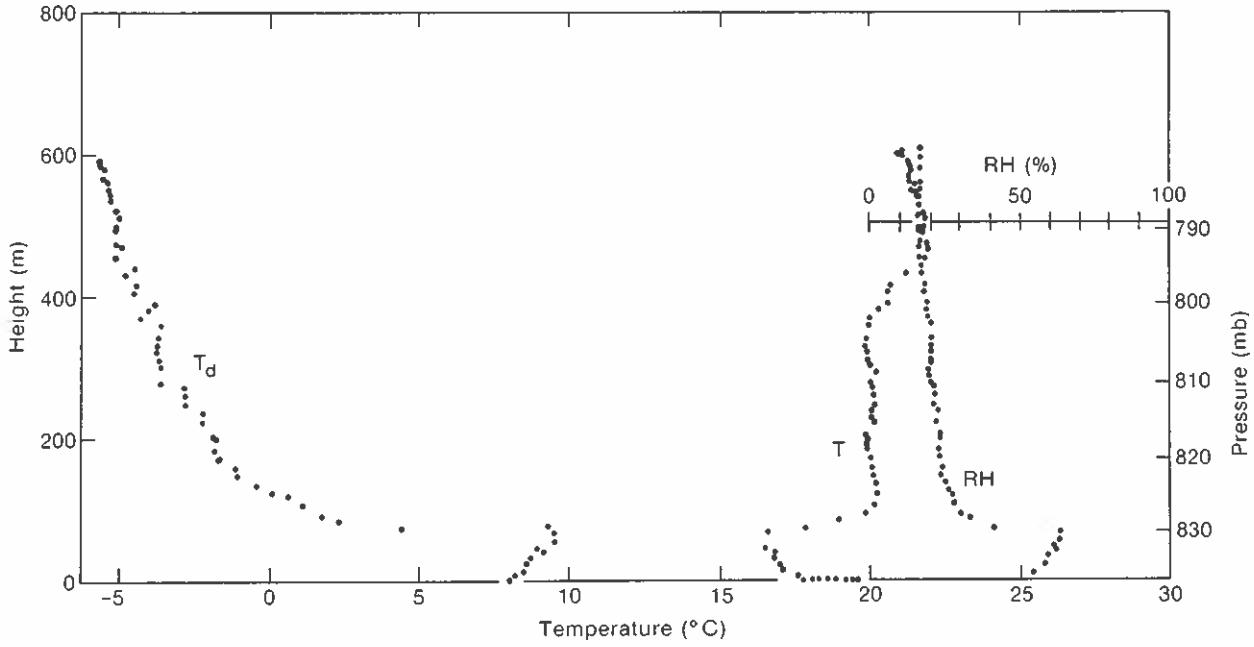

Figure 4.10. Example of T, T_d, and RH plots during ascent as a function of height. (Plot shown is redrawn from real-time plot, which shows points for both ascent and descent with different measurements indicated in different colors.) Taken at Boulder 28 August 1979 at 0930.

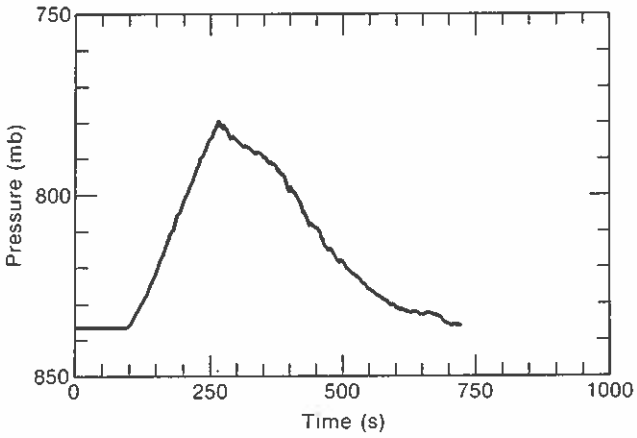

Figure 4.11. Pressure versus time plot recorded during flight.

fixed. Thirty-eight soundings were performed during 14 days, with time intervals varying from 1 h (around 0500 UT) to 20 min (around 1000 UT).

4.3.3 Plant Pollution Studies

During July 1979, SAM-C was used with a new sampling device consisting of 1.5-ℓ glass containers with an initial internal pressure of 1 mb. These containers were opened by a remote control system and were filled in approximately 5 s, then closed again. Analyses were conducted on the site immediately after each flight with an ultraviolet fluorescence method (SO_2).

5. COMPARISON OF AIRCRAFT AND BAO TOWER MEASUREMENTS

D. H. Lenschow and B. B. Stankov
National Center for Atmospheric Research
Boulder, Colorado, U.S.A.

5.1 INTRODUCTION

From 17 to 28 April 1978, a site evaluation study was conducted in the vicinity of the Boulder Atmospheric Observatory (BAO) tower to help determine the degree to which the tower measurements are representative of the surrounding area. This was the initial field research program involving the BAO tower. An NCAR Queen Air aircraft was used to obtain measurements along horizontal flight paths centered at the tower for comparison with concurrent tower measurements.

Intercomparisons of tower and aircraft measurements are carried out periodically by NCAR primarily to calibrate and check aircraft measurements of temperature, pressure, and humidity. This is particularly important for experiments involving several instrument platforms probing the same phenomena. Biter and Wade (1975) describe the techniques and equipment used for such an intercomparison during the National Hail Research Experiment (NHRE) and present some examples of the results. Their accuracy tolerances were ± 0.5 K for air and dewpoint temperature, and ± 1 mb for static pressure. Measurements of turbulence quantities such as variances and fluxes, however, are not routinely compared.

The region surrounding the tower is gently rolling terrain used for grazing, dryland and irrigated farming, and suburban living. As shown in Fig. 5.1, the general terrain slope is toward the northeast, although the local slope near the tower is toward the north. As pointed out by Lenschow et al. (1979), even very slight terrain variations can cause large variations in the overlying boundary layer, particularly at night and during the initial development of the daytime convective mixed layer. In addition to local terrain variations, the foothills of the Rocky Mountains rise to more than 600 m above the BAO site within 25 km west of the tower. About 25 km farther west, the Front Range towers about 2500 m above the BAO site. Therefore, we expect that, under certain conditions depending upon the height above the ground, the tower measurements will not represent the surrounding area.

5.2 EXPERIMENTAL DETAILS

The BAO tower was instrumented for measurements of wind velocity components, temperature, and humidity at heights of 10, 20, 50, 100, 150, 200, 250, and 300 m above the ground. Details of the tower, its instrumentations, and the data acquisition and recording are discussed by Kaimal (1978). Twenty-minute-block averages of winds and temperature, recorded at a sampling rate of 10 Hz, and standard deviations from the 20-min means were calculated and compared with the aircraft measurements.

The NCAR Queen Air, shown in Fig. 5.2, is a light twin-engine aircraft that can be equipped for a variety of research programs (Burris et al., 1973). The aircraft measurements in the site evaluation study included the three wind components, air and surface temperature, and humidity. Air motion measurements were calculated from the airplane velocity and attitude angles, measured with an inertial navigation system (INS), and the air velocity with respect to the airplane was obtained from sensors at the tip of the nose boom. A Rosemount platinum-resistance-wire thermometer, with a wire diameter of 25 μm, is also mounted near the tip of the nose boom. The measured total air temperature is then corrected for heating caused by the rapid air flow. Further details on the air motion sensing system are presented by Lenschow et al. (1978), and on airplane temperature and velocity measurements by Lenschow (1972).

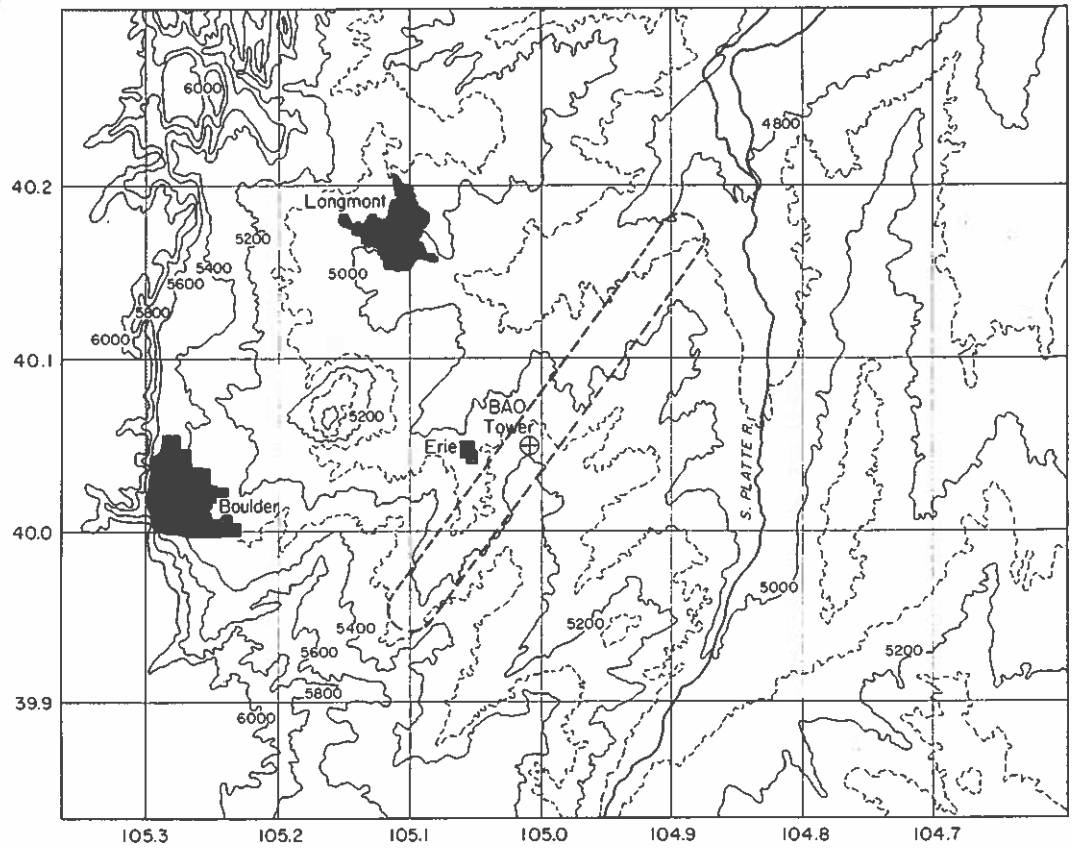

Figure 5.1. The region surrounding the Boulder Atmospheric Observatory tower and the research aircraft flight path (----).

The aircraft data were recorded at 20 Hz and divided into segments of 4096 samples. At an average aircraft speed of 70 m/s, this is equivalent to a length of 14.3 km. For comparison with the tower data, at a wind speed of 10 m/s, the equivalent averaging distance for a 20-min time series is 12 km. Before standard deviations were calculated, the mean and a least-squares linear trend were removed from each segment.

Because of flight restrictions over the suburban tower surroundings, the minimum aircraft flight altitude is 150 m above the ground. Therefore, intercomparison measurements were made only at the 150- and 300-m levels of the tower. The aircraft flight path is shown in Fig. 5.1. The aircraft was flown at a constant height above the ground, measured by a radar altimeter. Altogether, 13 flights totaling 28 h were conducted. Here we present a comparison of tower and aircraft measurements during Flight 6, from 1551 to 1751 MST on 21 April 1978.

A weak cold front had passed through the area several hours earlier and the wind was quite steady from the northwest. The sky was partly covered with cumulus clouds, with no precipitation. Solar heating was sufficient to generate a convective mixed layer well above the airplane flight path.

The flight path used on this day was a 30-km-long I-shaped pattern, centered at the tower, as shown in Fig. 5.1. This pattern, which took less than 15 min to complete, was flown continuously for eight cycles, all at 150 m above the ground, except for the last cycle, which was at 300 m. On most of the other days, an X-shaped flight path was

Figure 5.2. NCAR Queen Air research aircraft.

chosen to allow comparisons of aircraft and tower measurements at locations approximately uniformly surrounding the tower. However, it took 30 min to complete this pattern and, furthermore, on two of the four traverses by the tower, the airplane turned at the tower. Since turns can have an adverse effect on the accuracy of spatially averaged airplane wind measurements, reliable values centered at the tower were obtained for only half of the flight legs past the tower.

5.3 TOWER-AIRCRAFT INTERCOMPARISON

Tables 5.1-5.3 summarize the comparisons between the airplane and tower measurements. Since the length of an entire flight leg is only about 30 km, the north (Table 5.2) and south (Table 5.3) segments each overlap the center segment by about 6 km.

The mean values of tower and airplane measurements of horizontal wind components and temperature agree well with each other. The average difference of the velocity components is 0.6 m/s, with no significant difference between the segments by the tower and the other segments. Similarly, the average temperature difference is only about 0.4 K. Thus, horizontal variations were not large enough during this period to cause significant errors in the mean.

The standard deviations of the aircraft horizontal wind components are consistently somewhat larger and more variable than the tower measurements, particularly for the segments away from the tower. Although we do not know the reason for this, there are two possibilities:

(1) The wind may be affected somewhat by the terrain. On the north leg, we observed that u consistently reached a maximum in the middle of the segment, then decreased at the end of the leg. It is difficult to determine, however, even the scale of terrain variation that might cause such a perturbation.

(2) The airplane measurements may include contributions from longitudinal rolls (LeMone, 1973) since the airplane flight path is approximately perpendicular to the wind. If the rolls are aligned approximately with the wind, the tower may not pass through a complete cycle during the 20-min measurement period.

Tower and airplane measurements of the standard deviations of vertical velocity and temperature show good agreement with each other. This may be the result of relatively less contribution to the standard deviations by terrain-induced variations and longitudinal rolls than by the horizontal velocity components.

Table 5.1. Comparison of airplane (subscript A) and tower (subscript T) measurements of velocity components and temperature for the flight segments centered at the tower

MST Center of time period	M	m/s										K				
	h	N[1]	U_A[2]	U_T	σ_{UA}	σ_{UT}	V_A	V_T	σ_{VA}	σ_{VT}	σ_{WA}	σ_{WT}	θ_A	θ_T	σ_θ	$\sigma_{\theta T}$
1601	150	3	11.5	10.8	1.64	1.58	-5.0	-7.0	1.66	1.79	1.19	1.08	303.7	306.0	0.23	0.24
1621	150	3	12.1	12.0	1.63	1.15	-5.3	-5.5	1.72	1.33	1.00	1.07	305.3	305.3	0.27	0.32
1641	150	3	11.5	10.4	1.20	1.15	-4.0	-5.3	1.31	1.69	1.03	1.00	305.1	305.3	0.19	0.16
1701	150	3	10.0	10.4	1.07	1.05	-5.7	-5.8	1.16	0.93	0.78	.70	304.6	305.1	0.19	0.21
1721	150	2	8.7	8.8	1.42	1.06	-5.8	-7.1	1.04	0.93	0.70	.71	304.2	304.5	0.18	0.17
1741	300	2	8.0	7.0	1.38	1.36	-4.4	-5.0	1.61	1.35	.85	.85	304.0	304.1	0.21	0.14
Average			10.3	9.9	1.34	1.23	-5.0	-5.9	1.42	1.34	.93	.90	304.5	305.1	.20	.21
σ			1.7	1.7	0.19	0.21	0.7	0.9	0.29	0.36	0.18	0.17	0.63	0.67	.02	.07

[1] N is the number of 14-km flight segments during each time period.

[2] The horizontal velocity components are oriented towards the east (U) and north (V).

Table 5.2. Comparison of airplane (subscript A) and tower (subscript T) measurements of velocity components and temperature for the flight segments centered north of tower

MST	M		m/s										K			
Center of time period	h	N	U_A	U_T	σ_{UA}	σ_{UT}	V_A	V_T	σ_{VA}	σ_{VT}	σ_{WA}	σ_{WT}	θ_A	θ_T	σ_θ	$\sigma_{\theta T}$
1601	150	3	11.4	10.8	1.49	1.58	-3.8	-7.0	1.60	1.79	1.11	1.08	305.9	306.0	0.22	0.24
1621	150	3	12.8	12.0	1.57	1.15	-5.0	-5.4	1.54	1.33	1.05	1.07	305.7	305.3	0.22	0.32
1641	150	3	12.4	10.4	1.27	1.15	-4.5	-5.3	1.55	1.69	1.04	1.00	305.4	305.3	0.20	0.16
1701	150	3	10.4	10.4	2.20	1.05	-5.7	-5.8	1.47	0.93	0.83	0.70	305.0	305.1	0.20	0.21
1721	150	2	8.1	8.8	2.46	1.06	-6.5	-7.1	1.82	0.93	0.72	0.71	304.5	304.5	0.23	0.17
1741	300	2	7.7	7.0	1.94	1.36	-5.5	-5.0	1.73	1.35	0.87	0.85	304.4	304.1	0.26	0.14
Average			10.5	9.9	1.82	1.23	-5.2	-5.9	1.62	1.34	0.94	0.90	305.2	305.1	0.22	0.21
σ			2.2	1.7	0.46	0.21	0.9	0.9	0.13	0.36	0.15	0.17	0.62	0.67	0.02	0.07

Table 5.3. Comparison of airplane (subscript A) and tower (subscript T) measurements of velocity components and temperature for the flight segments centered south of tower

MST	M		m/s										K			
Center of time period	h	N	U_A	U_T	σ_{UA}	σ_{UT}	V_A	V_T	σ_{VA}	σ_{VT}	σ_{WA}	σ_{WT}	θ_A	θ_T	$\sigma_{\theta A}$	$\sigma_{\theta T}$
1601	150	3	11.1	10.8	1.93	1.58	-5.8	-7.0	1.60	1.79	1.22	1.08	305.7	306.0	0.23	0.24
1621	150	3	12.7	12.0	1.71	1.15	-5.4	-5.4	1.80	1.33	1.08	1.07	305.0	305.3	0.22	0.32
1641	150	3	11.5	10.4	1.35	1.15	-4.0	-5.3	1.79	1.69	1.19	1.00	304.5	305.3	0.20	0.16
1701	150	3	9.4	10.4	1.25	1.05	-5.8	-5.8	1.25	0.93	0.90	0.70	304.1	305.1	0.19	0.21
1721	150	2	7.3	8.8	1.20	1.06	-5.5	-7.1	1.05	0.93	0.85	0.71	303.9	304.5	0.17	0.17
1741	300	2	7.7	7.0	2.11	1.36	-4.0	-5.0	1.76	1.35	1.48	0.85	303.7	304.7	0.18	0.14
Average			10.0	9.9	1.59	1.23	-5.1	-5.9	1.54	1.34	1.12	0.90	304.5	305.1	0.20	0.21
σ			2.8	1.7	0.40	0.21	0.8	0.9	0.32	0.36	0.23	0.17	0.75	0.67	0.02	0.07

5.4 SUMMARY

The excellent agreement found in this initial comparison of mean values and standard deviations of velocity and temperature measured concurrently by the BAO tower and an aircraft is very encouraging. We can make useful comparisons of many other items of interest, such as covariances, time changes at the tower versus horizontal gradients from the aircraft, and spectral and cospectral quantities. These comparisons could help to determine the degree to which the tower measurements are affected by terrain inhomogeneities. Varying degrees of horizontal inhomogeneity in the boundary layer might be observed with different synoptic situations and at different times of day. Comparison of airplane and tower spectra may also be useful in determining the validity of Taylor's hypothesis, i.e., that time and space averages are interchangeable.

5.5 REFERENCES

Biter, C. J., and C. G. Wade (1975): Field calibration and intercomparison of aircraft meteorological measurements. Preprint Vol. 1, NHRE Symposium/ Workshop on Hail, September 1975, VIII.A.63.1-63.21. (Available from NCAR, P.O. Box 3000, Boulder, CO 80307.)

Burris, R. H., J. C. Covington, and M. N. Zrubek (1973): Beechcraft Queen Air aircraft. Atmos. Technol. 1:25-27.

Kaimal, J. C. (1978): NOAA instrumentation at the Boulder Atmospheric Observatory. Prepr. 4th Symp. on Meteorol. Obs. and Instrum., 10-14 April 1978, Denver, Colo., American Meteorological Society, Boston, Mass., pp. 35-40.

LeMone, M. A. (1973): The structure and dynamics of horizontal roll vortices in the planetary boundary layer. J. Atmos. Sci. 30:1077-1091.

Lenschow, D. H. (1972): The measurement of air velocity and temperature using the NCAR Buffalo aircraft measuring system. NCAR-TN/EDD-74. National Center for Atmospheric Research, Boulder, Colo., 39 pp.

Lenschow, D. H., C. A. Cullian, R. B. Friesen, and E. N. Brown (1978): The status of air motion measurements on NCAR aircraft. Prepr. 4th Symp. on Meteorol. Obs. and Instrum., 10-14 April 1978, Denver, Colo., American Meteorological Society, Boston, Mass., pp. 433-438.

Lenschow, D. H., B. B. Stankov, and L. Mahrt (1979): The rapid morning boundary layer transition. J. Atmos. Sci. 36:2108-2124.

6. TETHERED AERODYNAMICALLY LIFTING ANEMOMETER (TALA)*

Charles F. Woodhouse
Approach Fish, Inc.
Clifton Forge, Virginia, U.S.A.

6.1 INTRODUCTION

Variable altitude anemometry is a new method which is beginning to find application in low-level wind measurement. The principle is simple. Since wind-tunnel velocities are used to calibrate the lift and drag of an airfoil, if the characteristics of a free-flying airfoil are known then the velocity of the wind can be determined. The airfoil sensor or kite described here is stable in naturally turbulent winds to 50 m/s (Fig. 6.1).

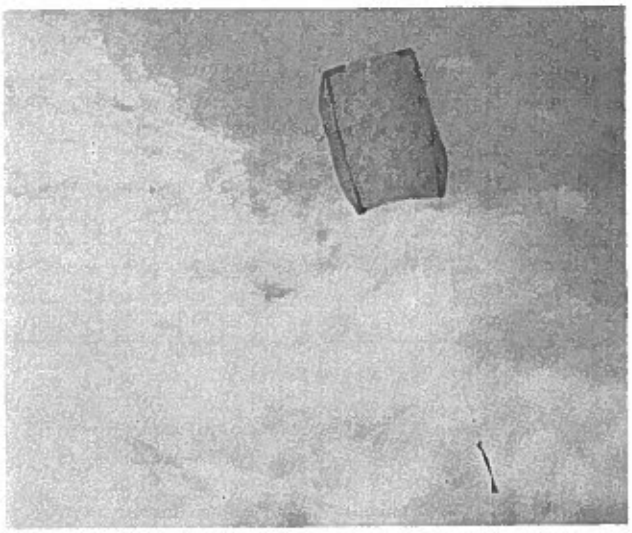

Figure 6.1. Patented sled airfoil is stable to 40 m/s. The tether line force is practically that of a theoretical flat plate:

$$q_k = \frac{\rho v^{1.967}}{2} \quad .$$

6.2 MEASUREMENT OF WIND SPEED

The tension on the tether line produced by lift and drag forces acting on the kite provides a measure of wind speed at kite level. The force on a flat plate is

$$q = \frac{\rho v^2}{2} \quad , \tag{6.1}$$

where q = force, ρ = density, and v = speed; q is quite close to the force on the sensor q_k as determined by wind tunnel calibration:

$$q_k = \frac{\rho v^{1.967}}{2} \quad . \tag{6.2}$$

*U.S. Pat. numbers 4,058,010 and 4,152,933.

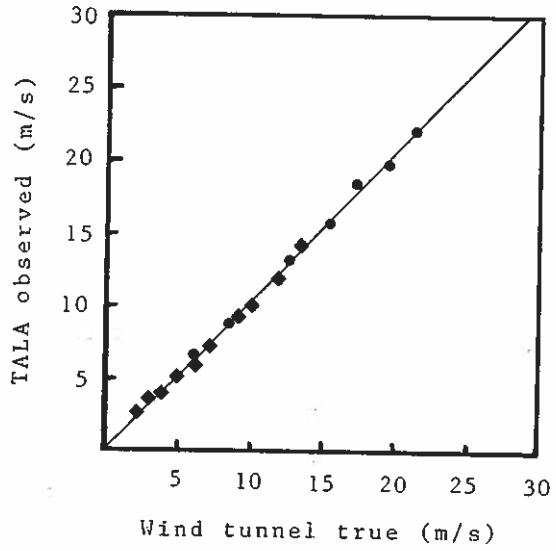

Figure 6.2. Original calibration of airfoil at NASA-Langley with correlation at NBS of electronic equipment built to Langley formula. ● = NASA-Langley data points (calibration 5 April 1976; correlation coefficient .999). ◆ = National Bureau of Standards data points (calibration 17 March 1978; correlation coefficient .997).

The force q_k is measured directly by a strain gauge attached to the end of the tether line. Correlation coefficients as determined in the large NASA-Langley and the NBS wind tunnels are 0.999 and 0.997 respectively (Fig. 6.2).

Car-tow calibration in still dawn air (Fig. 6.3) at 175 m altitude shows a wind drift between east and west runs. Car speed was calibrated by radar.

Calibration in natural winds against cup or propeller anemometers is difficult because the empirical and varying turbulence correction equations of these instruments (McMichael and Klebanoff, 1975) are in the 1% to 2% range (Baker et al., 1979). Previous calibration against the BAO sonic anemometers indicates accuracies within 0.65%. We will test this agreement more accurately during the BLIE intercomparison.

Catenary drag and the relationship between catenary cable curvature and height have been extensively studied. The present cable used is only 250 microns in diameter with a weight of 115 g/km. Computer analysis of the dynamics of this line (Shieh and Frost, 1979) has shown that for a cable of that type the maximum effect of catenary drag on the measured tension at the ground is five orders of magnitude smaller than the tension produced by the airfoil itself.

6.3 MEASUREMENT OF ALTITUDE

The kite altitude is a function of line length, corrected for catenary sag and the observed vertical angle to the kite. The following empirical relationship is used:

$$Z = 0.9 \sin\phi(0.3n - 2.2 \times 10^{-5} n^2) \qquad (6.3)$$

where Z is the kite altitude, ϕ is the observed sensor vertical angle and n is the reel count (Fig. 6.4). The 0.9% correction factor in (6.3) compensates for the effect of catenary curvature (Shieh and Frost, 1979). This correction is small because of the low weight and low drag of the line. The equation used for estimating decrease in reel diameter as line is payed out is found to be accurate to 1%.

Vertical angle ϕ can be determined from a hand-held clinometer. In the electronic model, altitude is computed automatically from measurements of the string angle at

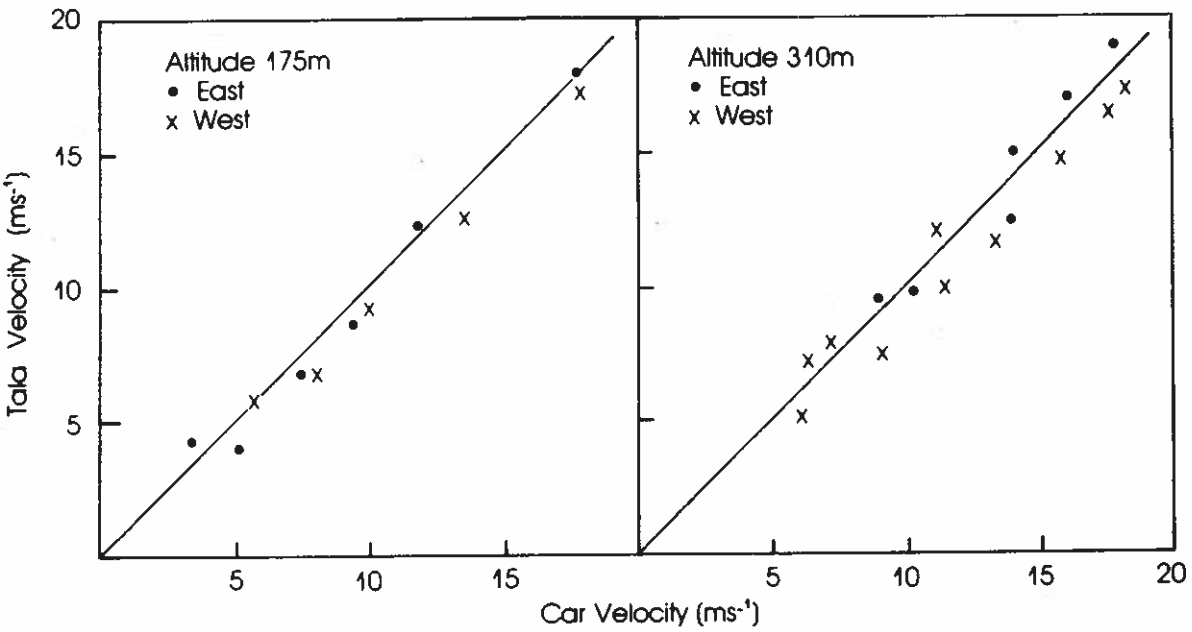

Figure 6.3. Car tow calibration at 175 m shows slight wind drift between east and west runs.

the base and of the line payout. A catenary correction control allows compensation for differences between visual angle and string angle, for different amounts of line length.

The kite flies at a constant angle of attack to its apparent wind. Wind-tunnel data show a tether repose angle of 53° at 5 m/s rising to 57° at 20 m/s. Car-tow data (Fig. 6.5) illustrate the constant flight altitude at speeds of 5 m/s to 20 m/s.

6.4 MEASUREMENT OF WIND DIRECTION

A simple potentiometer device attached to the end of the tether line measures azimuth wind direction. The potentiometer readings are referenced to true north. A pronounced lateral bend in the line will introduce errors in the wind direction reading, but this can be corrected by entering into the data acquisition system an initial visual reading of the direction of the upper section of the tether line. In order to make this measurement it will be necessary to move to either the left or right of the tether point with a precision magnetic compass.

6.5 CHARACTERISTICS OF THE KITE

The airfoil weighs 16 g and has a surface area of 1500 cm^2. It acts, when under tension in flight, much like a large electrostatic loudspeaker cone. Because of the low weight and large surface, its compliance is high. The tether, or force transmission line, is of inelastic Kevlar (DuPont) with a modulus of elasticity in the range of steel. Thus, the frequency response of the sensor is high. Field measurements from the sensor flying at 100- to 200-m altitude show a response of at least 10 Hz in a 10 m/s wind field.

The free-flying sensor orients directly and at constant angle of attack to its apparent wind. Thus its altitude of flight at specific line lengths is a direct function of the vertical component of the apparent wind vector. Similarly, horizontal position changes are a function of the lateral component. A measurement of the lateral and vertical turbulence may be obtained to altitudes of 300 m.

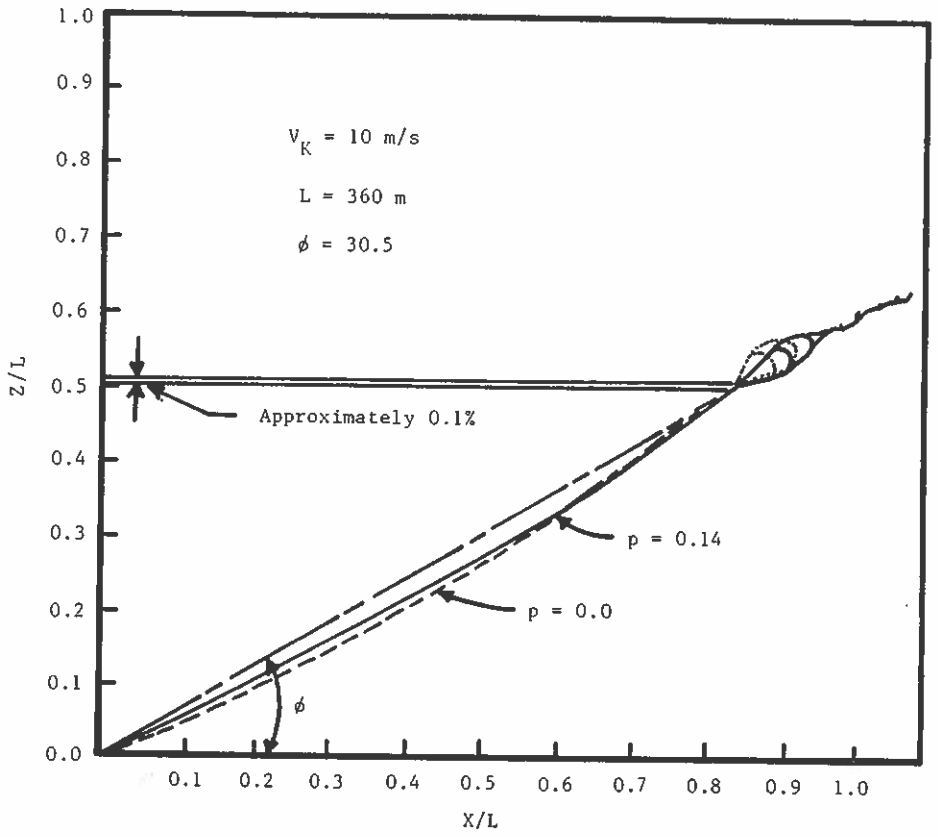

Figure 6.4. Analysis (Shieh and Frost, 1979) showing 0.1% effect of varying wind field on altitude where v = wind speed at sensor level; L = line length; ϕ = sensor elevation angle; Z = height; X = distance; p = power law exponent.

The kite will fly stably at wind speeds as low as 3 m/s. To lift the kite under such conditions, an ancillary balloon inflated with helium to a specific circumference may be attached with surgical silk, or mercerized cotton thread to the sensor. The surgical silk breaks away at wind speeds of 4 m/s.

At wind speeds of less than 3 m/s the helium-filled balloon lifts the sensor through calm inversions to upper altitude winds. The angle of the restraining tether is a function of lift/drag, and the altitude is a function of line length out and tether repose angle. As the sensor is lifted through the inversion into winds greater than 4 m/s the lifting balloon breaks away from the now flying sensor.

6.6 EQUIPMENT OUTPUT CHARACTERISTICS

Wind speed: The line tension strain gauge outputs are internally calculated to give 400 mV/m/s; thus, 10 V = 25 m/s.

Direction: Tether line direction is calculated from a reference centerline voltage of 5.0 V at $\pm$ 36° per volt.

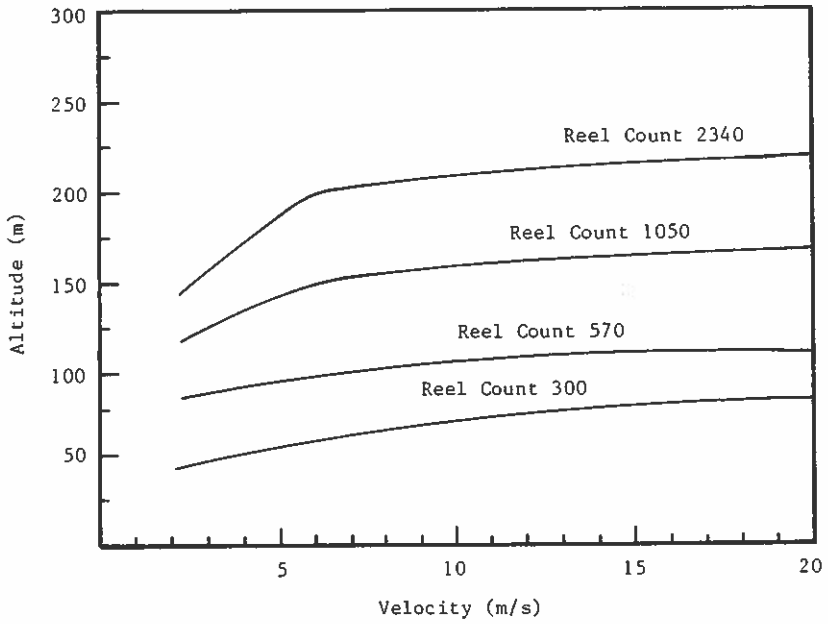

Figure 6.5. Altitude of sensor at increasing line length and speed, illustrating relatively constant altitude of flight at velocities above 5 m/s.

Altitude: Altitude from 0 to 300 m is calculated from line length and catenary angle at 33 mV/m; thus, 10 V = 300 m.

Digital: Analog oscillation-free outputs are sampled at 0.8 Hz by a portable digital recorder. Mean standard deviation and minimum and maximum values are calculated for each parameter each minute and stored on a cassette tape for later data reduction. The data output is RS232-compatible at 300 baud.

6.7 REFERENCES

Baker, R. W., R. L. Whitney, and E. W. Hewson (1979): A low level wind measurement technique for wind turbine generator siting. Wind Eng. 3:107-115.

Baker, R. W., R. L. Whitney, and E. W. Hewson (1979): Wind profile measurements using a tethered kite anemometer. Am. Wind Energy Conf., 16-18 April 1979, San Francisco, Calif., American Wind Energy Association, Washington, D.C.

Delaurier, J. D. (1972): A stability analysis of cable-body systems totally immersed in a fluid stream. NASA CR-2021, Stanford Univ., Dept. of Aeronautics and Astronautics, Stanford, Calif., 93 pp.

McMichael, J. M., and P. A. Klebanoff (1975): The dynamic response of helicoid anemometers. NBSIR 75-772, U.S. Dept. of Commerce, National Bureau of Standards, Washington, D.C., 54 pp.

Shieh, C. F., and W. Frost (1980): Tether analysis for a kite anemometer. Conf. on Wind Characteristics and Wind Energy Siting, 19-21 June 1979, Portland, Ore., Pacific Northwest Laboratory, Richland, Washington.

7. REMOTE ACOUSTIC ELECTRONIC SOUNDING (RACES)

P. Ravussin
Federal Institute of Technology
Lausanne, Switzerland

7.1 INTRODUCTION

The Remote Acoustic Electronic Sounding system (RACES) can measure in the lower layer of the atmosphere the vertical profile of the three-dimensional wind vector, the vertical profile of temperature, and the vertical profile of humidity. The version described here measures only the vertical profiles of vertical wind and temperature. As the measurements are made at the same time and in the same sampling volume, the system can calculate in time the vertical profile of the thermal coefficient of turbulent diffusivity K_h,

$$K_h = \frac{\overline{T'u_3'}}{\partial\bar{T}/\partial x_3} \tag{7.1}$$

where T is the aleatory variable of the temperature, and $T = \bar{T} + T'$, u_3 is the aleatory variable of the vertical component of the wind, and $u_3 = \bar{u}_3 + u_3'$. $\bar{T}$ and $\bar{u}_3$ are the statistical averages, defined in terms of probability density functions $p(T)$ and $p(u_3)$:

$$\bar{T} = \int_{-273}^{\infty} T \cdot p(T)\,dT \tag{7.2}$$

and

$$\bar{u}_3 = \int_{-\infty}^{+\infty} u_3 \cdot p(u_3)\,du_3. \tag{7.3}$$

Since the RACES system measures time series, the ergodic assumption of the stationarity of the measured phenomenon must be made, to replace the statistical averages by time averages. The averaging time is a critical parameter which depends on atmospheric conditions and topography.

7.2 OPERATION

The RACES system is based on the physical properties of transmission and diffusion of sound in the atmosphere. Thus the basis of the instrument is an electro-acoustic device which transmits vertically in the atmosphere.

7.2.1 Sound Transmitter

The sound transmitter (Fig. 7.1) contains an oscillator, which produces a sinusoidal electric signal at a very stable frequency f = 1600 Hz, $\Delta f/f < 10^{-6}$. The signal is transmitted through a switch (which is electronically operated) to a power amplifier and then to the electro-acoustic transducer. There the electric signal is transformed to an acoustic wave. The efficiency of the transducer is low:

$$\eta = \frac{P_s}{P_e} \tilde{=} 20\% \ , \tag{7.4}$$

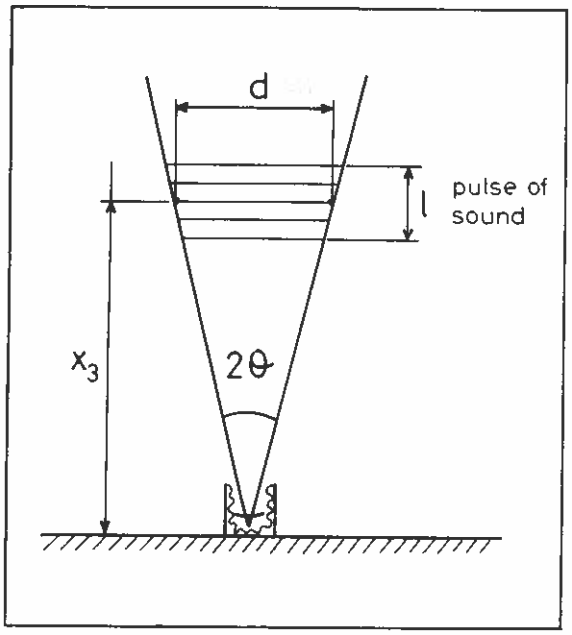

Figure 7.2. Sound propagation from acoustic antenna.

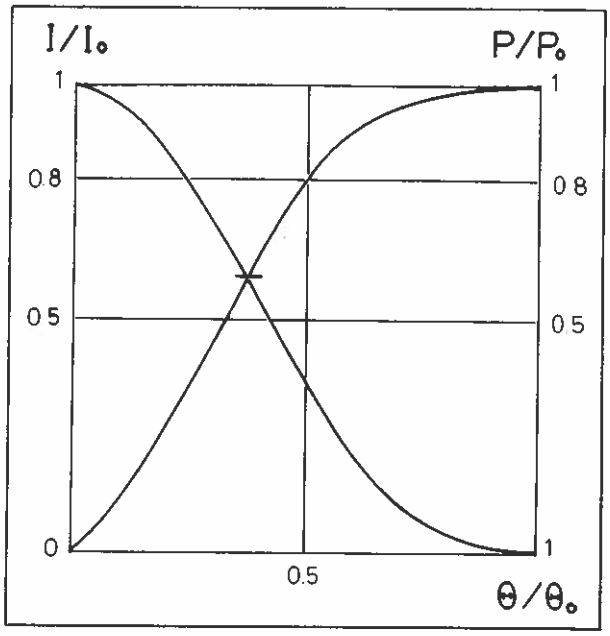

Figure 7.3. Acoustic intensity and power as a function of angle.

$$\lambda = \frac{c_s}{f} \quad . \tag{7.10}$$

For the 1600-Hz signal at 20°C,

$$\lambda = 0.21 \text{ m.}$$

For the present low-power version, the diameter of the antenna is 1.31 m. It is therefore possible to calculate at which altitude the diameter and the length of the pulse of sound will have the same value (Fig. 7.2):

$$x_3 = \frac{\ell}{2 \sin(1.22 \frac{\lambda}{d})} = 44 \text{ m} \quad . \tag{7.11}$$

The intensity of the sound is, however, not constant in the sampling volume. It varies according to the law

$$I = I_o \frac{2 J_1(\frac{d}{2} k \sin\theta)^2}{\frac{d}{2} k \sin\theta} \quad , \tag{7.12}$$

where I_0 = intensity at the center, J_1 = first-order Bessel function, k = wave number = $2\pi/\lambda$.

Figure 7.3 shows that 80% of the power is emitted in an angle

$$\theta \cong 0.5\ \theta_0 \quad .$$

For the RACES system, the length and the diameter of the sound pulse reach the same size at an altitude of ~90 m.

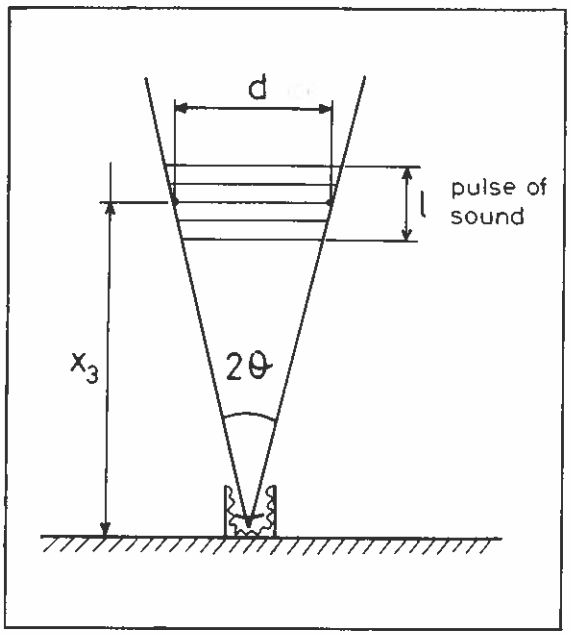

Figure 7.2. Sound propagation from acoustic antenna.

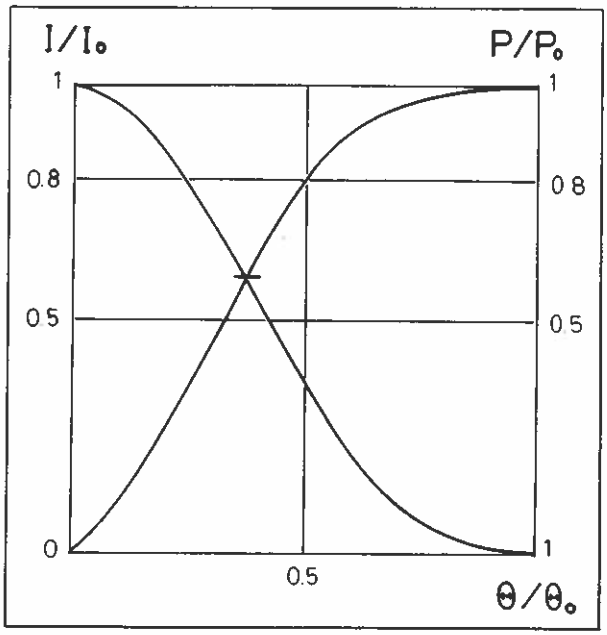

Figure 7.3. Acoustic intensity and power as a function of angle.

$$\lambda = \frac{c_s}{f} \quad . \tag{7.10}$$

For the 1600-Hz signal at 20°C,

$$\lambda = 0.21 \text{ m}.$$

For the present low-power version, the diameter of the antenna is 1.31 m. It is therefore possible to calculate at which altitude the diameter and the length of the pulse of sound will have the same value (Fig. 7.2):

$$x_3 = \frac{\ell}{2 \sin(1.22 \frac{\lambda}{d})} = 44 \text{ m} \quad . \tag{7.11}$$

The intensity of the sound is, however, not constant in the sampling volume. It varies according to the law

$$I = I_o \frac{2 J_1(\frac{d}{2} k \sin\theta)^2}{\frac{d}{2} k \sin\theta} \quad , \tag{7.12}$$

where I_o = intensity at the center, J_1 = first-order Bessel function, k = wave number = $2\pi/\lambda$.

Figure 7.3 shows that 80% of the power is emitted in an angle

$$\theta \cong 0.5\ \theta_0 \quad .$$

For the RACES system, the length and the diameter of the sound pulse reach the same size at an altitude of ~90 m.

Table 7.1. Corrections for relative humidity

Temp.	100% H	0% H
0°C	-0.23	+0.23
10°C	-0.48	+0.48
20°C	-0.93	+0.93
30°C	-1.78	+1.78

7.2.3 Time Constant

The time constant in the RACES system is the time that the sound takes to propagate along a distance equal to the length of the sound pulse. This is obviously the time duration of the pulse (50 ms). The RACES system is therefore capable of measuring the instantaneous value of the spatial average of the parameters T and u_3 in the sampling volume.

$$T_{ev} = \frac{1}{V} \iiint_V T \, dV \tag{7.13}$$

$$u_{3ev} = \frac{1}{V} \iiint_V u_3 \, dV \quad . \tag{7.14}$$

7.3 MEASUREMENT OF THE TEMPERATURE PROFILE

The speed of sound propagation in air is directly connected to the thermodynamical properties of the atmosphere. Because of this the RACES system measures directly the absolute value of the temperature.

7.3.1 Theory

The speed of sound in the air depends solely on the temperature. This can be deduced from the equation of the mechanics of fluids and the thermodynamic equations of the adiabatic processes,

$$C_s = \sqrt{\frac{\gamma R T}{\mu}} \quad , \tag{7.15}$$

where C_s = speed of sound (m/s), γ = ratio of the isobaric and isochoic specific heats, R = gas constant (J $mole^{-1}$ K^{-1}), μ = molecular weight ($mole^{-1}$), and T = absolute temperature (K).

In a dry atmosphere the proportions of the main gases, Ar, N_2, and O_2, are constant. In this case μ is also constant. γ does not vary with atmospheric pressure but does, very slightly, with temperature. However, the effect is negligible within a 10°C temperature variation.

7.3.2 Effect of the Air Moisture

Unfortunately the effect of the water vapor in the atmosphere is too strong to be negligible, especially at high temperatures. Because this version of the RACES system does not measure the vertical profile of humidity, the assumption of a constant 50% humidity profile was made. As seen in Table 7.1, the influence of moisture decreases rapidly with temperature. Table 7.1 gives the corrections for 100% and 0% relative humidity compared with 50% relative humidity, at different temperatures.

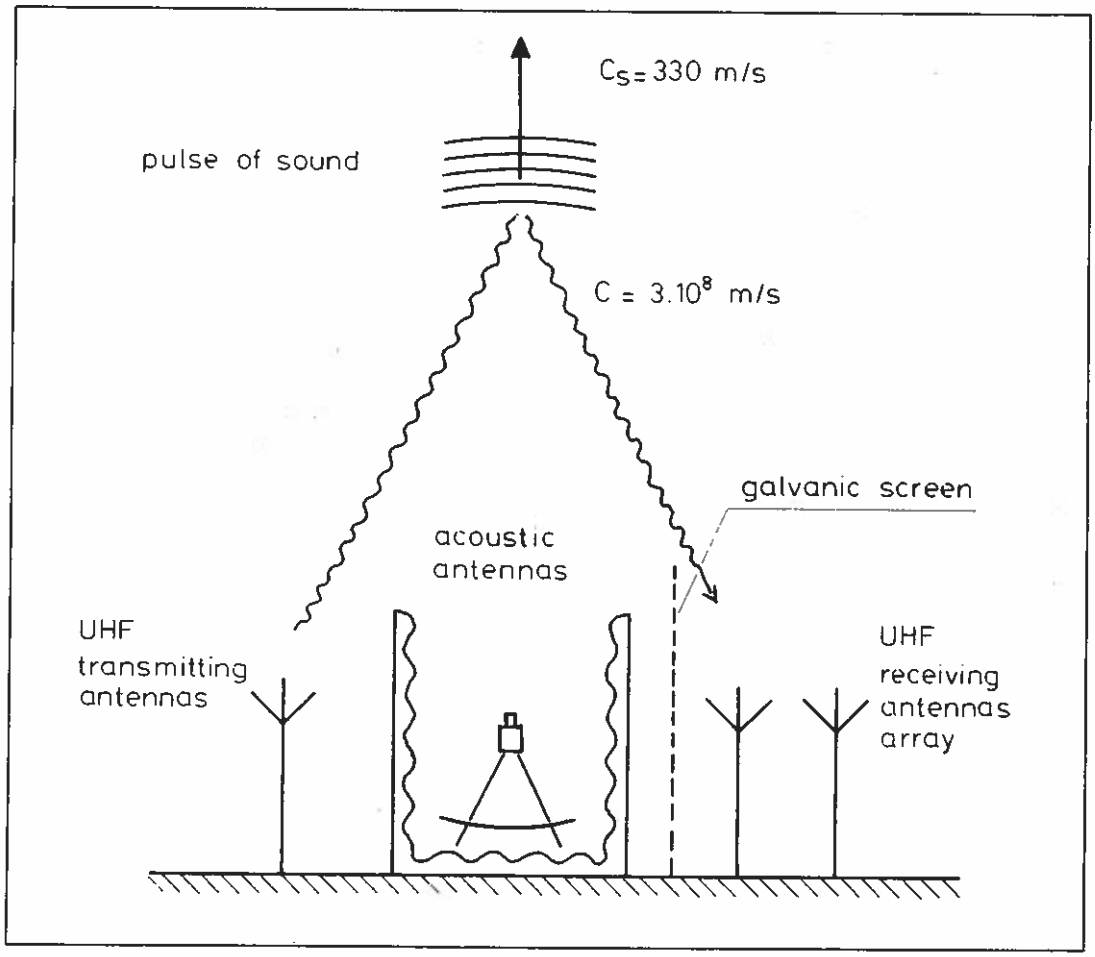

Figure 7.4. Measurement of speed of sound propagation in the atmosphere.

7.3.3 Effect of the Vertical Wind

The measured speed of sound is the sum of the effective speed of the sound and the vertical wind. Since the vertical wind is measured at the same time and in the same sampling volume, the computer can calculate this correction.

$$C_s = 20.05 \sqrt{T} + u_3. \tag{7.16}$$

7.3.4 Temperature Measurement

Since the speed of sound in the atmosphere depends mainly on the temperature, the propagation speed of the sound pulse is directly measured with a CW Doppler radar. The principle is illustrated in Fig. 7.4.

The wavelength of the radar must be exactly twice the wavelength of the sound pulse (which varies with the temperature). In order to improve the range, a feedback device was patented which corrects the frequency of the CW Doppler radar according to the frequency deviation of the return Doppler signal. The circuit used in this version is a phase-locked loop (PLL).

At the point of equilibrium the Doppler signal must have the same frequency as that of the sound pulse. Because of this, the same oscillator was used to produce the sound pulse and the reference signal for the feedback device. The relationship between the speed of sound and the radar frequency is given by the Doppler-Fizeau law:

$$\frac{\Delta\nu}{2\nu} = \frac{C_s}{C} \quad , \tag{7.17}$$

where Δv = received Doppler-Fizeau frequency, v = frequency of the emitter, C_s = speed of sound, and C = speed of the electromagnetic wave in the atmosphere. Since C is about 10^6 times faster than C_s, the speed of sound measurements made by RACES are essentially instantaneous.

The time interval between the starting of the sound pulse and the time of measurement gives the height of the measurement:

$$h = \int_{t_o}^{t} C_s \, dt \, . \tag{7.18}$$

The system measures the ratio $\Delta v/v$ directly and is therefore independent of the phase effect introduced by the low-pass filter of the PLL.

7.3.5 Description of the System

7.3.5.1 UHF transmitter

The UHF transmitter (Fig. 7.5) consists of a low-noise voltage-controlled oscillator (0.66 - 0.78 GHz) followed by a power amplifier (1 W) and a four-Yagi, 26-element, wide-band antenna system. The opening angle of the antenna is about 20°.

7.3.5.2 UHF receiver

The UHF receiver consists of an array of five 26-element (15.5-dB Yagi) antennas, electronically connected to the receiver. The purpose of the array is to compensate for the effect of sound pulse displacement by the horizontal wind. The antennas are followed by a 54-dB low-noise UHF preamplifier and the Doppler mixer. For practical reasons only one antenna was used for the Boulder comparisons.

7.3.5.3 LF receiver and converter

The low-frequency receiver consists of a low-noise preamplifier, a gyrator filter with adjustable Q factor from 0 to 1,000, a linear amplifier (0 - 40 dB), a log-amplifier, and a signal shaper circuit. The signal is then transmitted to an adjustable digital divider and to a UHF ratiometer with IEC-Bus interface. The measurement time is 12.5 ms. The measurement interval is 70 ms. This is because it takes about 35 ms to transmit the information to the computer through the IEC-Bus. Consequently, the temperature is measured every 20 m only.

7.4 MEASUREMENT OF THE VERTICAL WIND PROFILE

7.4.1 Theory

The sound pulse propagating vertically in the atmosphere is diffused by the small inhomogeneities of the air. The coefficient of diffusion σ_ϕ depends on the angle of diffusion of the thermal and wind turbulence according to the following expression:

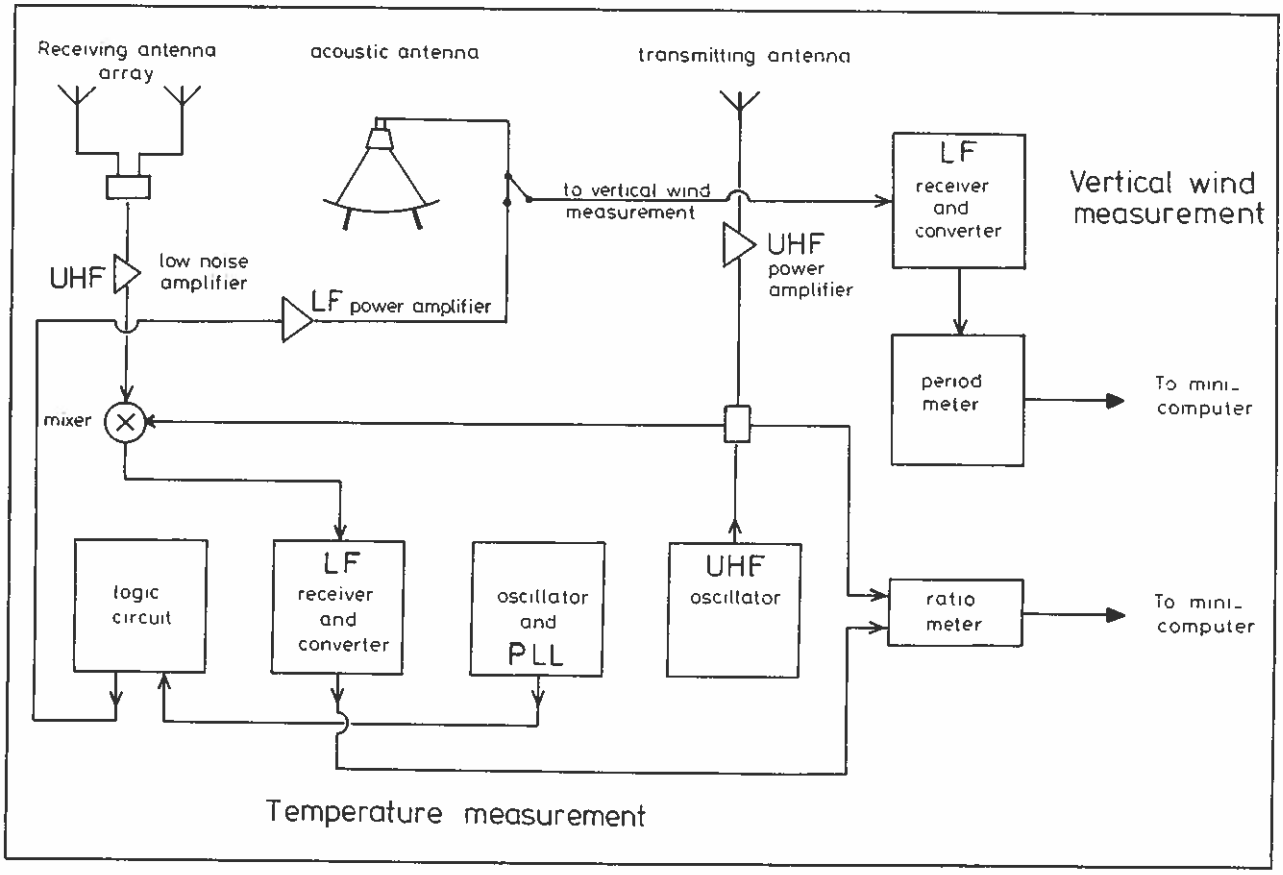

Figure 7.5. Block diagram of RACES system.

$$\sigma_\phi = 0.03\, k^{1/3} \cos^2\phi \left(\frac{C_v^2}{v^2} \cos^2\frac{\phi}{2} + 0.13\,\frac{C_T^2}{T^2}\right) \left(\sin\frac{\phi}{2}\right)^{-11/3}, \qquad (7.19)$$

where k = wave number of the sound, ϕ = diffusion angle, C_v = wind turbulence parameter, v = wind speed, C_T = thermal turbulence parameter, and T = temperature.

This law assumes that the wind turbulence and the thermal turbulence have a Kolmogorov's spectrum. A small part of the sound is back-scattered and reaches the acoustic antenna.

For $\phi = \pi$,

$$\sigma_\phi = 0.0039\, k^{1/3}\,\frac{C_T^2}{T^2}\,.$$

The sound is back-scattered only by the thermal inhomogeneities of the atmosphere.

7.4.2 Principle of the Wind Measurement

The small-scale thermal inhomogeneities in the atmosphere have an average general movement u_3 in relation to the receiver's antenna. In this case, according to the Doppler law, the back-scattered sound that reaches the acoustic antennas has a frequency slightly different from that of the emitting antenna.

$$\frac{\Delta f}{2f} = \frac{u_3}{C_s} \quad , \tag{7.20}$$

where Δf = Doppler frequency, f = frequency of the pulse of sound, u_3 = vertical wind, and C_s = speed of the sound in the atmosphere. C_s is measured by the temperature-measuring part of the RACES system.

Because the Fourier transform needs a stationary signal, the frequency measurement of the received signal was not made with a spectrum analyzer. Instead the average period of the signal was directly measured with a zero-crossing technique. The average is taken on 20 periods of the signal.

7.4.3 LF Receiver and Converter

The acoustic antenna signal is switched (a few milliseconds after the emission of the sound pulse) to a low-noise preamplifier, a gyrator filter with adjustable Q factor from 0 to 1000, a linear amplifier (0 - 40 dB), a log amplifier, and a signal shaper circuit. The signal is then transmitted to an adjustable digital divider and to a periodmeter (interval timer) with an IEC-Bus interface. The minimum time interval of the periodmeter is 0.1 μs. The timing considerations are exactly the same as in the temperature measurements. Consequently the vertical wind is measured approximately every 10 m.

7.5 DATA ACQUISITION AND PROCESSING

The RACES system uses a PDP11-03 16-bit minicomputer with 32-k-word RAM memory, display, an LA 35 printer, and an RX02 floppy disk driver with two single-side, double-density disk drivers.

The operator can choose the time interval from 0 (immediate) to 60 minutes, the number of soundings for averages from 0 to 400, and whether to print all the data, the selected data, or the statistical data, or to keep the data on file in a second floppy disk. A sample of the output is shown in Fig. 7.6.

7.6 PURPOSE OF THE COMPARISONS

Our purpose in BLIE will be to compare the measurements made by the RACES system with those made by the conventional tower instruments and by other remote sensing systems. It must, however, be considered that the RACES system has a sampling volume much larger and a sampling time much shorter than those of conventional instruments on the tower.

The range of the RACES system used will be rather low (~150 m) because the high-level version is too bulky and too heavy to be transported easily overseas. Another reason for the low range will be that we will have only one UHF receiving antenna instead of five.

300 SONDAGES---------- 04-SEP-79 --- 11:40:00 ----------

HAUTEUR (M)	T - BAR (DEG-C)	SIGMA (DEG-C)	NB. DE MESURES VALIDES (%)
394.	29.98	0.00	0.3
368.	0.00	0.00	0.0
343.	25.32	1.64	0.7
317.	24.76	0.44	0.7
291.	27.26	0.00	0.3
265.	27.69	0.91	1.3
239.	28.99	2.22	2.3
213.	28.23	2.37	3.7
186.	27.35	2.92	4.7
160.	27.95	2.42	5.3
134.	27.51	1.93	10.7
108.	27.91	2.27	13.0
82.	28.09	1.70	24.3
56.	28.68	1.53	61.3
30.	28.42	1.32	95.7

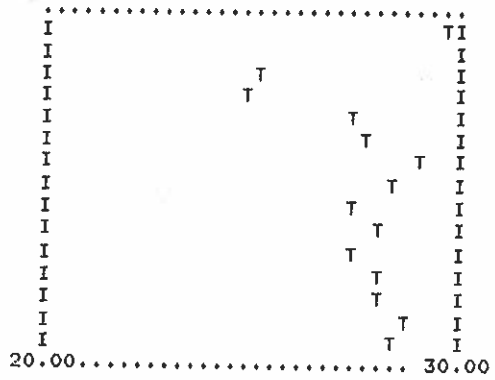

300 SONDAGES---------- 04-SEP-79 --- 11:40:00 ----------

HAUTEUR (M)	W - BAR (M/S)	SIGMA (M/S)	NB. DE MESURES VALIDES (%)
385.	-0.44	0.02	1.3
372.	0.00	0.00	0.0
360.	0.00	0.00	0.0
347.	0.00	0.00	0.0
335.	-0.46	0.00	1.0
322.	0.00	0.00	0.0
310.	-0.17	0.11	2.0
298.	0.00	0.00	0.0
285.	-0.33	0.02	1.0
273.	-0.43	0.01	1.3
260.	0.00	0.00	0.0
248.	0.00	0.00	0.0
235.	-0.29	0.21	3.0
223.	0.00	0.00	0.0
210.	-0.49	0.01	1.3
197.	-0.43	0.01	1.3
184.	-0.23	0.16	2.7
171.	0.00	0.00	0.0
158.	-0.35	0.12	1.3
145.	-0.13	0.13	3.0
132.	-0.06	0.01	1.3
119.	0.00	0.00	0.0
106.	0.00	0.00	0.0
93.	0.22	0.00	1.3
80.	0.00	0.00	0.0
67.	-0.01	0.01	1.7
54.	-0.24	0.01	1.7
41.	0.08	0.02	1.3
28.	0.33	0.02	1.7
15.	0.00	0.00	0.0

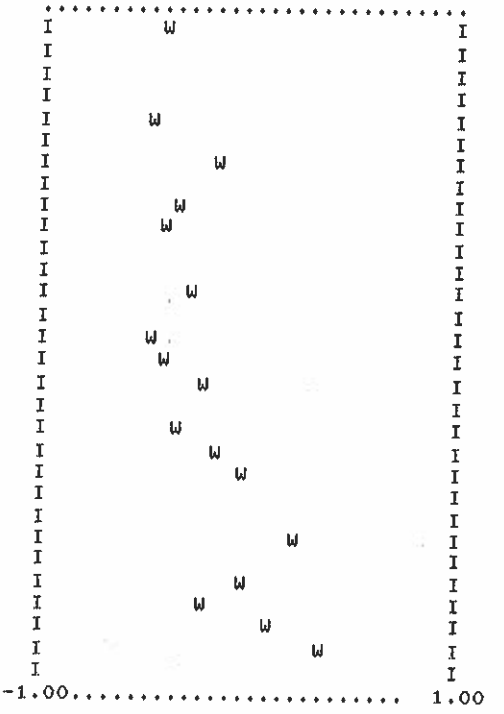

Figure 7.6. Sample output sheet.

8. FM-CW RADAR

R. B. Chadwick and K. P. Moran
NOAA/ERL/Wave Propagation Laboratory
Boulder, Colorado, U.S.A.

8.1 INTRODUCTION

The frequency-modulated, continuous-wave (FM-CW) radar first developed by Richter (1969) combines high sensitivity necessary for detection of clear-air echoes with ultra-high resolution (<1 meter) and virtual freedom from ground clutter, features which cannot be achieved in pulse radars used for monitoring atmospheric structures. Atlas et al. (1970), Gossard et al. (1970, 1971), and Bean et al. (1971) have described the use of this new tool in studying a variety of micrometeorological processes. Recently, however, FM-CW systems have enjoyed an added dimension: Doppler wind-measurement capability (e.g., Chadwick et al., 1976a,b; Chadwick and Strauch, 1979). The system can be operated in two modes: for high-resolution studies of atmospheric structure, the radar is operated in the range-only mode (to measure reflectivity as a function of range); for wind profiling, the radar is operated in the range-Doppler mode. The two modes of operation use the same equipment, differing only in sweep rates and sampling schemes.

In the range-only mode of operation, the antennas are usually pointed vertically, typically providing a maximum range of about 3 km or less in clear air, but much greater in the presence of targets such as hydrometeors, chaff, and insects. The WPL equipment provides 500 range cells within this altitude, yielding cells and hence resolution about 6 m or less in range. The beamwidth is some 0.05 radians, so that the interrogated cells are generally shaped like thin discs. In the range-only mode of operation, the output displays show regions of enhanced atmospheric refractive-index fluctuations. The time history of these records reveals the advection of structures passing overhead within the PBL during the observation period, as well as non-stationarity in the PBL itself (associated, for example, with the rise of the convectively mixed layer during the morning hours). From the resulting data set it is very easy to discern layers of high refractive-index variability and the behavior of these layers during the day.

In the range-Doppler mode the antenna can either be aligned in a given fixed direction or scanned in azimuth. The maximum range for clear-air measurements depends on the elevation angle. Looking vertically, the maximum range is about 3 km and this maximum range increases as the antenna beam is lowered toward the horizon. The number of range gates and the number of spectral points are variable, subject to the constraint that the product of range cells and the number of spectral points per range cell must equal 500, which is the number of points available at the output of the signal processor. Normally, ten range cells with 50 spectral points each are used, providing radial wind velocity measurements at ten equally spaced intervals out to the maximum range. Such a measurement yields only the radial component of the wind, i.e., the wind component parallel to the antenna beam direction. To derive profiles of the total vector wind, the airspeeds are measured with the radar looking in two or more directions. Horizontal homogeneity of the wind field within the scanning volume is assumed. Wind-velocity measurements made while the radar antenna is scanning azimuthally yield a so-called velocity-azimuth display (VAD). Total wind profiles as well as convergence profiles and estimates of shearing and stretching deformation can be obtained from a VAD scan. The time required for one vertical profile of wind speed and direction is 30 s. A large fraction of this time is expended in steering the antenna. Doppler sensing of the radial wind component profile is relatively rapid, typically once per second.

A recent improvement is the capability to operate the radar at very low elevation angles. Before these improvements, the minimum elevation angle was about 30° from horizontal. The increased return from the ground clutter at lower elevation angles caused saturation

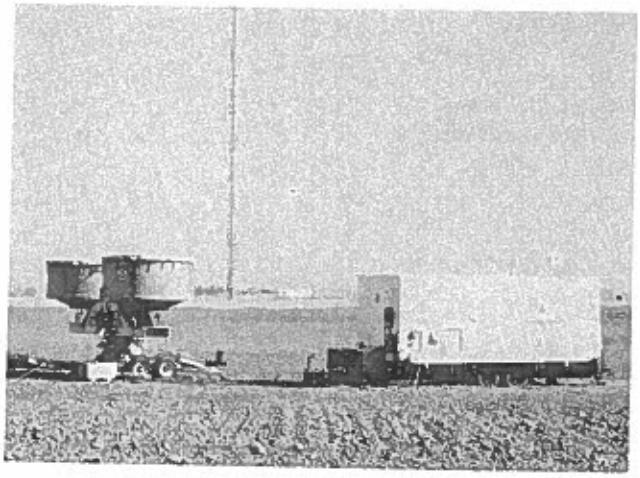

Figure 8.1. The transmitting and receiving antennas of the WPL FM-CW radar, shown pointed vertically. The BAO 300-m tower is in the background. The trailer on the right houses the electronics for the radar systems.

of the signal processor. Now the radar can operate at an elevation angle of 5°. The maximum range at these lower angles is greatly increased. In the summer-time clear air, ranges exceeding 10 km are possible at 8° elevation angle. For hydrometeor return, the maximum range can exceed 40 km. The radar has mapped thunderstorms at 40 km range.

As indicated above, the optically clear air targets for the FM-CW radar are half-radar-wavelength Fourier components of fluctuations in refractive index associated with atmospheric turbulence. Of course the radar detects other targets, including hydrometeors, insects, clouds, aircraft, and balloons. As a rule these other targets produce radar echoes of sufficiently distinctive character that they are readily distinguishable from clear-air returns, so that no misinterpretations arise. Indeed, to the extent that insects and chaff follow the mean flow, they simply increase the signal-to-noise ratio and actually aid the wind measurement process. However, when the backscattered power exceeds a certain level, the signal processor saturates and quantitative wind and backscatter intensity measurements deteriorate in quality and reliability.

8.2 DETAILS OF THE WPL FM-CW RADAR

The Wave Propagation Laboratory FM-CW radar is mobile and transported on two trailers. Figure 8.1 shows the radar receiving and transmitting antennas and their mount, with the BAO tower in the background. The radar transmitter, receiver, and data processing electronics are housed in a trailer that is not shown. The major parameters describing system performance are listed in Table 8.1. No maximum range is given since this depends upon atmospheric conditions and/or the availability of suitable targets, factors that vary diurnally and seasonally.

Table 8.1. FM-CW radar performance parameters

Average transmitted power	200 W
Antenna diameter	2.44 m
Wavelength	10 cm
Receiver noise figure	2.2 dB
Minimum range	15 m
Minimum detectable signal	-155 dBm
Range resolution (adjustable)	$\geq$1.65 m
Velocity resolution (adjustable)	$\geq$3 cm/s

During the intercomparison experiment, the FM-CW radar will be operated at an elevation angle of 60° with a maximum range less than 3 km. This will provide height coverage to about 2 km. Because of the requirement that wind profiles be available within 24 h after they are taken, the data will be reduced by hand. This means the radar will be operated only during selected data-taking intervals, mostly during the day. Also, this will preclude obtaining winds from the lowest range bin where special processing techniques are needed to determine the sign of the Doppler velocity.

To facilitate comparisons, the radar will be pointed either to the west or to the south during data-taking periods. While attempts will be made to measure both components for a few 20-min periods, the normal mode of operation will be to measure only one component during one 20-min period.

The hand processing algorithm that determines which bin of the velocity spectrum contains the peak assumes that the peak represents the mean value. This assumption could introduce errors beyond those normally expected in an intercomparison such as this. The first type of error is that due to simple human error in locating the spectral peak. This would normally be a large error. In some instances these points would be isolated; in other instances, the points in error may occur in sequences. Careful processing should minimize the occurrence of such errors. The second type of error is due to the discrete nature of the output velocity spectra and the fact that only 50 velocity values can be selected over the range of $\pm$10.5 m/s. This "discreteness" introduces errors in the range of $\pm$0.5 m/s. A third type of error is that caused by using the peak of a non-symmetric spectrum as the mean. The size of this error cannot be estimated without having some measure of the spectral asymmetry.

The radial velocity spectra taken by the FM-CW radar are on file and are available to any BLIE participants.

8.3 REFERENCES

Atlas, D., J. I. Metcalf, J. H. Richter, and E. E. Gossard (1970): The birth of "CAT" and microscale turbulence. J. Atmos. Sci. 27:903-913.

Bean, B. R., R. E. McGavin, R. B. Chadwick, and B. D. Warner (1971): Preliminary results of utilizing the high resolution FM radar as a boundary layer probe. Boundary Layer Meteorol. 1:466-473.

Chadwick, R. B., K. P. Moran, R. G. Strauch, G. E. Morrison, and W. C. Campbell (1976a): Microwave radar wind measurements in the clear air. Radio Sci. 11:795-802.

Chadwick, R. B., K. P. Moran, R. G. Strauch, G. E. Morrison, and W. C. Campbell (1976b): A new radar for measuring winds. Bull. Am. Meteorol. Soc. 57:1120-1125.

Chadwick, R. B., K. P. Moran, G. E. Morrison, and W. C. Campbell (1978): Measurements showing the feasibility for radar detection of hazardous wind shear at airports. Technical Report AFGL-TR-78-0160, Air Force Geophysical Laboratories, Hanscom Air Force Base, Bedford, Mass.

Chadwick, R. B., and R. G. Strauch (1979): Processing of FM-CW Doppler radar signals from distributed targets. IEEE Trans. Aerosp. Electron. Syst. AES-15:185-188.

Gossard, E. E., J. H. Richter, and D. Atlas (1970): Internal waves in the atmosphere from high-resolution radar measurements. J. Geophys. Res. 75:3523-3536.

Gossard, E. E., D. R. Jensen, and J. H. Richter (1971): An analytical study of tropospheric structure as seen by high-resolution radar. J. Atmos. Sci. 28:794-807.

Richter, J. H. (1969): High resolution tropospheric radar sounder. Radio Sci. 4:1261-1268.

9. DUAL-DOPPLER RADAR

R. A. Kropfli
NOAA/ERL/Wave Propagation Laboratory
Boulder, Colorado

9.1 INTRODUCTION

Although the Wave Propagation Laboratory developed its X-band dual-Doppler radars primarily to study motion fields within precipitating clouds (e.g., Miller and Strauch, 1974; Miller et al., 1975; Kropfli and Miller, 1976; Dye et al., 1978), the same radars have also been applied in PBL studies, both in small experiments (e.g., Wilson, 1970; Frisch and Clifford, 1974; Gossard and Frisch, 1976), and as part of large field programs such as METROMEX (e.g., Kropfli and Kohn, 1978). In such studies the radars use either hydrometeors, such as snowflakes (Wilson, 1970), or artificial chaff (e.g., Gossard and Frisch, 1976; Kropfli and Kohn, 1978) as tracers, deducing wind velocities from the Doppler shifts measured in the echoes from these targets. Scanning the radars through large volumes has provided a tremendous step forward in our visualization of boundary-layer flow fields.

Despite the wide variety of field programs in which these radars have been used, there has not been an opportunity until now to make detailed comparisons of the Doppler radar wind fields with data from other remote sensors or in-situ instruments. An experiment called PHOENIX provided this opportunity in September of 1978, and the first results of this experiment are presented here. The focus of this experiment was a 300-m instrumented tower, the Boulder Atmospheric Observatory (BAO) (Kaimal, 1978). The instruments on this tower, along with other remote, ground-based, and aircraft-borne sensors, were used in these intercomparisons.

One of the many components of PHOENIX was an array of three Doppler radars: two NOAA/WPL X-band radars, and an NCAR C-band (CP-4) radar. Analyses described here involve only the two X-band radars. These radars were located to optimize observations near the 300-m-high, instrumented BAO tower. Short (~15-km) radar baselines were chosen to optimize spatial resolution, a luxury not possible in past multiple Doppler radar experiments.

In addition to these intercomparisons, an important goal of PHOENIX was to improve our understanding of physical processes in the PBL. Understanding of a physical process almost always follows our ability to observe and measure that process in a better way. We are therefore hopeful that the first PBL flow visualizations presented here, and the ones that will be produced later, will be followed by a corresponding increase in our understanding of the PBL.

9.2 DESCRIPTION OF THE EXPERIMENT

Since the backscattered signal from the convective PBL is usually too weak to be observed reliably by the radars involved in PHOENIX, chaff must be dispensed from an aircraft over an area of several hundred square kilometers. X-band chaff was distributed for several hours at a time along 15-km crosswind flight legs. Usually, the flight patterns were adjusted to dispense chaff about 30 to 45 min upwind of the target area. When the winds were weak and variable in direction, a zig-zag pattern covering an appropriate box was chosen. Convective activity was usually sufficiently strong between 1100 and 1800 (all times are given in MDT) each day to disperse the chaff uniformly throughout the convective PBL in the test area. Radar echoes from the resulting chaff cloud were usually greater than 10 dB above noise power within most of the region of interest. The two identical NOAA systems were operating at a wavelength of 3.22 cm, peak transmitted power of 20 kW, pulse width of 1.0 μs, and beamwidth of 0.8°.

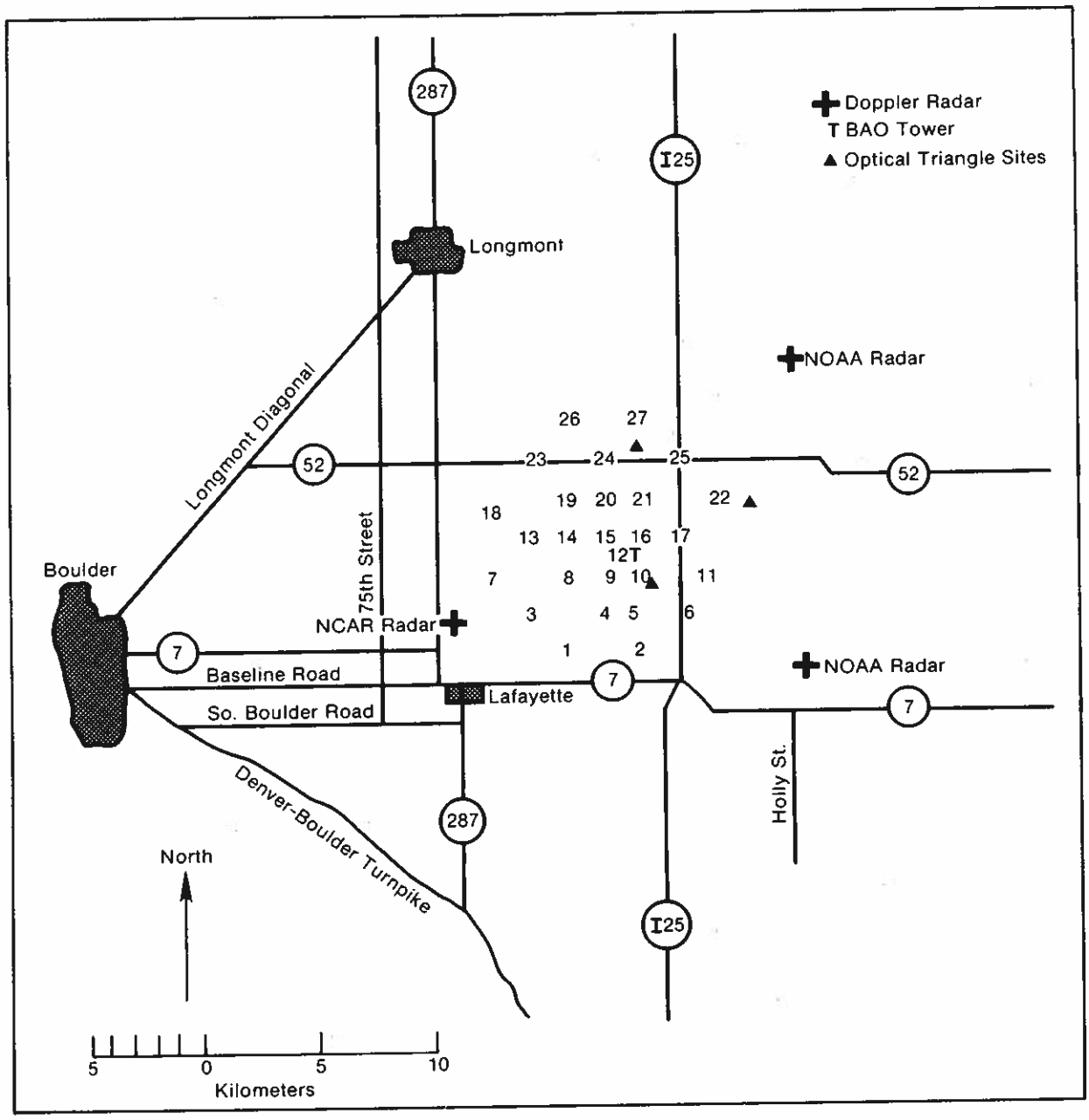

Figure 9.1. Positions of radars and optical triangle relative to BAO tower. PAM stations are indicated by numbers.

Figure 9.1 shows the location of the radars relative to the tower. The NCAR portable automated mesonetwork (PAM) and the NOAA optical triangle are also shown. The 13- to 18-km separation between radars is much smaller than is normally used in multiple Doppler radar experiments. Thus, the radars were able to scan the entire depth of the PBL (~2 km) over an area of several hundred square kilometers while observing air motions at wavelengths as small as 600 or 700 m. Volume scans were completed in less than 90 s. Siting the radars equidistant from the tower also had the important advantage of equalizing the radial and tangential dimensions of the three radar pulse volumes to about 150 m at the BAO.

Table 9.1. Summary of radar scan characteristics for PHOENIX

Scan number/name	Volume time (s)	Cartesian grid element ΔX, ΔY, ΔZ (km)	Sample density number (km^3)	Half-amplitude wavelength after filtering (km)	Area covered (km^2)
100/Standard	72<T<96	0.25, 0.25, 0.20	170<N<270	0.85	20<A<110
200/Fast-standard	40<T<80	0.20, 0.20, 0.20	300<N<400	0.70	20<A<110
300/Over-sampled	40<T<90	0.15, 0.15, 0.15	600<N<1300	0.50	A ≈ 4
400/Optical triangle	50<T<180	----------	160<N<300	----	A ≈ 25
600/Large scale	140<T<180	0.40, 0.40, 0.30	80<N<160	1.40	A = 270

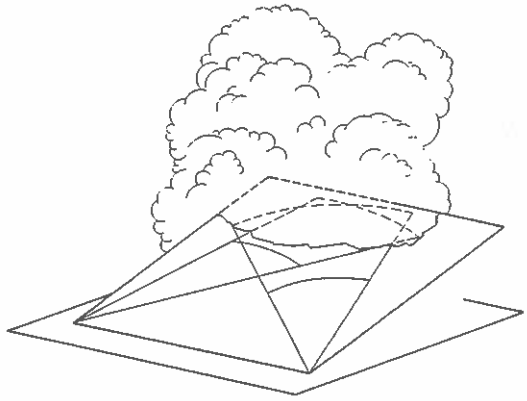

Figure 9.2. Schematic representation of COPLAN scanning method.

Five different scan types, summarized in Table 9.1, were designed in order to satisfy the experimental objectives and, in addition, to allow us to evaluate the relative merits of different radar sampling schemes for future experiments. The routine that was followed throughout the experiment was to perform pairs of the five scans as rapidly as possible. Taking two identical volume scans in rapid succession has, in effect, given us the redundant data set that is helpful in distinguishing statistical fluctuations in the measurement from actual features in the flow field. It also allows convenient temporal interpolations between scans whenever necessary. Each pair of scans was completed in about 3 min and the entire sequence was completed in 15 to 20 min. All scans were predetermined to reduce operator errors.

The two NOAA radars operated during the entire PHOENIX experiment in the COPLAN scanning mode (Miller and Strauch, 1975), as shown in Fig. 9.2. Specifically, they scanned in tilted planes passing through the baseline between them. Having taken the data in this fashion provides the option of either COPLAN or Cartesian processing with the existing software.

Of the wide variety of processing options available to generate three-dimensional wind fields, we chose the following sequence: 1) computation of mean radial velocity estimates for each radar by a pulse-pair method (Rummler, 1968), 2) thresholding the pulse-pair velocities to eliminate noise-contaminated estimates, 3) interpolation to a common Cartesian grid so that the radial velocities can be vectorially combined to yield two-dimensional velocity and divergence fields within each horizontal plane, and 4) integration of the anelastic continuity equation in Cartesian coordinates to yield the vertical velocity component. The integration is performed with the usual boundary conditions; i.e., the vertical velocity is zero everywhere at the surface. Many refinements are currently being added to this process.

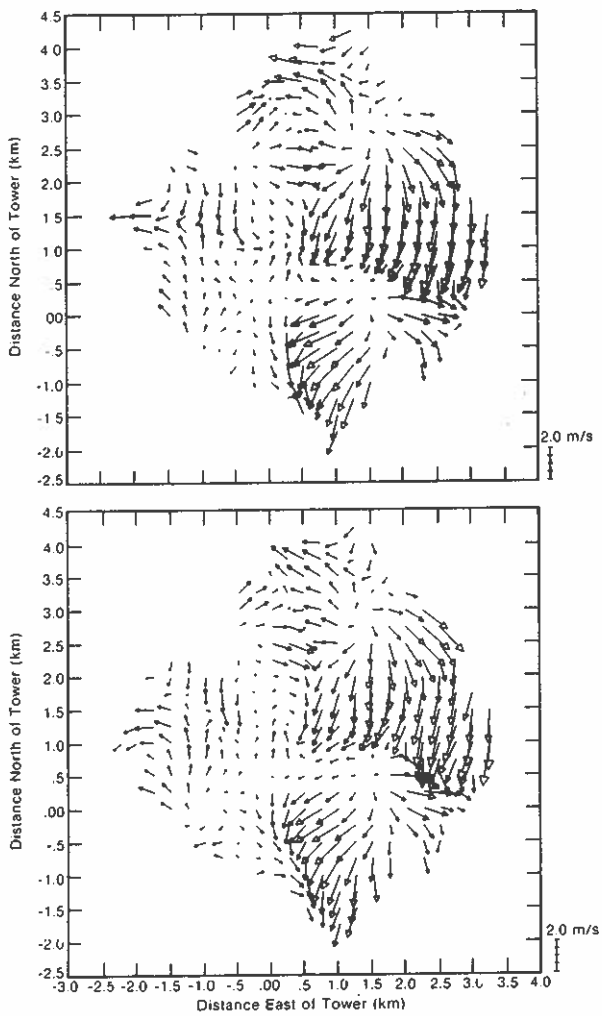

Figure 9.3. Horizontal eddy wind fields (volume mean removed) for Z=0.1 km at 1512 MDT (top) and at 1513 MDT (bottom) on 21 September 1978.

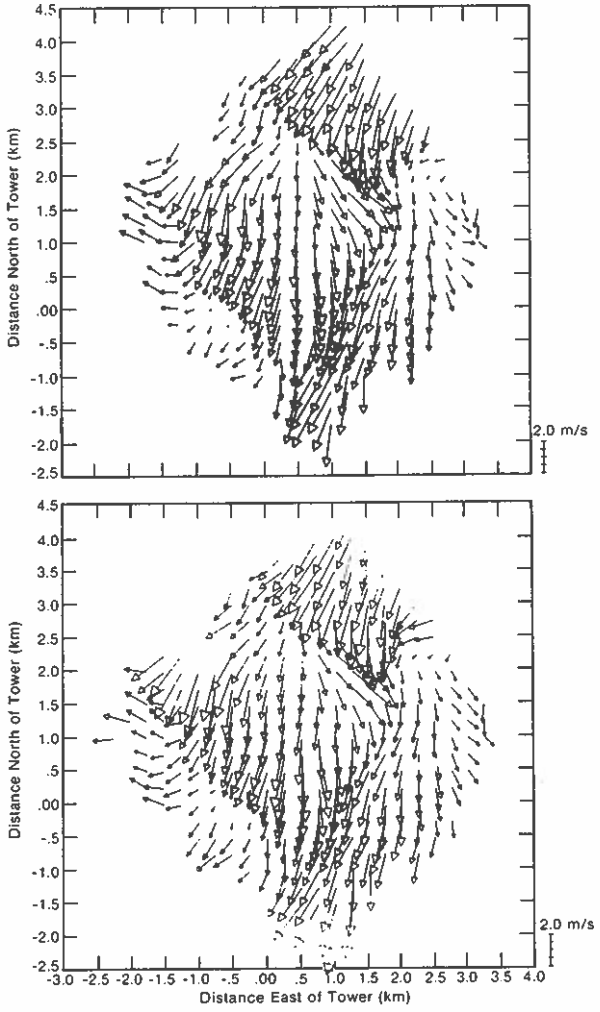

Figure 9.4. Horizontal eddy wind fields (volume mean removed) for Z=0.1 km at 1531 (top) and at 1533 (bottom) MDT on 21 September 1978.

9.3 INTERCOMPARISONS

Figure 9.3 shows the eddy flow patterns (volume mean removed) for two scans that were begun about 1 min apart. Clearly, their appearances are very similar. In Fig. 9.4 we have shown two similar wind field patterns 20 min later, and again the repeatability is excellent. This is borne out even when looking at the vertical cross sections as in Fig. 9.5. It is reassuring to observe this short-term repeatability while the entire pattern changes completely during the 20-min interval. The RMS difference between U, V, and W wind components generated by scans such as these is about 0.3 m/s.

Comparisons of wind components derived from the radars were made with those measured by a sonic anemometer at the 300-m level on the BAO tower (Kaimal, 1978). Figure 9.6 shows these results. The tower data were obtained by averaging the sonic anemometer record for 90 s, the time required for an air parcel to pass through one radar

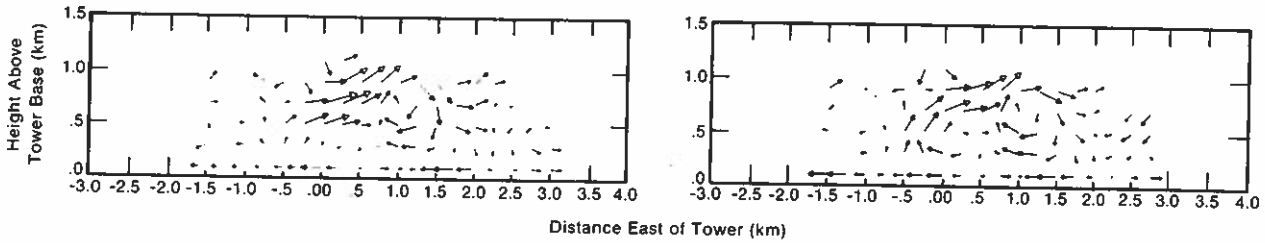

Figure 9.5. Vertical (XZ) sections through the wind field at 1531 (left) and 1533 (right) MDT on 21 September 1978 for Y=0.5 km.

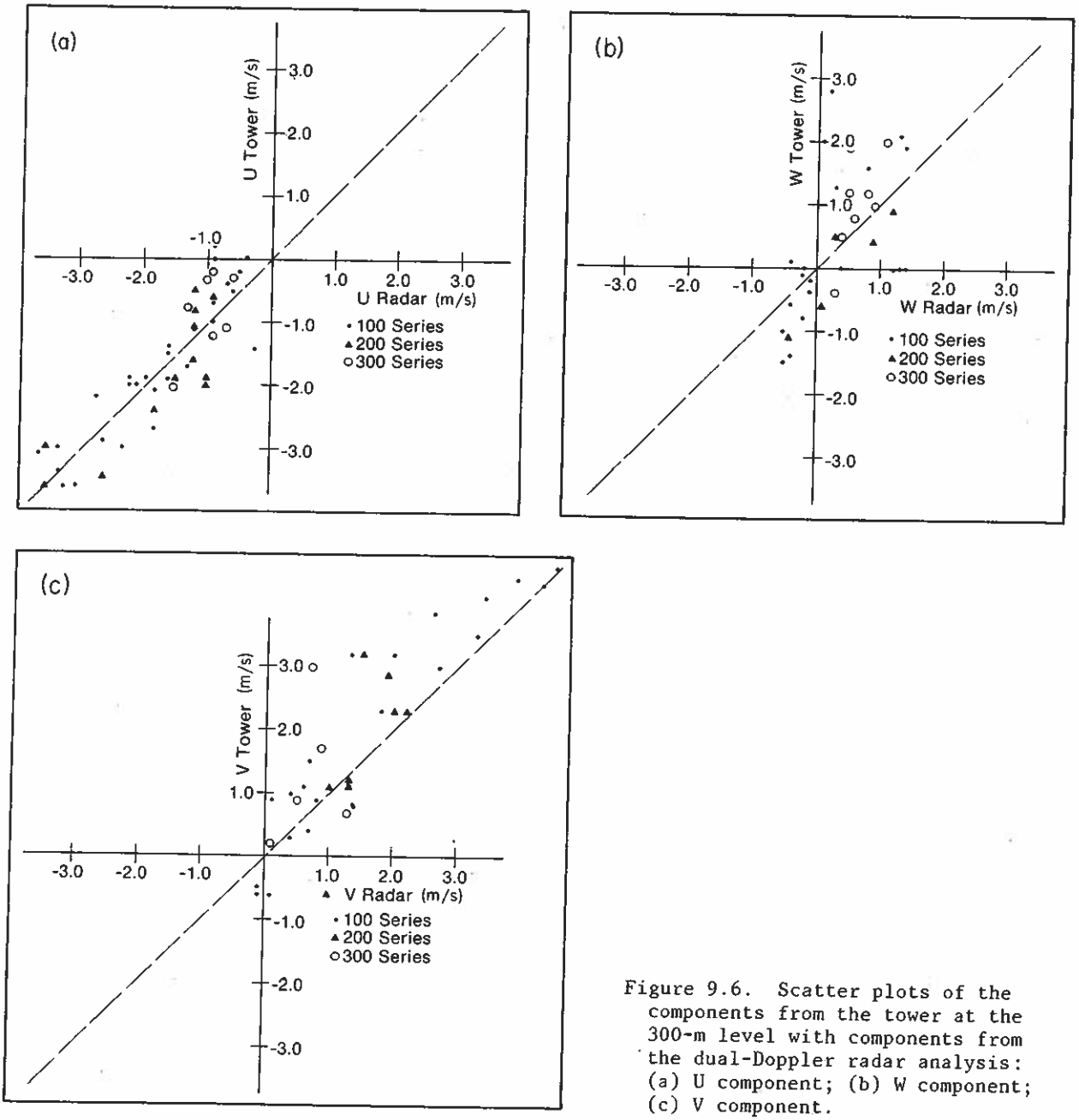

Figure 9.6. Scatter plots of the components from the tower at the 300-m level with components from the dual-Doppler radar analysis: (a) U component; (b) W component; (c) V component.

grid volume. The two methods generally agree to within 0.5 m/s despite the volume averaging by the radar, as opposed to the line average represented by the tower values. There is a slight underestimation in the magnitudes of the three components, which could be the result of this volume averaging and ground-clutter biasing.

Whenever comparisons of radar- and aircraft-derived fields are made two problems should be considered to ensure accurate and valid comparisons. First, the aircraft must be positioned accurately in time and space with respect to the radar data. Spatial agreement within at least 0.2 km and temporal agreement within 1 min are needed for the assumption of stationarity of the turbulent wind fields to be valid. For differences much larger than about 0.2 km and 1 min, changes can occur that seriously degrade the comparison of radar and aircraft data. Although the inertial navigation system of the aircraft can drift significantly, visual fixes were used in this experiment to correct the aircraft locations to within 0.2 km. Even though every effort was taken to produce simultaneous measurements, some data comparisons had to be made with aircraft and radar data separated by as much as 2 to 3 min.

The second problem to be considered is that of filtering aircraft and radar data such that the spectral content is as similar as possible. The aircraft velocity data are collected at a rate of about 20 Hz, with the samples being essentially independent. The radars collected radial velocity data that were interpolated to Cartesian grids having grid elements 200 or 250 m on a side. These radar data were processed as described in the preceding section. In order to match the radar-derived scales, a Gaussian filter with a half width of 0.2-km was applied to the aircraft data.

Sample comparisons of multiple Doppler radar data and aircraft data are presented in Figs. 9.7 and 9.8. Single data points have been added in Fig. 9.7 to indicate BAO tower wind values (The tower is 0.75 km north of the east-west flight track.) These measurements and others like them indicate agreement between multiple Doppler radar, aircraft, and tower measurements to better than 1 m/s in most cases.

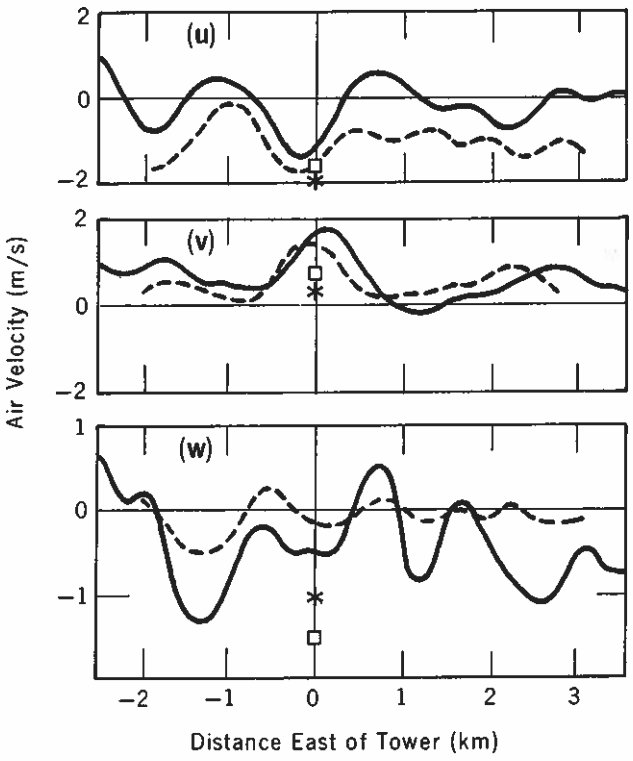

Figure 9.7. Comparison of wind components (U, V, and W) derived from Doppler data (at 1100 hours) and aircraft data (at 1108 to 1110) on the same day. Solid lines represent aircraft data; dashed lines represent radar data. Heights are 0.15, 0.10, and 0.50 km for radar, aircraft, and inversion respectively. BAO tower data are indicated by * (at 0.1 km) and □ (at 0.15 km).

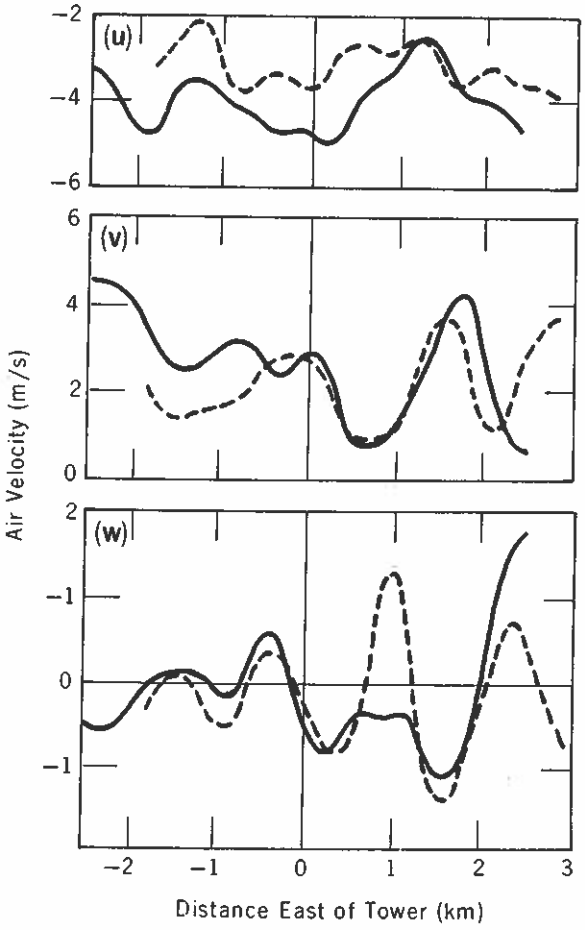

Figure 9.8. Comparison of wind components derived from Doppler data (at 1335 hours) and aircraft data (at 1336 to 1338) as in Fig. 9.7. Heights are 0.5, 0.6, and 0.8 km for radar, aircraft, and inversion, respectively.

9.4 FLOW VISUALIZATION IN THE PLANETARY BOUNDARY LAYER

Figure 9.9 is an example of how the use of the various scan types summarized in Table 9.1 allows us to see the PBL motions with different magnifications. The figure contains a large-scale 600 series scan, a 200 series scan, and a high-resolution 300 series scan, all taken within 8 min. Boxes have been drawn over the 600 series grid to indicate where the 200 and 300 series grids lie. The same features seen in the 600 series grid can be seen with increased detail in the 200 series. The 600 series display shows a very chaotic wind field with sharp wind gradients aligned roughly along the mean wind direction, which was 2.8 m/s from the SSE. Scales of motion here are about 3 km or about three times the depth of the convective boundary layer at this time.

An example of an unusual feature, suggestive of flow around a jet, is depicted in the 200 series and 300 series displays of Fig. 9.10. An updraft of about 1.5 m/s was observed by radar at the location (0.5, 0.8) at a height of 0.825 km. Such a weak updraft would not be expected to act as a barrier to the prevailing flow. This feature was clearly evident in the wind patterns for about 10 min and was observed to track with the mean wind. Recognizable features in the eddy field could usually be tracked along the mean wind for about 10 or 15 min.

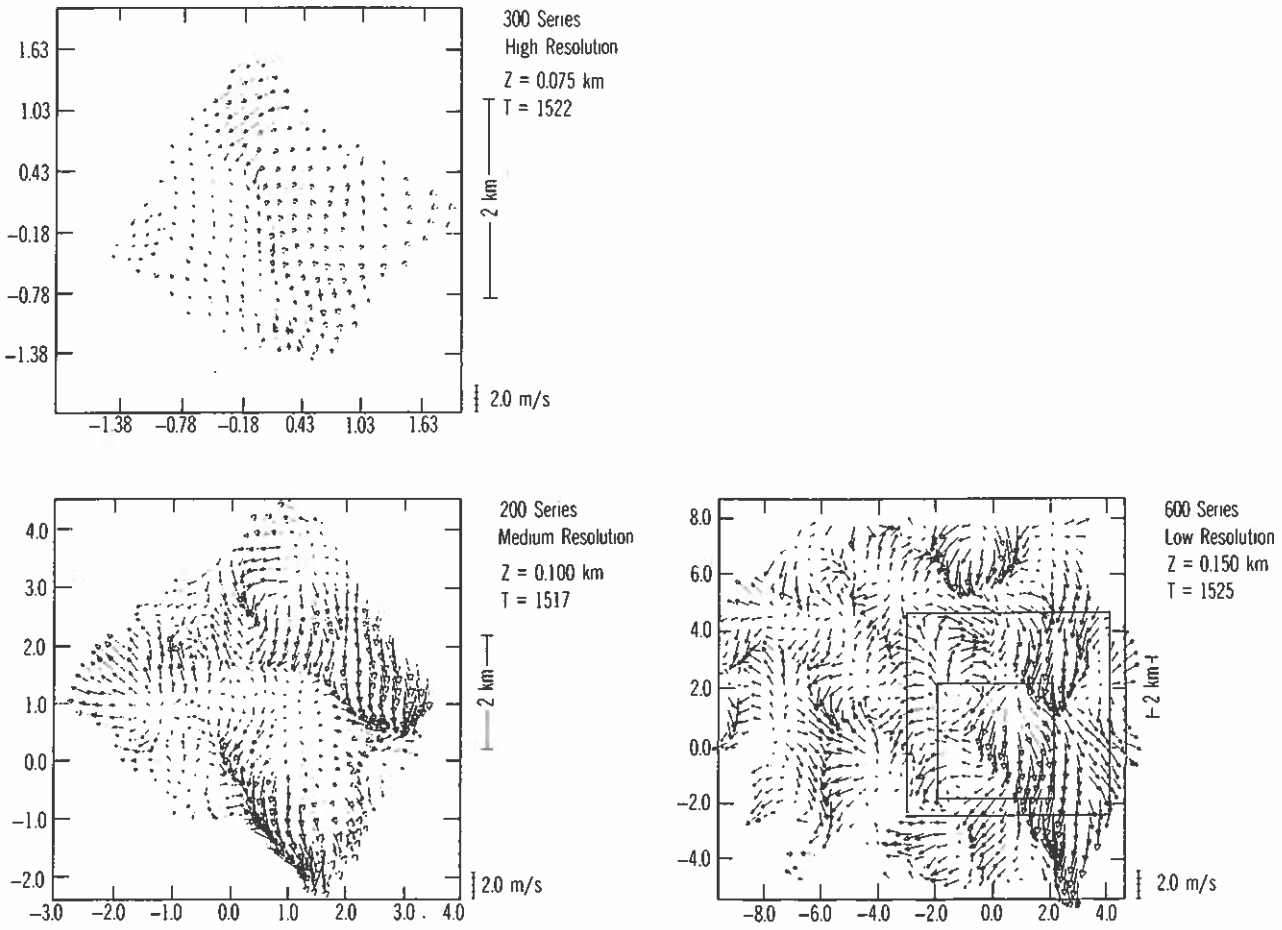

Figure 9.9. Horizontal eddy fields at high, medium, and low resolutions.

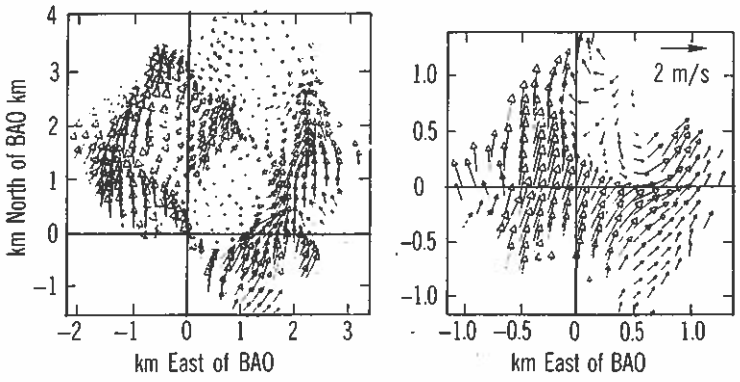

Figure 9.10. Horizontal eddy fields on 21 September 1978: (left) at Z=0.9 km, obtained from 200 series scan at 1538; (right) at Z=0.825, obtained from 300 series scan at 1540.

9.5 SUMMARY

We have presented a brief description of the dual-Doppler technique for measuring three-dimensional wind fields, intercomparisons with other in-situ measurements of the three wind components, and a sample of the flow fields obtained during the recent PHOENIX experiment at the BAO. Although the analysis of these data is far from complete, we expect these data and similar data sets to have important impacts on remote sensor techniques and also on our understanding of the dynamics of the PBL.

9.6 REFERENCES

Dye, J. E., L. J. Miller, B. E. Martner, and Z. Levin (1978): Growth and recirculation of precipitation in an evolving convective storm. Prepr. Conf. on Cloud Phys. and Atmos. Electr., 31 July-4 August 1978, Issaquah, Washington, American Meteorological Society, Boston, Mass., pp. 528-533.

Frisch, A. S., and S. F. Clifford (1974): A study of convection capped by a stable layer using Doppler radar and acoustic echo sounders. J. Atmos. Sci. 31:1622-1628.

Gossard, E. E., and A. S. Frisch (1976): Kinematic models of a dry convective boundary layer compared with dual-Doppler radar observations of wind fields. Boundary Layer Meteorol. 10:311-330.

Kaimal, J. C. (1978): NOAA instrumentation at the Boulder Atmospheric Observatory. Prepr. 4th Symp. Meteorol. Obs. and Instrum., 10-14 April 1978, Denver, Colorado, American Meteorological Society, Boston, Mass., pp. 35-40.

Kropfli, R. A., and N. M. Kohn (1978): Persistent horizontal rolls in the urban mixed layer as revealed by dual-Doppler radar. J. Appl. Meteorol. 17:669-676.

Kropfli, R. A., and L. J. Miller (1976): Kinematic structure and flux quantities in a convective storm from dual-Doppler radar observation. J. Atmos. Sci. 33:520-529.

Miller, L. J., and R. G. Strauch (1974): A dual-Doppler radar method for the determination of wind velocities within precipitating weather systems. Remote Sensing Env. 3:219-235.

Miller, L. J., J. D. Marwitz, and J. C. Fankhauser (1975): Kinematic structure of a Colorado thunderstorm. Prepr. 16th Radar Meteorol. Conf., 22-24 April, Houston, Texas, American Meteorological Society, Boston, Mass., pp. 128-133.

Rummler, W. O. (1968): Two pulse spectral measurements. Tech. Memo. MM-68-4121, Bell Telephone Laboratories, Whippany, N.J.

Wilson, D. A. (1970): Doppler radar studies of boundary layer word profile and turbulence in snow conditions. Prepr. 14th Radar Meteorol. Conf., Tucson, Arizona, American Meteorological Society, Boston, Mass., pp. 191-196.

10. REMOTE SENSING OF TEMPERATURE PROFILES WITH COMBINED ACTIVE AND PASSIVE SENSORS

M. T. Decker
NOAA/ERL/Wave Propagation Laboratory
Boulder, Colorado, U.S.A.

10.1 INTRODUCTION

Project PHOENIX (Hooke, 1979), carried out at the Boulder Atmospheric Observatory (BAO) during September 1978, involved a variety of atmospheric sensors including aircraft, the NCAR PAM network, radars, lidar, acoustic sounders, microwave radiometers, optical wind sensors, radiosondes and fixed level balloons, and the 300-m BAO instrumented tower. The many goals of this project included evaluation and comparison of various remote sensing systems. Among these was the comparison of atmospheric temperature profiles obtained from microwave radiometers with profiles from standard tower and radiosonde sensors, and especially the usefulness of information from active sensors such as microwave radars and acoustic sounders in improving the resolution of vertical structure in the radiometric temperature profiles. It will be shown that the active sensor information can indeed be useful but that questions remain regarding the proper interpretation of the observed echoes.

10.2 INSTRUMENTATION

The measurements reported here were made by microwave radiometer, FM-CW radar, and radiosondes colocated at the BAO site. Radiosonde equipment was a standard GMD system operated by the NCAR Field Observing Facility, and 38 flights were made during the month.

Three microwave radiometer systems were operated at the BAO site during the PHOENIX experiment. Data reported here are from the Scanning Microwave Spectrometer (SCAMS) operated by personnel from the Jet Propulsion Laboratory. This is a 5-channel instrument similar to that flown aboard the Nimbus 6 satellite. It has one frequency at the water vapor absorption line at 22.235 GHz, three frequencies (52.85, 53.85, and 55.45 GHz) in the oxygen absorption complex, and a frequency of 31.65 GHz in the window between these absorption bands. The instrument scans in a vertical plane from a zenith angle of 58.3°, through the zenith, and to 28.1° on the other side of zenith. The scan steps in 7.2° increments with a dwell time of about 1 s at each step. Two additional steps are used to point the antennas at calibration targets, and the entire sequence is repeated approximately once each 16 s. The sky radiation measurements for all channels at zenith and for 55.45 GHz at 58.3° zenith angle were used to retrieve the temperature profiles reported here. The 1-s measurements (at 16-s intervals) were averaged over a period of about 7 min before being used in the profile retrieval algorithm.

The FM-CW radar was operated during PHOENIX by the NOAA Wave Propagation Laboratory. This radar (Chadwick et al., 1976) operates at a wavelength of 10 cm with an average transmitted power of 200 W. The 2.44-m transmit and receive antennas are steerable in elevation and azimuth. The radar operates in either of two modes: a high-resolution range-only mode or a range-Doppler mode with a wind-measurement capability. In the measurements reported here the radar operated in the range-only mode with the antennas pointed at the zenith. The high-sensitivity, high-resolution, low-ground-clutter qualities of this radar allow detection of the detailed structure of atmospheric refractive-index fluctuations in the lower atmosphere. Minimum range is 15 m, and in clear air the typical maximum range is 3 km. The presence of persistent layer echoes is used here as evidence of thermal structure, specifically an elevated temperature inversion.

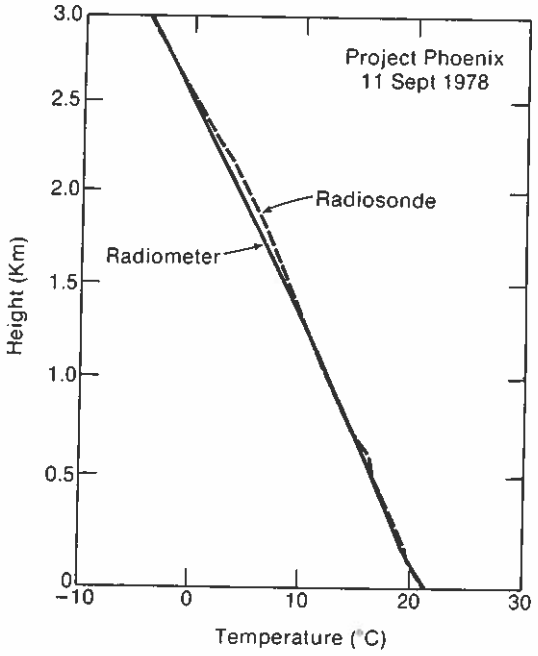

Figure 10.1. Comparison of radiosonde and radiometer temperature profiles for a case with simple vertical structure.

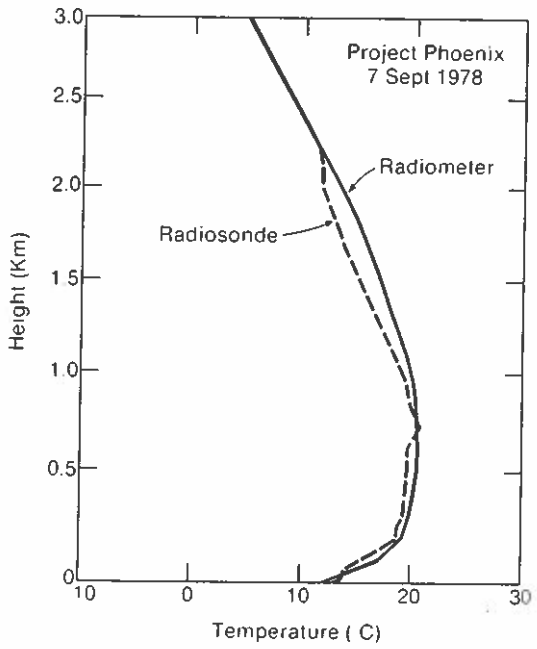

Figure 10.2. Comparison of radiosonde and radiometer temperature profiles for the case of a ground-based inversion.

10.3 TEMPERATURE PROFILE RETRIEVAL

Statistical retrieval algorithms (Waters et al., 1975; Westwater et al., 1975) are used to extract temperature profiles from the radiation measurements. In these algorithms we use a nine-element data vector consisting of the six radiation measurements as well as surface temperature, pressure, and relative humidity to obtain a minimum variance estimate of the temperature at any level. The available measurement frequencies also allow us to correct for the effect of radiation from clouds as described by Westwater et al. (1976). Examples of the effectiveness of this cloud correction technique are contained in a series of measurements reported by Decker et al. (1978). It has been further demonstrated by Westwater (1978) that if the presence and height of an elevated temperature inversion can be observed, the retrieval algorithm may be derived from a statistical ensemble of atmospheres all of which contain temperature inversions at this height (or realistically, within some representative height range). This method of conditional statistics has been applied to a number of cases from PHOENIX, and examples are shown here.

10.4 RESULTS

A sample comparison of temperature profiles from the radiometer and radiosonde for a case with little vertical structure is shown in Fig. 10.1. In the example of Fig. 10.2 the profile shows a ground-based temperature inversion. In cases such as these the radiometer profile is generally in good agreement with the radiosonde profile. An example of an elevated temperature inversion is shown in Fig. 10.3. In this case the structure of the profile is smoothed by the radiometer to the extent that the temperature inversion is not observed. It is in this type of profile that knowledge of inversion height would be a very useful piece of information. The FM-CW radar record at this time shows a persistent echo with maximum intensity at 507 m above the surface. The profile retrieval algorithm is

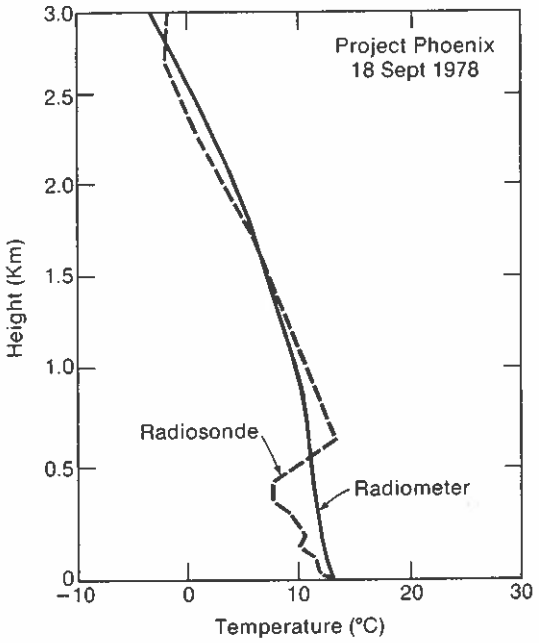

Figure 10.3. Comparison of radiosonde and radiometer temperature profiles for the case of an elevated inversion.

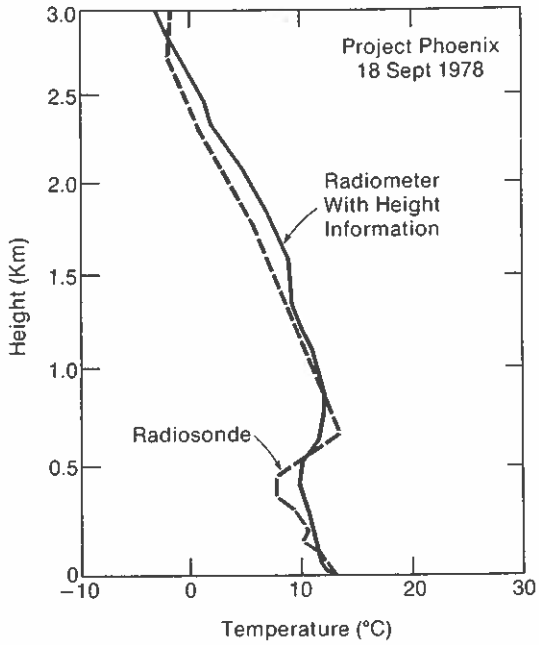

Figure 10.4. Comparison of radiosonde and radiometer temperature profiles for the case of an elevated inversion, in which the radiometer profile is retrieved with knowledge of the height of the temperature inversion derived from radar echoes.

then derived from a statistical ensemble, each member of which contains an elevated inversion with base in the height range from 400 to 600 m above the surface at Denver, Colorado. The profile retrieval resulting from the use of this algorithm is shown in Fig. 10.4. This profile is an improved representation of the radiosonde profile, and it is evident that the inversion height information has been helpful. It should be noted that the 200-m interval was used in the statistical ensemble so that enough profiles could be found in our data base to give a representative sample. A larger data base would allow this interval to be narrowed and presumably improve the retrieved radiometer profile.

It must be pointed out that the above procedure required the assumption that the echo observed by the FM-CW radar was associated with an elevated temperature inversion. Such, of course, is not always the case; in fact, at the time of the profile of Fig. 10.2 the radar was observing an echo at a height of 157 m. If it is assumed that this echo is associated with an elevated inversion rather than the ground-based inversion, and the temperature retrieval is performed using conditional statistics with inversions between 100 and 300 m, the resulting profile is as shown in Fig. 10.5. It is obvious (when Fig. 10.5 is compared with Fig. 10.2) that this procedure has degraded the radiometrically retrieved profile. In view of a number of examples such as this observed during PHOENIX, additional work must be done to assure proper use of the echo height data. Methods for characterizing the echo data are being studied. A more basic study of the relation between the radio refractive index structure parameter which is observed by the radar and the profile or gradient of refractive index which is related to temperature and water vapor is being pursued. It is expected that the combination of active and passive sensors will result in improved remote sensing of profiles for research and operational use.

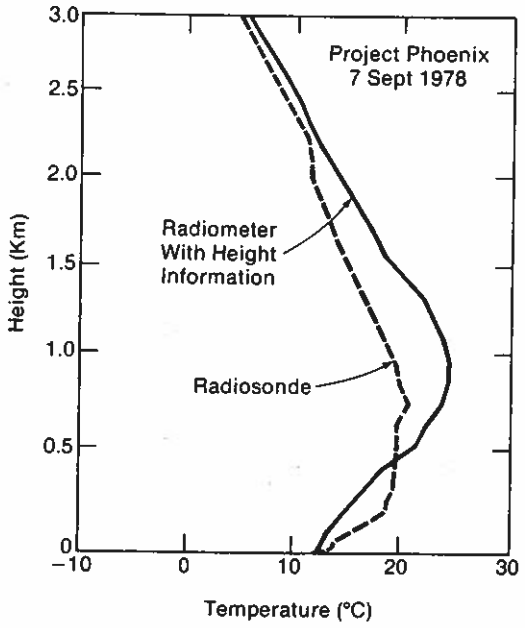

Figure 10.5. Comparison of radiosonde profile from Fig. 2 with radiometer profile derived with incorrect use of radar echo information.

10.5 ACKNOWLEDGMENTS

The radiometric measurements used here were made under the direction of Bruce L. Gary of the Jet Propulsion Laboratory, Pasadena, California. Russell B. Chadwick directed the work with FM-CW radar; Ed R. Westwater developed the retrieval algorithms for the radiometer data. Both are with the NOAA/ERL Wave Propagation Laboratory.

10.6 REFERENCES

Chadwick, R. B., K. P. Moran, R. G. Strauch, G. E. Morrison, and W. C. Campbell (1976): Microwave radar wind measurements in the clear air. Radio Sci. 11:795-802.

Decker, M. T., E. R. Westwater, and F. O. Guiraud (1978): Experimental evaluation of ground-based microwave radiometric sensing of atmospheric temperature and water vapor profiles. J. Appl. Meteorol. 17:1788-1795.

Hooke, W. H. (ed.) (1979): Project PHOENIX: The September 1978 Field Operation. NOAA/NCAR Boulder Atmospheric Observatory Rept. No. 1, available from NOAA/ERL, Boulder, Colo. 80303, and from NCAR Publications Office, Boulder, Colo. 80307.

Waters, J. W., K. F. Kunzi, R. L. Pettyjohn, R. K. L. Poon, and D. H. Staelin (1975): Remote sensing of atmospheric temperature profiles with the Nimbus 5 microwave spectrometer. J. Atmos. Sci. 32:1953-1959.

Westwater, E. R., J. B. Snider, and A. V. Carlson (1975): Experimental determination of temperature profiles by ground-based radiometry. J. Appl. Meteorol. 14:524-539.

Westwater, E. R., M. T. Decker, and F. O. Guiraud (1976): Feasibility of atmospheric temperature sensing from ocean data buoys by microwave radiometry. NOAA Tech. Rept. ERL 375-WPL 48, NOAA/ERL, Boulder, Colo. [NTIS No. 262-421].

Westwater, E. R. (1978): Improved determination of vertical temperature profiles of the atmosphere by a combination of radiometric and active ground-based remote sensors. 4th Symp. on Meteorol. Obs. and Instrum., 10-14 April 1978, Denver, Colo., American Meteorological Society, Boston, Mass., pp. 153-157.

11. WPL DOPPLER SOUNDER

W. D. Neff, H. E. Ramm,* and C. Wendt
NOAA/ERL/Wave Propagation Laboratory
Boulder, Colorado, U.S.A.

11.1 INTRODUCTION

This paper describes the use of the "complex covariance" frequency estimation technique in a microprocessor-controlled acoustic sounding system. A bistatic scattering arrangement was used during BLIE with fan-beam transmitters, a central receiver, and two orthogonal 300-m baselines. A frequency of 1250 Hz with a 100-ms pulse of 300 electrical watts was implemented.

The Wave Propagation Laboratory has developed and tested a number of Doppler acoustic sounders during the past ten years. These used a variety of frequency estimation techniques and transmitter-receiver configurations. Direct spectral calculation, analog tracking devices (Kaimal and Haugen, 1977), and adaptive filter techniques were utilized. However, all these techniques required either expensive microcomputers or hardware to implement. With the development of microprocessors capable of using higher-level languages such as Fortran, an effort began in this laboratory to reduce the complexity and expense of Doppler sounding systems.

Owens (1977) simplified the acoustic sounder electronics to a single printed circuit board and examined a simple frequency estimation technique referred to as "real covariance" for possible implementation with an LSI-11 microprocessor. The simplicity of the technique and the hardware developed by Owens led to more extensive field tests during the September 1978 Project PHOENIX experiment (Neff and Brown, 1979). However, these comparisons with tower data showed a systematic bias, leading to further laboratory testing in early 1979. Both real and complex covariance techniques were analyzed for the effect of white noise on the mean and variance of the frequency estimates. This analysis led to the choice of complex covariance as the preferred technique and the basis for the system described in this paper. An outline of the system to be described in the following sections is shown schematically in Fig. 11.1.

11.2 SYSTEM DESIGN AND DOPPLER ALGORITHMS

The hardware for this system, with slight modification, was developed by E. J. Owens of WPL (Owens, 1977; also E. J. Owens, NOAA/ERL, Boulder, Colo., personal communication). Owens developed separate printed circuit boards for the acoustic sounder electronics and for the heterodyning and filtering of the signals required for the real covariance frequency estimation technique. Corresponding software was written for the 1978 Project PHOENIX experiment (Neff and Brown, 1979).

The basis for the real covariance technique is the following algorithm (Owens, 1977):

$$\Delta f = \frac{1}{2\pi\tau_s} \cos^{-1} \frac{N}{N-1} \frac{\sum_{i=1}^{N-1} A_i A_{i+1}}{\sum_{i=1}^{N} A_i A_i} - f_c \quad , \tag{11.1}$$

*NOAA Commissioned Officer assigned to WPL.

where τ_s is the sampling period, f_c the heteordyned carrier frequency, N the number of samples, and A_i the discrete sample of the signal. Sampling frequencies range from 500 to 1000 Hz, corresponding to reduced center frequencies of 125 or 250 Hz. The large number of samples results in either large memory requirements or a reduced number of samples per range gate to allow time for processing.

The complex covariance technique is based on the following algorithm (Sirmans and Bumgarner, 1975):

$$\Delta f = \frac{1}{2\pi\tau_s} \tan^{-1} \frac{\sum_{i=1}^{N} (Q_{i+1} I_i - Q_i I_{i+1})}{\sum_{i=1}^{N} (Q_i Q_{i+1} + I_i I_{i+1})} , \qquad (11.2)$$

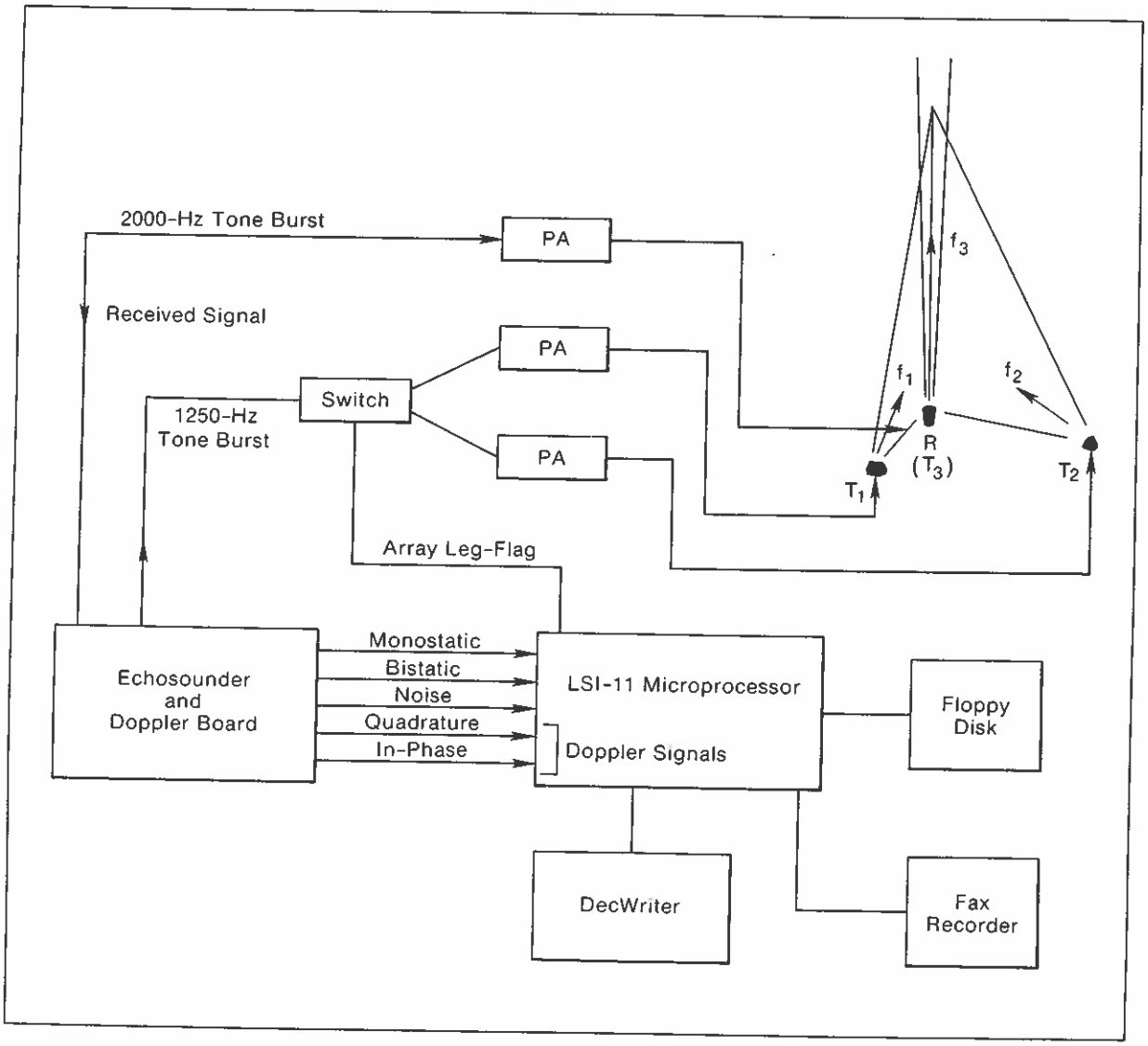

Figure 11.1. Block diagram of LSI-11-controlled Doppler sounder.

where the complex time signal $Z_i (\equiv I_i + iQ_i)$ is given by

$$Z_i = A(t_i) \cos t_i \, 2\omega_o + i \, A(t_i) \sin t_i \, 2\omega_o \quad .$$

In this application, after the received signal is filtered (with a 300-Hz bandwidth) it is multiplied first by the carrier and then separately by the carrier phase-shifted 90 degrees, providing the in-phase and quadrature components required in (11.2). After mixing, a low-pass filter (0 $\pm$ 200 Hz at the -3 dB point) provides the final processing of the signals going to the computer, where the Nyquist frequency must be near the half-power point in the bandpass of these filters to avoid aliasing by the noise (R. J. Keeler, NOAA/ERL, Boulder, Colo., personal communication).

First-moment spectral estimators do not provide any information as to the noise content of the spectrum. A variety of techniques can be used to provide an approximate estimate of the signal-to-noise ratio. In our case we filtered and detected the noise below 1 kHz. Since normal background noise falls off with increasing frequency, we adjusted the gain of the noise circuit to match the output of the signal circuit with the transmitters shut off. By using a broadband filter for the noise, we eliminated Doppler shifts calculated from nonwhite noise transients. Under most conditions, we observed that the variations in noise estimate between these two techniques were about 25 percent.

A bistatic sounding arrangement similar to that described by Kaimal and Haugen (1977) was utilized. The fan-beam transmitters operated at 1250 Hz. The central receiver normally also acts as a monostatic transmitter at 2000 Hz. These choices of frequencies appear to avoid aliasing problems in the processing of the data. At present we do not calculate the vertical velocity, but rather assume that it averages to zero.

11.3 DIGITAL PROCESSING

The details of the microprocessor system and its interfacing with an acoustic sounder have been provided by Owens (1977). To process complex covariance data we designed a general purpose program to sample a variety of acoustic data as well as the in-phase and quadrature components for use in equation (11.2) at 200 Hz and several additional channels at 100 Hz. These latter channels were used for the monostatic and bistatic intensities as well as the noise channel. An assembly language program is called shortly after the transmit gate. After the maximum range gate is reached, control is returned to the Fortran main program, signal-to-noise tests applied, and frequency shifts calculated and accumulated for a specified number of pulse repetition periods. For a maximum range of 600 m, a pulse repetition period of 5 s is used, with the last second dedicated to the Fortran processing. Following the required averaging period (normally 18 min) the wind components, speed, and azimuth are obtained from the individual components. These data, together with the signal intensities, noise level, and number of samples retained for each range gate, are printed out and also recorded on floppy disk for later analysis. A line-printer profile of wind speed and direction is also obtained for a quick visual impression of the data as shown in Fig. 11.2.

11.4 SIGNAL-TO-NOISE TESTS

The hardware described in Section 11.2 was first tested in the laboratory by use of a signal from a waveform generator mixed with the output from a white noise source. These measurements were designed to test the relative merits of the two techniques. (The usual method of evaluation (e.g., Sirmans and Bumgarner, 1975) is to define a Gaussian spectrum, add a noise spectrum, and then perform an inverse Fourier transform.) Signal and noise levels were measured for reference purposes with two identical receivers set to the carrier frequency of 1250 Hz with a centered bandwidth of 300 Hz. These mixed signals then served as inputs to the real and complex covariance pre-processor boards. Fifty 100-ms samples were then obtained at frequency shifts of 0, 10, 30, and 60 Hz. Mean and standard deviations were obtained by using the resulting frequency estimates. The results are shown in Figs. 11.3 and 11.4.

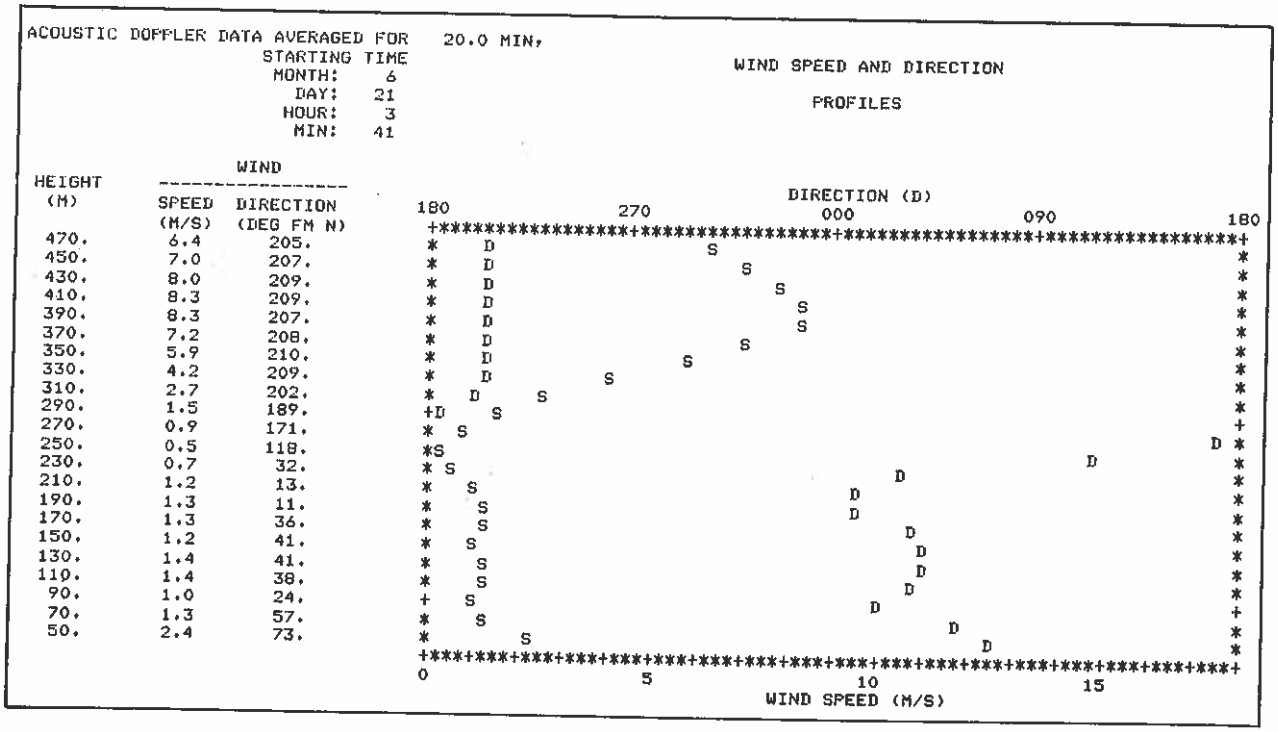

Figure 11.2. Sample output. Wind speed (S) uses scale along bottom of output in 0.25-m/s intervals. Wind direction (D) uses scale along top of graph in 5° intervals.

11.4.1 Conclusions

11.4.1.1 Real covariance

The estimates described above were biased by noise with the magnitude of the error found to be a function of the magnitude of the frequency shift. Since the real covariance utilizes a signal heterodyned to a frequency centered on 125 Hz, fractional errors in the frequency estimate provide a larger error in the estimate of the differential frequency shift.

11.4.1.2 Complex covariance

(1) The complex-covariance technique showed results unbiased by white noise for a sufficiently large number of samples.

(2) The standard deviation was a function of the signal-to-noise ratio. The mean error was also within $1/\sqrt{N}$ of the standard deviation with N samples.

(3) With pure noise, the frequency estimate was biased towards zero-shift because of the centering and non-flatness of the filters.

(4) Errors in the frequency estimates were independent of the magnitude of the frequency shift from that of the carrier.

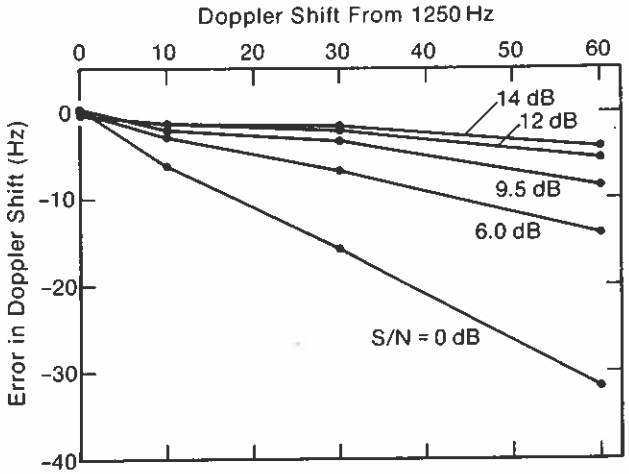

Figure 11.3. Real covariance error analysis showing error in Hz for given amount of Doppler shift from carrier frequency of 1250 Hz, as a function of signal-to-noise ratio (as defined in text.)

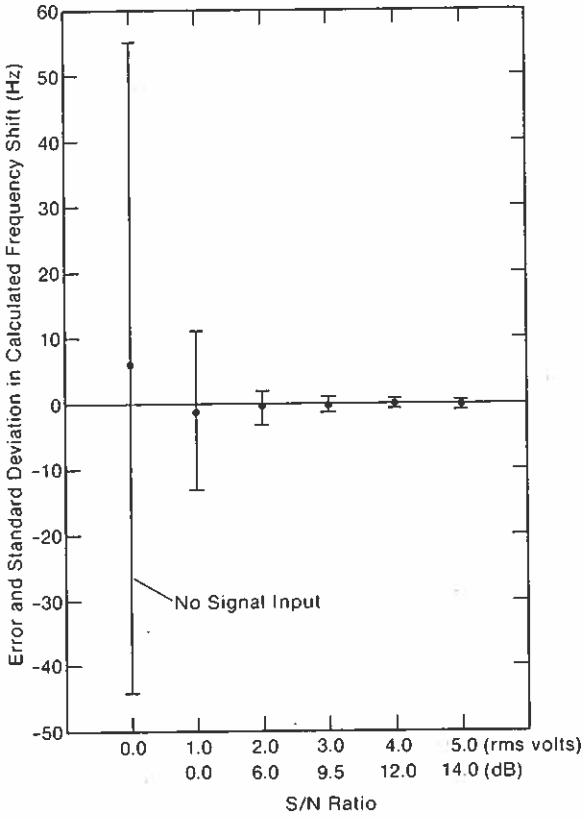

Figure 11.4. Complex covariance error analysis showing errors and standard deviations of frequency estimates as a function of signal-to-noise ratio.

11.4.2 Consequences for Field Measurements

(1) Under noisy conditions averaging times must be increased.

(2) Wind variance measurements under windy (surface) conditions should be inspected carefully since the background noise level increases with surface wind speed. Thus, although the variance might be expected to increase with wind speed and the data might be observed to behave properly, such increases in the variance cannot necessarily be disassociated from S/N effects. However, for white noise, such variances in the frequency estimates will be equal to those obtained by using direct spectral techniques (R. J. Keeler, personal communication).

11.5 FIELD TESTS

The results of the limited number of field tests to date have been encouraging. Following the construction of a prototype system during May 1979 we were able to obtain several nights of tower data with which to compare the new system's results. We found, at that time, zero bias in the mean values averaged over the total data set of three nights

and a mean difference in direction of 3 degrees. This system was then moved to a field site and has been running since 4 July with about 95 percent data recovery to a height of 600 m. A second device was then built several weeks before the BLIE experiment. During testing some biasing was evident. Further inspection showed two sources of error. The first was the presence of other transmitting frequencies. We found that sufficiently strong signals, although normally outside the bandwidth of our receiver, can pass through the wings of the filter and be aliased into the estimate of the mean spectrum. The choice of a second operating frequency for backscatter sounding must, therefore, be made carefully. A second source of error was the presence of nonwhite noise produced by the tower. We analyzed the background noise with a real-time spectrum analyzer before, during, and after data runs. With a delayed trigger, spectra were averaged for signals characteristic of the 300-m range gate. Figure 11.5 shows a typical spectrum obtained with winds from the southwest greater than 4 m/s. Strong peaks in the noise are evident near 500 Hz and again near our operating frequency of 1250 Hz. The peak in this latter region occurred typically between 1100 and 1300 Hz, depending on conditions. We also calculated the errors in our measurements as a function of wind direction; the results are shown in Fig. 11.6. Underestimates are most prevalent with winds from the southwest. This is also the direction toward which the carriage support on the tower is oriented. This support consists of two grids of 1000 elements each spaced 0.3048 m apart with an opening of 0.267 m. At 25°C these dimensions correspond to acoustic frequencies of 1135 and 1297 Hz.

11.6 REFERENCES

Sirmans, D., and B. Bumgarner (1975): Numerical comparison of five mean frequency estimators. J. Appl. Meteorol. 14:991-1003.

Owens, E. J. (1977): Microcomputer-controlled acoustic echo sounder. NOAA Tech. Memo. ERL WPL-21, NOAA/ERL, Boulder, Colo., 76 pp.

Neff, W. D., and E. H. Brown (1979): Acoustic echo sounder operations during PHOENIX, Chapter 14. In Project PHOENIX: The September 1978 Field Operation, W. H. Hooke (Ed.), NOAA/NCAR Boulder Atmospheric Observatory Rept. No. 1, available from NOAA/ERL, Boulder, Colo. 80303, and from NCAR Publications Office, Boulder, Colo. 80307.

Kaimal, J. C., and D. A. Haugen (1977): An acoustic Doppler sounder for measuring wind profiles in the lower boundary layer. J. Appl. Meteorol. 16:1298-1305.

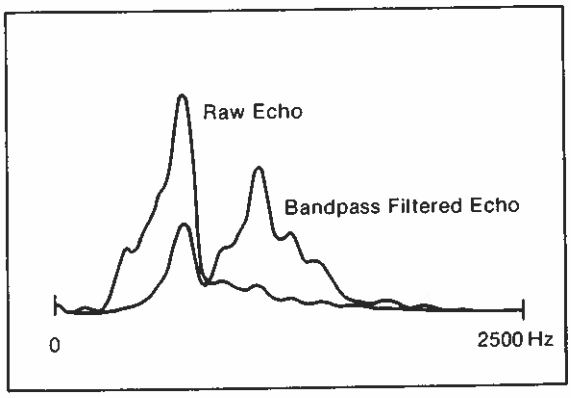

Figure 11.5. Spectrum analysis of tower noise in the range 0 to 2500 Hz with a 6 m/s wind from the south before and after bandpass filtering.

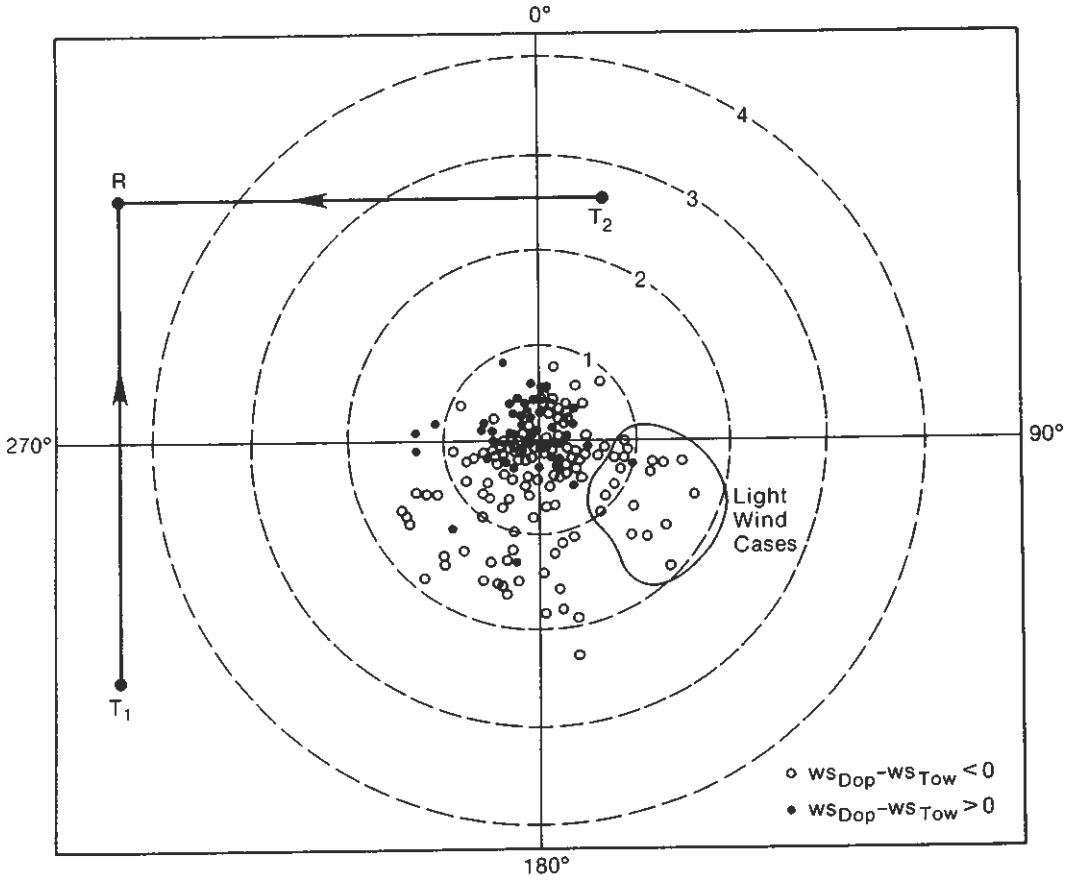

Figure 11.6. Error analysis of winds (in m/s) showing the dependence of the errors on wind direction, which correlated with noise estimates made by spectral analysis.

12. DOPPLER ACOUSTIC SYSTEM FOR WIND PROFILING (AVIT)

Paul MacCready
AeroVironment Inc.
Pasadena, California, U.S.A.

12.1. INTRODUCTION

The AVIT (AeroVironment Invisible Tower) system is a pulse Doppler acoustic unit continuously monitoring air motions aloft (mean winds and turbulence). The system parameters have been chosen to provide all the atmospheric inputs for modeling the dispersion of atmospheric pollutants, on both research projects and operational programs. Considerations of economy, portability, simplicity of installation, reliability, and satisfactory operation in noisy environments are as important to the design as the basic accuracy and high-altitude capability.

Since 1975, AeroVironment has developed and operated Doppler wind systems that use various antenna beam configurations, several Doppler shift analysis methods, and numerous transducer and enclosure designs. Before 1975 Ian Bourne at the University of Melbourne began development of high-altitude Doppler acoustic systems, with an emphasis on monostatic configurations and a full spectrum analysis technique for ascertaining Doppler shift. A formal collaboration between AeroVironment (AV) and the University of Melbourne began in 1978; AVIT is the system that evolved from this collaboration. The basic algorithms and electronics concepts used in AVIT were developed by Bourne. At AeroVironment, John Worden has been in charge of the AVIT program. Bourne's early two-component monostatic system is described by Bourne and Brann (1978), who also give examples of observations and comparisons with radiosonde data. Hopper (1978) briefly reviews the system and also gives examples of measurements taken with it.

12.2. THE SYSTEM AND ITS PERFORMANCE

AVIT is a flexible, modular system. The basic three-axis system uses three adjacent pencil-beam antennas. One tilts N (or S) 30° from the vertical to observe the N-S wind; one tilts E (or W) similarly to observe the E-W wind; and one points vertically to observe the vertical component. The antennas are operated sequentially, in the monostatic mode. Figure 12.1 shows a three-antenna array. Figure 12.2 shows a two-axis array mounted on a trailer.

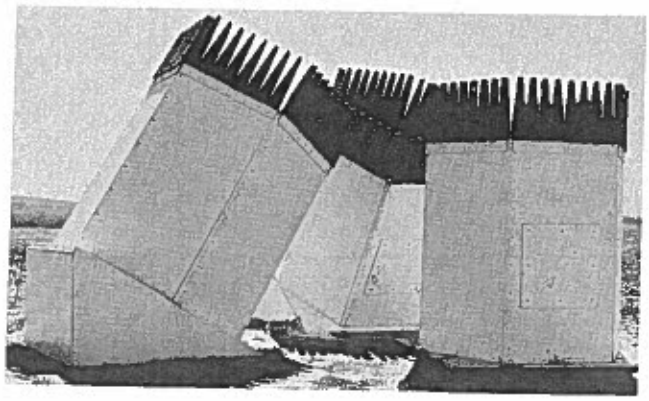

Figure 12.1. The three acoustic enclosures for the three-antenna system. Each contains a 1.8-m-diameter parabolic reflector.

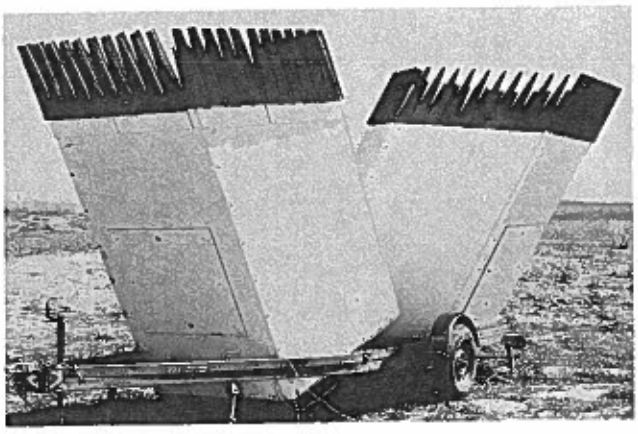

Figure 12.2. Acoustic enclosures for a two-antenna system mounted on a trailer for easy portability. The enclosures are oriented vertically for transport. Parabolic reflector size is 1.2 m.

A sound pulse (150 to 200 W) is transmitted at a frequency of 1500 Hz (2000 Hz also available), with a duration of 180 ms for the tilted beams. The received echo is heterodyned and then processed through an electronic comb filter with 31 teeth, to yield continuously the full spectrum. For each 33.3-m (100-ft) altitude range gate, the spectrum is examined for acceptance or rejection, and then if accepted it is smoothed and curve-fitted, and the resulting peak frequency and amplitude are stored. At the end of the selected averaging period, say 20 min (variable from 5 to 30 min), the assemblage of peaks is explored by a number of histograms, spectra, and interpolation techniques, and the best estimate of Doppler shift is ascertained along with an estimate of an observation reliability factor.

The resulting wind profiles for each period are printed out on a Texas Instruments Silent 700 printer. In a three-axis system the display gives three components (vertical turbulence, and horizontal speed and direction) for every range gate, starting with 67 m (200 ft) and continuing up to the maximum height selected (up to 47 range gates) or the maximum height observed. The data can also be recorded on digital tape.

Two other displays are available. One is a facsimile recorder giving a time plot of signal intensity vs. height. The signal intensity represents the strength of the echo after initial processing by the comb filter, i.e., it shows only "accepted" range gates. Thus this recorder conveniently displays the overall height and quality of the data.

The other display is an oscillograph showing the spectra in real-time sequence for each range gate. It is a convenience when evaluating the contribution of ambient noise to the echoes. Finally, a speaker is available to make the echoes audible and to give the trained listener a good bit of information. Figure 12.3 shows a version of the complete data processing and display system. (Only item missing is the oscillograph.)

The velocity component range is $\pm$15 m/s, limited by comb filter width. An automatic frequency alteration for the transmit pulse can be selected by the operator. Then, on the basis of the wind measurements during the preceding integration period the frequency is adjusted for the next period to keep the comb filter operating in its middle range. This extends the working range of the filter to component speeds of $\pm$25 m/s, and so in some directions wind speed can be covered to vector speeds of 35 m/s. This technique permits the total frequency band evaluated to be narrow and minimizes spurious noise acceptance.

Speeds are printed out to 0.1 m/s resolution, and directions to 3° resolution. Nominal reproducibility during periods of strong signals is deemed to be about 0.2 m/s, although examination of data runs often shows consistency between range gates to be within 0.1 m/s and 3°.

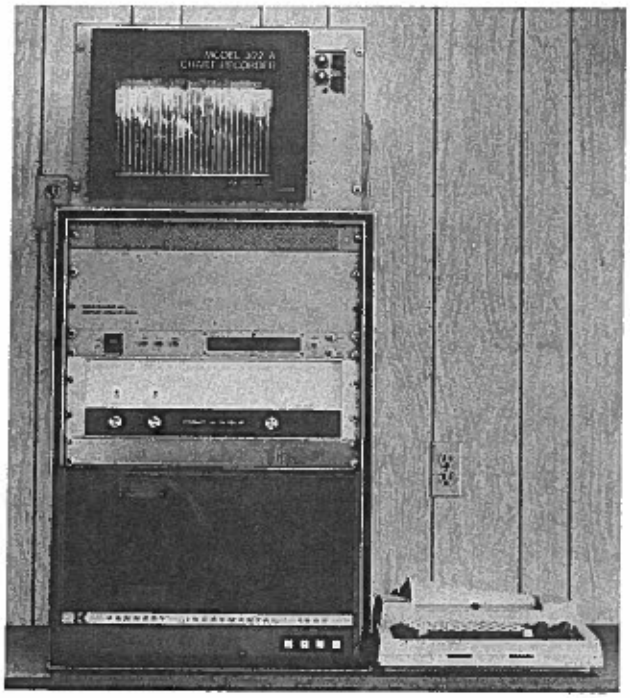

Figure 12.3. AVIT data processing and display system in operation, with digital tape recording as well as data printout and facsimile display.

The maximum altitudes at which data are obtained vary widely with meteorological conditions. An estimate from all operations with AVIT in Australia and the United States over the last year indicates that the 95% and 5% data recovery percentiles correspond to 300 m and 1000 m, with percent vs. altitude varying linearly between these heights.

The clock has battery backup to maintain time accuracy during power outages. The system features automatic restart after power failure. It is also designed for unattended operation.

12.3. OUTPUTS

Figure 12.4 presents a typical printout on the Texas Instruments Silent 700 printer. This is a 20-min interval display. The time during which data were taken is indicated at the top of the printout (date code, time 0622:02 to 0640:21). The left column gives height in units of 33.3 m (Range 2 = 66.7 m, Range 3 = 100 m, Range 9 = 300 m, etc.). Range 1 is omitted in this long-pulse, high-altitude version because there is insufficient time for the high-output driver to recover completely from its transmit power pulse before serving as the receiver transducer. Range 0 is an option not included in this example; it gives the near-surface wind component information from two propeller anemometers mounted on a 10-m mast.)

The numbers across the top give instrument operating codes and automatic gain control (AGC) levels. The columns from left to right are as follows:

HT	Height ranges in units of 33.3 m
NS	The N-S component (+ from N; m/s)
R	Data reliability assessment for this component (0 is best, 9 is worst; data from 0 to 7 are generally deemed suitable for meteorological application).
NO	Number of pulses utilized in deriving N-S component.
EW	The E-W component (+ from E).

START TIME= 0019 06 22 02
END TIME= 0019 06 40 21

28 1 1 24 0 0 70 86 69

HT	NS	R	NO	EW	R	NO	VERT	R	NO	SD	VEL	ANG	R	NO
32	-2.7	3	34	-6.1	0	34	0.0	1	34	0.3	6.6	246	3	34
31	-2.8	3	31	-5.4	0	32	0.2	1	26	0.3	6.0	243	3	31
30	-3.7	1	29	-4.3	3	28	0.2	0	23	0.3	5.7	228	3	28
29	-4.2	0	33	-3.9	0	30	0.2	0	25	0.3	5.8	225	0	31
28	-4.5	2	33	-3.6	1	28	-0.0	1	30	0.4	5.8	219	2	30
27	-4.5	1	33	-2.1	0	32	-0.1	2	27	0.4	5.0	204	1	32
26	-4.7	2	30	-1.4	0	31	0.0	3	28	0.3	4.9	195	2	30
25	-5.3	5	33	-0.7	1	28	0.0	1	31	0.2	5.2	186	5	30
24	-5.8	2	34	-0.4	0	33	0.2	5	32	0.2	5.8	183	2	33
23	-6.2	0	33	0.3	0	34	0.1	3	34	0.1	6.1	177	0	33
22	-6.2	0	34	0.2	0	33	0.0	4	34	0.4	6.2	180	0	33
21	-6.1	0	34	0.3	0	33	0.0	1	34	0.1	6.1	177	0	33
20	-5.9	0	34	0.2	0	34	0.0	2	32	0.2	6.0	180	0	34
19	-5.8	0	34	-0.2	0	34	-0.0	4	34	0.3	5.8	180	0	34
18	-5.6	4	34	-0.8	1	34	0.2	4	34	0.3	5.6	186	4	34
17	-5.4	0	34	-1.9	0	34	0.2	4	34	0.2	5.7	198	0	34
16	-5.3	0	34	-2.0	0	34	0.1	4	34	0.3	5.7	201	0	34
15	-5.3	0	34	-1.1	2	34	0.0	4	33	0.1	5.4	192	2	34
14	-5.3	0	34	-0.2	0	34	-0.2	7	33	0.2	5.3	180	0	34
13	-5.6	2	34	0.1	0	34	0.1	5	33	0.1	5.6	180	2	34
12	-6.5	3	34	0.0	0	34	0.0	4	32	0.1	6.4	180	3	34
11	-6.9	0	34	0.2	0	34	0.1	6	34	0.2	6.9	180	0	34
10	-7.3	0	34	0.2	0	34	0.1	6	34	0.1	7.2	180	0	34
9	-7.4	1	34	0.4	0	34	0.0	4	34	0.0	7.3	177	1	34
8	-7.4	1	34	0.5	3	34	0.1	4	34	0.1	7.4	177	3	34
7	-7.6	2	34	0.4	0	34	0.1	7	34	0.1	7.5	177	2	34
6	-7.6	2	34	0.5	0	34	0.1	7	34	0.1	7.6	177	2	34
5	-7.6	5	34	0.5	0	34	0.1	5	33	0.1	7.5	177	5	34
4	-7.3	1	34	0.8	3	34	0.1	5	34	0.1	7.3	174	3	34
3	-6.9	0	34	0.8	0	34	0.1	7	34	0.1	7.0	174	0	34
2	-6.8	0	34	0.5	2	33	-0.1	2	13	0.4	6.8	177	2	33

Figure 12.4. Sample data printout of AVIT system.

R	Data reliability assessment for E-W component.
NO	Number of pulses utilized in deriving this component.
VERT	Vertical wind (+ denotes upcurrent)
R	Data reliability assessment for vertical component.
NO	Number of pulses utilized in deriving vertical wind.
SD	Standard deviation of vertical wind (calculated with respect to zero vertical wind).
VEL	Total horizontal wind speed (m/s).
ANG	Horizontal wind direction (degrees)
R	Data reliability assessment for speed and direction.
NO	Number of pulses utilized in deriving speed and direction.

The operator commands a wide variety of printout options. Figure 12.4 represents a common selection for operational uses, the main variations being different altitudes (the lower the altitudes, the faster the pulse repetition rate and so the greater

the amount of information available for processing); longer or shorter averaging times; and, for the two-component system, omitting the vertical component.

In the example given, the horizontal data (components, speed, and direction) are derived from the horizontal components only. Since the vertical velocity averaged over 20 min is usually small, even in convective conditions, the error in omitting the vertical velocity correction is also usually small. The correction involves taking 1.73 times the vertical component, adding that to the N-S component and subtracting that from the E-W component (for the N-pointing and W-pointing antenna orientation employed in this example) to correct the components and hence the speed and direction. This correction can be selected in the computer and then the speed and direction printouts are for the corrected data. If the vertical velocity data observation is missing at that height, or has a bad reliability assessment number, the correction computation can assume a zero vertical velocity.

For research purposes, the operator can choose to print out more information. The integrated full spectra for each component can be printed. Alternatively, the display will give the components calculated from each of six different histograms or spectra or combined analysis approaches. It is the agreement between these component estimates, plus a weighting depending on the number of pulses selected, that is used to derive the reliability assessment quantity. A combination of a specific histogram and spectrum were used to obtain the numbers presented in Fig. 12.4.

The output can also be recorded on tape. We have used a Texas Instruments Silent 700 ASR cassette recorder for recording the results of each 20-min run, essentially the data illustrated in Fig. 12.4. We also use a Kennedy 1600 digital tape machine to record the integrated data and, if desired, to record fully every spectrum tooth output for every range gate for every pulse. This second option yields basic data for research on improving the algorithms for data selection and for exploring alternative methods of deriving turbulence from the echoes.

12.4. MAIN FEATURES

The primary design options of a pulse Doppler acoustic system are (1) overall beam configuration, (2) transducer/antenna characteristics, and (3) the Doppler shift processing technique. (Features such as pulse generation, preamplifier, and data display, are not significant in differentiating systems.) For AVIT, the design choices are as follows:

(1) The overall beam configuration is monostatic. There is also a narrow angle bistatic variation available for special tasks.

(2) The transducer/antenna system uses horn-driver-reflector-enclosure geometry and materials tailored from theory and considerable experimentation. In addition, a special treatment of the enclosure edges lessens diffraction at these edges, cuts sidelobes substantially, and makes the system suitable for use in noisy or urban locations.

(3) Doppler shift for each pulse and range gate is ascertained in real time by a continuous full-spectrum technique coupled with versatile data selection/rejection criteria (and the data quality assessment factor is one of the system outputs).

The following sections explore the rationale behind the first two design choices. The Doppler shift subject has already been treated briefly in previous sections. Suffice it to note here that the analog filter teeth (4.3 Hz wide) are both economical and stable; that the comb filter method substitutes for the more conventional full spectrum method, the digital FFT, while decreasing the demands on the computer; and that the comb filter method automatically weights the information in the previous range gate and adds it, to yield more significant information than that which can be derived solely by FFT examination of echoes from a single range gate.

12.4.1 Overall Beam Configuration

In comparison with a bistatic beam configuration, the monostatic system offers several distinct advantages:

(1) The antennas can be located adjacent to each other (even all on a single trailer) for convenience of installation.

(2) The tilted monostatic antenna senses the same percentage of the horizontal wind at all heights. This is simpler than the bistatic case, which involves altered geometry at each range gate, and which has very strong sensitivity to vertical components at the high range gates.

(3) Only pencil-beam antennas are used in the typical monostatic system, while fan beams are used in bistatic systems. The broad fan beams have poorer sidelobe suppression, even when used with complex enclosures. When used for receiving, the fan beams are relatively inefficient in keeping out noise from low elevation angles; when used for transmitting, they can be disturbing to persons nearby.

(4) Tilted beams can be tilted away from noise sources, to minimize interference.

There is one significant disadvantage to the monostatic system. It operates on echoes scattered only at 180°, and such scattering comes only from the temperature microstructure field. The bistatic systems utilize echoes from both the velocity and temperature fields. With moderate turbulence but near-neutral stability, one would expect monostatic scattering to be weak whereas bistatic scattering would be strong. Another disadvantage, but one which is generally insignificant, is that the sensed volumes at a given height are not at exactly the same location. This is of little concern when data are averaged over a few minutes, since the data are then deemed representations of an air volume large in horizontal extent.

It turns out that in virtually all conditions the monostatic approach is practical because the high efficiency inherent in having the transmit and receive beams line up exactly compensates partially for the weaker scattering cross section. Thus the main disadvantage of the monostatic system is not overwhelming; one can use the system and benefit from its good features. The average altitudes reached (see Section 12.2) demonstrate the general suitability of the technique. At night, with stability aloft, particularly in complex terrain, there are good monostatic signals at 500 m even with very light turbulence (less than $\varepsilon^{1/3} = 0.5\ cm^{2/3}\ s^{-1}$ where ε is the dissipation rate). The worst period for monostatic echoes (and bistatic) is typically in weak pressure gradient conditions in late afternoon when solar heating shuts off, heat flux up into the atmosphere stops, the lapse rate remains close to neutral, and the turbulence dissipates. To cover this period we have tested an approach that merges the bistatic method with a monostatic system.

12.4.2 Antenna Systems

AVIT employs a standard driver feeding downward into a tuned horn, spreading sound out to a parabolic reflector from which a pencil beam is emitted upward. The assembly is housed in a large acoustic enclosure that decreases the sidelobes for transmitting or receiving. The research instrument configuration uses a 1.8-m reflector, and a parallel-sided enclosure built of six sheets of 1.2-m by 2.4-m plywood or chip board. The enclosure is lined with 5-cm-thick glass wool for sound absorption. The glass wool is used instead of plastic foam because rain water drains better with the wool. The parabolic reflector can be heated for snow removal.

The two-component portable instrument version uses 1.2-m reflectors in five-sided enclosures, with both enclosures optionally mounted on a trailer for easy portability. During transit the enclosures are set upright. They are then set up for operation by tilting 30° from vertical in the N and W directions (or other orthogonal orientation).

The top edges of the enclosure are equipped with Thanadners, at Lockheed Co. Thanadners are teeth, here 0.6 m high and 0.1 m wide, covered on both sides with absorbing material, which have the effect of acoustically "feathering" the top edges and greatly decreasing diffraction. Our tests have shown the additional sidelobe suppressions at low angles to be as much as 12-14 dB. The amount will depend greatly on the sidelobes initially present, and on whether or not the wall attenuation is adequate. The Thanadners help make the acoustic system suitable for operation in urban environments.

The wind speed at which wind noise becomes a problem has not been determined for these enclosures, either with or without Thanadners. On several installations we worried about possible wind noise, but avoided the problem by erecting a fence upwind.

12.5. THE FUTURE

AVIT is satisfactory as a high-altitude remote probe for many purposes, but improvements are always desirable. Work will continue in order to reach higher altitudes or to cover a given altitude a larger percentage of the time. The main approaches are to increase power and to apply more sophisticated algorithms for extracting valid Doppler shift information when the signal/noise ratio is low. Work will also continue to obtain additional turbulence parameters, and to validate the observations by aircraft measurements.

Our goal is to have an instrument that provides all the meteorological inputs needed to supply a rational diffusion model covering a wide range of conditions. Wind and turbulence profiles are obviously essential inputs. Temperature gradients are needed only to assist in calculating plume rise, and they need not be precise; the standard plume rise equation can use only a few broad categories, such as unstable, neutral, stable, and very stable. It may prove possible in many cases to derive such categories from the profiles of wind and turbulence.

12.6. REFERENCES

Bourne, I. A., and H. N. Brann (1978): AIRMET Conf. R. Met. Soc. (Aust.), Bureau of Meteorology, Melbourne, Australia.

Hopper, V. D. (1978): Acoustic sounding of the atmosphere. Endeavour (new series) 2:121.

13. RADIAN CORPORATION MODEL 800 ECHOSONDE

M. A. McAnally
Radian Corporation
Austin, Texas, U.S.A.

13.1 INTRODUCTION

The Doppler acoustic sounding system is used to characterize the thermal structure and wind profiles in the lower atmosphere (below 1 km). Transmitted acoustic tones are scattered by the turbulent atmosphere. The strength of the direct backscatter depends on the temperature fluctuations in the scattering volume. The frequency of the scattered energy is shifted by an amount dependent on the motion of the scattering volume. Therefore the returned echo strength as a function of time provides information about the thermal structure as a function of altitude. The mean Doppler frequency shift is proportional to the average velocity of the scattering volume along a line that bisects the transmit and receive beams. By measuring the mean Doppler frequency shift in three independent directions, the three wind components can be determined as a function of altitude. Only recently with the availability of low-cost digital systems has it been possible to estimate the Doppler frequency shift in a cost-effective system. Radian's Model 800 Doppler Echosonde utilizes the LSI-11 microcomputer to perform complex covariant processing to measure the Doppler frequency shift of the returned echo.

The Radian Echosonde system comprises five basic subsystems:

(1) Acoustic antenna and transducer assembly.

(2) Acoustic noise suppression (Septacuff).

(3) Bistatic transmit horn.

(4) Microcomputer and control electronics.

(5) Display terminal.

13.2 ACOUSTIC ANTENNA ASSEMBLY

The antenna assembly consists of an exponential horn and transducer which directs acoustic energy into a parabolic reflector to form a 10° acoustic beam. Because of the high magnetic field strength in the compression driver coil gap, the assembly also functions well as a return echo detector. The electrical signal from the compression driver-detector is amplified at the antenna to minimize electrical noise effects on the receiver system.

The transmitted tone is 2000 Hz in the standard configuration; however, other frequencies have been used. The transmitted tone power is 150-W electric input power with a selectable pulse duration of 0 to 990 ms in 10-ms steps. The pulse repetition rate is also selectable from 1 to 99 s in 1-s steps. The pulse duration is the controlling variable for altitude resolution, and the repetition rate sets the maximum travel time, and thus the maximum altitude.

13.3 ACOUSTIC NOISE SUPPRESSION

The acoustic enclosure design, based on theoretical and experimental studies by the NOAA Wave Propagation Laboratory, isolates the receiving antenna from ground-based

interfering noise sources. The fully portable Septacuff is constructed of seven sides and a bottom, all of which are lined with acoustic foam and a sandwiched lead sheet septum for maximum sound control. The Septacuff shape was selected to minimize diffracted ground-level noise. The sides of the enclosure are flared away from the 1.2-m parabolic antenna/reflector at the bottom. The total weight of the enclosure is 250 kg (550 lb); it can be disassembled down to parts that weigh less than 50 kg (110 lb).

13.4 BISTATIC TRANSMIT HORN

The bistatic exponential transmit horn is constructed of fiberglass and shaped to form a broad vertical beam to provide information over a range of altitudes. The bistatic transmitter uses the same type of transducer as the monostatic antenna assembly. The transmitter provides a fan-shaped beam with 50° vertical beamwidth, and 10° horizontal width.

13.5 MICROCOMPUTER AND CONTROL ELECTRONICS

This subsystem consists of a microcomputer, amplifiers and filters, controls, and power supply. The central processing unit is a Digital Equipment Corporation LSI-11 with 4-K memory and hardware multiply/divide. Because the control program resides in programmable read-only memory (PROM), the system will automatically restart after power failure. The Echosonde signal-generating and processing electronics are assembled on printed circuit boards designed for plug compatibility with the LSI-11 microcomputer. The modular system design provides many optional system configurations by exchanging or adding circuit boards. For example, a user may select the option that provides only single axis measurement, i.e., only the vertical wind components and temperature structure, and upgrade to a full three-axis system by adding the bistatic transmitters, and changing the PROM board, which contains the system software.

13.6 DISPLAY TERMINAL

The display unit is a dot-matrix digitally controlled line printer. The printer has a special optical shading character set for displaying the intensity of the backscatter return. Figure 13.1 shows a sample of the display terminal output. The standard alpha-numeric character set is used to print the wind data determined by the Doppler frequency shift. The figure shows horizontal wind speed (tenths of m/s), horizontal direction (degrees east of north), vertical and horizontal wind direction variance (degrees), and a vertical wind indicator. The display can also provide an estimate of the returned signal-to-noise ratio.

13.7 OPTIONS

In addition to the basic subsystems, the Echosonde system offers the following optional features:

(1) 220 V a.c., 50-Hz input power.

(2) Telecommunications (serial ASCII) over two-wire or standard telephone with standard modems.

(3) Optional peripheral storage units including 9-track magnetic tape, cassette tape, disk, or paper tape.

(4) Heated antenna/reflector.

(5) Tilting base for Septacuff.

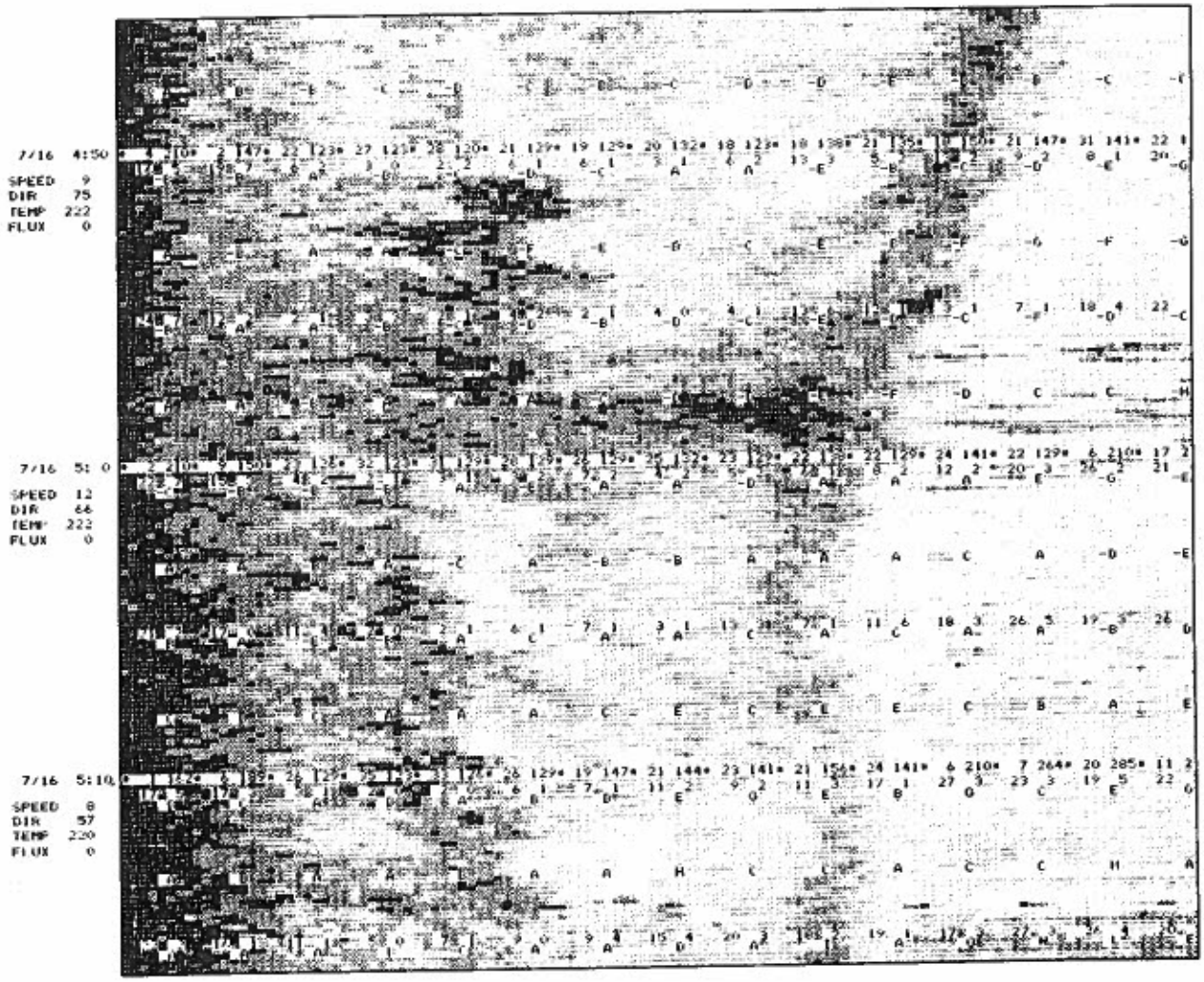

Figure 13.1. Sample format of display from printer.

13.8 SYSTEM CONFIGURATION OPTIONS

The optimum acoustic sounder configuration is dependent on the specific requirements of the application. The user of the acoustic sounder system must consider the following:

(1) Altitude range required.

(2) Sampling interval required.

(3) Noise interference as well as potential noise nuisance.

Radian's Model 800 Doppler Echosonde can be configured in a variety of ways tailored to each specific application. All configurations determine thermal structure and display on the line printer, but the user may elect to record the following:

(1) Single-axis (vertical) wind component.

(2) Two-axis (vertical and one horizontal) wind components.

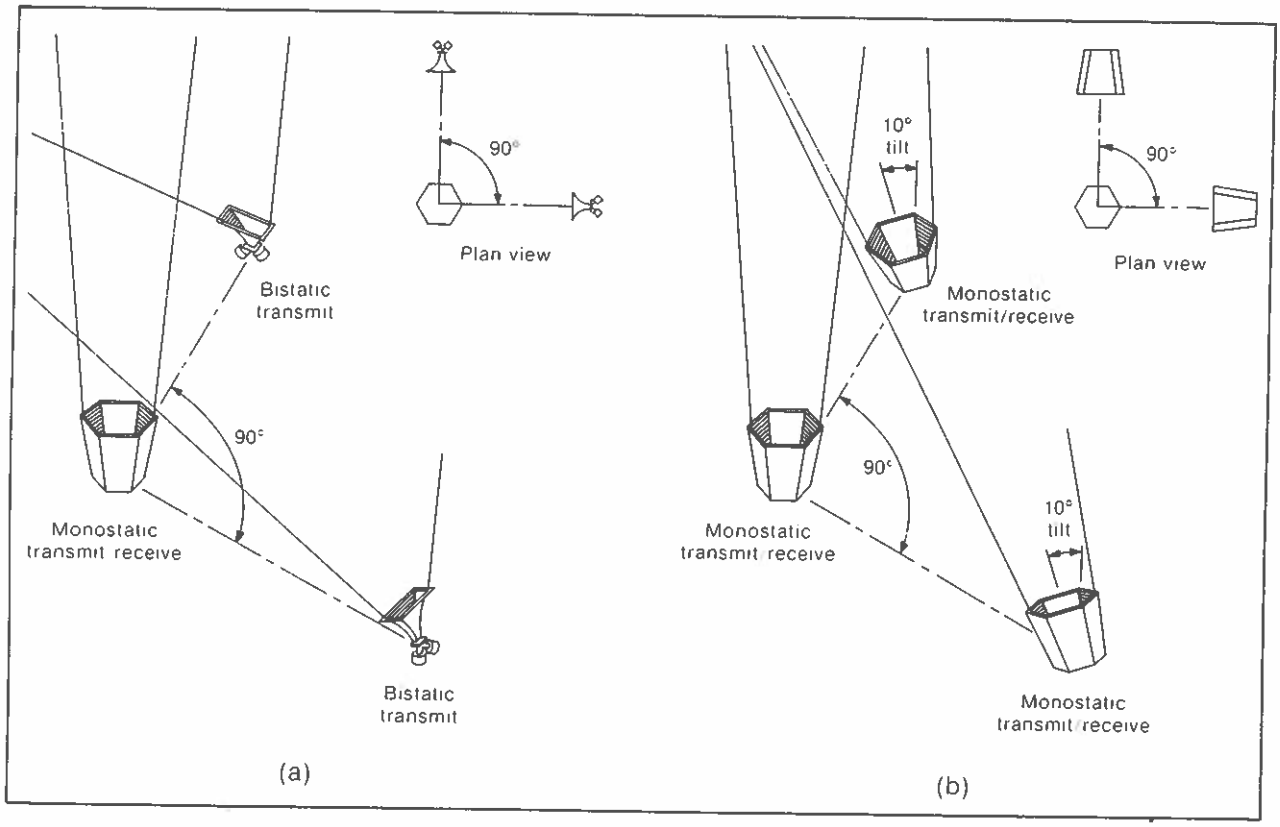

Figure 13.2. Optional three-axis (u, v, w) configurations for the Model 800 Doppler Echosonde: a) bistatic, b) monostatic.

(3) Three-axis (vertical plus orthogonal horizontal) wind components.

Figure 13.2 illustrates two choices for arranging the transmit/receive antennas to record wind components. The bistatic arrangement separates the transmit and receive antennas for resolving the horizontal wind components. This arrangement provides the simplicity of receiving all returned echoes at one receiver. The monostatic arrangement provides one to three transmit/receive modules complete with acoustic enclosure. Two of the acoustic enclosures are tilted to obtain the horizontal wind components. The monostatic arrangement has the advantage of directional focusing of the transmitted acoustic energy.

13.9 CALIBRATION VERIFICATION

The Model 800 Echosonde normally requires no field calibration after installation. The instrument is fully calibrated and tested prior to shipment. It is usually advantageous, however, to verify several critical aspects of the Echosonde operation following a field installation. The sound level of each of the acoustic transmitters is normally checked after installation. The sound level of each bistatic transmitter should be 133 dB relative to 20 $\mu N/m^2$. The monostatic transmitter sound level should be 128-130 dB relative to 20 $\mu N/m^2$. The preamplifier d.c. offset is also normally checked after installation. This is accomplished by injecting a 100-μV signal into the preamplifier and adjusting the zero trim pots for less than 1-mV offset voltage. The remaining analog adjustments are not usually possible in the field without the use of specialized equipment.

14. SWEDISH SODAR SYSTEM

Sören Salomonsson
Department of Meteorology
University of Uppsala
Uppsala, Sweden

Mats Hurtig
Sensitron AB
Stockholm, Sweden

14.1 INTRODUCTION

During the period 1970-1975 a monostatic acoustic sounding system was developed at the Swedish Research Institute of National Defence under the leadership of Hans Ottersten. This sodar system was then utilized in research projects in Sweden and other European countries (Ottersten and Eklund, 1973; Ottersten et al., 1974; Ottersten, 1975a and 1975b).

Starting in 1975, the Swedish sodar system was further developed in joint projects between the Department of Meteorology of the University of Uppsala and the electronic company Sensitron AB of Stockholm (Holmgren et al., 1976). A new monostatic Doppler system was built in 1976 by applying a phase-locked loop (PLL) circuit for tracking the frequency shift of the return signal. The sodar project is supported by the Swedish Board for Space Activities and the Swedish Board of Technical Development.

A first application of the Doppler unit was done in cooperation with the Swedish Meteorological and Hydrological Institute in a boundary layer study during the first two weeks of May 1977. The vertical wind velocity was derived from the Doppler shift at 100, 175, 250, and 350 m at some brief periods. Figure 14.1 shows a set of these measurements.

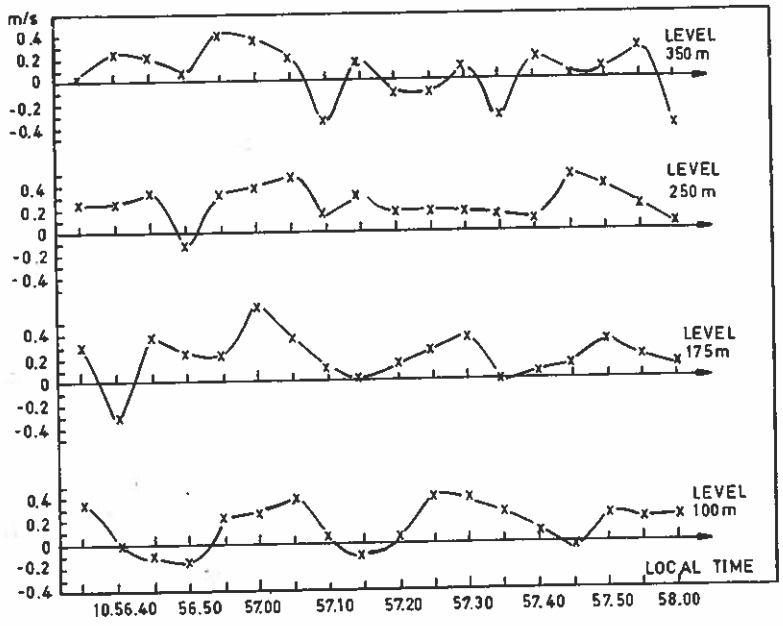

Figure 14.1. Vertical wind velocities derived from the acoustic Doppler measurements for different heights on 5 May 1977.

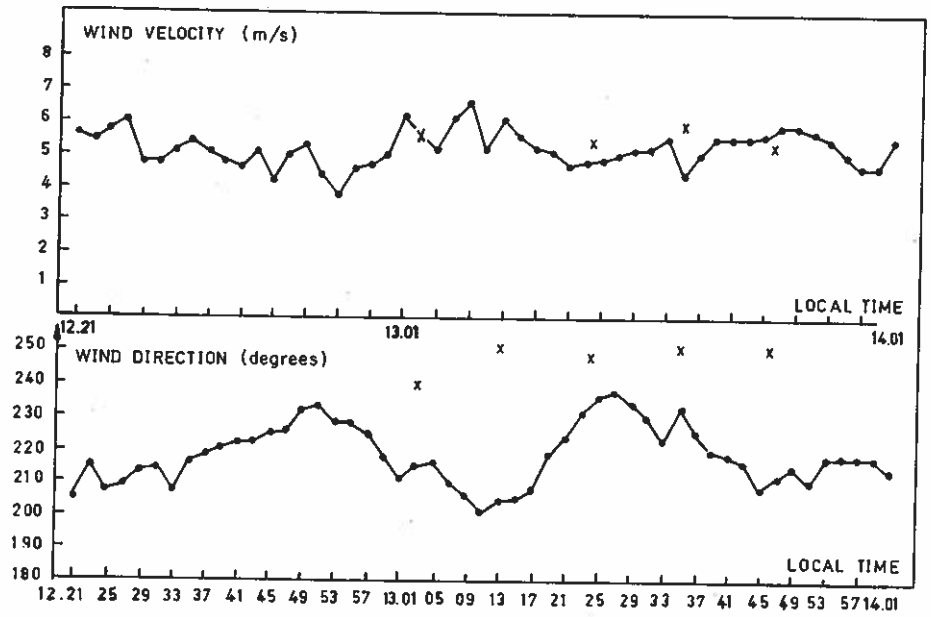

Figure 14.2. Example of the horizontal wind velocity and wind directions measured by Doppler (solid line) and pibal tracking (crosses) at a height of 60 m. Each data point is centered on the corresponding 2-min averaging interval.

A preliminary description of the sodar measurements obtained during this field project is given in Salomonsson and Ivarsson (1978).

Measurements of the horizontal wind velocity were carried out during the autumn of 1978 for the benefit of a project that aimed at finding the best location for a wind power station in the area. Two monostatic sodar systems, with tilted antennas, were used to determine the horizontal wind components. The derived wind velocity was compared with simultaneous wind measurements obtained from double theodolite pibal trackings. An example of these measurements is shown in Fig. 14.2.

14.2 TECHNICAL DESCRIPTION

The monostatic system used at the intercomparison in Boulder is a commercial system manufactured by Sensitron AB. It consists of two antennas for measuring the two horizontal wind components. Figure 14.3 shows the relationships of the parts of the system. Table 14.1 lists the specifications. The system uses two antennas, but a third antenna can be added to measure the vertical wind velocity. The antennas can be clustered together, with the tilting antennas pointing out from the central point along the orthogonal planes, or they can be separated as shown in Fig. 14.4. The antennas are fed by compressor drivers of 100 W. They give an acoustic beam pattern like that in Fig. 14.5.

14.2.1 Description of the Monostatic System

During transmission, a tone-burst is generated in the transceiver unit SR 20 by the combined band-pass filter and tone generator. The tone-burst is fed through a power amplifier to the transducer of one of the selected antenna channels. The received echo signals are amplified in the preamplifier and transferred by balanced cables to the receiver in the transceiver unit SR 20.

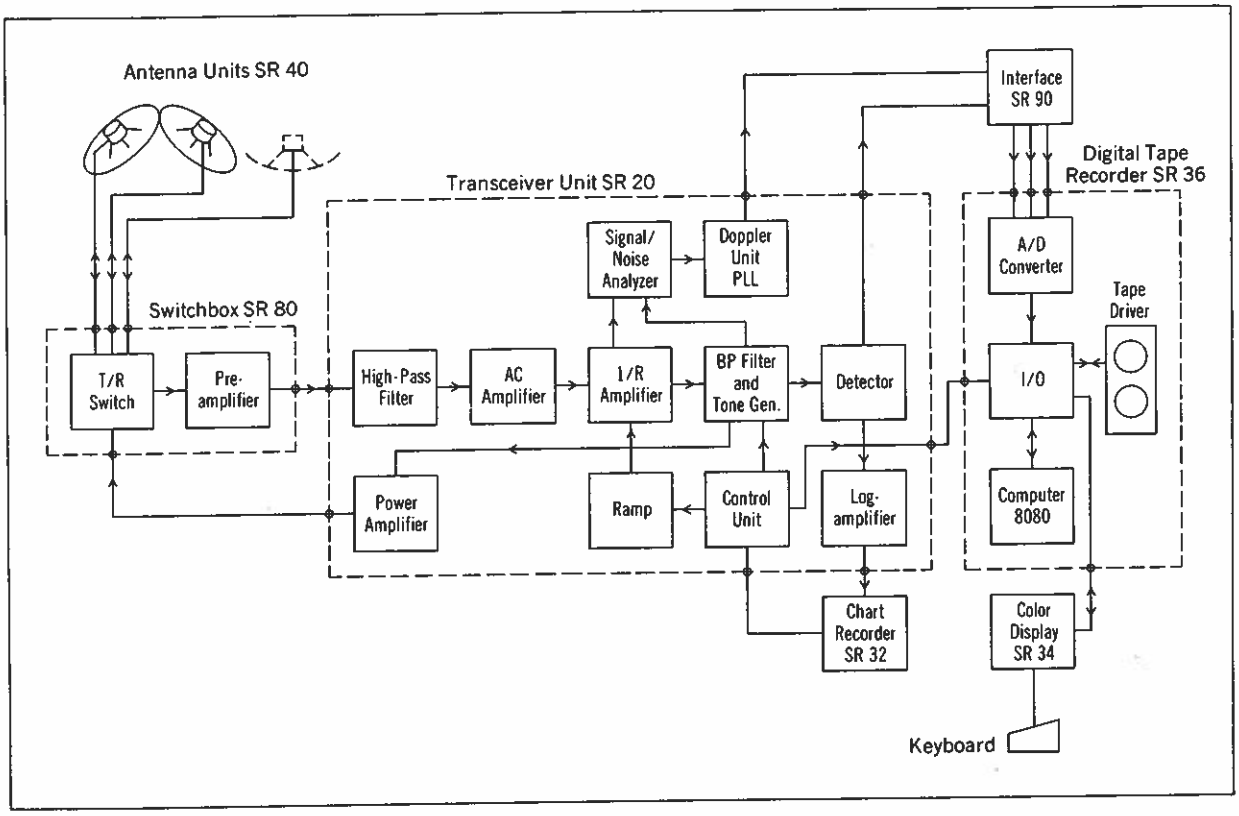

Figure 14.3. Block diagram of the acoustic Doppler sounder.

The echo signals are high-pass filtered to eliminate high energy components of the background noise at frequencies below 800 Hz. A linear-gain amplifier is used to compensate for spherical divergence of the scattered acoustic wave. The PLL circuit gives an output signal proportional to the Doppler shift of the incoming signal. To reduce noise the echo signals are passed through a signal-to-noise analyzer, which selects signals that have a given ratio to the background noise level. The detected Doppler signal is connected by the interface SR 90 to the microprocessor in the tape recorder unit SR 36 for determination of the wind vector. The other channel works in exactly the same way. The wind information received and processed by the microprocessor is presented on the color display SR 34 (Thomson and Scheib, 1978).

The intensity for the temperature fluctuation received at one of the antennas is band-pass filtered and detected. The signals are processed and presented on the color display SR 34. Even chart recorder SR 32 presents temperature fluctuation and is fed by a log amplifier, which compensates for the difference in the dynamic range of the detected signal to the recorder.

14.2.2 Data Presentation

The color display SR 34 is an eight-color CRT screen that contains a microprocessor for the color representation. The wind information is presented on the screen in different pictures which can be selected from the keyboard. Profiles of wind speed and direction, columns of wind speed and direction, and a combination of wind speed and the intensity of the temperature fluctuation can be displayed. The intensity of the temperature fluctuations is classified in five colors and presented in a height/time diagram. Integration time of data, color representation, program start-up, etc., can be controlled from the keyboard.

Table 14.1. Technical specifications of the Swedish sodar system

Equipment	Specifications
Antennas (two)	Parabolic dish Fiberglass Diameter: 1.2 m Transducer Altec Lansing 291-16B
Transceiver SR 20	Transmitter Frequency: 2,400 Hz (1,800 Hz) Pulse power: 100 W Pulse width: 30, 90, 180 ms Pulse repetition rate: 0.1 - 0.2 Hz Receiver Balanced input: 600 Ω High pass filter: 800 Hz Range correction: 1/R within height range 20-1,000 m Bandwidth: 20, 40, 80 Hz (for recorder SR 32) Sounding range: 20-1,500 m

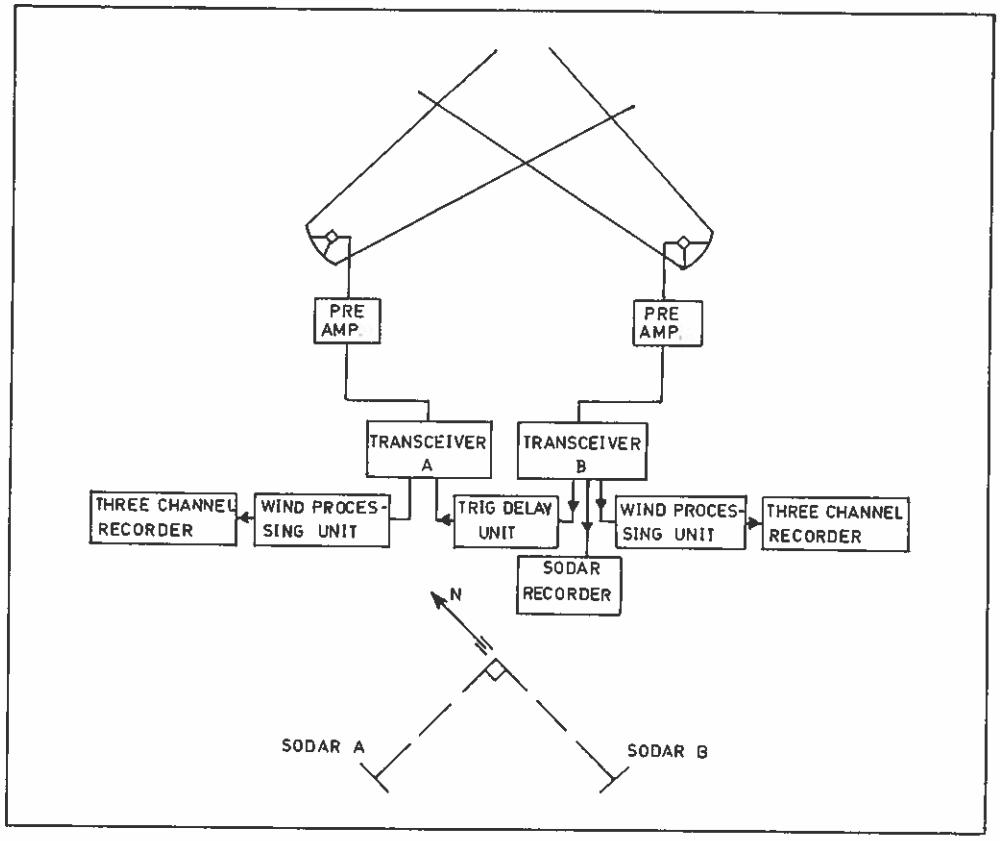

Figure 14.4. Block diagram of the monostatic Doppler system used in the project on Gotland and the horizontal orientation of the two antennas (A and B) in relation to the north axis.

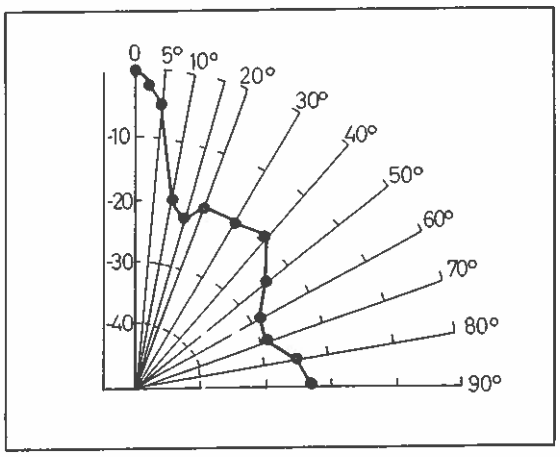

Figure 14.5. Polar pattern of the acoustic beam for the transmitting antenna at 2,400 Hz. (The lobe width is about 8°.)

All data are recorded on tape in data blocks. Every block contains number of day, time, wind information, and intensity of the temperature fluctuations for one sounding interval.

Another presentation unit is recorder SR 32 which gives the intensity of the temperature fluctuation along one axis. Recorder SR 32 works on a new principle, presenting grey shades on metallized paper. This recorder is almost free of maintenance compared with earlier recorders.

14.3 EXAMPLES OF DOPPLER MEASUREMENTS

Figure 14.1 shows graphs of vertical wind velocities derived from the Doppler shift at four selected levels obtained in an atmosphere of a slightly stable thermal stratification. It may be noted that the measuring period is only about 1.5 min. Therefore, a discussion of average wind velocities has no significance in this case. During ideal conditions one may expect to get zero mean vertical velocity if the averaging interval is long enough (Kaimal and Haugen, 1977). Variations in the vertical velocities indicate a "wavy" pattern with a tendency for crests and troughs to coincide at the four levels. In order to discuss the vertical wind structure in detail a much longer time series is needed.

During the autumn of 1978 an extensive project aimed at finding the best location for a wind power station was carried out in selected high-wind areas on the Swedish island Gotland (Smedman-Högström and Faxén, 1980). In connection with this wind-prospecting project, supported by the Swedish National Board for Energy Source Development, two monostatic sodar systems were used. The sodar measurements were carried out in a joint project between the Department of Meteorology of the University of Uppsala and the Swedish Meteorological and Hydrological Institute, with technical support by Sensitron AB.

A simplified block diagram of the two monostatic sodar systems (A and B) used in the wind-prospecting project is shown in Fig. 14.4. The system was built around two standard sodar units. The Doppler frequency received at each antenna was analyzed in the wind-processing unit and presented on the analog 3-channel recorder. The two sodar systems operated at the same frequency (2.4 kHz). To avoid interference between the two systems each transmitter was pulsed separately in time by the trigger delay unit, with a pulse repetition frequency of 0.25 s^{-1}. The antennas were tilted 50 degrees from the horizontal plane, with the intersection of the antenna beams at a height of 60 m.

The radial velocities were derived from the 3-channel recorders. By using the assumption of a zero mean vertical velocity for the time-averaging interval and trigonometric relationships the horizontal wind vector was computed. Figure 14.2 shows a preliminary

result of the horizontal wind measurements. The wind velocity derived from the Doppler shift was then compared with simultaneous wind measurements from double theodolite pibal trackings (Alexandersson and Bergström, 1979).

Wind velocities show satisfactory agreement, but the wind directions show more differences. These differences could probably be explained to some extent by considering the uncertainties in the determination of the Doppler shift (Beran and Clifford, 1972). A small error in the determination of the Doppler frequency in one or both of the components affects the wind direction more than the wind velocity. Another reason for the discrepancy is that in general the actual position of the balloon does not coincide with the intersection of the antenna beams. Furthermore, the vertical wind velocity will also influence the measurements, especially when the averaging period is not long enough to make the mean vertical component negligible.

A more detailed analysis of the whole series of tests of the Doppler measurements from the wind-prospecting project will be published in the series of reports from the Department of Meteorology of the University of Uppsala.

14.4 REFERENCES

Alexandersson, H., and H. Bergström (1979): Evaluation of double theodolite pibal tracking data. Report No. 55, Dept. of Meteorol., Univ. of Uppsala, Uppsala, Sweden.

Beran, D. W., and Clifford, S. F. (1972): Acoustic Doppler measurements of the total wind vector. Preprints AMS 2nd Symp. on Meteorol. Obs. and Instrum., San Diego, Calif., 27-30 March 1972. American Meteorological Society, Boston, Mass., pp. 412-417.

Holmgren, B., C. Jacobsson, and H. Ottersten (1976): Sondering av atmosfärens gränsskikt med vertikalsodar. FOA rapport C 30077-E1, National Defence Research Institute, Stockholm, Sweden.

Kaimal, J. C., and D. A. Haugen (1977): An acoustic Doppler sounder for measuring wind profiles in the lower boundary layer. J. Appl. Meteorol. 16:1298-1305.

Ottersten, H. (1975a): Fjärranalys av atmosfärens gränsskikt med sodar och radar. Styrelsen för Teknisk Utveckling. Slutrapport STU 71-727/U 957b, April 1975.

Ottersten, H. (1975b): Swedish sodar investigations and results. Paper presented at the URSI XVIIIth General Assembly, Lima, Peru, August 1975, International Union of Radio Science, Brussels, Belgium.

Ottersten, H., and F. Eklund (1973): Remote sensing av troposfären. Styrelsen for Teknisk Utveckling. Lägesrapport STU 71-727/U 597.

Ottersten, H., M. Hurtig, G. Stilke, B. Brummer, and G. Peters (1974): Shipborne sodar measurements during JONSWAP II. J. Geophys. Res. 79:5573-5584.

Salomonsson, S., and J. Ivarsson (1978): Sodar measurements of the boundary layer during the field project "Stenungsund-77." Report No. 50, Dept. of Meteorol., Univ. of Uppsala, Uppsala, Sweden.

Smedman-Högström, A.-S., and T. Faxén (1980): To be published in report series. Dept. of Meteorol., Univ. of Uppsala, Uppsala, Sweden.

Thomson, D. W., and J. P. Scheib (1978): Improved display techniques for sodar measurements. Bull. Am. Meteorol. Soc. 59:147-152.

15. THE XONDAR

Robert L. Peace, Jr.
Xonics, Inc.
Van Nuys, California, U.S.A.

15.1 INTRODUCTION

The XONDAR (Xonics Doppler acoustic radar) is an operational, commercially available system. It is designed for a broad range of applications, from mean wind measurements to turbulence and diffusion studies. It can also be used in environments ranging from benign to hostile. The XONDAR can vary several key parameters, such as pulse length, pulse repetition frequency, summation time, and observing altitudes, in the field with a simple computer command. It can also suppress the effects of ambient noise (Balser et al., 1976a). Optional equipment includes a sounder printer (to display the time-height distribution of relative stability), hardware to melt ice and snow, and telephone or radio modems.

15.2 THE BASIC XONDAR ACOUSTIC ANEMOMETER

A basic XONDAR wind-profile measuring system consists of five subsystems: the sound-producing and -sensing hardware, the computer, the printer, the program input and storage device, and the command keyboard. Two models of the XONDAR are offered, the Model 300 and the Model 600. These differ primarily in hardware attributes that give the first system finer vertical, temporal, and velocity resolution, and the second system a greater altitude range. The characteristics and attributes of both models are given in Table 15.1, although only the longer range Model 600 participated in the intercomparison.

Table 15.1. XONDAR wind sensor technical specifications

Characteristic	Model 300	Model 600
Antenna diameter (inside)	3 ft (0.9 m)	4 ft (1.2 m)
Peak power to transducer (electrical)	250 W	250 W
Peak output power (acoustic)	40 W	80 W
Transmitted frequency	4000 Hz	2000 Hz
Pulse duration (computer-controlled)	80/40 m s	160/80 m s
Altitude resolution	25/12 m	50/25 m
Velocity accuracy (one component)	0.2/0.4 m/s	0.2/0.4 m/s
Maximum velocity (one component)	±25 m/s	±25 m/s
Pulse repetition interval (normal)	2.5 s	5 s
Nominal maximum altitude for velocity	200 m	500 m
Maximum altitude for sounder	400 m	800 m
Number of altitudes sampled	10	10
Averaging time (typical)	2 min	2 min
Power requirements	115 V ±10% @ 30 A, 50-60 Hz	

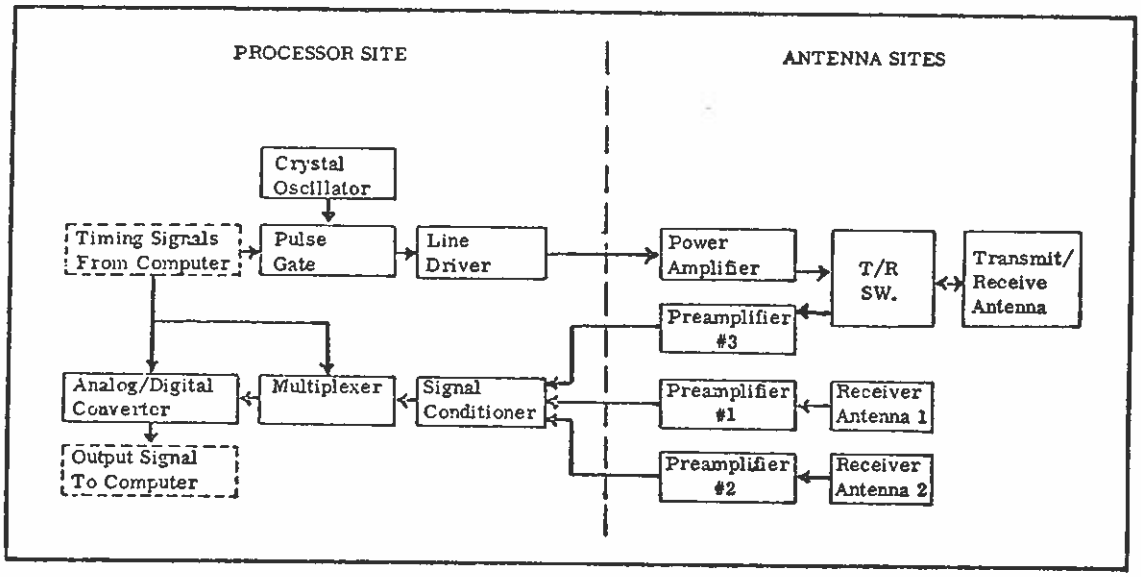

Figure 15.1. Block diagram of XONDAR sensor subsystem.

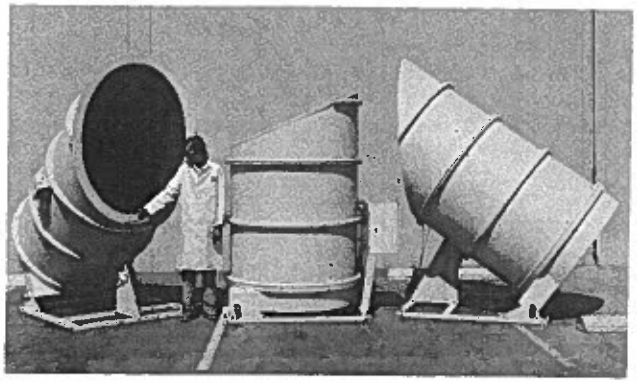

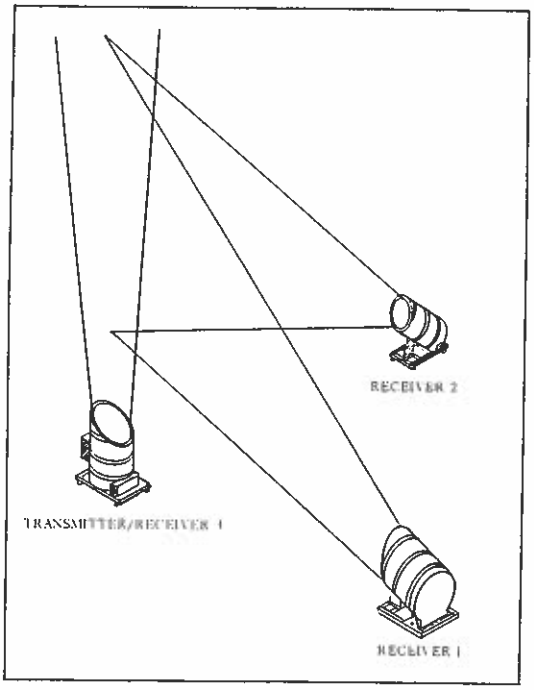

Figure 15.2. (Above) The three XONDAR antenna housings. (Right) The standard antenna configuration of a Xonics three-component air-motion measuring system.

15.2.1 The Sensor Subsystem

The sensor subsystem for both models of XONDAR is composed of one transceiving and two receiving antennas and their supporting electronics (Fig. 15.1). Each of the three antenna assemblies consists of an aluminum parabolic reflector mounted in the bottom of a foam rubber and lead-lined acoustic shield (Fig. 15.2, above). This shield effectively prevents sound from escaping from the transceiver housing or entering any of the housings

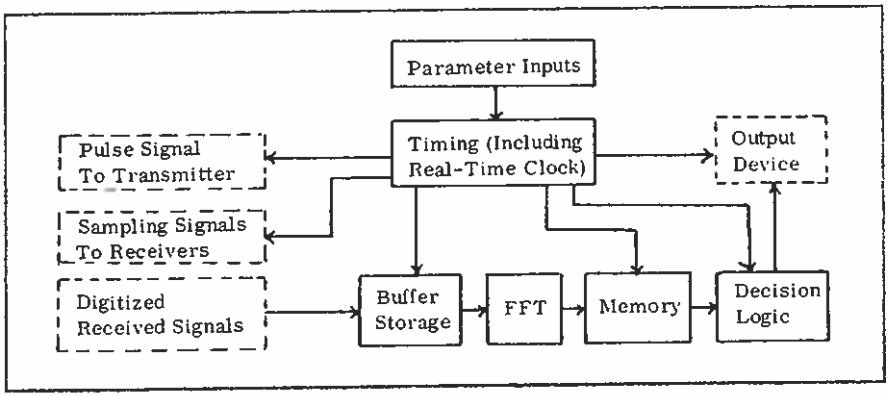

Figure 15.3. Block diagram of basic computer functions.

except in the desired direction. At the focal point of the transceiving antenna is an acoustic transducer that both emits high-power pulses of sound in a narrow circular beam and detects sound returning from the atmosphere.

The two outlying receiver antennas are equipped with transducers and feedhorns that detect sound from a range of angles that is narrow in the horizontal but fan-shaped in the vertical and centered on the transmitter beam boresight.

In operation, the three XONDAR antennas are nominally located in the right-triangle configuration diagrammed in Fig. 15.2 (right) with an antenna separation equal to, or somewhat less than, the maximum altitude to be observed. To avoid loss of sensitivity of the horizontal components of air motion, the elevation of the receiving antennas should not exceed 50° to 55°. For the nominal 500-m maximum altitude of the Model 600, antenna spacing should be 350 to 400 m. Although the antenna specifications and the configuration shown in Fig. 15.2 (right) are optimum, the computer program that performs data reduction is sufficiently versatile to allow considerable variation in antenna spacing, orientation, and relative height where site constraints dictate.

The electrical power requirements of the XONDAR systems are 100-120 V, 50-60 cycles at 30 A, supplied only at the computer location. The low-voltage power requirements of the receiving antennas are provided through the interconnecting cables supplied with the system. These cables also carry all intelligence to the computer and commands to the antennas.

15.2.2 The Computer Subsystem

The heart and brain of the XONDAR system are a minicomputer with 32,000 words of memory, a real-time calendar clock, a precision lapsed-time clock, and a nonvolatile memory sufficient to read in and restart the program after a power failure. Figure 15.3 is a diagram of the basic functions performed by the computer.

The system has considerable flexibility in its configuration, operational mode, and data format. The standard selectable system configuration elements are relative antenna height, spacing, and orientation. Selectable operational modes are pulse duration (which determines velocity and height resolution), pulse repetition frequency (which determines maximum unambiguous observable height as well as the number of samples per summation period), integration interval (which must balance the frequency of observations against the statistical significance of the data), duration of observation versus no observation (if intermittent operation is desirable), and height levels to be sampled (up to 10). The data

output for the basic system can be in either the vector component form (V_x, V_y, V_z, σ_x, σ_y, σ_z), with or without the standard deviation of the velocity component (σ_x, σ_y, σ_z), or the more common polar coordinate form (A_z, S_p, E_l, σ_a, σ_s, σ_E), with or without the standard deviations. Additional types of output are available, but they were not used for this intercomparison.

15.2.3 The Program-Storage Subsystem

The computer program to control the XONDAR's operations, including the default values of the system configuration, operational mode, and output data format, is provided on a floppy disk. This disk is read into the computer each time the system is activated after a period of disuse, or when changes in the program or default parameters are desired. Once read in, the program automatically begins operation of the XONDAR. If power is interrupted during operation, the disk drive automatically rereads the program and default parameters into the computer and begins operation whenever power resumes. The real-time calendar clock continues to operate for long periods on its own storage battery. Thus, the system resumes operation without loss of date or time reference.

The residence of both the controlling program and a default value of all operational parameters on a floppy disk makes it possible for Xonics to rapidly and economically provide a user with different default values whenever the basic XONDAR use changes. If a variety of operational modes or system configurations is anticipated, Xonics can provide a diskette for each. These are easily inserted into the reader. Thereafter the system will operate in accordance with the new instructions until a different diskette is inserted or parameters are changed through the keyboard. Should it be desirable to add optional hardware or data-analysis capabilities, the computer program necessary to accomplish the changes is also provided by Xonics on a system-compatible floppy disk.

15.2.4 The Printer

The system printer is a stand-alone 40-column printer connected to the computer through a simple cable. This arrangement makes it possible to locate the printer wherever most convenient within several feet of the computer. The unit prints data, heading information, and command prompts and echoes keyboard entries on a 3½-in-wide roll of ordinary paper. A take-up reel rewinds the paper a few inches beyond the print roller. Sufficient paper is exposed to allow examination of two complete 10-level sets of air-motion data without removing the take-up reel from the printer.

15.2.5 The Keyboard

All operational communication with the XONDAR system is accomplished through a standard computer-type keyboard mounted in the computer cabinet. Temporary changes in one or more of the operating commands or parameters are easily entered through the keyboard. The new command or parameter overrides the corresponding value in the computer. The new value is then used until it is changed through the keyboard or overridden by the contents of the diskette subsequent to a power interruption or an operator command to read the diskette.

15.3 PREVIOUS TESTS OF THE XONDAR

This intercomparison of acoustic Doppler radar systems is not the first for Xonics systems. The earliest prototype XONDAR (a three-antenna, bistatic, two-component system) was compared with cup anemometers and wind vanes mounted on a 150-m tower at White Sands Missile Range in 1973 (Balser et al., 1976b). In October 1974, a four-antenna, fully bistatic system (made for the Air Force Cambridge Research Laboratory) was compared with anemometers on a 500-m tower at the Atomic Energy Commission test site in Nevada (Kaimal and Haugen, 1975).

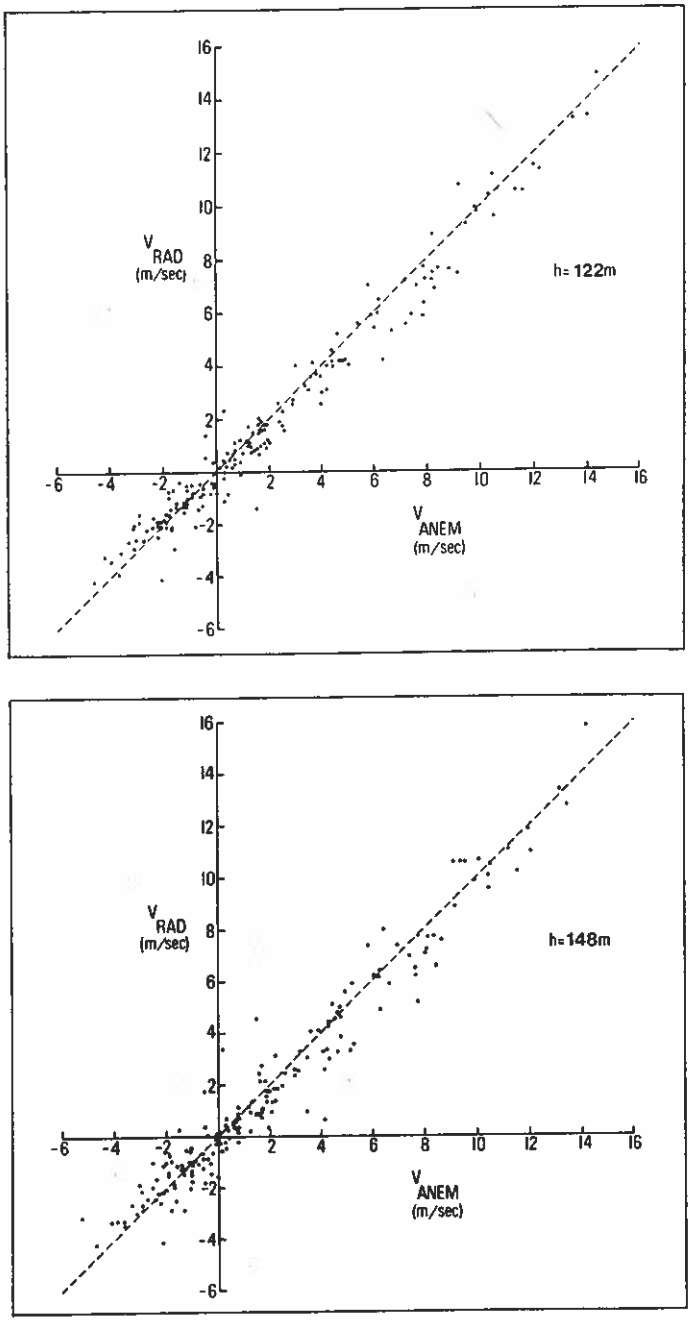

Figure 15.4. Overall comparison between XONDAR-observed wind speeds (V_{rad}) and those reported by an anemometer (V_{anem}) mounted at the 122-m level (upper) and 148-m level (lower) of a tower near Boulder, Colorado, in 1975.

In 1975, a prototype, two-component (wind only) XONDAR was compared against instruments on NOAA's 150-m tower at Boulder, Colorado. Figure 15.4 shows the results of comparisons made by NOAA between the XONDAR and conventional anemometers located at two levels on the tower. Each point in Fig. 15.4 represents a 10-min average speed from both the XONDAR and the corresponding anemometer.

Model 300 and Model 600 XONDARs have recently undergone a series of comparisons against tower-mounted anemometers in Japan. Preliminary comparisons were made between a 4-kHz Model 300 system and anemometers mounted on a 213-m tower in Tsukuba, Japan, in December 1977. Figures 15.5 and 15.6 show the comparison results.

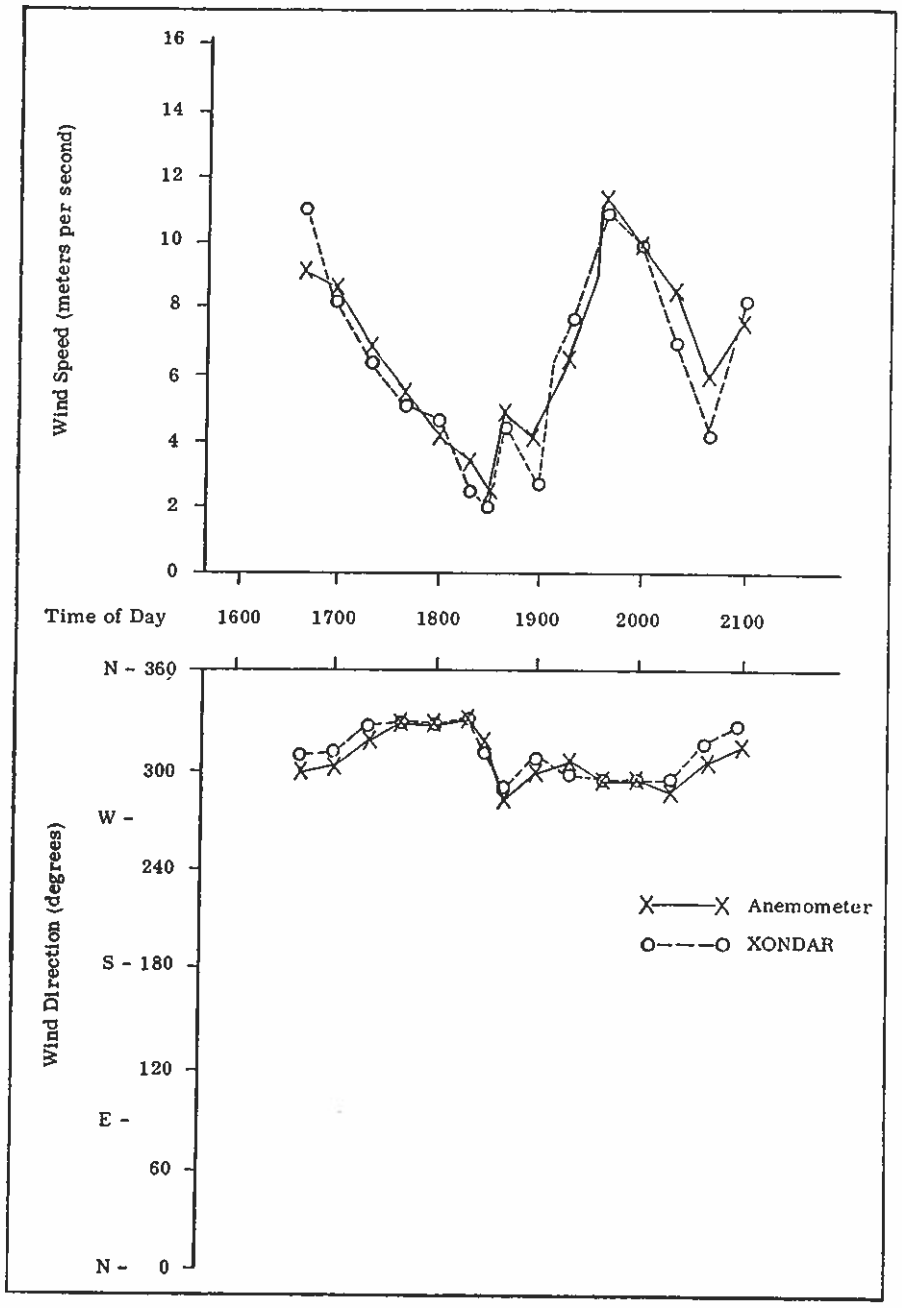

Figure 15.5. Comparison of wind speed and wind direction measurements from a Model 300 XONDAR and an anemometer mounted at the 100-m level of the 213-m high Meteorological Research Institute (MRI) tower, Tsukuba, Japan, in December 1977.

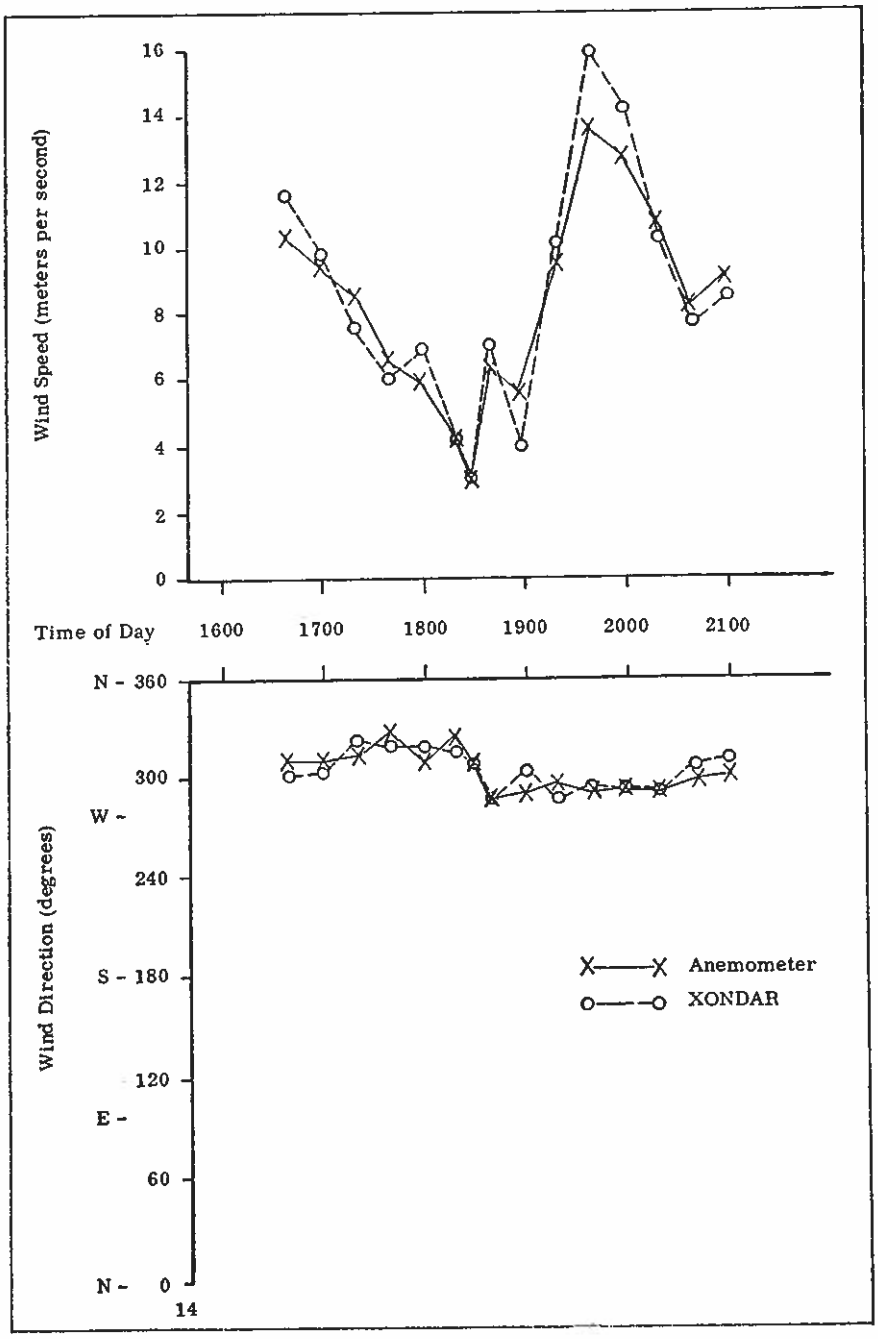

Figure 15.6. Comparison of wind speed and wind direction measurements from between a Model 300 XONDAR and an anemometer mounted at the 150-m level of the MRI tower in December 1977.

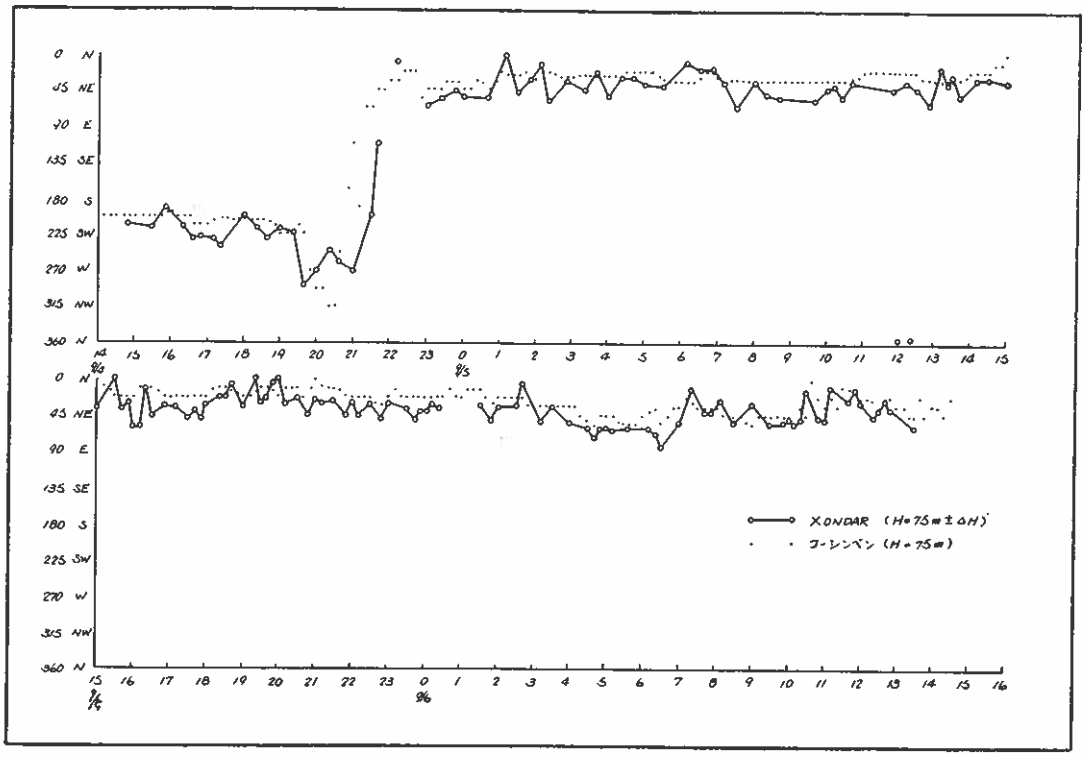

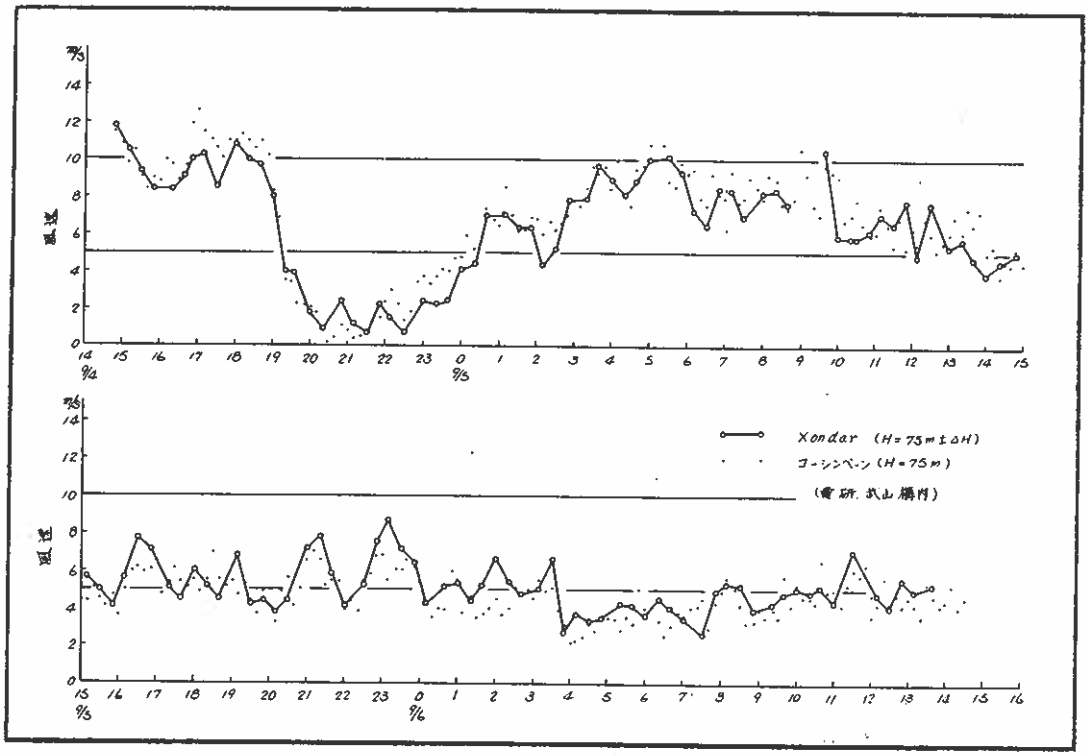

Figure 15.7. A 2-day wind direction comparison (upper) and wind speed comparison (lower) between a Model 600 XONDAR and an aerovane mounted on top of a 75-m tower in Japan in September 1978.

In September 1978, a 2-kHz Model 600 underwent a series of tests including comparisons against an aerovane mounted on top of a 75-m tower. Figure 15.7 shows comparisons of the direction and speed data acquired during these tests (Nishinomiya and Akai, 1979).

The disparity between XONDAR and anemometer wind measurements is symptomatic of one of the principal weaknesses of this kind of comparison. By their very nature, tower-mounted anemometers of any type measure only the temporal distribution of air-motion conditions at a fixed point in space. In contrast, Doppler acoustic radars or sounders intermittently measure the spectrum of velocities in a rather large volume of air within the dimensions of the pulse length and beam width of the system. These two types of measurements will agree only to the extent that Taylor's hypothesis—that time variations at a point are due only to displacement of a steady-state field—is valid and that the turbulence is vertically and horizontally isotropic on a scale commensurate with the acoustic Doppler's pulse volume. Since these conditions are rarely completely fulfilled in the lower atmosphere, acoustic Doppler and tower-mounted sensor statistics can be expected to differ, even if both have measured accurately.

15.4 XONDAR APPLICATIONS AND EXAMPLES OF DATA

Only a few accounts of the applications of XONDAR systems have been published (Balser, 1976; Balser et al., 1974, 1976a and b; Noonkester, 1978). These articles refer only to their use for general winds-aloft measurement, wind and wind shear measurements at the end of airport runways, and measurements related to ocean-based convective activity. They have also been used in conjunction with wind-energy exploration, transport and diffusion, and environmental impact studies.

Samples of data from one of these applications, part of a Department of Energy program conducted by Battelle Pacific Northwest, show vertical velocity characteristics of interest to both meteorologists and Doppler acoustic radar designers. These measurements were made near Pittsburg, California (close to the mouth of the Sacramento River) in 1978.

Figure 15.8 (left) shows the sequential change in vertical velocity from the highest level downward. The shift has just begun during the 2 min ending at 2308, with all but the 400-m level showing upward velocities of 2 to 2.4 m/s. In 2 min the upper two levels have reversed direction of vertical velocity, and the upward velocity has halved at the 300-m level. By 2312 all levels show downward velocity with the greatest downward velocity at the higher levels. The data also show a similar downward progression of wind direction shifts.

In contrast, Fig. 15.8 (center) shows vertical velocity reversal at all levels in the 2-min data interval between 1812 and 1814. The horizontal speed shows little change with time, but the 150-m level direction changes 12° in the same 2-min interval that the vertical velocity reverses and 5° more in the next 2 min. Direction changes at higher levels follow.

Figure 15.8 (right) is a 12-min sample of persistent vertical velocity averaging more than 1 m/s at most levels. The significance of such persistence to wind-measuring systems that do not measure vertical velocity was pointed out by Kaimal and Wescott (1976). If bistatic antennas had been located so that the elevation angle to the higher altitudes was about 60° and vertical velocity was not measured, the error in wind measurement would have been 3 to 4 m/s, which is 25% to 30% of the measured values. Furthermore, these persistent vertical velocities occurred in the absence of orographic effects, frontal activity, or precipitation, all of which can cause significant vertical velocities (or the apparent acoustic indication of them) to persist for extended periods. Examination of samples of XONDAR records indicates that persistent vertical velocities are sufficiently common to cast doubt on any wind data acquired by a Doppler acoustic radar without the benefit of vertical velocity information.

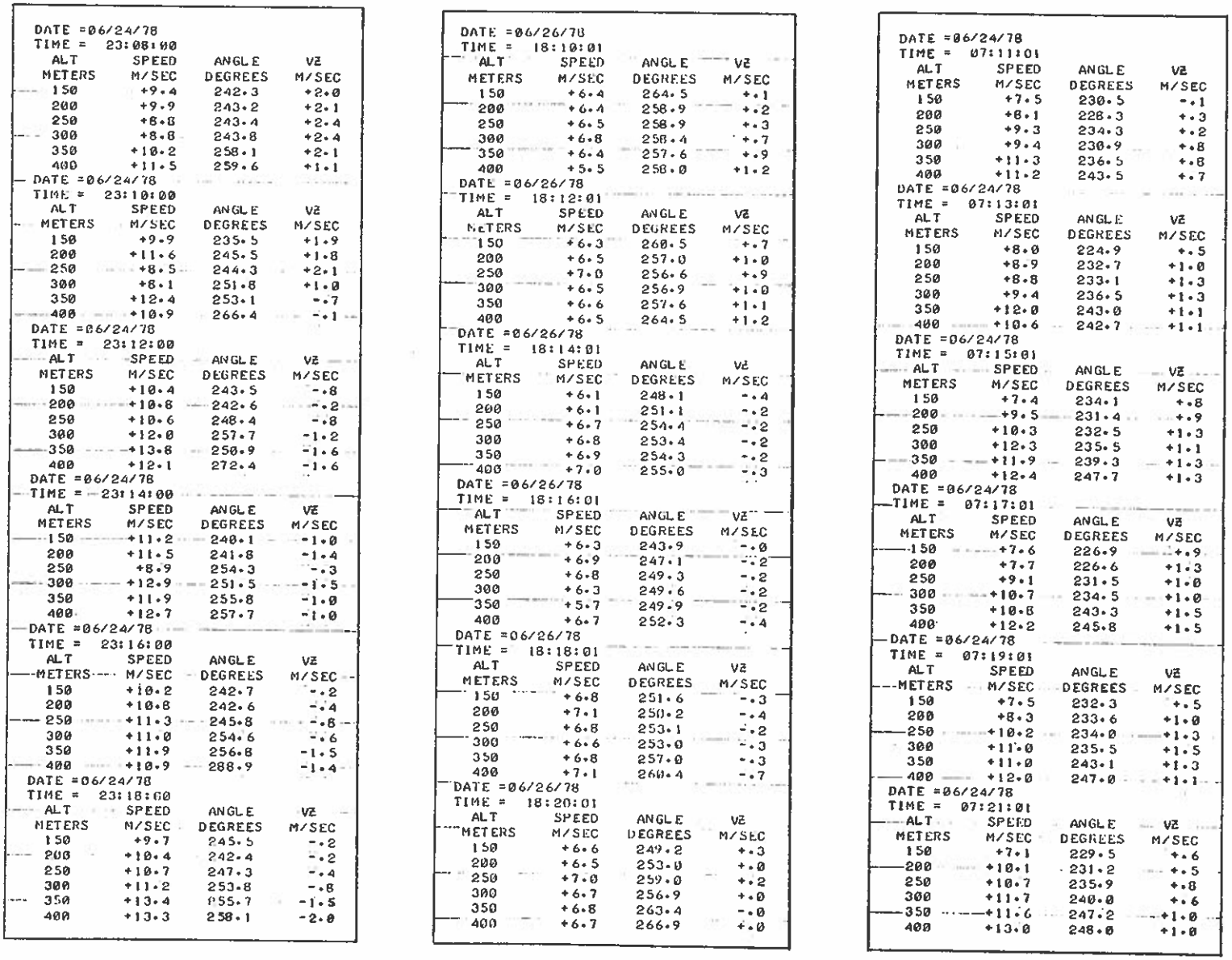

DATE =06/24/78
TIME = 23:08:00

ALT METERS	SPEED M/SEC	ANGLE DEGREES	VZ M/SEC
150	+9.4	242.3	+2.0
200	+9.9	243.2	+2.1
250	+8.8	243.4	+2.4
300	+8.8	243.8	+2.4
350	+10.2	258.1	+2.1
400	+11.5	259.6	+1.1

DATE =06/24/78
TIME = 23:10:00

ALT METERS	SPEED M/SEC	ANGLE DEGREES	VZ M/SEC
150	+9.9	235.5	+1.9
200	+11.6	245.5	+1.8
250	+8.5	244.3	+2.1
300	+8.1	251.8	+1.0
350	+12.4	253.1	-.7
400	+10.9	266.4	-.1

DATE =06/24/78
TIME = 23:12:00

ALT METERS	SPEED M/SEC	ANGLE DEGREES	VZ M/SEC
150	+10.4	243.5	-.8
200	+10.8	242.6	-.2
250	+10.6	248.4	-.8
300	+12.0	257.7	-1.2
350	+13.8	250.9	-1.6
400	+12.1	272.4	-1.6

DATE =06/24/78
TIME = 23:14:00

ALT METERS	SPEED M/SEC	ANGLE DEGREES	VZ M/SEC
150	+11.2	240.1	-1.0
200	+11.5	241.8	-1.4
250	+8.9	254.3	-.3
300	+12.9	251.5	-1.5
350	+11.9	255.8	-1.0
400	+12.7	257.7	-1.0

DATE =06/24/78
TIME = 23:16:00

ALT METERS	SPEED M/SEC	ANGLE DEGREES	VZ M/SEC
150	+10.2	242.7	-.2
200	+10.8	242.6	-.4
250	+11.3	245.8	-.8
300	+11.0	254.6	-.6
350	+11.9	256.8	-1.5
400	+10.9	288.9	-1.4

DATE =06/24/78
TIME = 23:18:00

ALT METERS	SPEED M/SEC	ANGLE DEGREES	VZ M/SEC
150	+9.7	245.5	-.2
200	+10.4	242.4	-.2
250	+10.7	247.3	-.4
300	+11.2	253.8	-.8
350	+13.4	255.7	-1.5
400	+13.3	258.1	-2.0

DATE =06/26/78
TIME = 18:10:01

ALT METERS	SPEED M/SEC	ANGLE DEGREES	VZ M/SEC
150	+6.4	264.5	+.1
200	+6.4	258.9	+.2
250	+6.5	258.9	+.3
300	+6.8	258.4	+.7
350	+6.4	257.6	+.9
400	+5.5	258.0	+1.2

DATE =06/26/78
TIME = 18:12:01

ALT METERS	SPEED M/SEC	ANGLE DEGREES	VZ M/SEC
150	+6.3	260.5	+.7
200	+6.5	257.0	+1.0
250	+7.0	256.6	+.9
300	+6.5	256.9	+1.0
350	+6.6	257.6	+1.1
400	+6.5	264.5	+1.2

DATE =06/26/78
TIME = 18:14:01

ALT METERS	SPEED M/SEC	ANGLE DEGREES	VZ M/SEC
150	+6.1	248.1	-.4
200	+6.1	251.1	-.2
250	+6.7	254.4	-.2
300	+6.8	253.4	-.2
350	+6.9	254.3	-.2
400	+7.0	255.0	-.3

DATE =06/26/78
TIME = 18:16:01

ALT METERS	SPEED M/SEC	ANGLE DEGREES	VZ M/SEC
150	+6.3	243.9	-.0
200	+6.9	247.1	-.2
250	+6.8	249.3	-.2
300	+6.3	249.6	-.2
350	+5.7	249.9	-.2
400	+6.7	252.3	-.4

DATE =06/26/78
TIME = 18:18:01

ALT METERS	SPEED M/SEC	ANGLE DEGREES	VZ M/SEC
150	+6.8	251.6	-.3
200	+7.1	250.2	-.4
250	+6.8	253.1	-.2
300	+6.6	253.0	-.3
350	+6.8	257.0	-.3
400	+7.1	260.4	-.7

DATE =06/26/78
TIME = 18:20:01

ALT METERS	SPEED M/SEC	ANGLE DEGREES	VZ M/SEC
150	+6.6	249.2	+.3
200	+6.5	253.0	+.0
250	+7.0	259.0	+.2
300	+6.7	256.9	+.0
350	+6.8	263.4	-.0
400	+6.7	266.9	+.0

DATE =06/24/78
TIME = 07:11:01

ALT METERS	SPEED M/SEC	ANGLE DEGREES	VZ M/SEC
150	+7.5	230.5	-.1
200	+8.1	228.3	+.3
250	+9.3	234.3	+.2
300	+9.4	230.9	+.8
350	+11.3	236.5	+.8
400	+11.2	243.5	+.7

DATE =06/24/78
TIME = 07:13:01

ALT METERS	SPEED M/SEC	ANGLE DEGREES	VZ M/SEC
150	+8.0	224.9	+.5
200	+8.9	232.7	+1.0
250	+8.8	233.1	+1.3
300	+9.4	236.5	+1.3
350	+12.0	243.0	+1.1
400	+10.6	242.7	+1.1

DATE =06/24/78
TIME = 07:15:01

ALT METERS	SPEED M/SEC	ANGLE DEGREES	VZ M/SEC
150	+7.4	234.1	+.8
200	+9.5	231.4	+.9
250	+10.3	232.5	+1.3
300	+12.3	235.5	+1.1
350	+11.9	239.3	+1.3
400	+12.4	247.7	+1.3

DATE =06/24/78
TIME = 07:17:01

ALT METERS	SPEED M/SEC	ANGLE DEGREES	VZ M/SEC
150	+7.6	226.9	+.9
200	+7.7	226.6	+1.3
250	+9.1	231.5	+1.0
300	+10.7	234.5	+1.0
350	+10.8	243.3	+1.5
400	+12.2	245.8	+1.5

DATE =06/24/78
TIME = 07:19:01

ALT METERS	SPEED M/SEC	ANGLE DEGREES	VZ M/SEC
150	+7.5	232.3	+.5
200	+8.3	233.6	+1.0
250	+10.2	234.0	+1.3
300	+11.0	235.5	+1.5
350	+11.0	243.1	+1.3
400	+12.0	247.0	+1.1

DATE =06/24/78
TIME = 07:21:01

ALT METERS	SPEED M/SEC	ANGLE DEGREES	VZ M/SEC
150	+7.1	229.5	+.6
200	+10.1	231.2	+.5
250	+10.7	235.9	+.8
300	+11.7	240.0	+.6
350	+11.6	247.2	+1.0
400	+13.0	248.0	+1.0

Figure 15.8. Twelve-minute samples of XONDAR data acquired near Pittsburg, California. (Left) Note the character of the vertical velocity reversal with height and time. (Center) Note rapid reversal of vertical velocity at all levels. (Right) Note consistent upward vertical velocity near 1 m/s at all but the lowest level.

15.5 REFERENCES

Balser, M. (1976): Measuring wind shear. In Airports International, IPC Business Press, Surrey, England.

Balser, M., C. A. McNary, and A. E. Nagy (1974): Acoustic backscatter radar system for tracking aircraft trailing vortices. J. Aircraft 11:556-562.

Balser, M., C. A. McNary, and D. Anderson (1976a): A remote acoustic wind sensor for airport approaches. J. Appl. Meteorol. 15:665-668.

Balser, M., C. A. McNary, A. E. Nagy, R. Loveland, and D. Dickson (1976b): Remote wind sensing by acoustic radar. J. Appl. Meteorol. 15:50-58.

Kaimal, J. C., and D. A. Haugen (1975): Evaluation of an acoustic Doppler radar for measuring winds in the lower atmosphere. Proc. 16th Radar Meteorol. Conf., 22-24 April 1975, Houston, Tex., American Meteorological Society, Boston, Mass., p. 312.

Kaimal, J. C., and J. W. Wescott (1976): An acoustic Doppler sounder for measuring wind profiles in the lower boundary layer. Proc. 17th Radar Meteorol. Conf., 26-29 October 1976, Seattle, Wash., American Meteorological Society, Boston, Mass., pp. 290-296.

Nishinomiya, S., and Y. Akai (1979): Wind profile measurements with a Doppler-acoustic remote sensor in the lower atmosphere. Central Research Institute for Electric Power Industry, Iwato 1, 229, Komae City, Tokyo, Japan (in Japanese), 28 pp.

Noonkester, V. R. (1978): Multi-sensor measurements of ocean based convective activity. Proc. 18th Radar Meteorol. Conf., 28-30 March 1978, Atlanta, Ga., American Meteorological Society, Boston, Mass., pp. 55-64.

16. GMD-1 RADIO WIND SOUNDING SYSTEM

Robert B. McBeth
National Center for Atmospheric Research
Boulder, Colorado, U.S.A.

16.1 PURPOSE AND USE

The GMD-1 rawin set is a transportable radio direction finder that automatically tracks a balloon-borne radiosonde transmitter. A radio signal containing meteorological information in the form of amplitude or frequency modulation is received, amplified, and detected by this equipment. The detected radiosonde signal is passed to separate equipment in the system where it is recorded. By reference to calibration data, these recorded data are converted to values of temperature, humidity, and pressure. Recordings of time versus progressive changes of the elevation and azimuth positions of the ascending balloon, as determined by tracking of the signal from the radiosonde, are converted to wind speed and direction.

16.2 SYSTEM COMPONENTS

16.2.1 Radiosonde VIZ 1680 MHz

This equipment consists of a transmitter, a modulator, an antenna, a battery, and pressure-, temperature-, and humidity-sensing elements. The pressure capsule employed is temperature-compensated and constructed to give approximately logarithmic response over the operating range. The temperature element is a rod of ceramic material with a high negative resistance coefficient. The humidity sensor is a plastic strip with a gelatinous cellulose coating that contains finely divided carbon particles in suspension. Resistance of the sensor increases with relative humidity.

The radiosonde in use for the low-level experiment was the VIZ 1680-MHz radiosonde equipped with ACCU-LOK sensors. These sensors are calibrated at the factory, thus eliminating the need for a baseline check before each observation. The assembled instrument weighs about 800 g and can be carried to an altitude of 30 km by a helium-filled balloon. The battery furnishes power to the transmitter and modulator. The transmitter operates in the 1660- to 1700-MHz band, and its carrier is amplitude-modulated by an audiofrequency pulse, the rate of which is determined by the pressure-, temperature-, and humidity-sensing elements.

Switching between temperature, relative humidity, and a calibration signal (reference) is achieved by a pressure-operated device called a baroswitch. With the ascent of the radiosonde the expansion of an aneroid capsule, through connecting mechanical linkage, causes a contacting pen to travel across a printed circuit board array of silver conducting strips mounted on insulated material. This is termed the commutator.

When the baroswitch pen rests on an insulated portion of the commutator the value of air temperature is transmitted by the radiosonde unit. The silver segments of the circuit board are used to switch the sonde to reports of relative humidity or references. The first four of every five silver segments on the commutator switch the radiosonde to report values of relative humidity whereas the fifth, tenth, fifteenth, etc., silver segments direct the sonde to a circuit which provides a fixed frequency of about 190 Hz. When this frequency is received at the ground station the meteorological recorder pen moves to approximately the 95th ordinate of the recording chart. This provides the radiosonde operator with a reference that enables him to adjust the setting of the recorder to exactly 95 ordinates and thus remove any subsequent linear errors in the temperature and

humidity values to be received until the next reference. On most U.S. radiosonde devices the 30th, 45th, 60th, etc., contact reports a slightly greater frequency, termed the high reference, which is used to facilitate counting the number of contacts received at the ground station.

Every radiosonde unit is delivered with a calibration chart which provides a value of pressure for each contact of the particular sonde.

16.2.2 Rawin Set

The rawin set automatically tracks by continuous homing on the radiosonde signal. The equipment indicates and records the azimuth and elevation angles of the radiosonde. These angles are plotted with the height (computed from the pressure and temperature data) to determine wind direction and speed.

16.2.3 Recording Equipment

Radiosonde meteorological data (temperature, humidity, reference data) are recorded on a time-frequency strip chart recorder. Elevation, azimuth angles, and elapsed time after balloon release are printed on paper tape.

16.3 TECHNICAL CHARACTERISTICS

Power input to the system is 105-129 V a.c., 50-65 Hz, 1,000 W. The frequency range is 1660-1700 MHz, and either an AM or FM signal can be used.

The RF system features conical scanning with a single dipole antenna and a parabolic reflector. The receiving system uses a superheterodyne receiver and an IF frequency of 30 MHz; its tracking accuracy is 0.05° maximum error between 10° and 60° elevation.

The antenna positioning system features automatic tracking, with the option of manual control locally.

16.4 DATA PROCESSING

At most operational GMD radiosonde stations data are manually processed. Temperature and humidity strip chart records and printed elevation and azimuth angles from the control recorder are analyzed with the aid of slide rules, graphs, and scales to yield profiles of temperature, humidity, and wind. For the BLIE, with six scheduled soundings per day (two of these on the tower carriage), there was not enough time for manual processing. Instead the operator manually transcribed data from the two hard-copy records onto a magnetic tape from which the data were entered by phone line into a Bureau of Reclamation computer. When conventional radiosonde reduction programs were used, the computer yielded processed data on a printer at the field site with a normal turnaround time of 1 min.

17. TDFS LOW-LEVEL RADIOSONDE SYSTEM

C. Fink and E. Schöllmann
Upper-Air Research Station
Deutscher Wetterdienst
Munich, Federal Republic of Germany

A. Kölbl
Instrument Division
Deutscher Wetterdienst
Munich, Federal Republic of Germany

17.1 LOW-LEVEL SONDE TDFS

The low-level sonde TDFS is a lightweight weather sonde for measuring temperature, humidity, and atmospheric pressure in the free atmosphere up to about 600 mb. For dry- and wet-bulb temperatures, bead thermistors with negative temperature coefficient (NTC) resistance, having diameters of 0.4 mm, are used. The measuring range is from -40°C to +40°C. The frequency of a subcarrier oscillator is changed in the range of 300-900 Hz by the temperature behavior of the NTC resistance. This subcarrier frequency modulates a crystal-controlled transmitter with a frequency between 402 and 406 MHz. The exact frequency can be determined subsequently for each sonde by a plug-in crystal. The modulated signal is transmitted by a half-wavelength antenna, which also serves as a means for suspension. Two small 9-V dry batteries are used for the power supply. The pressure-measuring element is an aneroid capsule of copper beryllium, which is temperature compensated over the entire measuring range. The measuring range of about 1,050 mb to about 600 mb is subdivided by gold-plated contacts in pressure steps of about 25 mb. The features of the sonde are listed in Table 17.1.

The case is made of white plastic that insulates well against cold. Its dimensions are 206 x 170 x 85 mm; the weight including batteries is 300 g. Both temperature sensors are housed in a foamed plastic tube that protects the sensors from mechanical influences and direct solar radiation and provides for an optimal air flow. Three views of the sonde are shown in Fig. 17.1.

17.2 RECEIVING STATION KS 75

The signals of the radiosonde are received by the UHF radiosonde receiver. Here the demodulation takes place; i.e., the measuring signals (frequencies of 300-900 Hz) are separated from the high frequency carrier and are available for further processing at the receiver output.

The special data-handling unit allows the low frequency signals of the sondes to be automatically evaluated. For this purpose four coefficients have to be inserted to describe the corresponding calibration curve. On the basis of the inserted sonde calibration curve, a microprocessor calculates the digitally measured low frequency values and shows a temperature in degrees Celsius in a digital display, at 1-s intervals.

During sonde reception the dry- and wet-bulb temperatures are received alternately, interrupted at irregular intervals by pressure signals that are represented on the strip chart recorder as rectangular steps. Figure 17.2 illustrates a portion of a typical strip chart record. Temperature values of -50°C to +50°C can be recorded with a resolution of 0.4°C/mm.

Two digital outputs (TTL level, BCD 1,2,4,8) available at the back of the receiving station make it possible to connect tape punches (e.g., hp 3,489 A) or computers

Table 17.1. Description of the low-level sonde TDFS

Feature	Description
Dimensions	Height 206 mm Width 170 mm Depth 85 mm
Weight with battery	300 g
Sensors	For dry- and wet-bulb temperature, matched bead thermistors, varnished in white; diameter 0.4 mm.
Temperature-measuring range	-40°C to +40°C
Pressure-measuring element	Aneroid capsule, CuBe
Pressure-measuring range	1,050 mb to ~600 mb in pressure steps of ~25-mb intervals; every fifth pressure step is a double step.
Resolution	Pressure ±0.5 mb Temperature ±0.1°C
Accuracy of system	Pressure ±2 mb Temperature ±0.4°C Psychrometric difference ±0.2°C
Transmitter frequency range	402 to 406 MHz crystal-controlled
Transmitter power	~25 mW
Modulation	Frequency modulation
Subcarrier frequency	300 to 900 Hz
Frequency bandwidth	±6 kHz
Frequency stability	±30 ppm
Antenna	Half-wavelength omnidirectional
Polarization	Vertical
Duration of operation	~45 min with alkali-manganese cells, Mallory MN 1604

for further processing of the data. The features of the receiving station are summarized in Table 17.2. The receiving station and the radiosonde were developed for the Deutscher Wetterdienst by Instrumentenamt München.

17.3 EVALUATION

Receiving station KS 75 produces an analog record (see Fig. 17.2) containing atmospheric pressure in the form of pressure steps and the dry- and wet-bulb temperature, in the correct physical units. The dry-bulb data are recorded during a period of about 6 s, and the wet-bulb data during a period of about 3 s. From the calibration table attached to each sonde the values of the pressure levels are obtained and the pressure time curve is plotted as shown in Fig. 17.2. Intermediate pressures may be interpolated

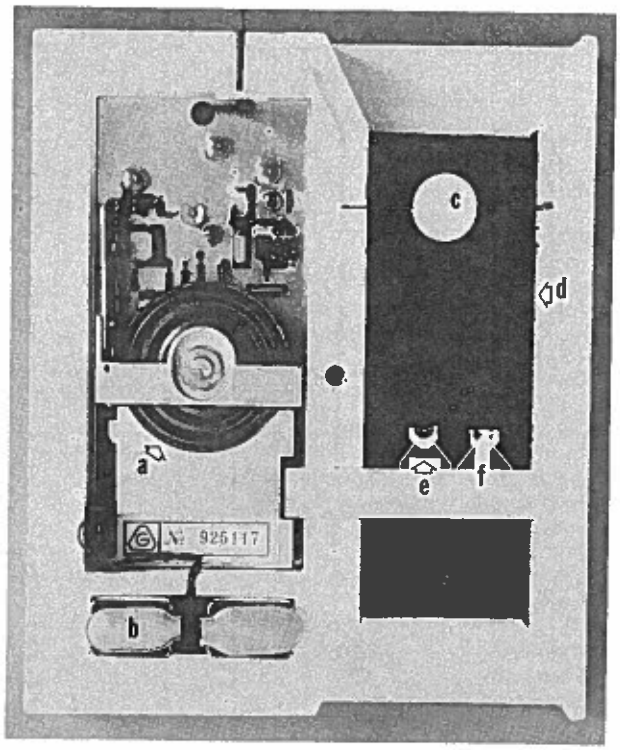

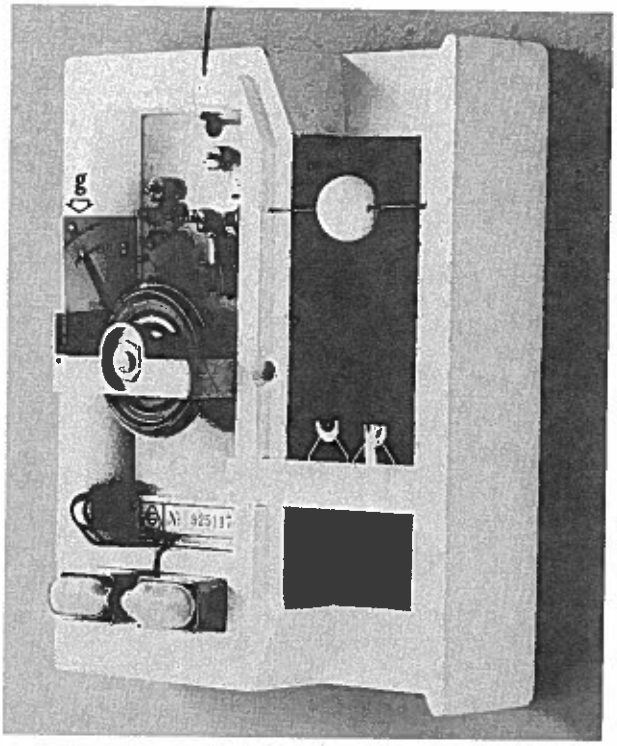

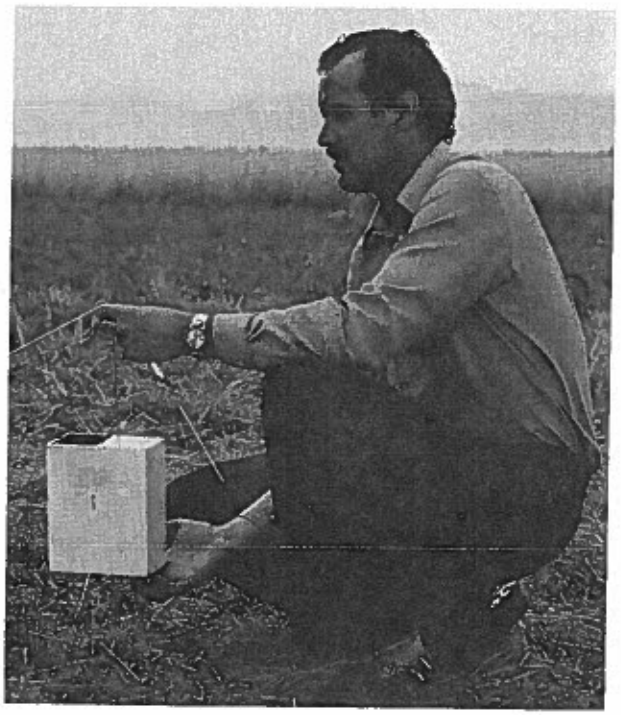

Figure 17.1. Low-level radiosonde of the Deutscher Wetterdienst: (above, left and right) cover removed to show (a) aneroid capsule, (b) batteries, (c) sphere, to create a turbulent air flow, (d) blackened air-duct, (e) dry-bulb thermistor, (f) wet-bulb thermistor, and (g) array of pressure contacts; (left) cover on for balloon launch.

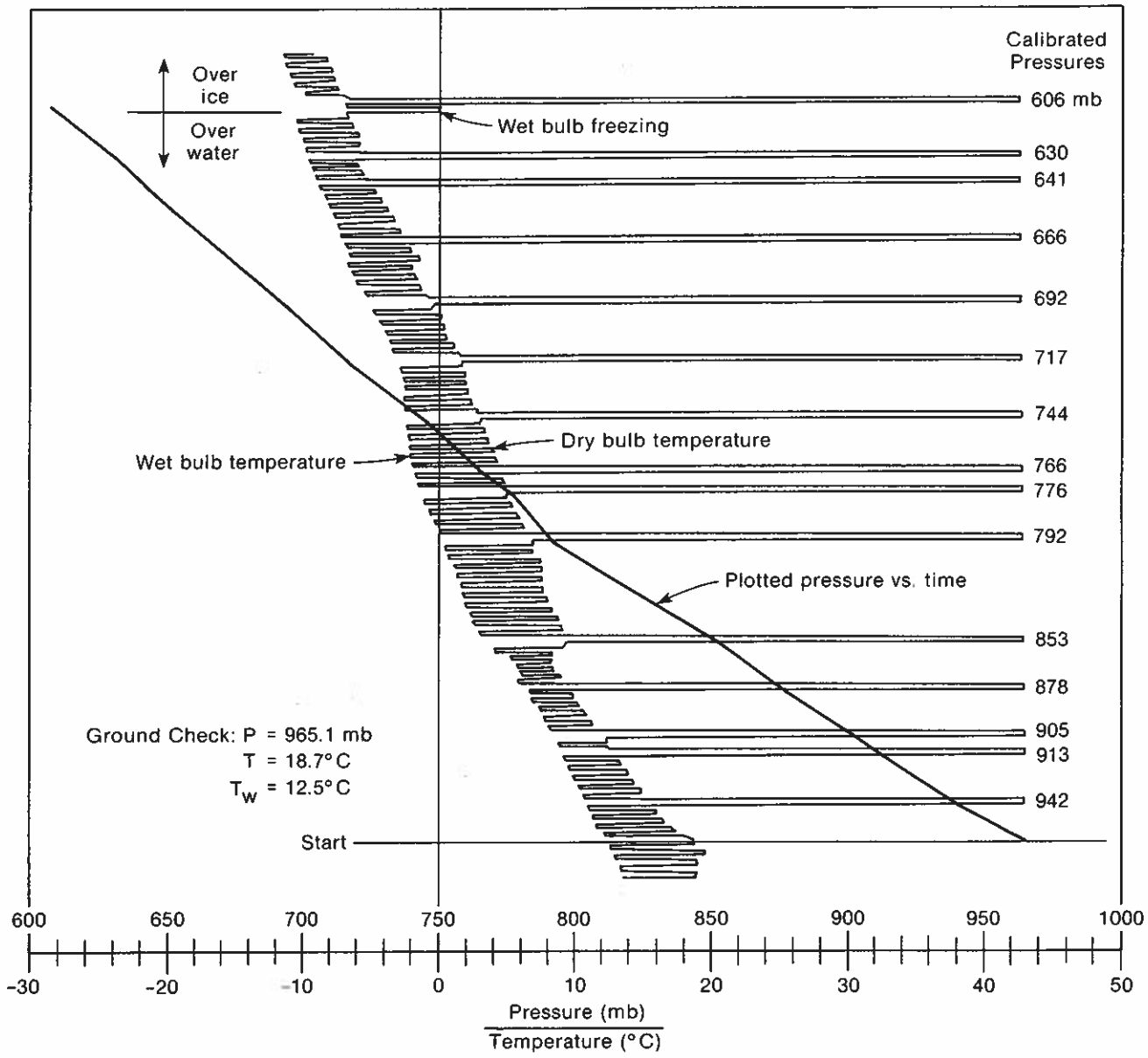

Figure 17.2. Analog record of a sounding showing the pressure vs. time curve plotted from the pressure calibration of the sonde and the occurrences of pressure readings. Note the warming to 0°C of the wet bulb at the instant of freezing.

from this curve. Then the significant levels of the dry- and wet-bulb temperature are selected. Pressure and dry- and wet-bulb temperatures for each significant level and for any mandatory pressure levels are inserted in a small programmable calculator to yield relative humidity, dew point, and height. The data for mandatory height levels are determined by interpolation. If a calculator is not used, the relative humidity has to be determined from psychrometric tables. The computation of the height is then made by using the Stüve diagram.

Table 17.2. Description of receiving station KS 75

Feature	Description
Dimensions	Height 440 mm Width 520 mm Depth 400 mm without paper cassettes and dust cover; 490 mm with cassettes and cover.
Weight	40 kg
Power input	220 V ± 10%, 50 Hz ± 20%, 100 VA
Input of calibration curve	4 coefficients
Temperatures	Digital indication
Analog recording	Alternating between dry- and wet-bulb temperatures, interrupted by pressure steps; temperature range -50°C to +50°C.

17.4 ACCURACY

Each sonde is calibrated by the manufacturer. The conversion of frequency into temperature is made by means of a polynomial of the third degree. Since only the coefficients of one calibration curve can be inserted into the receiving station KS 75, the thermistor for dry- and wet-bulb temperatures have to be matched. A deviation of ±0.1°C is acceptable. Because of digitalizing, the resolution of the station amounts to 0.1°C. When all sources of error are combined, the system accuracies are ±0.4°C for temperature and ±0.2°C for psychrometric difference. The lag-coefficient of the bead thermistors is about 2 s; it is larger with ice accretion. The change of the water from liquid to solid on the wet-bulb thermometer takes about 30 to 60 s, depending on the degree of supercooling and the moisture content of the air.

When a pressure step is reached during the ascent, a fixed resistor is switched in instead of the temperature sensor. The resulting step change in frequency provides an indication of the pressure contact on the strip chart. When the points are connected it yields the pressure versus time curve in Fig. 17.2. The leading edge is chosen for the calibration value. The calibration accuracy is ±0.5 mb. The occurrence of the event is reported with a maximum delay of 0.5 s. The accuracy of the entire system is ±2 mb.

18. CORA RADIOSONDE SYSTEM USING FREE-FLYING BALLOONS

Ilkka Ikonen
Vaisala Oy
Helsinki 42, Finland

CORA is an automatic upper-air system commercially available from Vaisala. The system is equipped with automatic computation and analog output for monitoring purposes. Manual evaluation is possible by using the analog output of radiosonde frequencies. The program for upper-air sounding stations, which make soundings for meteorological networks, is called CORA 6. In the BLIE a special computer program called CORA 8 EXP was used. The radiosonde used by the system is the Vaisala RS 21-12 CN, shown in Fig. 18.1.

18.1 RADIOSONDE RS 21-12 CN

18.1.1 General Characteristics

The general characteristics of radiosonde 21-12 CN are as follows:

Output frequency: 46.1 to 50.8 kHz.

Carrier frequency: 403 MHz (adjustable ±3 MHz).

Sensors: Low-altitude pressure P, aneroid barometer.
High-altitude pressure PP (above 150 mb), aneroid barometer.
Humidity U, Humicap thin film capacitor.
Temperature T, NiFe-alloy bimetal.
Two reference capacitors K1 and K2.
VLF receiver for the Omega system (13.6 kHz).

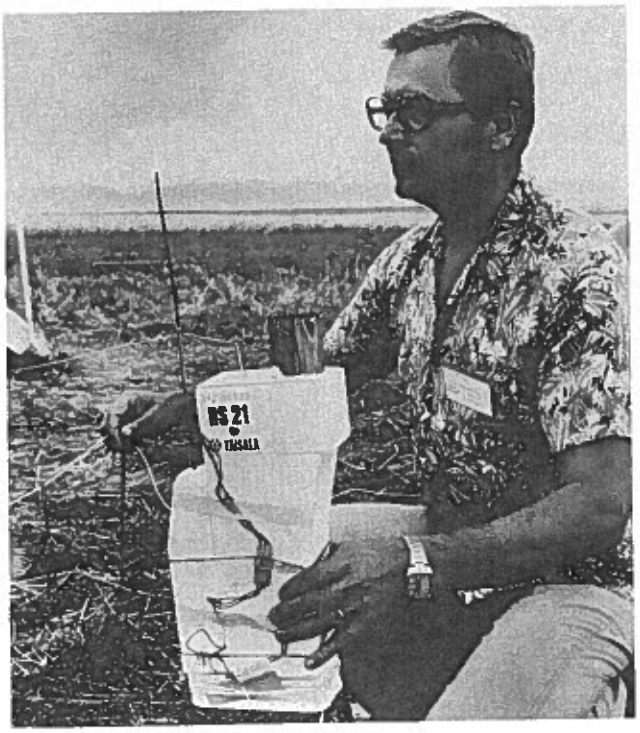

Figure 18.1 Vaisala radiosonde RS 21-12 CN before launch during BLIE.

The pressure and temperature sensors are linked mechanically to variable capacitors. Each of the six elements is connected in sequence to the modulating circuit by a switch attached to a rotating reel. The sonde is tied to the balloon by a line running from the reel. During ascent the weight of the sonde pulls line from the reel, causing it to rotate. During one cycle each element transmits for about 1.6 s. Winds are derived from the VLF reception of Omega signals.

18.1.2 Calibration

Each radiosonde is individually calibrated in the factory. Numeric calibration coefficients for P, PP, and T are available for automatic computation. U calibration is carried out during baselining.

18.2 GROUND EQUIPMENT

Hardware consists of the following main parts:

Teletype 43 ASR.
NOVA 2 minicomputer with 64-Kbyte memory.
NOVA cassette (3-drive C-cassette).
400-MHz receiver.
Omega receiver.
Radiosonde signal sampling unit.
Antennas for 400-MHz and local Omega reception.
Analog output devices for monitoring and manual evaluation.
Baselining equipment.

18.3 AUTOMATIC COMPUTATION

18.3.1 Output Format

The system offers two possibilities for data output: teletypewriter and C-cassette. Output made on the teletype has the following format:

tttt ZZZZZ PPPPP ±TTT UU DDD FFF,

where tttt is time for the level in seconds;

ZZZZZ is height in geopotential meters computed from pressure, temperature, and humidity using the hydrostatic equation;

PPPPP is pressure in 0.1 mb;

TTT is temperature in 0.1°C;

UU is relative humidity in %;

DDD is wind direction in degrees;

and FFF is wind speed in 0.1 m/s.

The system offers a wide variety of post-ascent processing capabilities using the data stored on the magnetic cassettes. Programs can be written and run in BASIC language using the CORA equipment.

18.3.2 Automatic Computation of PTU

Radiosonde signals from the six elements are received continuously, six frequencies in sequence per data frame. Each of the six frequencies is passed through its own digital filter that rejects impossible values.

Meteorological values are computed using the following procedure:

(1) Compute the corrected element value for P, PP, T, and U using the element in question and both reference capacitors.

(2) Compute the humidity value using a predefined calibration equation that is fixed during baselining.

(3) Compute pressure and temperature using individual calibration equations of second degree.

Pressure, humidity, and temperature at a specified time are computed as weighted averages of the two nearest observed values. Weighting is in proportion to nearness to the specified time.

18.3.3 Manual Computation of PTU

Manual computation is easily carried out by an operator using the automatic radiosonde receiver and evaluation ruler.

18.3.4 Wind Computation Specification

Wind computation is based on the Omega network. All eight Omega stations are always used. Both local wind and remote wind are determined, and a differential correction is made optionally. Wind is reported each 10-s interval, which corresponds to a full Omega sequence. In derivative computation a sliding second-degree curve across 4 min is used. A weighting is carried out to get an optimal solution in the sense of least squares fitting. If the quality is under a certain pregiven level, the weight of that particular signal is zero. Although the accuracy of Omega-derived winds depends on local Omega reception conditions, it is the experience of Vaisala that, in most cases, the wind vector is accurate within 1-2 m/s.

18.4 INTERCOMPARISON DATA

(1) Automatic computation listing in the format described in 18.3.1, at 10-s intervals.

(2) Pressure, temperature, and humidity transferred on the Vaisala low-level sounding aerogram.

(3) Manual readings from automatic radiosonde receiver, transferred on the Vaisala low-level sounding aerogram.

19. THE AIRSONDE SYSTEM

David B. Call
Atmospheric Instrumentation Research, Inc.
220 Central Ave.
Boulder, Colorado, U.S.A.

Alvin L. Morris
Ambient Analysis, Inc.
3300 Arapahoe Ave.
Boulder, Colorado, U.S.A.

19.1 INTRODUCTION

The Airsonde™ meteorological sounding system (Fig. 19.1) is a complete, highly portable system in which precision sensors and solid-state electronics are combined to yield digital data in standard meteorological units in real time. It is designed for use with small (30- and 100-g) balloons and is capable of reaching heights greater than 10 km.

The Airsonde sensor package (hereafter called the Airsonde) is contained in an expanded polystyrene package (see Fig. 19.2) in the form of a helicoid propeller. As it rises or descends, its spinning aspirates two bead thermistors mounted in radiation shields at the tips of the propeller. One is covered by a wick that is wetted by water contained in a small reservoir, and the two form a psychrometer. Pressure is sensed by an aneroid capsule whose temperature is measured by a third bead thermistor. No baseline measurements are required for most uses of the Airsonde system.

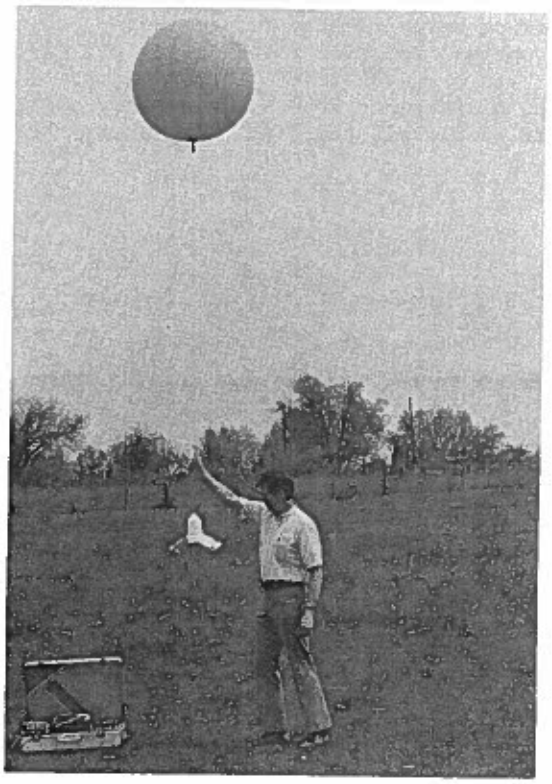

Figure 19.1. The Airsonde system with an inflated 30-g balloon. The aluminum case to the left contains the ground station.

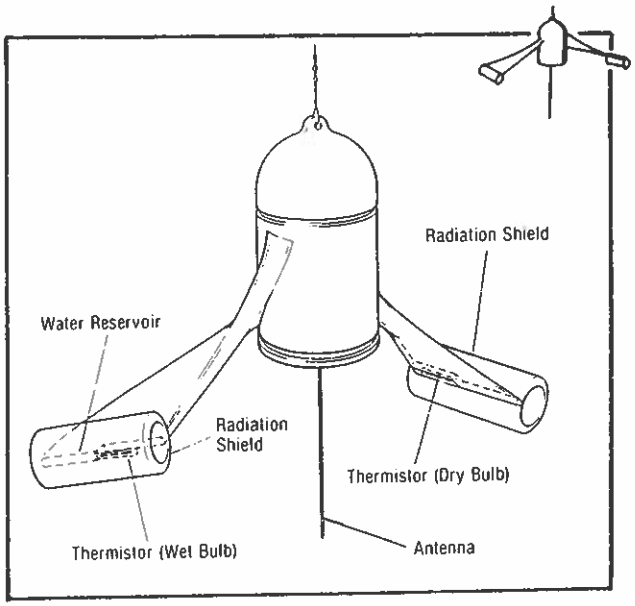

Figure 19.2. Schematic diagram of an Airsonde.

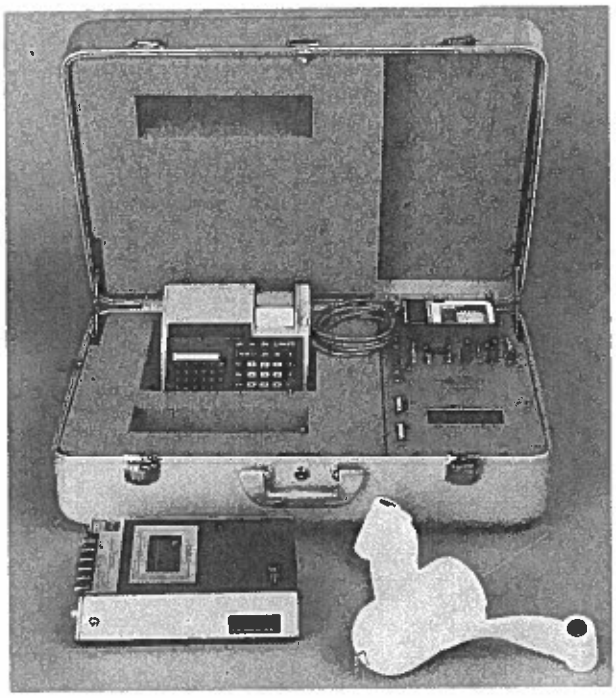

Figure 19.3. Airsonde ground station mounted in aluminum suitcase. Modified HP-97 is shown in foam cutout. Similar cutout is for tape recorder beside Airsonde in front of case.

An electronic multiplexer samples the sensors sequentially once every 6 s. The Airsonde mass, complete with battery, is 130 g. The transmitter, a narrow-band, crystal-controlled, solid-state device, transmits data in analog form, radiating 25 mW of power at a frequency of 403.5 MHz.

The Airsonde ground station (Fig. 19.3) is interchangeable with that of the Tethersonde, described in Chapter 20. Enclosed in an aluminum case, the ground station consists of a receiver, a small strip chart recorder, a microcomputer, a visual digital display, a battery charger, and a power supply. It may be operated on either 110 V a.c. or 12 V d.c. For soundings up to 300 mb the ground station may be used with an omnidirectional, half-wave antenna; for higher-level soundings a higher-gain antenna is used.

In the ground station the incoming analog telemetry signal is converted to a digital signal, which is then processed by the microcomputer. Digital data from the ground station may be printed on a modified Hewlett-Packard Model HP-97 programmable printing calculator, or recorded on either digital or analog tape recorders. Table 19.1 shows sample printout information from an HP-97 during an Airsonde flight. Figure 19.4 is a graph of the Airsonde sounding data from a flight.

19.2 OPERATIONAL CHARACTERISTICS

The Airsonde used in BLIE measured pressure, temperature, and wet-bulb temperature. Complete profiles of these variables, or of variables such as relative humidity or potential temperature that can be derived from the measured variables, are attainable.

Table 19.1. Examples of Airsonde system data printouts from a modified HP-97 printing calculator

Observed data printout*		Observed and calculated data printout†	
Variable§	Printout	Variable§	Printout
Time	20.8 ***	Time	9.2139 ***
T (°C)	15.4 ***	P (mb)	818.6 ***
Tw(°C)	8.6 ***	T(°C)	9.0 ***
P(mb)	820.4	RH (%)	43.8 ***
		w(g/kg)	6.0 ***
		z(m)	17.6 ***
		θ(K)	305.6 ***

* A real-time printout of observed data only. The time, 20.8, is elapsed time in decimal minutes after the ground station was set to receive and process data. Real-time printout is for every second or third frame of data.
† A printout of observed and calculated data from post-flight playback of tape recorded data. The time is read 9 h, 21 min, and 39 s. On playback every data frame can be printed out if desired.
§ Note that the variable columns shown here are not part of the HP-97 printout.

The basic Airsonde ground station is quite versatile because it has both analog and digital outputs and because it interfaces with a number of peripheral devices. Communication with these devices is through two 25-pin connectors, one of which provides RS-232C and 20-mA signal levels to operate a cathode ray terminal, teletypewriter, or modified HP-97 printing calculator, whereas the other provides a terminus of 16 bi-directional data lines, 8 of which are control lines. The latter connector gives the user a general-purpose programmable interface and provides control and data signals as well as power for recording data in ASCII FSK on an analog cassette tape recorder.

The most commonly used peripherals are a magnetic tape recorder and a modified HP-97 calculator. Digital data are tape recorded during flight. In addition the HP-97 may be used to calculate data shown in Table 19.1(right) for every fifth frame or to print every third frame in real time. After the flight the taped record may be played back through the ground station to the HP-97 at a selectable slower rate, and the HP-97 may be programmed to do various calculations with every data frame, printing calculated as well as measured variables.

The program has certain editing features. For example, while integrating the hydrostatic equation to calculate height, the program compares current and previous frames of data for apparent discrepancies. If the difference in either temperature or pressure is excessive according to the criteria programmed into the calculator, the program rejects the current data for calculations, but prints current time, pressure, and temperature. The operator can observe these and override the program decision at will.

The Airsonde is normally flown on either a 30- or 100-g balloon. Guidelines for balloon inflation are provided by the curves of Fig. 19.5, which relate ascent rate of the Airsonde to weigh-off mass. (Weigh-off is the total mass, including inflation device, suspended from the balloon during inflation. Gas is added until the balloon is in neutral equilibrium with the weigh-off mass.) Separate curves are given for both helium and hydrogen and for 30- and 100-g balloons. The curves are approximate and are based on data obtained by dropping the Airsonde from a tower and considerations of balloon drag and buoyancy. An ascent rate of more than 1 m/s is necessary to assure adequate aspiration of the psychrometer. In the intercomparison experiment the Airsonde was flown in tandem with other types of radiosondes from a single 300-g balloon.

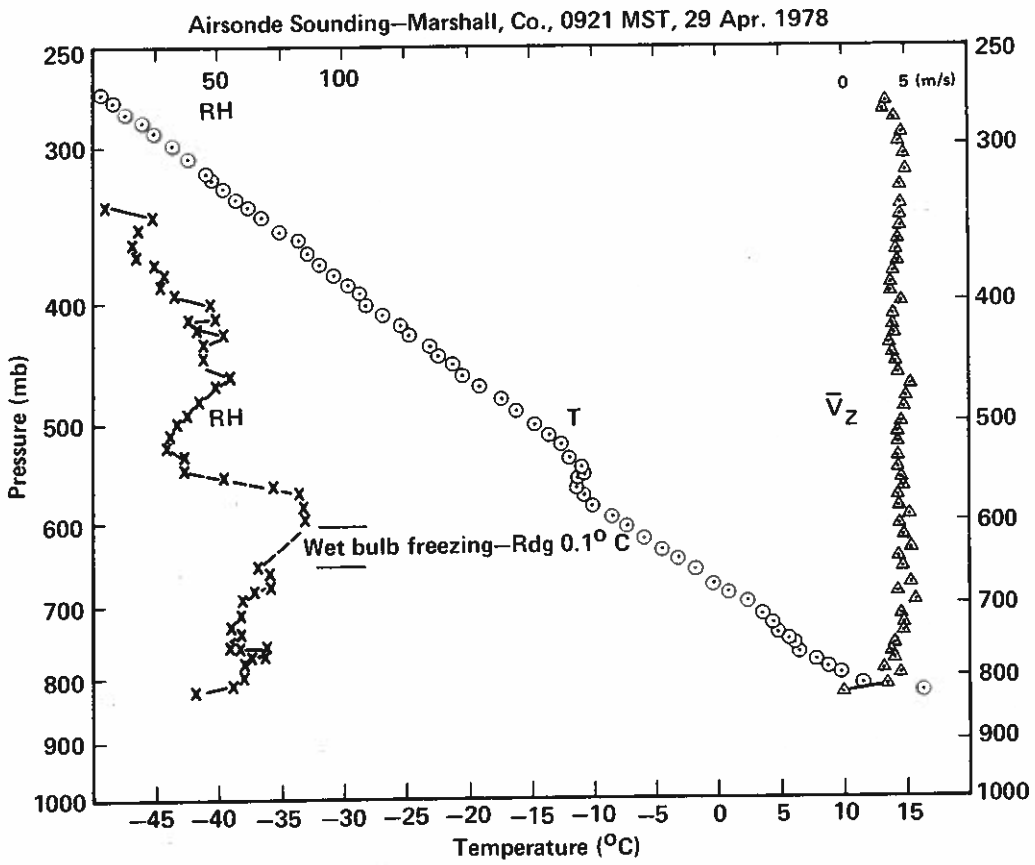

Figure 19.4. Sample Airsonde sounding, every fifth data frame, with additional detail between 750-760 mb and 550-560 mb. Note that the wet-bulb freezing temperature provides a convenient temperature check. The HP-97 program used for this sounding calculates vapor pressure over ice for all values of $T_w < 0°C$.

19.3 SENSOR CHARACTERISTICS

19.3.1 Temperature-Humidity

The precision bead thermistors used in the Airsonde are epoxy-coated sensors manufactured to precise tolerances. Interchangeability and accuracy of ±0.2°C from +50° to -20°C are stated by the manufacturer; typical performance is better.

The Airsonde system ground station measures the resistance of each thermistor and interpolates data from a table to derive dry-bulb and wet-bulb temperatures. Error introduced by the mathematical computation is an insignificant 6.0×10^{-3} °C in the worst case.

Since the psychrometric technique of measuring humidity is more sensitive to wet-bulb depression than to either dry- or wet-bulb temperature, the circuitry was designed to assure an accurate measure of the depression. An electronic multiplexer switches the dry- and wet-bulb thermistors into the measurement circuitry within 1 s of each other during each 6-s frame. This is considerably faster than an Assmann psychrometer can be read. A possible 0.1°C error, traceable to manufacturing tolerances in reference resistors and to

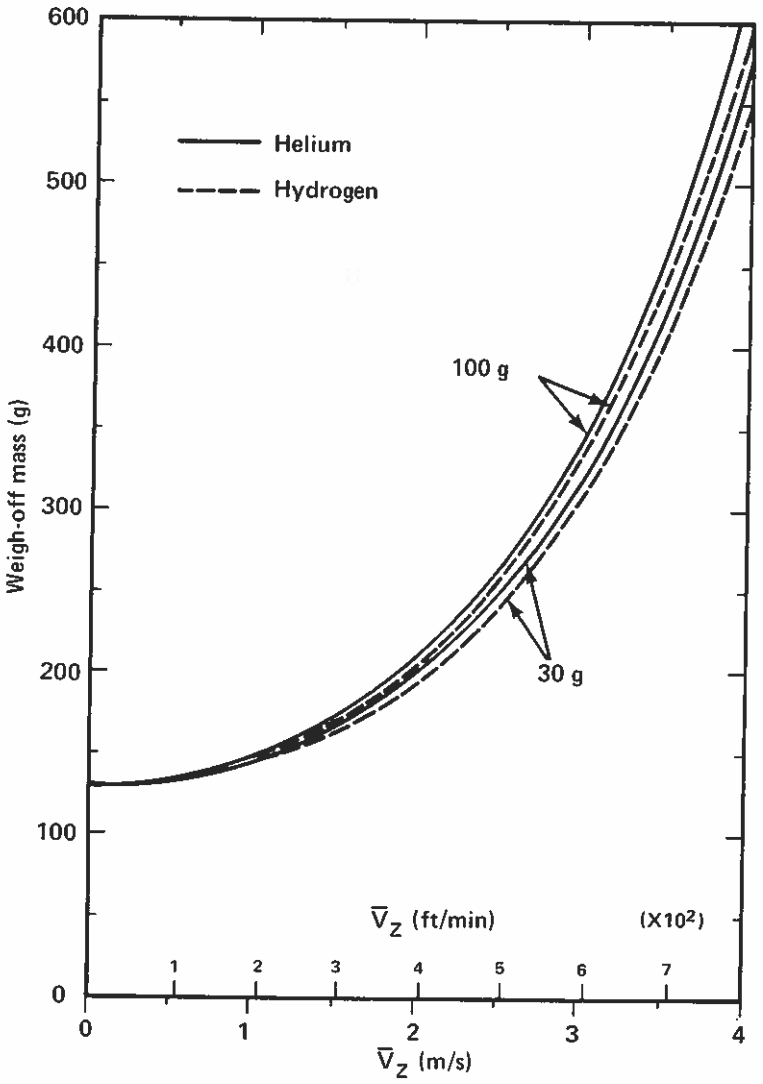

Figure 19.5. Graphic aid for calculating the weigh-off mass to be used when inflating Airsonde balloons.

switch resistance, is common to both dry- and wet-bulb temperatures and is therefore absent from the wet-bulb depression.

Good psychrometry requires that the sensors be properly exposed. They must be adequately aspirated and protected from the effects of radiation. Fast response is essential in a sounding system that moves rapidly through strata in which humidity gradients are large. The dry-bulb thermistor has a time constant of 10 s in still air and 3 to 5 s with the rotational aspiration that occurs at nominal ascent rates (2 to 4 m/s). The wet-bulb response time, which has been observed only in a very limited way, is believed to be about three times that of the dry bulb.

Each thermistor is mounted in its own radiation shield. The shield, a tube of molded expanded polystyrene, has small thermal mass and is a good insulator. Since the Airsonde rotates about a vertical axis during flight, direct insolation to the bead can occur for only a small fraction of each rotation and is therefore not significant. Diffuse radiation is minimized by blackening the inside surfaces of the shields.

Aspiration is achieved by the spinning of the helicoid propeller-shaped Airsonde as it ascends or descends. A minimum aspiration rate of 3 m/s is recommended (Bindon, 1965). The Airsonde is designed to produce an airspeed past the propeller tips equal to

three times its ascent rate. The helicoid shape also assures that airflow over the entire propeller is parallel to the surface. Thus, the air flows axially through the radiation shield tubes at the propeller tips.

19.3.2 Pressure

The Airsonde pressure transducer is a variable capacitance aneroid cell consisting of a square ceramic substrate with the aneroid capsule bonded symmetrically to both sides. A metalized area of the ceramic substrate forms one plate, and the capsule forms the other plate of the sensing capacitor. Hence, the sensing capacitor is inside the cell where the dielectric is an unchanging vacuum, resulting in a small and rugged sensor. A similar pressure sensor has been in use at NCAR for several years (Pike and Bargen, 1976). The cell is 3.18 cm on a side and 0.76 cm thick. It has a capacitance of 10 pF at 1,000 mb. Its sensitivity is 0.03 pF/mb.

Unlike the dry- and wet-bulb thermistors, whose calibration and interchangeability are well defined, each aneroid cell must be calibrated individually. The calibration yields a curve of pressure versus capacitance that can be fitted adequately by a second-degree polynomial. Four coefficients, one of which is a temperature compensation coefficient, are provided with each Airsonde. These are placed in the computer through thumbwheel switches before launch. The computer executes a program that does the curve fitting in real time for every frame of Airsonde data. This technique gives pressure readings in millibars with a characteristic absolute accuracy of ±3 mb from 1,000 to 300 mb. Accuracies of ±1 mb can be achieved through that pressure range if a baseline correction from a good reference barometer is entered into the ground station. Under standard procedures the Airsonde is not calibrated for pressures less than 300 mb. Hence, flights above 300 mb may have errors that are considerably greater than ±3 mb, unless the Airsonde has been calibrated at those pressures and an additional correction is made to the data.

19.4 ELECTRONICS

19.4.1 Airsonde

Figure 19.6 is a block diagram of the Airsonde. The transmitter is a conventional frequency-modulated crystal-controlled circuit. It uses a voltage-controlled crystal oscillator and 9X frequency multiplication to generate 25 mW at 403.5 MHz. Temperature stability and narrow ±5-kHz frequency deviation permit use of narrow band receivers with very high sensitivity. The combination of small transmitter power and high receiver sensitivity allows a standard 9-V transistor radio battery to serve as the transmitter power source. This battery is widely available, lightweight, sealed, and inexpensive.

Sensor conditioning circuitry is simple, requires little power, and uses inexpensive, readily available components. The use of precision references for both resistive and capacitive sensors eliminates the need for calibration of each sonde.

The Airsonde has two RC data oscillators. One provides a frequency whose period is linearly proportional to resistance. An electronic switch acts as a timing element and inserts three reference resistors and then three sensing thermistors sequentially in this RC oscillator. The first resistor (R_{SYNC}) has a low value that establishes a high synchronization frequency, which the microcomputer interprets as the start of a frame. The next two reference resistors (R_{LOREF} and R_{HIREF}) are precision components whose accuracy allows the microcomputer to calibrate the data link in software during each data frame. Knowing the values of these two reference resistors (10 kΩ and 100 kΩ), the microcomputer can measure the resistance of three subsequent thermistors (R_{TINT}, R_{TDRY}, and R_{TWET}) to an accuracy of 1%, from which it can compute temperature to ±0.2°C, the inherent thermistor accuracy. The circuit has particular advantages in psychrometry because both dry- and wet-bulb sensors use exactly the same measurement circuitry separated in time by 1 s. The only error sources in the circuitry that can contribute to a differential error are switch resistance differences and digitalization errors in data processing. The electronic switches

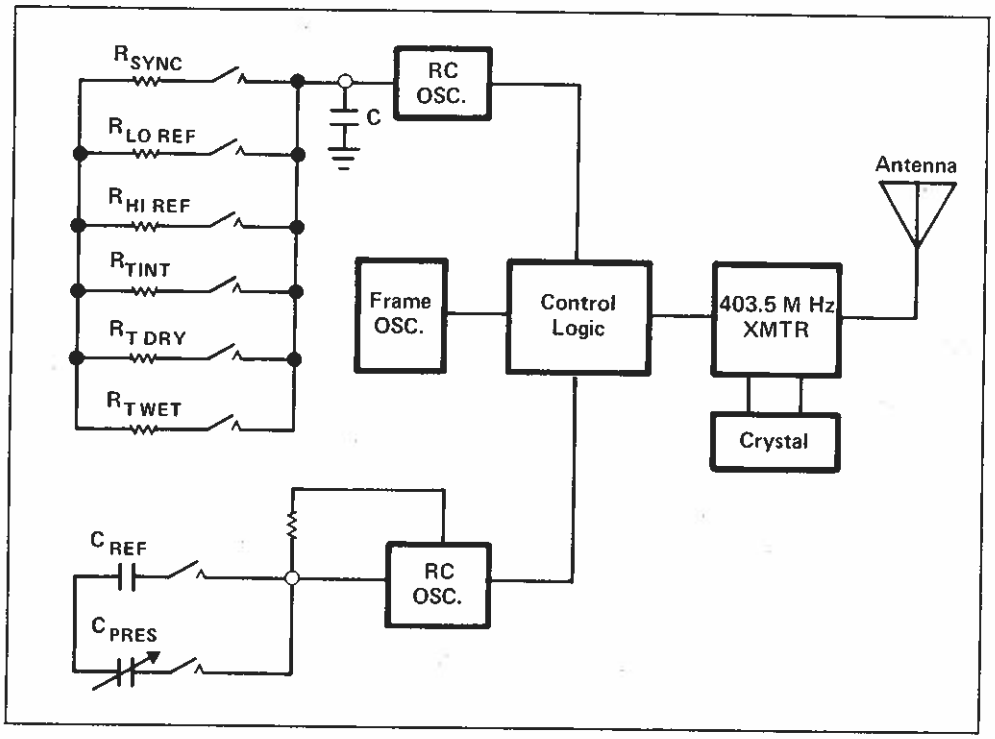

Figure 19.6. Block diagram of an Airsonde.

are contained in a single, mass produced, integrated circuit. The typical ON resistance of these is matched within a few ohms, an insignificant difference.

A second RC oscillator uses a CMOS gate as the frequency source. It switches sequentially first to a stable reference capacitor (C_{REF}) and then to the aneroid pressure-sensitive capacitor (C_{PRES}). The ratio of these two frequencies is proportional to pressure. The thermistor that measures internal Airsonde temperature (R_{TINT}) is mounted on the pressure sensor, and its temperature is used by the microcomputer to correct the pressure measurement for the temperature coefficient of capacitance of the aneroid cell.

19.4.2 Ground Station

The Airsonde-Tethersonde ground station (Fig. 19.3) is designed for the field environment. Mounted in an aluminum suitcase it is portable and ruggedly constructed. All electronics, including the four receiver modules, are installed on one 7½-in x 9½-in printed circuit card that is mounted on six standoffs to the aluminum front panel. This configuration is easy to service and transport.

The ground station can be logically divided into analog and digital sections, as shown by Fig. 19.7. The analog section includes the FM receiver, audio active filters, and phase-locked loops (PLL). One PLL is tuned for 500 ± 125 Hz. This 500-Hz PLL is used with the Tethersonde continuous analog channel and has no function with Airsonde operations. A second PLL, tuned for 2,500 Hz, acts as a bandpass filter with excellent signal-to-noise ratio performance for Airsonde or Tethersonde data. It converts the sine wave signal to a square wave for input to the 16-bit frequency counter.

The 8080-A microprocessor and associated memory and peripheral integrated circuits form a general purpose microcomputer. All system software resides in memory where it is available whenever the system power is turned on.

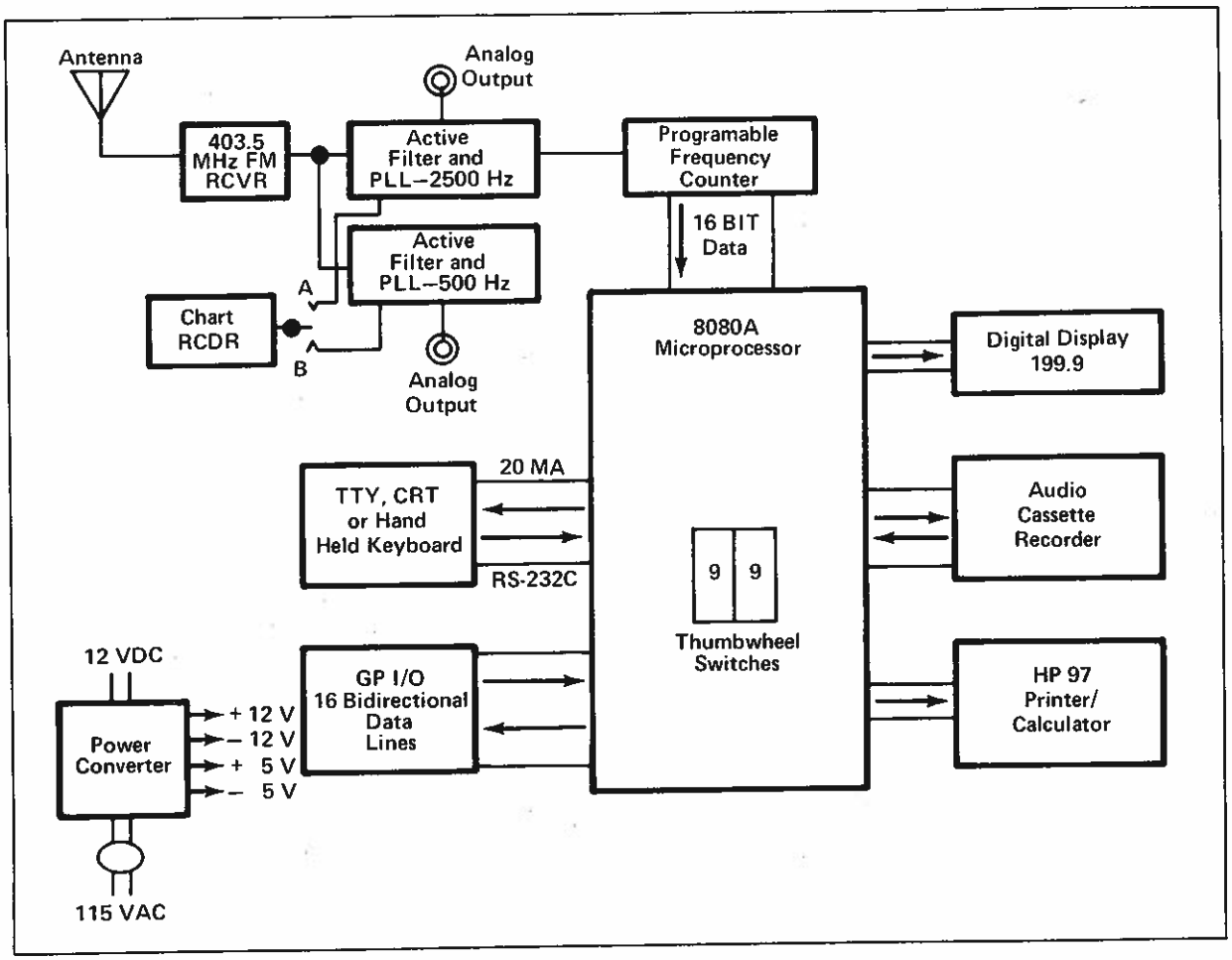

Figure 19.7. Block diagram of an Airsonde-Tethersonde ground station.

The ground station displays and stores Airsonde data in various ways. The primary display is a 3½-digit light-emitting diode (LED) display. All data are displayed in real time. One of seven individual LEDs also lights above an engraved legend that identifies the parameter currently being displayed and gives its meteorological units.

Hardcopy records can be printed on ASR-33 teletypewriter or HP-97 printing calculator (see Table 19.1). The same records can be displayed on most common CRT terminals and line printers. The standard HP-97 calculator has been modified for this application by a small printed circuit card to give the microcomputer access to various storage registers in the calculator. The microcomputer sends data to HP-97 storage registers and initiates execution of programs stored in the programmable HP-97.

Permanent storage of data in a form readable by external computers is provided by microcomputer circuitry that controls standard audio magnetic cassette recorders. The Sony TC-142 gives excellent performance and is battery powered. Digital data are converted into a series of discrete audio tones for audio recording. A standard cassette will record several hours of Airsonde or Tethersonde data. These data may be played back into the ground station at any time for conversion to other computer-compatible media. On playback the data are converted to the same format as real-time data, so all peripherals that are used with real-time data will work without change on recorded data.

19.5 DATA CONSISTENCY TESTS

To determine the consistency of the overall data processing subsystem during flight, the wet-bulb thermistor was replaced by a precision reference resistance equivalent to a 25.0°C wet-bulb reading. During the course of a flight from 843 mb to 314 mb, the average wet-bulb temperature reading was 24.94°C, and the standard deviation of the values was 0.05.

In a second flight test, the wet-bulb thermistor was left bare so that it was sampling dry-bulb temperature. The two sets of dry-bulb temperatures were compared for temperatures ranging from 27°C at the surface to -5° at 550 mb. The mean difference was 0.08°C, and the standard deviation of the differences was 0.04, which is within the specifications for interchangeability of the thermistors.

19.6 REFERENCES

Bindon, H. H. (1965): A critical review of tables and charts used in psychrometry. In Humidity and Moisture, Measurement and Control in Science and Industry, Vol. 1, Robert E. Ruskin (ed.), Reinhold, New York, pp. 3-15.

Morris, A. L., D. B. Call, and R. B. McBeth (1975): A small tethered balloon sounding system. Bull. Am. Meteorol. Soc. 56:964-969.

Pike, J. M. and D. W. Bargen (1976): The NCAR digital barometer. Bull. Am. Meteorol. Soc. 57:1106-1111.

20. THE TETHERSONDE SYSTEM

Alvin L. Morris
Ambient Analysis, Inc.
3300 Arapahoe Ave.
Boulder, Colorado, U.S.A.

David B. Call
Atmospheric Instrumentation Research, Inc.
220 Central Ave.
Boulder, Colorado, U.S.A.

20.1 INTRODUCTION

A small tethered balloon system, developed at the National Center for Atmospheric Research (NCAR), has been described by Morris et al. (1975). The Tethersonde™ system, successor to the NCAR system, is similar to it in many ways. Probably the most significant difference to the user is the treatment of data in the ground station. The Tethersonde Model TS-2A described here provides analog data quite similar to those provided by the NCAR system; it also provides digital data in conventional meteorological units.

A Tethersonde system ready for flight is shown in Fig. 20.1. The principal components of the system are (1) an airborne sensor package, (2) an aerodynamically shaped balloon (blimp) that carries the sensor package aloft, (3) a variable-speed reversible electric winch used to control tether line, (4) a ground station, and (5) several items of ancillary equipment. The components of a Model TS-2A system, excluding the balloon but including a modified HP-97 printing calculator, are shown in Fig. 20.2.

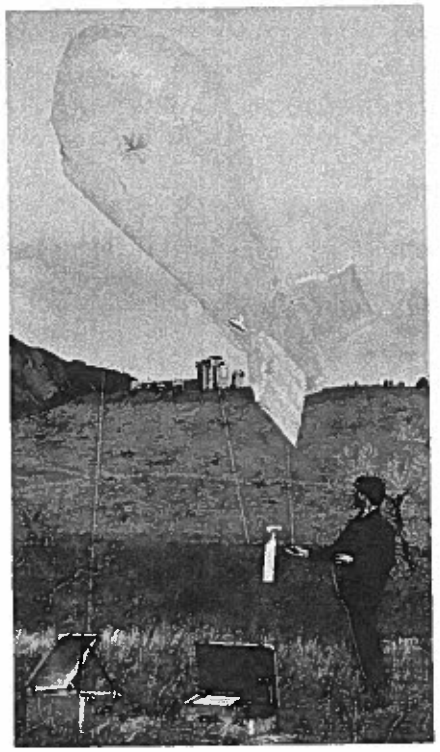

Figure 20.1. Tethersonde system ready for flight. The balloon and sensor package fly better if a rigid spacer (not shown) is placed between the suspension lines at about the level of the lowest part of the bottom tail fin and tied to the tail fin. The properly inflated 3.25 m^3 balloon is about 5 m long.

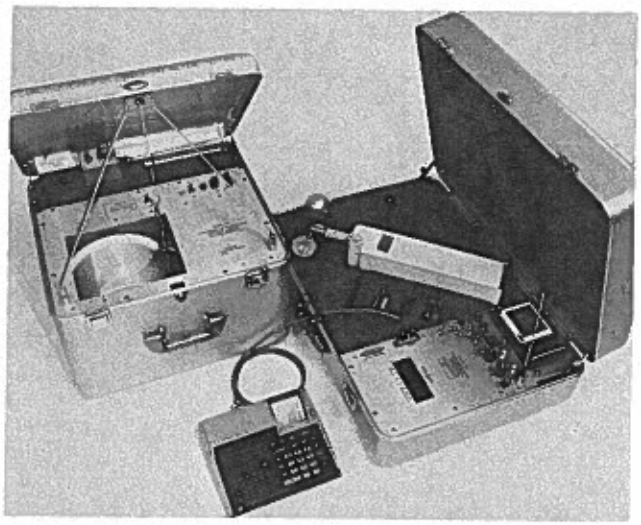

Figure 20.2. Tethersonde system, including winch, ground station with the sensor package in its cradle, and modified HP-97 printing calculator. The case containing the ground station is 24 x 47 x 67 cm. The mass of the winch is 20 kg; the mass of the ground station and sensor package is 11.5 kg.

During operation, the tethered balloon lifts the sensor package, which samples pressure, temperature, wet-bulb temperature, and wind direction and wind speed in its normal operational mode. With additional, attachable sensors, ozone, carbon monoxide, and the temperature structure parameter C_T have also been measured by the Tethersonde system.

Sensed values are transmitted to the ground station through two data channels on FM-FM telemetry using a carrier frequency of 403 MHz. One of the data channels carries continuous data from a selectable sensor; the other uses a time multiplex format to carry data from one to eight sensors.

At the ground, the telemetry signal is converted to an analog voltage that may be recorded on a strip chart recorder and to digital data that are displayed by light-emitting diodes. The digital data are also available to external data storage and processing devices.

20.2 OPERATIONAL CHARACTERISTICS

20.2.1 Sensor Package

The standard instrument package contains circuits which automatically interrogate the sensors and condition sensor signals for transmission to the ground. Temperature is measured over the range of -50°C to +50°C; relative pressure is measured over the range 0 to 100 mb. Signals are scaled directly for these ranges; signals are also scaled for four 25°C and four 25-mb ranges. By using two range scales for temperature and pressure, adequate resolution may be obtained on a small strip chart recorder without causing ambiguity.

The telemetry system consists of an FM, crystal-controlled transmitter and receiver. Data are transmitted at 403 MHz in two formats on separate frequency multiplexed audio channels. One channel uses an FM-FM PAM time multiplex format which may be recorded immediately on a single strip chart or audio magnetic tape or both simultaneously. In this format data quality is ensured by including high and low reference data in the recordings. On the second channel, data from any one sensor are transmitted continuously in FM-FM so that spectral information to 10 Hz can be telemetered.

A data frame in the time multiplex format consists of a wide sync pulse whose amplitude is full scale, followed by eight sensor channels separated by zero reference values. All sensor data are linear and are scaled in meteorological units for convenient chart interpretation. Standard sensor ranges are the following:

Dry-bulb temperature: 25°C and 100°C.
Wet-bulb depression: 25°C.
Pressure: 25 mb and 100 mb.
Wind speed: 20 m/s.
Wind direction: 360°.

All sensors are calibrated as part of the system using standards which are traceable to NBS or are based on fundamental physical principles. Periodic recalibration and certification service is available at the factory, but no baseline or reference calibration of any kind is required in the field. It is necessary to have a separate barometric reading if absolute pressure is required.

20.2.2 Ground Station

The Model TS-2A-GS ground station receives a telemetry signal from the sensor package, processes the signal, and yields both analog and digital outputs. The analog output may be recorded on an external recorder or on a small strip chart recorder contained in the ground station or on both. Digital data are displayed by light-emitting diodes. Two 25-pin connectors permit the transfer of data in several modes. One provides RS-232C and 20-mA signal levels for cathode ray tube, teletypewriter, or an optional programmable, printing calculator. The second connector is the terminus of 16 bi-directional data lines, 8 of which are control lines, giving the user a general purpose programmable interface. This connector also provides power, control, and data signals so that digital data in ASCII FSK may be recorded on and read from an inexpensive audio cassette recorder. All ground-station functions are controlled by a built-in, 8-bit microcomputer (8080A).

The ground station also processes Airsonde signals as described elsewhere in this report. It may be operated on 12 V d.c. or 120 V a.c. (220 V a.c. option available).

20.2.3 Winch

The electric winch is enclosed in a suitcase-size aluminum case that protects all parts, including the line, during shipping and storage. When in use, the lid of the case and a small A-frame (which folds inside the case, Fig. 20.2) form the support for a line guide a short distance above a second line guide on a level-wind. The level-wind assures proper winding of the tether line on the winch drum.

Controls on the winch are contained in a small hand-held box at the end of a cable. This enables the user to stand under the balloon as shown in Fig. 20.1 while launching and recovering the sensor package. The controls consist of a switch with UP, DOWN, and OFF positions and a knob with which to control the speed of the drum.

20.2.4 Ancillary Equipment

20.2.4.1 Additional sensors

Five of the eight sensor channels in the time multiplex format are used for standard meteorological variables. The other three can be used to repeat a variable or for additional sensors.

20.2.4.2 Output devices

The most common devices for receiving output from the ground station are a chart recorder, a modified Hewlett-Packard printing calculator, and a tape recorder. The analog output is a voltage. To record it a chart recorder should respond to an input of 0 to 5 V and have a full-scale response time of less than 0.5 s.

Digital data may be sent to a teletypewriter or a modified HP-97 printing calculator. The modified HP-97 is capable of receiving data, making calculations, and printing both the original and computed data. Since the calculator is easy to program, the user can readily calculate any quantity permitted by the meteorological data from the ground station and the capacity of the calculator. Potential temperature and mixing ratio are two commonly calculated quantities.

20.3 SENSOR CHARACTERISTICS

20.3.1 Temperature-Humidity

Temperature and wet-bulb depression are measured by thermistor networks which form the sensing elements of a psychrometer. Each network produces a voltage output that is linear with temperature. The manufacturer of the networks claims $\pm$0.15°C accuracy and interchangeability, and a deviation from linearity of $\pm$0.16°C. The deviation from linearity is a known function of temperature; consequently it can be removed if desired.

Both the dry- and wet-bulb temperature sensors are placed along the axis of a double-walled, cylindrical radiation shield that is pointed into the wind. The temperature element is ahead of the wet-bulb element in the flow, and the two are separated enough to prevent evaporation from the wet-bulb from affecting the dry bulb. A small fan at the rear of the tube aspirates the sensors. Water from a small reservoir flows along a wick and keeps the cover of the wet-bulb sensor wet.

The circuitry in the sensor package measures temperature and wet-bulb depression; it does not measure wet-bulb temperature. This assures an accurate wet-bulb depression even when temperature or wet-bulb temperature may be changing rapidly with time. If wet-bulb depression is less than 5°C, the deviation from linearity of the depression never exceeds $\pm$0.1°C. With a wet-bulb depression of 10°, the linearity error could reach $\pm$0.17°C.

The time constant (i.e., the time for the sensor to reach 63% of a step change in temperature) of the dry-bulb sensor is about 5 s in the aspirated psychrometer. The time constant of the wet-bulb sensor is believed to be about 15 s, but this value is not well established.

Tests under steady-state conditions have shown the Tethersonde psychrometer to be the equal of any good Assmann psychrometer.

20.3.2 Pressure

Pressure is measured by a barometer that is similar to the NCAR digital barometer described by Pike and Bargen (1976). The barometer is also essentially the same as the one described in the companion paper on the Airsonde system. In the Tethersonde system, however, pressure measurements are relative. By using a potentiometer in the sensor package, pressure output is adjusted to read zero at the ground. After launch the output is the difference from surface pressure rather than the absolute pressure.

20.3.3 Wind Speed

A three-cup anemometer mounted on top of the sensor package turns a small tachometer generator. According to the anemometer manufacturer, the threshold is 0.4 m/s, the distance constant is 2.4 m, and the voltage output is directly proportional to wind speed. Wind tunnel tests of the anemometer on a sensor package indicate that the body of the package does not affect the calibration. The response of a cup anemometer to a wind velocity vector that is not normal to the axis of rotation is such that tilting of the axis in horizontal flow has little effect if the tilt angle is 15° or less. This response is summarized by Moses (1968). The tilt of the vertical axis of the anemometer on the sensor

package is difficult to observe, but except for brief spells of turbulence it is generally less than 15°.

20.3.4 Wind Direction

The balloon is used as a wind vane. When it is tethered at the nose, fully inflated, and the sensor package is suspended just in front of the tail fins, the balloon heads into the wind. This behavior has been verified by tying a light streamer to the tether line a short distance below the balloon and comparing its orientation to that of the balloon. The sensor package is suspended by two lines, one from each side of the balloon. To assure constant orientation relative to the balloon, a rigid spacer about a meter in length is placed between the suspension lines at a distance of 1 m below the tie points on the balloon. A magnetic compass in the sensor package detects the orientation of the balloon relative to magnetic north. The compass needle is momentarily locked in place on a potentiometer each time direction is sampled, and is free to find magnetic north between samples. To determine true wind direction a compass deviation correction must be made.

Wind direction is difficult to determine by another method that can serve as a check on the direction measured by the Tethersonde system. Comparisons made with tower data and careful visual checks suggest that in smooth air the Tethersonde indicates true wind direction to within 5°.

20.4 ELECTRONICS

20.4.1 Sensor Package

The TS-1A sensor package circuitry is divided into five major sections: (1) voltage regulator and battery, (2) sensors and conditioning circuitry, (3) analog multiplexer, (4) voltage controlled oscillators and filters, and (5) FM transmitter (Fig. 20.3).

20.4.1.1 Voltage regulators and battery

The sensor package is powered by a 12-V, 500 mA-h, nickel-cadmium rechargeable battery. The battery voltage varies from 13.6 V at full charge to 10.5 V, the recommended low discharge point.

Three regulated voltages are provided in the sensor package. These are 7 V $\pm$ 0.01 V, 3 V $\pm$ 0.01 V, and 9 V $\pm$ 0.25 V. The 7-V regulator is the primary reference, and both the 3 V and 9 V refer to this voltage.

20.4.1.2 Sensors

Both temperature and wet-bulb temperature are sensed with bead thermistors. Each bead is a composite of two nonlinear thermistors. The composite, with a precision resistor network, produces a voltage that varies linearly with temperature. The voltage from the temperature sensor is amplified and scaled for direct input to the analog multiplexer. The voltage from the wet-bulb sensor is compared electronically with the temperature sensor voltage, and the difference is scaled and amplified for input to the multiplexer.

The anemometer cups drive a small d.c. generator whose voltage is linearly proportional to wind speed. This voltage is amplified and scaled for input to the multiplexer.

Wind direction is sensed by an electronically actuated magnetic compass as described in section 20.3.4. The compass consists of a circular potentiometer element, a wiper mounted on a small bar magnet, and a coil surrounding the magnet. The Earth's magnetic field aligns the bar magnet and wiper. Current is passed through the coil, and the

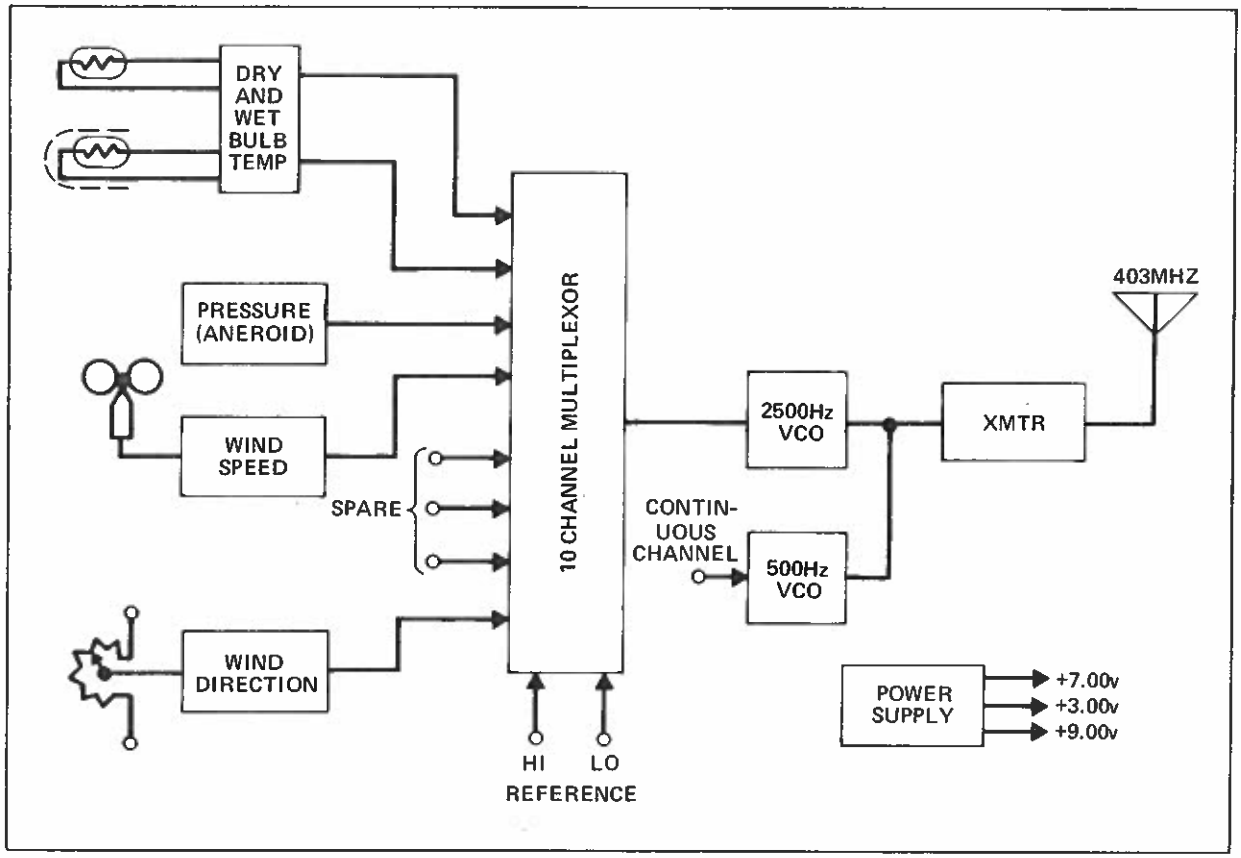

Figure 20.3. Circuitry of Tethersonde.

large magnetic field created causes the wiper to contact the potentiometer element producing a voltage linearly proportional to package orientation.

Pressure is sensed by an aneroid barometer. The transducing element is an aneroid capacitor of special design (Pike and Bargen, 1976). This capacitor is a timing element for an RC oscillator. A second fixed capacitor is also used as the timing element in the same RC oscillator. The two capacitors are switched in alternately. The ratio of the resultant frequencies is proportional to pressure. The pressure transducer produces a d.c. voltage that varies linearly with pressure. This voltage is compared electronically with the voltage from a "zero" potentiometer, and the difference is scaled for pressure change from the initial setpoint.

20.4.1.3 Analog multiplexer

A 10-channel analog multiplexer and associated timing logic generate the Tethersonde frame format. A frame consists of 20 time-clock periods. The frame starts with three periods of high reference. The eight data channels follow, each one period long and preceded and followed by a one-period low reference.

A unique automatic scale expansion circuit works in combination with the multiplexer logic to give a 4:1 gain in the temperature and pressure sensor outputs. The circuit automatically switches the reference at 25%, 50%, and 75% of full scale to give four times the normal resolution for chart record interpretation.

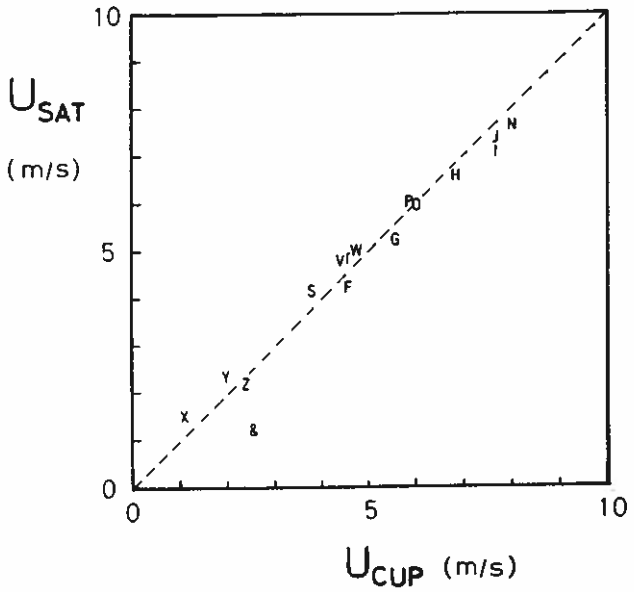

Figure 22.7. Comparison of mean wind speed measured by a cup anemometer and a sonic anemometer in turbulent atmosphere. The plotted letters identify different runs.

This response is about 4.5 m for this cup anemometer. The second-order perturbation shows the nonlinear response of the cup anemometer, i.e., the over-run (rotation) of the cup assembly. This is one of the most distinctive features of a cup anemometer, i.e., that it overestimates the mean wind speed in turbulent air flow. The cup anemometer calibrated in the wind tunnel was compared with the sonic anemometer, Kaijo model TR-32, in the real atmosphere. Both instruments were mounted on top of a 13-m tower. The overestimate of the cup anemometer amounts at most to 7%, as shown in Fig. 22.7.

The relationship between the wind speed, U, and the cut-off frequency, f_c, is obtained by comparing spectra. The cut-off frequency is $U/2\pi L$. The comparison gives the frequency response function of the cup anemometer, as shown in Fig. 22.8. The turbulent intensity measured by the cup anemometer is about 83% of that measured by the sonic anemometer, as shown in Fig. 22.9.

22.3.2 Vane

The transient response of the vane was tested by Yokoyama (1969) with a wind tunnel. Figure 22.10 shows an example of the time response of the vane to a step-function direction change. The response of the vane angle, Θ, can be represented by the following equation of simple damped oscillation:

$$\frac{d^2\Theta}{dt^2} - 2\omega_n\zeta \frac{d\Theta}{dt} - \omega_n{}^2\Theta = F(t) ,$$

where ω_n is the natural angular frequency of the vane, ζ is the damping ratio (the ratio of the actual damping to the critical damping), t is the time, and F(t) is a time-dependent forcing function. The damping ratio, ζ, and natural frequency, ω_n, are obtained from the measurements of the time response to a step-function direction change for various wind speeds by use of a solution of the equation for the case of $\zeta < 1$. The distance constant of the vane, $U/\omega_n\zeta$, is used as an index of the response characteristics and regarded as a constant for high wind speeds. It is approximately 1.6 m for this type of vane. An example of the frequency response for typical wind speeds is shown in Fig. 22.11.

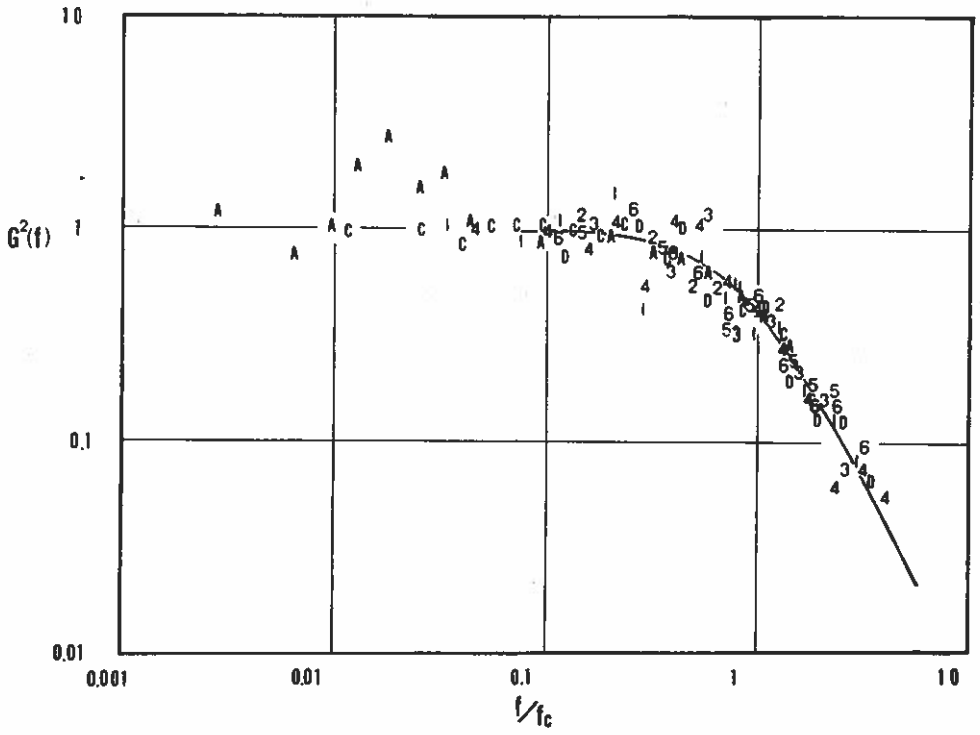

Figure 22.8. The frequency-response function as a ratio of power spectra from the cup and those of the sonic anemometer. The plotted letters and numbers identify different runs.

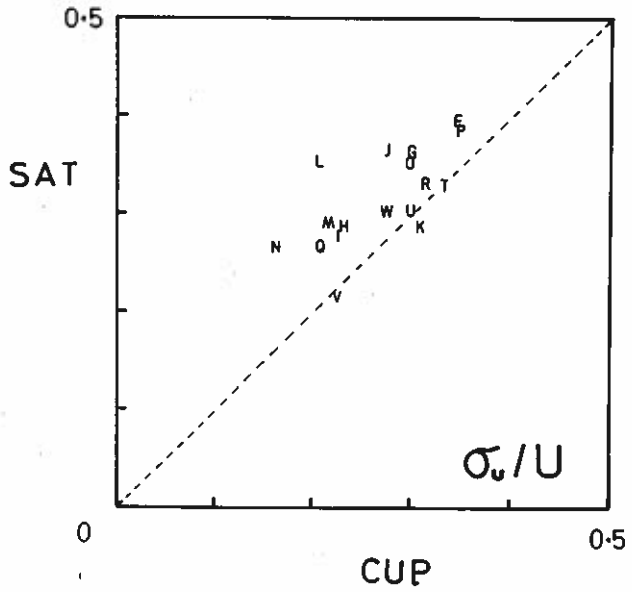

Figure 22.9. Comparison of σ_u/U as measured by cup and by sonic anemometer. The plotted letters identify different runs.

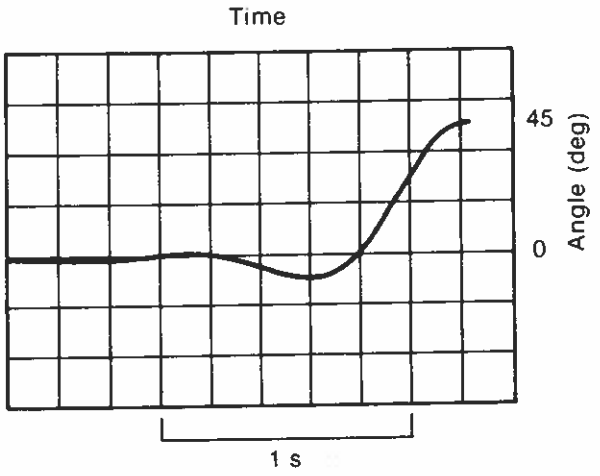

Figure 22.10. Example of the measured time response of the vane to a step-function direction change. (Mean wind speed is 3.0 m/s and angle of attack is 45.0°.)

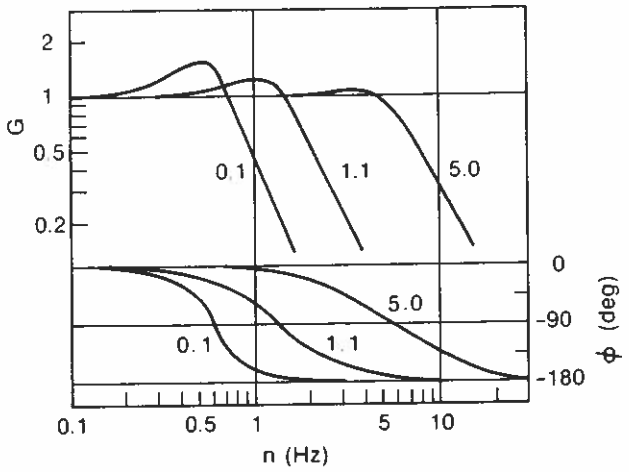

Figure 22.11. Frequency response of the vane for various wind speeds. (G is the ratio of amplitudes and ϕ is the difference of the phases. Entries are wind speed in m/s.)

22.4 OUTPUT FORMAT

The raw tape recorded data are contained within an FM multiplexed signal in the IRIG standard. The signal is separated by a discriminator into separate signals of each sensor. The output range depends on the discriminator. The discriminator used in the BLIE is for the simplest boundary layer package. It has only four channels, one each for wind speed, elevation angle, and dry- and wet-bulb temperatures. The range of the voltage is from 0.0 to 1.0 V. The corresponding outputs are 0.0 to 10.0 m/s for wind speed, -45 to +45 degrees for elevation angle, and one of the ranges -10°C to +10°C, 0°C to 20°C, 10°C to 30°C, or 20°C to 40°C, for wet- and dry-bulb temperatures. To obtain the signals from the other two sensors, hot wire and thermocouple, we need a discriminator with more channels.

22.5 REFERENCES

Hayashi, M., and M. Miyake (1973): Some characteristics of cup anemometers. Kogai (Japan) 9:53-61.

Hayaski, M., O. Yokoyama, H. Yoshikado, and K. Nemoto (1974): A boundary layer package with tape recording system inside. Tenki (Japan) 21:45-47.

Nakajima, S., (1967): On the meteorological observation in the lower atmosphere by a captive balloon. Weather Serv. Bull. (Japan) 34:1-65.

Ootsuka, S., N. Shishido, N. Honda, S. Nemoto, S. Koinuma, M. Hayashi, and M. Miyake (1975): Observations of the planetary boundary layer by tethered ballons and lower tropospheric radionsonde. Scientific Report of the Fourth AMTEX Conference, 26-29 September 1975. AMTEX Report No. 8, Tokyo, Japan, pp. 70-73.

Yokoyama, O. (1969): Measurements of wind fluctuations by a vane mounted on the captive balloon cable. J. Meteorol. Soc. Japan 47:159-166.

23. NCAR BOUNDARY PROFILER SYSTEM

Robert B. McBeth and Steven Semmer
National Center for Atmospheric Research
Boulder, Colorado, U.S.A.

23.1 INTRODUCTION

The NCAR Boundary Profiler (BP) system is a small tethered-balloon system (Morris et al., 1975) providing the user with five meteorological parameters: dry-bulb temperature, wet-bulb temperature, pressure, wind speed, and wind direction. Data information is transmitted, in a time multiplex format, to a ground station, where it is recorded on magnetic tape for later processing and on a strip chart recorder for real-time analysis. The system is portable and can be operated by one person.

23.2 DESCRIPTION

The BP system consists of a sensor package attached to an aerodynamic balloon, a tether line controlled by a winch, and a ground station.

The balloon's approximate dimensions are length, 4.8 m; maximum diameter, 1.4 m; volume, 3.25 m^3. It has a lifting capability of 1.9 kg at sea level. In calm weather the balloon has been flown to heights of 600 m. With its aerodynamic shape, the balloon acts as a wind vane and is used in computing wind direction. Because of its small size, it can be flown without a special FAA waiver.

The winch consists of a drum wheel driven by a 1/3-hp motor. The tether line, 100-lb test nylon cord, is wrapped around the drum wheel. The motor operates on 110 V a.c. An SCR controller sets the rate of ascent and descent of the package. The operator can vary the rate from 0 to 3 m/s depending on weather conditions.

The telemetry package was purchased off the shelf. A brief description of the package is given here; more detailed information can be found in the description of the Tethersonde. The package gets its power from 12 1.22-V nicad batteries, giving an average flight time of 2 h. A d.c. signal from each sensor circuit is fed into a time multiplexer. From there the signal is passed on into a voltage-controlled oscillator where it is converted to a frequency in the range of 2.6 to 3.4 kHz. The data signal is then used to modulate a 403-MHz crystal-controlled transmitter. The power output of the transmitter is about 10 mW.

The ground station is made up of three parts: a receiver, an Esterline Angus strip-chart recorder, and a digital cassette system. The receiver picks up the 403-MHz signal and passes the audio portion on to a discriminator circuit and the cassette system. The audio discriminator converts the audio tone to an electrical signal ranging from 0 to 5 V. This signal is then fed into the chart recorder to provide a real-time look at the data. The audio tone going into the cassette system is filtered and passed on into a frequency-detector circuit. The detector circuit determines when to take a sample of data and record it on tape. Between all data samples there is a down signal. The down signal has a frequency outside the range of the detector so the detector will be turned off during this signal and on during a data signal. The down frequency is at 2.3 kHz, and the data frequencies are in a range of 2.6 to 3.4 kHz. When the detector circuit is set, a short time delay takes place to allow for a clear signal, and then the data signal is passed on into a counter for 0.256 s. The lower eight bits of the counter become the digital representation of the data sample and are recorded on tape. The frequency span of 0.8 kHz represents a span of 205 counts. The cassette tape is then processed on a microcomputer system. The cassette system also contains a real-time clock, and at the beginning

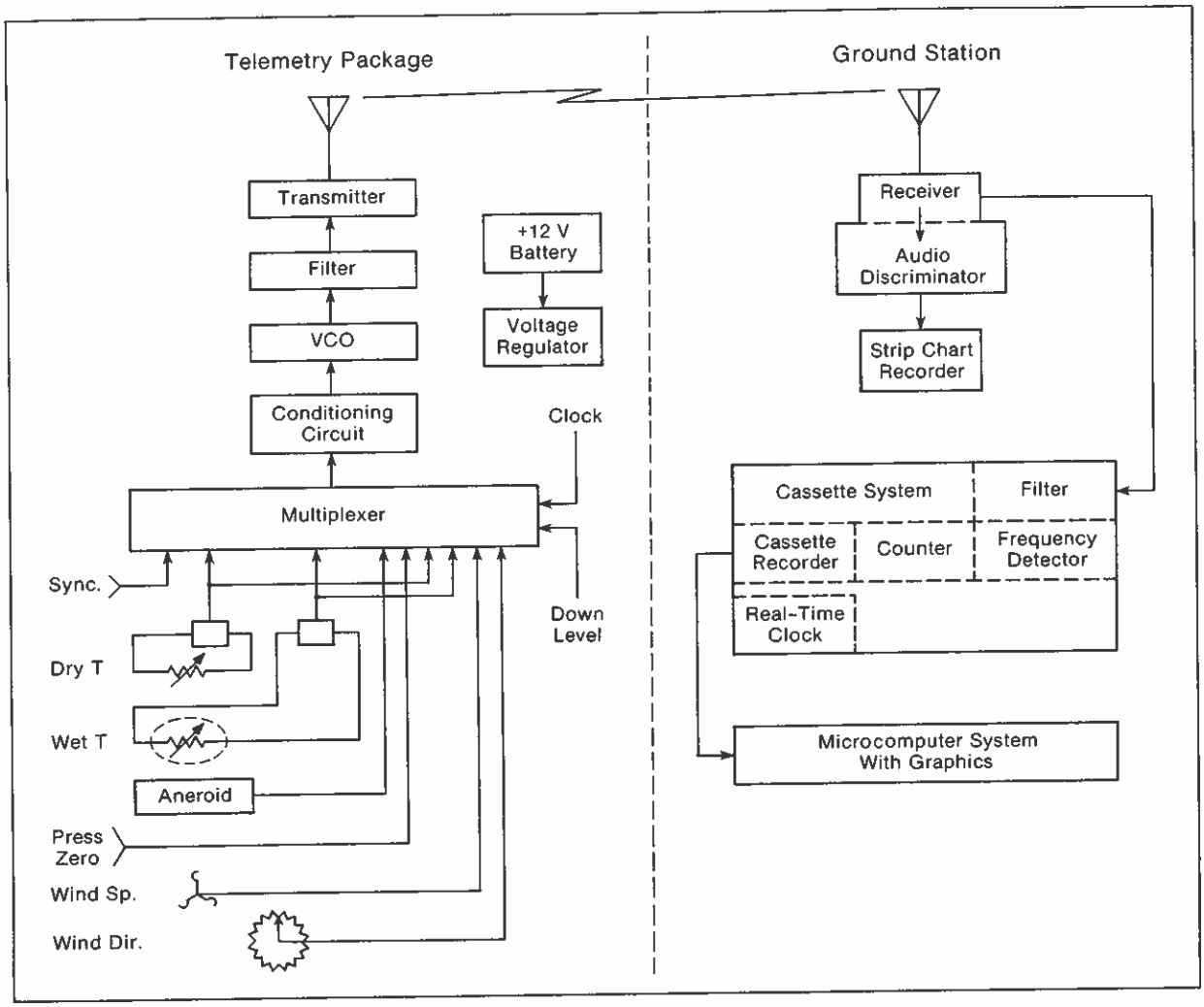

Figure 23.1. Block diagram of NCAR Boundary Profiler electronics.

of each data frame time is recorded on the magnetic tape. Figure 23.1 is a block diagram of the BP system.

23.3 SENSORS

Bead thermistors are used to measure dry- and wet-bulb temperatures. The sensors are mounted in a radiation shield tube and are aspirated by a small fan located at the end of the tube. The wet-bulb thermistor is covered by a sock, which is connected to a small reservoir.

Pressure is measured with an aneroid capsule. The pressure sensor is set up to make a relative reading, not an absolute one. The relative reading has a total differential range of 100 mb.

Wind speed is measured with a three-cup anemometer connected to a small d.c. generator. Wind direction is determined by using the balloon as a wind vane in conjunction

Table 23.1. Sensor characteristics

Sensor	Total range	Set range	Precision
Thermistor	-30° to 45°C*	25°C	±0.5°C
Aneroid capsule	Relative†	100 mb	±1 mb
Cup anemometer	0.5 to 10 m/s	0 to 10 m/s	±0.25 m/s
Magnetic compass and balloon	0° to 360°	0° to 360°	±5°

*Six switches set temperature ranges in 25°C increments.
†Pressure is set at ground level relative to launch site.

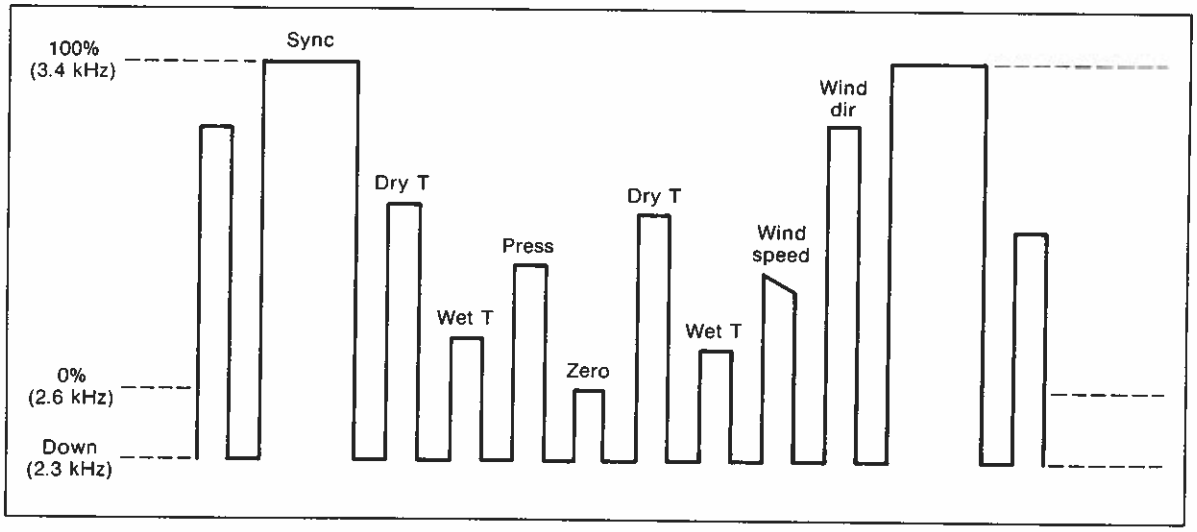

Figure 23.2. Data frame on strip chart recorder.

with a magnetic compass. The magnetic compass is a potentiometer with the compass needle acting as the arm of the pot. When it is time to sample wind direction an electric field locks the needle to the pot windings. This gives a clean reading when a sample is taken.

Table 23.1 gives more information about each sensor.

23.4 DATA FORMAT AND PROCESSING

Figure 23.2 is an example of one data frame recorded on the strip chart. The average frame duration is 30 s but can range from 20 to 40 s. The sync pulse represents 100% or 3.4 kHz, whereas the zero pulse is 0% or 2.6 kHz. Data are transmitted in the following order: (1) sync, (2) dry-bulb temperature, (3) wet-bulb temperature, (4) pressure, (5) zero, (6) dry bulb, (7) wet bulb, (8) wind speed, and (9) wind direction. The user can change this sampling order. The down signal is used to separate each channel sample from the next one. The scale ranges for each data parameter are listed in Table 23.1. The zero reference level for temperatures can be set by the user in 10°C increments

BAO/WMO

AUGUST 30,1979 FLIGHT (10)

TIME (H:M:S)	DBULB (C)	WBULB (C)	DP (C)	PRESS (MB)	WS (M/S)	WD (DG)	RH (%)	HEIGHT (M)	HT/MSL (M)
8:30:23	17.21	11.47	8.55	839.60	0.00	309	53	10.17	1587.17
8:30:45	17.24	11.49	8.58	838.50	0.00	310	53	21.36	1598.36
8:31:36	16.73	11.17	8.31	835.80	0.00	306	53	48.88	1625.88
8:33: 4	16.87	10.55	6.69	830.90	2.73	306	48	99.01	1676.01
8:34:54	17.95	10.07	4.33	826.10	4.24	332	39	148.48	1725.48
8:36:34	18.31	10.65	5.56	821.20	4.81	332	41	199.40	1776.40
8:38:35	18.55	10.22	4.16	816.40	4.32	322	37	249.63	1826.63
8:40:31	18.27	10.00	3.92	811.50	3.27	320	37	301.19	1878.19
8:43:28	19.89	10.73	4.27	804.00	2.51	325	34	380.91	1957.91
8:47:32	21.18	10.00	0.61	795.00	1.56	258	25	478.02	2055.02
9: 1:23	21.89	10.34	0.83	795.00	1.84	223	25	480.42	2057.42
9: 7:53	20.81	11.08	4.26	804.00	4.48	298	32	383.04	1960.04
9: 9:36	20.59	10.31	2.10	811.50	4.76	321	29	302.90	1879.90
9:10:56	19.83	10.11	2.33	816.40	5.11	326	31	251.03	1828.03
9:12:17	19.26	10.83	5.04	821.20	5.07	321	37	200.62	1777.62
9:13:19	18.65	11.47	7.32	826.10	4.80	320	45	149.55	1726.55
9:14:11	19.03	10.83	5.19	830.90	3.10	335	38	99.82	1676.82
9:15:12	19.46	11.80	7.28	835.80	0.55	311	42	49.29	1626.29

Figure 23.3. Example of data listing for a BLIE flight.

starting at -30°C and going up to 20°C. The user also has the ability to set a ground level reference for the pressure. Data recorded on magnetic tape have a similar format, except that no down channels are recorded and time information is placed on the tape after each sync signal.

Although the strip chart provides a real-time look at the data, the final analysis is done with the digital cassette tapes. With the use of a microcomputer graphics system, the cassette data are transferred to a digital cartridge tape. Each frame of raw data is then converted to physical units, with the sync and zero data being used for maximum and minimum levels. When all data have been converted, they are interpolated to one time point per frame, and the height, dewpoint, and relative humidity can be computed. The user can now use the graphics to obtain a listing of the flight data in tabular form or an XY plot of time versus data. Figure 23.3 is an example of a listing of flight data.

23.5 REFERENCE

Morris, A. L., D. B. Call, and R. B. McBeth (1975): A small tethered balloon sounding system. Bull. Am. Meteorol. Soc. 56: 964-969.

24. DETAILS OF THE EXPERIMENT

J. C. Kaimal and J. E. Gaynor
NOAA/ERL/Wave Propagation Laboratory
Boulder, Colorado, U.S.A.

H. W. Baynton
National Center for Atmospheric Research
Boulder, Colorado, U.S.A.

24.1 INTRODUCTION

The Boulder Low-Level Intercomparison Experiment commenced on schedule at 0800 MDT on 27 August 1979. Favorable weather conditions and the absence of major equipment problems contributed to a highly productive first week (27-31 August). As a result, no tests were run during the 3-day weekend. On 2 days during the following week (4-5 September) observations were resumed primarily for participants who needed more data. Some had made improvements in their sensors after the first week and were eager to see the effect; others simply wanted more observations.

The BAO tower instrumentation and associated data acquisition and processing systems (see Chapter 1 of this report) were operated continuously for the entire 2 wk. Functioning in a 20-min averaging mode, the data acquisition system printed out summary listings of BAO data at the end of each averaging period. The listings provided a set of common reference data for comparison of all sounding systems. Although each listing was withheld from the participants during the core observing periods until after the 24 h allowed for submission of their data, it was subsequently available for system checks and calibration.

A major problem in planning the experiment was crosstalk and interference between systems operated concurrently. Most radiosonde and tethered balloon systems used telemetering frequencies that overlapped. Balloons and kites served as reflecting targets for sodars, interfering with their Doppler measurements. The remotely piloted aircraft, besides being a reflector, generated its own acoustic noise and used radio frequency bands shared by the radiosonde and tethered balloon systems. Doppler sodars are known to interfere with one another even when their operating frequencies are far apart.

Coordinating this complex set of interactions called for optimal use of time sharing, spatial separation, and frequency tuning. The major crosstalk problems were solved before the experiment started by planning the location of sensors in the field and assigning specific observing windows for each sensor. In this chapter we describe the experiment and detail the specific problems and solutions, which should serve as background for interpreting the results in Chapter 25.

24.2 SENSORS COMPARED

Essential information on all sensors that participated in the BLIE is given in Table 24.1. The numbers indicate the order in which the papers are presented in Part 1 of this report. The sensors omitted from the list required unacceptable lead times for data processing. As mentioned in the Preface, participants in the BLIE were required either to submit data from each run within 24 h or to provide analog signals for sampling and processing in the BAO acquisition system.

Table 24.1. Sensors used in the BLIE

Sensor number	Sensor type	Parameters* measured	Country	Principal scientist	Affiliation
1	Tower system (BAO)	U,V,W,T,T_d	U.S.A.	J. C. Kaimal	Wave Propagation Laboratory, NOAA, Dept. of Commerce
2	Sonic anemometer-thermometer (Kaijo Denki)	U,V,W,T	Japan	T. Hanafusa	Meteorological Research Institute, Japan Meteorological Agency
3	Tower system (Vaisala)	S,D,T,RH	Finland	I. Ikonen	Vaisala Oy
4	Remotely piloted aircraft (SAM-B)	T,RH,P	France	D. Martin	Établissement d'Études et de Recherches Météorologiques
6	Kite anemometer (TALA)	S,D	U.S.A.	C. F. Woodhouse	Approach Fish, Inc.
7	Radio acoustic sounding system (RACES)	T	Switzerland	P. Ravussin	Federal Institute of Technology of Lausanne
8	FM-CW radar	U,V	U.S.A.	R. B. Chadwick	Wave Propagation Laboratory, NOAA, Dept. of Commerce
11	Bistatic sodar	U,V	U.S.A.	W. D. Neff	Wave Propagation Laboratory, NOAA, Dept. of Commerce
12	Monostatic sodar (AVIT)	U,V,W	U.S.A.	P. B. MacCready	AeroVironment, Inc.
13	Bistatic sodar (Echosonde)	U,V,W	U.S.A.	M. A. McAnally	Radian Corp.
14	Monostatic sodar (Sensitron)	U,V	Sweden	S. Salomonsson	University of Uppsala
15	Bistatic sodar (XONDAR)	U,V,W	U.S.A.	R. L. Peace, Jr.	Xonics, Inc.
16	GMD-1/VIZ radiosonde	S,D,T,RH,P	U.S.A.	R. B. McBeth	National Center for Atmospheric Research
17	TDFS low-level radiosonde	T,T_w,P	F.R.G	E. Schöllmann	Deutscher Wetterdienst
18	CORA radiosonde	S,D,T,RH,P	Finland	I. Ikonen	Vaisala Oy
19	Airsonde radiosonde	T,T_w,P	U.S.A.	D. B. Call	AIR, Inc.
20	Tethersonde profiler	S,D,T,T_w,P	U.S.A.	A. L. Morris	Ambient Analysis, Inc.
21	Tethered balloon profiler	S,T,RH,P	Poland	K. Stefanicki	Institute of Meteorology and Water Management
22	Tethered balloon profiler	S,E,T,T_w	Japan	M. Hayashi	National Institute for Pollution and Resources
23	Tethered balloon profiler	S,D,T,T_w,P	U.S.A.	R. B. McBeth	National Center for Atmospheric Research

*U - wind component (positive from west)
V - wind component (positive from south)
W - vertical wind component (positive up)
S - wind speed
D - wind direction
T - temperature
T_d - dew point temperature
T_w - wet-bulb temperature
RH - relative humidity
P - pressure
E - elevation angle

The variables measured by the different systems were reduced to the following common parameters for comparison:

(1) Horizontal wind component U (positive from west).
(2) Horizontal wind component V (positive from south).
(3) Vertical wind component W (positive upward).
(4) Temperature T.
(5) Dew point temperature T_d
(6) Relative humidity RH.
(7) Height above ground Z.

All measurements were reported for heights corresponding to the fixed levels on the tower. Reporting levels for radiosonde observations above tower heights were set at pressure levels corresponding to 400, 500, 750, 1,000, 1,250, 1,500, 1,750, 2,000, 2,250, 2,500, 2,750, and 3,000 m.

The unit of time for data comparison was a 20-min period coincident with the BAO averaging period. In-situ and remote sensors were expected to provide time-averaged data compatible with the BAO tower profiles. For immersion sensors, which use a single instrument package to probe the layer, a full ascent or descent had to be completed within the 20-min period. When this was not possible, the period containing the most profile points was used for comparison.

24.3 LOCATION OF SENSORS

Assignment of sensor locations (Fig. 24.1) was based on several considerations: the crosstalk problem, the availability of a.c. power, and the need for certain sensors to be far from (or close to) the tower. Groups operating in shifts or flying instruments on the same balloon train had to be close together for easy communication.

Major areas of activity centered around the tower base, anchor point B, and the temporary building. Air-conditioned office trailers were provided at each of these locations to house equipment and personnel. The circled numbers in Fig. 24.1 indicate the sensors occupying each trailer.

The electronics for the tower systems were situated in the trailer close to the tower to keep signal lines short. Radiosonde and tethered balloon activities were located near the temporary building to be far away from the tower and its guy wires. Since by arrangement the remotely piloted aircraft would not be operated when the balloons were flown, its landing strip was placed close to the balloon launch area. The installations around the building can be seen in Fig. 24.2.

The sodar antennas (see Fig. 24.3) were laid with their axes aligned E-W and N-S and their centers close to anchor point B. With this arrangement, the sampling volumes of the bistatic sodars and the lower levels of the monostatic sodars were close to each other. Their remoteness from the tower was intentional; to avoid reflections the sodars were placed at a distance from the tower equal to or greater than the expected height range of the devices.

Operating around anchor point A and sometimes around anchor point C (see Fig. 24.1), the kite anemometer was sufficiently removed from the other sensors to avoid interference. Its only potential conflict was with the remotely piloted aircraft, but this was avoided by scheduling kite and aircraft operations at different times.

24.4 OPERATING SCHEDULE

In the initial plan three observing periods with 2-h breaks for rest and refreshments were scheduled for each day:

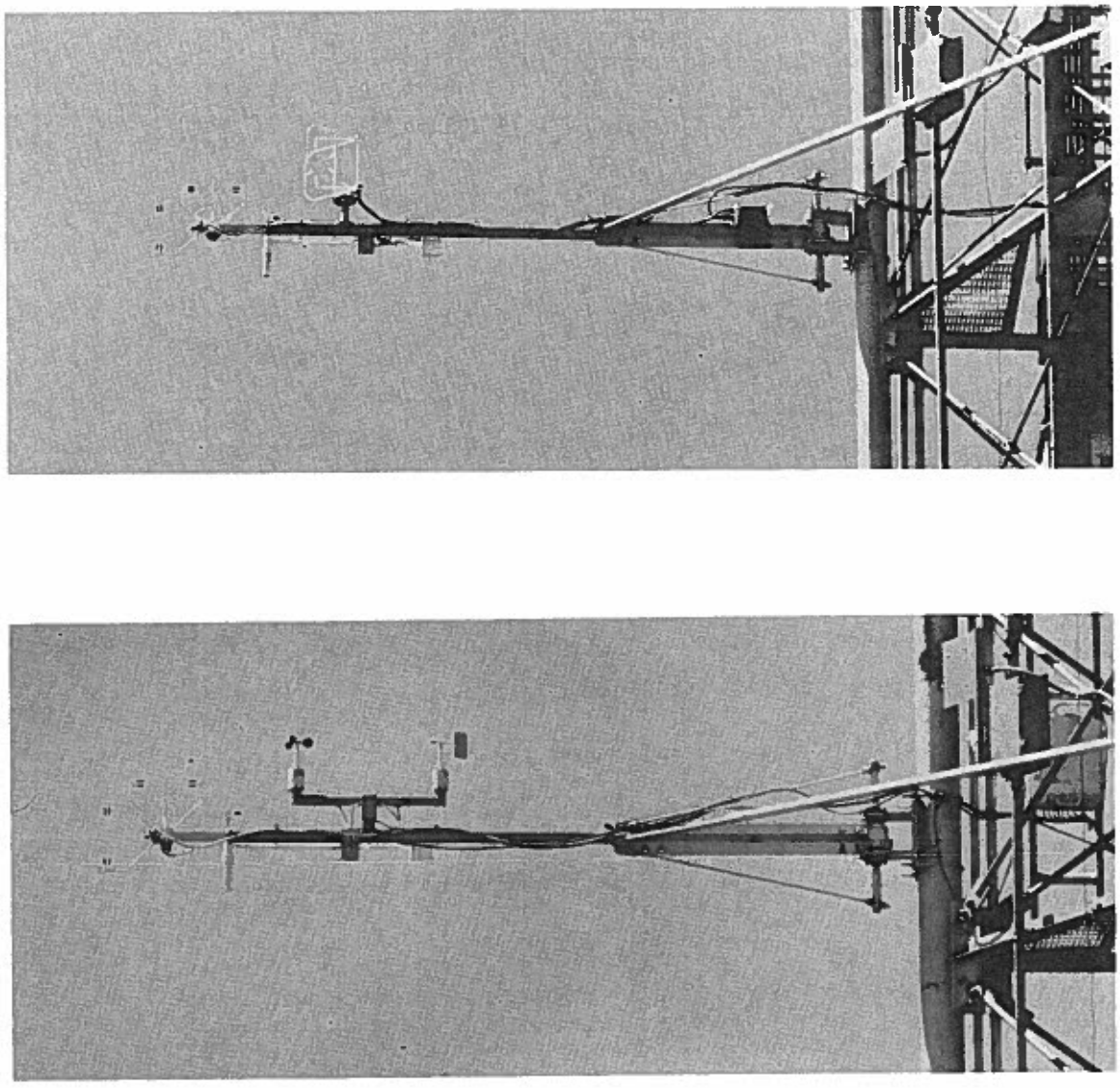

Figure 24.5. Vaisala cup and vane system at the 22-m level.

examine the effect of separation to determine if the 20-min averaging specified for BLIE is effective in reducing this variability.

Terrain irregularities of length scales comparable to separation distances between sensors can introduce systematic differences between their measurements. These differences cannot be removed by time averaging. The terrain around the BAO site rolls gently down toward the west and north but is relatively smooth. Thus the effect of the slope should be very small.

Obviously the sampling volumes of the different systems are not at the same distance from the tower. The bistatic systems have their sampling volumes oriented vertically over the central transmitter (or receiver), but the tilted beams of the monostatic systems point away from the tower toward the west and north, so their separation from the tower increases as a function of height.

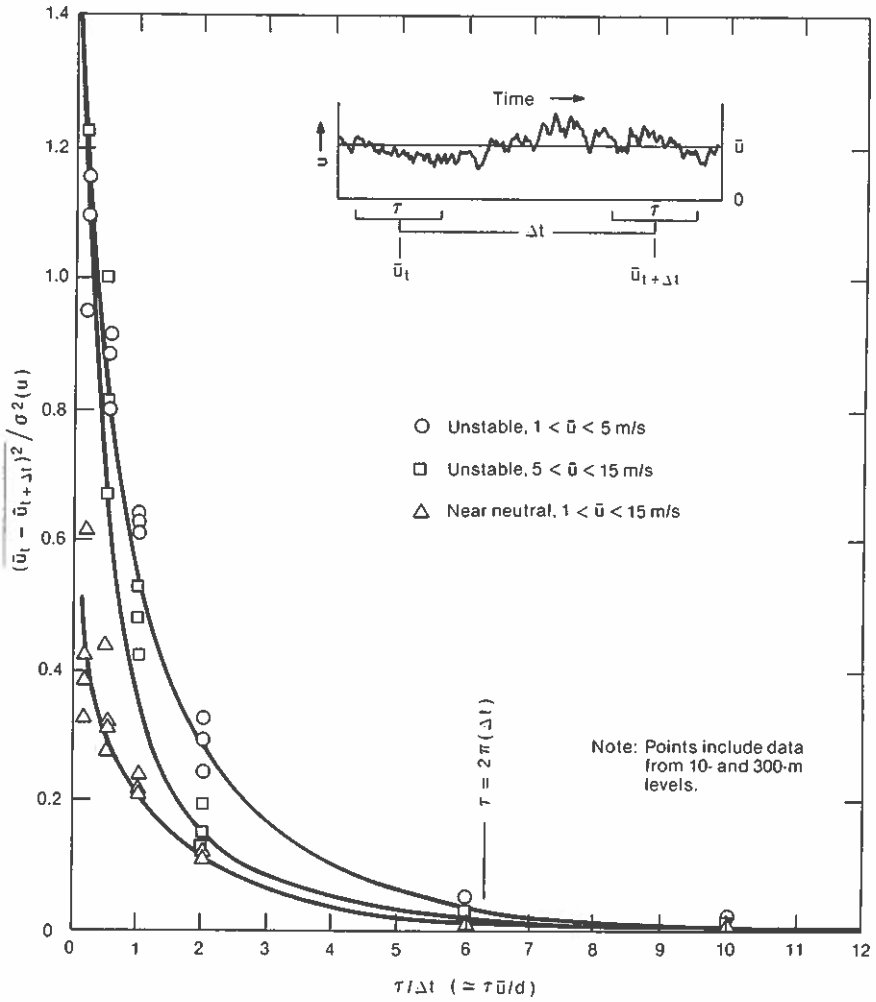

Figure 24.6. Simulated two-point variance for a downstream separation of sensors plotted as a function of averaging time. Plotted here are variance ratios for τ = 1/6, 1/2, 1, 2, 6, and 10 min with Δt fixed at 1 min.

The effect of averaging can be demonstrated for the simple case where the two sensors are aligned along the direction of the mean wind. If the flow is assumed to be horizontally homogeneous and the distance between the sensors small enough that the wind field can be considered frozen, the spatial separation converts to a time lag $\Delta t = d/\bar{u}$, where d is the distance and $\bar{u}$ is the mean wind. For typical d = 300 m and $\bar{u}$ = 5 m/s, the lag corresponds to 1 min. In a truly frozen field, 19 of the 20 min would be the same in both measurements, bringing the two averages very close together.

The above assumption is tested in Fig. 24.6 with single-point time series of the stream-wise wind component, u, measured at two levels on the BAO tower. The variance of the difference across a fixed time lag, normalized by $\sigma^2(u)$, the variance of the time series, is plotted as a function of $\tau/\Delta t$ where τ is the averaging time and Δt is the time lag between the two points. For $\tau << \Delta t$, the difference variance approaches $2\sigma^2(u)$, the limiting value for no correlation between the measurements, but becomes negligible as τ exceeds $2\pi\Delta t$. The 20-min averaging should therefore be adequate down to a mean wind speed of 2 m/s.

In practice the wind could be blowing from any direction with respect to the line joining the two sensors. The frozen-field assumption is no longer applicable, and the variance of the two-point difference increases as the two signals become increasingly uncorrelated. The most rapid drop in correlation with distance occurs in the lateral direction. Here one can resort to turbulent time scale arguments to determine the minimum required averaging time for comparison. Under daytime convective conditions, the logarithmic spectral peak for horizontal winds typically falls between 0.002 and 0.005 Hz, which corresponds to a wave period between 3.3 and 8.3 min. Our 20-min averaging period should therefore be adequate even for comparisons between two laterally spaced measurements provided, of course, that the flow is horizontally homogeneous.

Since sensor separation has a large effect on the sodar/tower sensor comparison, the configuration of the sodar systems is summarized in Table 24.3 for quick reference.

Table 24.3. Doppler sodar configurations

Sensor	Transmit frequency (kHz)	Configuration	Details
WPL	1.25	Two-axis, bistatic	Central pencil-beam receiver, two fan-beam transmitters
AVIT	2.0	Three-axis, monostatic	Pencil-beam transmit-receivers: one pointing vertical, one tilted west, one tilted south
Echosonde	2.0	Three-axis, bistatic	Central pencil-beam receiver, two fan-beam transmitters
Sensitron	2.4	Two-axis, monostatic	Pencil-beam transmit-receivers: one tilted west, one tilted north
XONDAR	2.0	Three-axis, bistatic	Central pencil-beam transmitter-receiver, two fan-beam receivers

24.5.3 Sampling the Same Air Space

The problems encountered in the radiosonde intercomparisons differed from those in the sodar intercomparisons. The tower measurements have limited value as a common reference because of the short time required for the radiosondes to cover the first 300 m. Radiosondes launched a few seconds apart sample different air, and even when released in clusters are likely to ascend at different rates. Thus a useful comparison of radiosondes can be achieved only by flying the four sondes on a single balloon train.

The resolution of the radio frequency crosstalk problem was a matter of critical importance. The Vaisala, TDFS, and AIR sondes (see Table 24.1) operated in the 403-MHz band, whereas the VIZ sonde used with the GMD-1 operated at 1,680 MHz. Fortunately, some of the sondes were tunable to more than one frequency in the 403-MHz band. By adjusting the frequencies (see Table 24.4 for details) and assigning different time periods for the radiosonde and tethered balloons (which also shared the 403-MHz band), it was possible to eliminate crosstalk between the different systems. A trial run before the main intercomparison demonstrated that the radiosondes could be released simultaneously.

Table 24.4. Telemetering frequencies for radiosondes and tethered balloon profilers

Radiosondes		Tethered profilers	
Sensor type	Frequency (MHz)	Sensor type	Frequency (MHz)
GMD-1/VIZ	1,680	BP/NCAR	403
CORA	Between 400 and 403	NIPR	In-flight recording
TDFS	404.17 or 404.59	IMWM	393 to 407, with peak at 400
Airsonde	403.5	Tethersonde	403.5

To attach the four sondes to the single balloon, a yoke consisting of string and two horizontal pieces of dowel suspended 2 m below the balloon was devised. The Vaisala sonde, which must be free to lower itself to operate its reel-activated switch, was suspended from the lower dowel along with the TDFS sonde. The AIR sonde was suspended from the midpoint of the upper dowel, halfway between the vertical string risers that connected the two dowels at their ends, and was thus free to rotate and aspirate its dry and wet thermistors. The VIZ sonde was suspended above the upper dowel from the point where the yoke was tied to the string from the balloon. Several pairs of hands were needed to handle the balloon train at launch (see Fig. 24.7). The technique described above resulted in 19 successes out of 20 attempted launches.

24.5.4 Operation of the Tethered Systems

To solve the radio crosstalk problem, the Polish profiling system was assigned a separate operating time. The NCAR, AIR and NIPR systems continued to operate simultaneously. Although the winches were spaced as far apart as practical, operators had to be alert for tangled lines. Since the line and balloon had to be watched constantly at all times, tethered balloons could not be flown after dark.

24.5.5 Comparisons on the Moving Carriage

Direct comparisons of all immersion sounding systems (free balloon, tethered balloon, and aircraft) were carried out with the aid of the moving carriage on the SW face of the tower. The carriage operated at a constant speed, ascending at a rate of 0.55 m/s and descending at a rate of 0.57 m/s. As a result, the exact time of arrival of the carriage at each of the instrumented levels was known within a second. A cross arm was attached to the end of the boom on the carriage to support the instruments being compared (see Fig. 24.8).

For the radiosondes, the procedure was to obtain simultaneous profiles to a height of 250 m with the same four sondes that would be subsequently taken aloft on the single balloon train. At the times corresponding to the tower levels, their observed values would be compared with the values observed by the tower sensors. Special measures were required to adapt the sondes to the slow ascent rate of the carriage. For example, since the Vaisala sonde was not free to lower and operate its switching reel, a small motor was attached to rotate the reel. The TDFS and AIR sondes were designed to operate at ascent rates almost an order of magnitude faster than the carriage. A special fan was therefore provided for the TDFS sonde. Initially, the AIR sonde was rotated as if in free flight by a motor attached to a stiff wire. Because of problems with this approach, small motors were inserted in the dry- and wet-thermistor ducts. These steps proved to be successful.

Figure 24.7. Radiosonde operators preparing to release balloon train with all sondes in tow.

Instrumentation packages used with the tethered balloons and the remotely piloted aircraft were carried aloft on the carriage, one at a time, during the evening or at other times when they would not interfere with other instruments.

24.5.6 Baselining Procedures

A conventional, white wooden thermometer shelter was installed in the radiosonde launch area. A single Assman psychrometer manufactured by Casella and a digital barometer manufactured by Negretti and Zambra were used to obtain baseline data. For the carriage intercomparisons, these instruments were transported to the tower base; at other times they were located in the thermometer shelter. Since the exact instant of a balloon launch or carriage ascent was not known in advance, baseline readings of pressure, temperature, and humidity were made at about 5-min intervals and the most recent ones used when the ascent or launch was imminent.

24.6 COLLECTION AND PROCESSING OF DATA

According to the terms of the experiment, the participants were required to submit their data to the BLIE organizing committee within 24 h of each observation period. The ability of experimenters to provide processed data within that time was an important innovation. The use of microprocessors and minicomputers in field equipment made this possible; besides providing immediate feedback it enabled participants and observers to

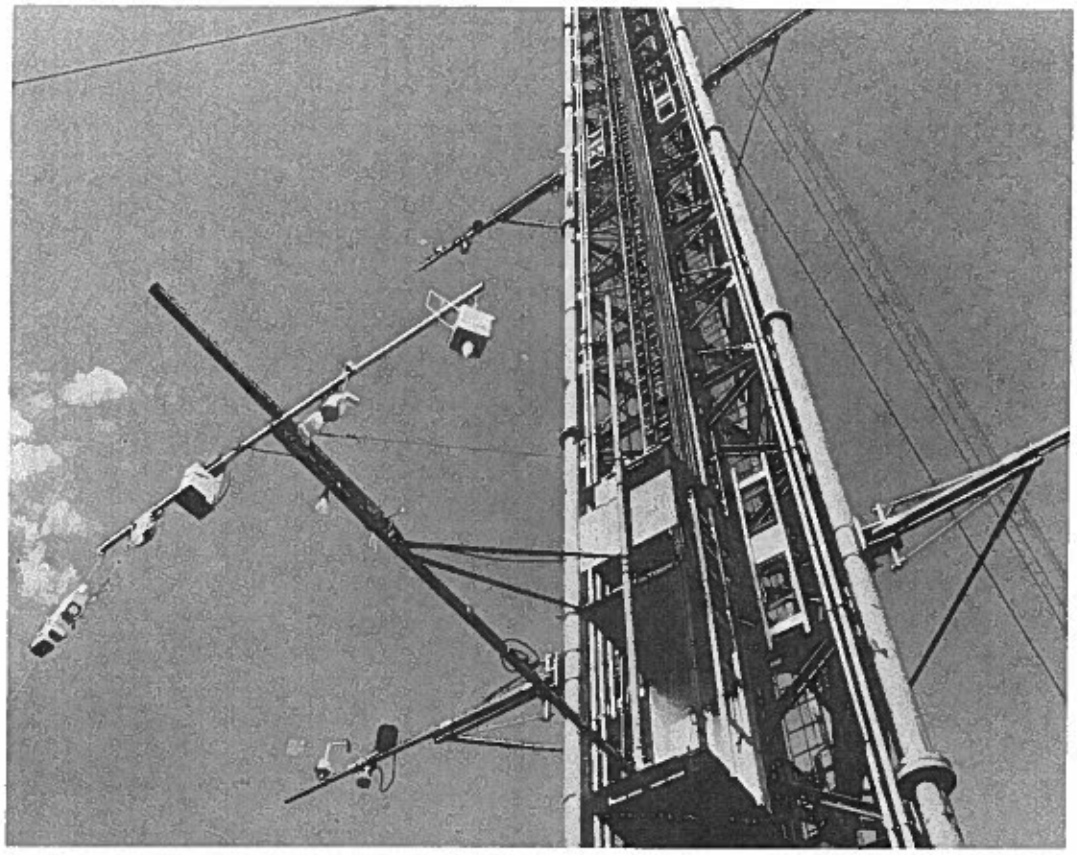

Figure 24.8. Radiosondes on cross arm attached to moving carriage on the BAO tower.

reach agreement before they left Boulder on how the sensors compared. Photocopying equipment at the site offered the participants access to other data collected during the experiment for their own analysis.

The task of entering all data into the processing computer at Boulder was formidable. Although the data acquired by the on-site computer were transmitted by phone lines to the processing computer, the data on sheets turned in by the participants had to be entered manually. A team of computer operators worked steadily to keep up with 200 data sheets turned in every 24 h. As all data were entered, they were separated according to sensor and stored on individual flexible disks. Months of painstaking editing and plotting followed. These data are presented in scatter plots and statistical summaries in Chapter 25.

25. SUMMARY OF RESULTS

J. C. Kaimal and J. E. Gaynor
NOAA/ERL Wave Propagation Laboratory
Boulder, Colorado, U.S.A.

H. W. Baynton
National Center for Atmospheric Research
Boulder, Colorado, U.S.A.

25.1 INTRODUCTION

Although the BLIE data justify a wide range of analyses, only a brief overview of the results is presented in this report. Our objective is to make available the comparison results in the form of statistical summaries and scatter diagrams. In keeping with WMO policy we make no attempt to rank the sensors by performance.

Tables 25.1 to 25.9 summarize all data submitted by participants. They include information on sensor mean, rms difference from reference, and correlation between sensor and reference. For all measurements below 300 m, BAO tower data are used as the reference. For radiosonde data, which are measured to a height of 3 km, averages of all sonde measurements are used as well.

The scatter diagrams (Fig. 25.1 to 25.24) include all data included in the statistical summaries. In several figures we present additional plots at the request of participants who wished to highlight certain aspects of the data. In some cases exclusion of certain levels (or time periods) improved agreement between sensor and tower data. Accompanying the figures are comments by BLIE participants and notes from the editors of this report that explain factors which influenced comparison results but were not discussed in Chapter 24. The circumstances and limitations described therein should be considered when the figures are interpreted.

The reader is alerted to some errors and discrepancies in the BAO tower reference wind data.

(1) The 300-m Propvane direction reading was in error by +7° from the beginning of the experiment until 1300 MDT on 30 August. Since data from the Propvanes were used only for wind directions between 244° and 64° (clockwise), the number of points affected constitutes 0.5% of the total number of points (including all 8 levels).

(2) The direction readings from the Propvanes and the sonic anemometers differed by as much as 10° (for winds from about 64° azimuth) to 5° (for winds from about 244° azimuth) for directions normal to the two booms; this is clearly the result of distortion in the flow field around the tower. For wind directions from about 64° azimuth, the direction difference exceeded 7° for about 1% of the total data points; for directions around 244° azimuth the direction difference was smaller, exceeding 4° for about 2.5% of the data points.

Errors in the computed wind components U and V, resulting from the direction errors detailed above, tend to be small, and since the number of readings affected is also small compared with the total sample, the effect on the statistical summaries is negligible. On the plots, the affected points are lost in the general scatter, so no attempt was made to flag or delete them.

25.2 STATISTICAL SUMMARIES

The notations used in this section follow the conventions adopted by the participants as outlined in Section 24.2. U and V represent wind components from the west and the south, respectively (in m/s), T and T_d are the dry-bulb and dew point temperature, respectively (in °C), RH is the relative humidity (in %), and Z is the height (in m) computed from pressure readings. In earlier sections authors may have used different notations to represent the same variables.

Table 25.1. Statistical summary of data from tower sensors

Variable	Sensor	No. of points	BAO mean	Sensor mean	rms diff.	Correlation
U*	Kaijo Denki	105	0.74	0.69	0.37	0.99
	Vaisala	365	-0.31	-0.33	0.59	0.99
V*	Kaijo Denki	105	3.17	2.76	0.62	0.99
	Vaisala	365	2.66	2.59	0.49	0.98
W*	Kaijo Denki	168	0.03	0.06	0.09	0.70
	Vaisala	-	-	-	-	-
T	Kaijo Denki	179	23.05	24.08	1.15	1.00
	Vaisala	969	22.64	22.81	0.33	1.00
T_d	Kaijo Denki	-	-	-	-	-
	Vaisala	963	4.25	4.32	0.77	0.99
RH	Kaijo Denki	-	-	-	-	-
	Vaisala	572	32.80	32.15	1.89	1.00

* Includes only winds between 64° and 244° azimuth.

Table 25.2. Statistical summary of data from RACES and SAM-B sensors

Variable	Sensor	No. of points	BAO mean	Sensor mean	rms diff.	Correlation	Mode*
T	RACES†	52	21.67	21.48	1.40	0.92	
	SAM-B	88	22.31	21.90	0.72	0.99	(air. ascent)
	"	88	22.31	22.13	0.81	0.98	(air. descent)
	"	14	25.24	25.68	0.90	0.89	(car. ascent)
	"	14	25.24	26.29	1.18	0.98	(car. descent)
T_d	SAM-B	85	6.30	5.87	1.95	0.89	(air. ascent)
	"	85	6.30	5.81	2.02	0.90	(air. descent)
	"	14	6.04	7.74	2.07	0.99	(car. ascent)
	"	14	6.04	8.35	2.56	1.00	(car. descent)
RH	SAM-B	85	39.45	38.68	5.20	0.96	(air. ascent)
	"	85	39.45	38.42	4.41	0.97	(air. descent)
	"	14	30.43	34.29	5.51	1.00	(car. ascent)
	"	14	30.43	34.36	5.44	1.00	(car. descent)

* Sonde operated in remotely piloted aircraft (air.) or on carriage (car.).
† RACES measured only temperature.

Table 25.3. Statistical summary of data from TALA and FM-CW sensors

Variable	Sensor	No. of points	BAO mean	Sensor mean	rms diff.	Correlation	
U	TALA 1*	25	0.94	0.97	0.96	0.94	(4.31)†
	TALA 2*	12	3.89	2.94	1.72	0.92	(8.64)†
	FM-CW	124	0.36	-0.17	3.32	0.75	
V	TALA 1*	25	1.12	1.24	0.82	0.98	(4.31)†
	TALA 2*	12	6.51	5.99	1.15	0.97	(8.64)†
	FM-CW	19	-0.34	-0.90	2.66	0.66	

* TALA 1 is the small kite used during light winds. TALA 2 is the large kite used during strong winds.
† Mean wind speed for comparison periods.

Table 25.4. Statistical summary of data from sodars

Variable	Sensor	No. of points	BAO mean	Sensor mean	rms diff.	Correlation
U	WPL	201	0.71	1.04	0.95	0.97
	AVIT	308	0.04	0.01	0.82	0.97
	Echosonde	127	0.99	1.21	1.57	0.87
	Sensitron	111	0.36	-0.93	2.52	0.80
	XONDAR	201	0.09	-0.06	0.97	0.97
V	WPL	201	0.64	0.36	1.25	0.92
	AVIT	308	0.82	0.77	0.85	0.97
	Echosonde	127	1.52	0.68	2.12	0.86
	Sensitron	102	0.88	1.30	2.21	0.71
	XONDAR	205	1.04	1.05	1.03	0.96
W	WPL	-	-	-	-	-
	AVIT	244	-0.03	0.07	0.34	0.32
	Echosonde	83	-0.05	0.08	0.28	0.03
	Sensitron	-	-	-	-	
	XONDAR	154	0.07	0.18	0.30	0.62

Table 25.5. Statistical summary of data from balloon-borne radiosondes (10-300 m)*

Variable	Sensor	No. of points	BAO mean	Sensor mean	rms diff.	Correlation
T	GMD-1/VIZ	234	23.15	23.33	0.86	0.98
	CORA	152	23.81	23.48	0.83	0.98
	TDFS	138	23.63	23.08	0.80	0.99
	Airsonde	160	23.82	23.93	1.09	0.95
T_d	GMD-1/VIZ	188	5.55	6.48	2.06	0.86
	CORA	150	3.57	3.88	1.41	0.97
	TDFS	136	3.81	4.51	1.85	0.95
	Airsonde	158	3.83	6.35	3.41	0.90
RH	GMD-1/VIZ	188	36.73	37.90	4.99	0.96
	CORA	150	30.14	31.70	4.10	0.98
	TDFS	136	31.17	34.01	4.89	0.98
	Airsonde	160	31.05	35.76	7.03	0.95
U	GMD-1/VIZ	-	-	-	-	-
	CORA	149	0.26	0.14	2.13	0.77
	TDFS	-	-	-	-	-
	Airsonde	-	-	-	-	-
V	GMD-1/VIZ	-	-	-	-	-
	CORA	149	0.90	0.96	2.04	0.80
	TDFS	-	-	-	-	-
	Airsonde	-	-	-	-	-

* GMD-1/VIZ wind data not computed for this height range. TDFS and Airsonde did not measure wind.

Table 25.6. Statistical summary of data from balloon-borne radiosondes (10 m - 3 km)*

Variable	Sensor	No. of points	Mean of all sondes	Sensor mean	rms diff.	Correlation	
T	GMD-1/VIZ	255	17.83	18.03	0.58	1.00	
	CORA	255	17.83	17.71	0.36	1.00	
	TDFS	255	17.83	17.37	0.58	1.00	
	Airsonde	255	17.83	18.18	0.71	1.00	
T_d	GMD-1/VIZ	204	1.90	1.38	1.31	0.99	
	CORA	204	1.90	1.16	1.16	0.99	
	TDFS	204	1.90	1.67	1.02	0.99	
	Airsonde	204	1.90	3.37	1.98	0.98	
RH	GMD-1/VIZ	204	37.92	35.96	3.60	0.98	
	CORA	204	37.92	36.09	3.39	0.98	
	TDFS	204	37.92	38.97	3.21	0.98	
	Airsonde	204	37.92	40.68	4.57	0.96	
Z	GMD-1/VIZ	255	-	-	10.28	1.00	(-1.01)†
	CORA	255	-	-	5.28	1.00	(1.37)†
	TDFS	255	-	-	6.45	1.00	(2.41)†
	Airsonde	255	-	-	11.59	1.00	(-2.78)†

* Only periods when all four sondes functioned satisfactorily are included in this comparison. Complete wind data provided only by CORA. GMD-1/VIZ gave wind data for two levels below 3 km.

† Difference in reported height from mean for all sondes.

Table 25.7. Statistical summary of data from radiosondes on carriage (10-300 m)

Variable	Sensor	No. of points	BAO mean	Sensor mean	rms diff.	Correlation
T	GMD-1/VIZ	126	23.44	23.41	0.82	0.97
	CORA	133	23.62	23.86	0.66	0.99
	TDFS	113	23.89	23.42	0.71	0.99
	Airsonde	126	23.60	24.07	0.92	0.98
T_d	GMD-1/VIZ	40	5.08	5.43	1.98	0.90
	CORA	131	4.82	5.09	1.31	0.97
	TDFS	112	4.28	3.83	1.34	0.97
	Airsonde	124	4.63	5.08	1.08	0.98
RH	GMD-1/VIZ	40	34.25	34.22	5.15	0.95
	CORA	131	33.09	33.42	2.61	0.99
	TDFS	112	31.47	31.53	2.28	0.99
	Airsonde	118	32.61	32.66	2.70	0.99

Table 25.8. Statistical summary of data from tethered balloon sensors

Variable	Sensor	No. of points	BAO mean	Sensor mean	rms diff.	Correlation	
T	Tethersonde	112	21.28	21.17	0.88	0.99	
	IMWM	119	21.49	21.56	1.24	0.96	
	NCAR	59	25.18	28.07	5.19	0.31	
T_d	Tethersonde	106	6.19	8.36	3.09	0.83	
	IMWM	109	6.09	7.15	2.34	0.82	
	NCAR	59	-1.28	7.17	11.74	0.53	
RH	Tethersonde	106	42.48	46.86	6.66	0.97	
	IMWM	109	41.67	44.24	8.53	0.89	
	NCAR	59	18.07	29.73	19.01	0.58	
Z*	Tethersonde	141	-	-	17.33	1.00	(5.33)†
	IMWM	-	-	-	-	-	
	NCAR	78	-	-	22.28	0.99	(4.63)†
S§	Tethersonde	111	3.05	2.85	0.98	0.86	
	IMWM	53	4.46	5.47	1.92	0.91	
	NCAR	59	3.25	3.56	1.16	0.69	

* Height above ground determined from pressure.
† Mean difference with respect to actual height.
§ Wind speed used for this comparison since IMWM did not measure wind direction.

Table 25.9. Statistical summary of data from tethered balloon sensors on carriage

Variable	Sensor	No. of points	BAO mean	Sensor mean	rms diff.	Correlation	
T	Tethersonde	14	20.89	21.15	0.35	0.99	
	IMWM	55	24.60	24.31	0.65	0.97	
	NIPR	-	-	-	-	-	
	NCAR	14	24.70	24.92	0.43	0.97	
T_d	Tethersonde	13	9.73	10.82	1.26	0.99	
	IMWM	51	5.69	6.06	1.36	0.98	
	NIPR	-	-	-	-	-	
	NCAR	14	6.01	6.79	1.19	0.84	
RH	Tethersonde	13	50.93	54.08	3.94	0.99	
	IMWM	51	32.49	34.48	3.90	0.99	
	NIPR	-	-	-	-	-	
	NCAR	14	30.47	31.66	2.26	0.92	
Z	Tethersonde	14	-	-	6.04	1.00	(2.23)*
	IMWM	55	-	-	12.26	0.99	(-0.39)*
	NIPR†	5	-	-	3.85	1.00	(-3.20)*
	NCAR	14	-	-	5.88	1.00	(-0.37)*
S§	Tethersonde	14	6.52	6.15	0.53	0.98	
	IMWM	53	4.46	5.47	1.92	0.91	
	NIPR†	5	1.63	2.06	1.67	0.64	
	NCAR	-	-	-	-	-	

* Mean difference from actual heights.
† NIPR data were not processed electronically but averaged by eye.
§ Wind speed used for this comparison since IMWM did not measure wind direction.

25.3 SCATTER DIAGRAMS AND NOTES

In the following scatter diagrams the scales on the axes convert directly to meteorological units when multiplied by the factor (10, 100, or 1000) indicated in parentheses. The wind components U and V are given in m/s; temperatures and dew points in °C; heights in m; relative humidities in %.

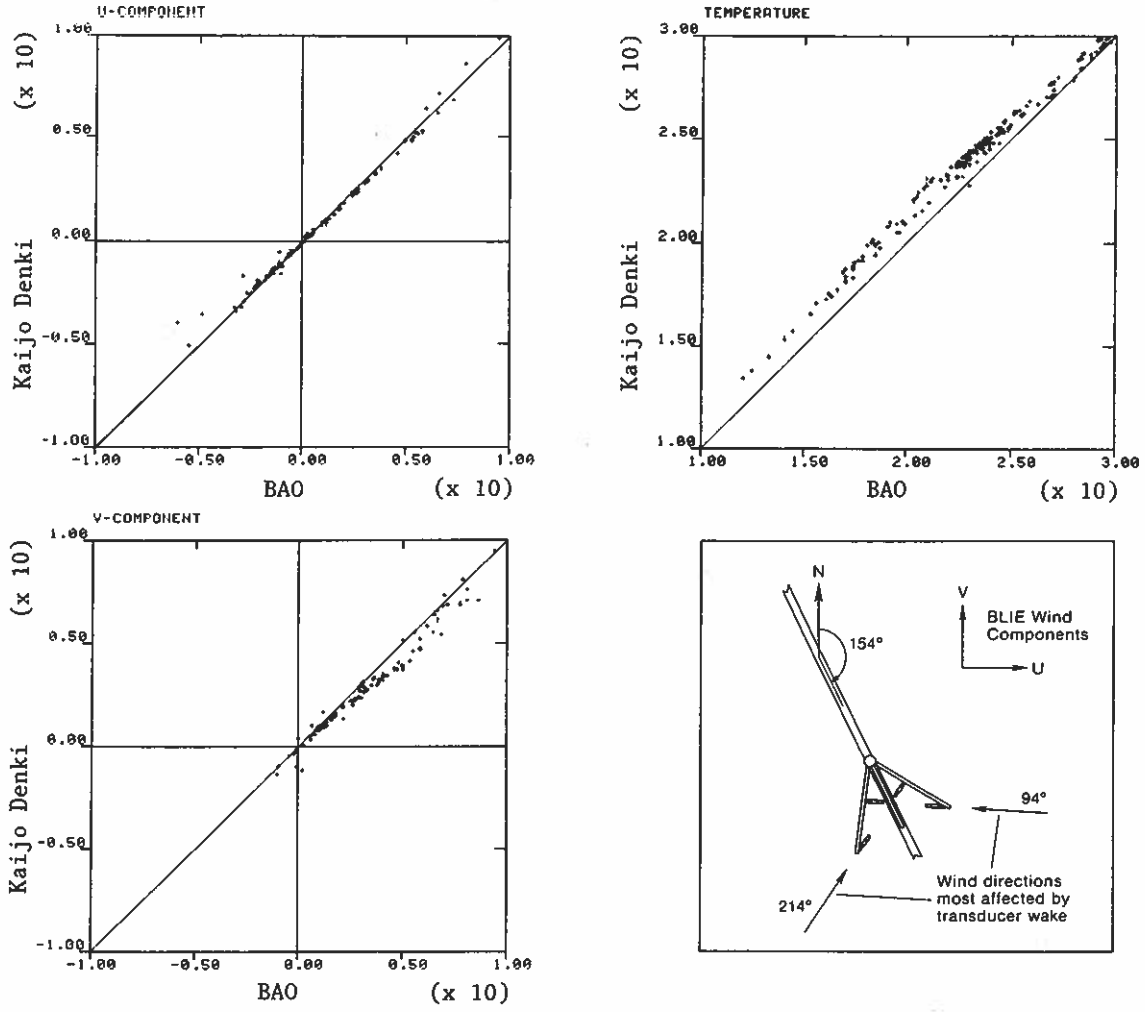

Figure 25.1. Scatter plots of data from Kaijo Denki sonic anemometer-thermometer at 50-m level vs. data from BAO tower sensors. Sketch shows orientation of the Kaijo Denki probe on the SSE boom.

Notes on Fig. 25.1

1. Only wind directions from 64° to 244° (clockwise) are included in this comparison. Not many data points occur on the negative side of V because of this restriction.

2. Significant departures from the 1-to-1 lines (for U ≅ -5 m/s and V ≅ 5 m/s) may be attributed to (1) absence of correction for transducer blockage of flow along the Kaijo Denki axes (see sketch in Fig. 25.1), (2) overcorrection for same effect in the BAO sonic anemometer, or (3) distortion of flow field around the tower. The lack of such a clear trend away from the 1-to-1 line in the Vaisala-BAO plots (see Fig. 25.2) suggests that the absence of correction in the Kaijo Denki data is a major factor.

3. The sonic temperature setting on the instrument appears to be offset by about +1°C; otherwise, the Kaijo Denki temperature data seem to track the BAO temperature data quite well. The sonic thermometer measures relative changes in temperature more accurately than the absolute temperature.

Notes on Fig. 25.2

1. The same restriction on wind direction (see Note 1 on Fig. 25.1) applies here for the U and V comparisons. Large scatter for light winds exists because wind components are resolved from 20-min averaged speeds and directions in the Vaisala data.

2. Temperature comparisons with and without restricting wind directions show no significant difference in overall scatter. In the former, wind directions are restricted to ranges of 34° to 94° and 214° to 274°. Vaisala and BAO temperatures were measured from opposite booms (see Section 24.3).

3. No direction restrictions were imposed for the humidity comparisons.

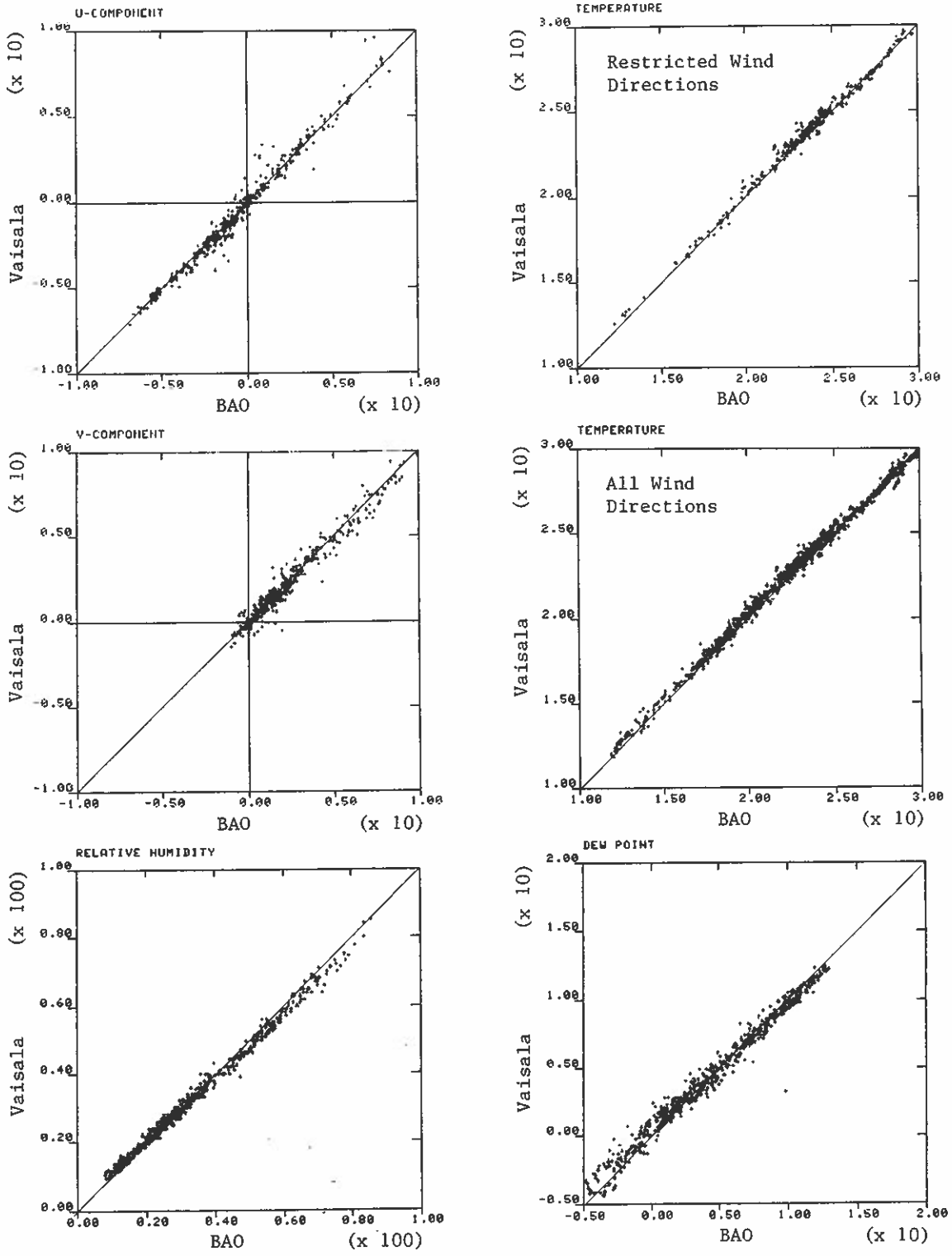

Figure 25.2. Scatter plots of data from Vaisala tower sensors vs. data from BAO tower sensors.

Notes on Fig. 25.3

Comments from D. Martin, EERM

1. SAM-B temperature readings during flight appear to be lower than tower temperature readings by about 0.4°C for ascents and 0.2°C for descents. Although this may be caused by calibration error, the probability is low.

2. In a 20-min period when temperatures are rising, instantaneous temperatures obtained from SAM-B at the beginning of the period will be lower than the mean temperature for that period.

3. Consideration must be given to possible perturbations of the temperature field caused by the tower or the lack of ventilation in tower sensors.

Editors' response

The temperature sensors on the tower are aspirated and shielded. Periodic comparisons between measurements on the tower and the NCAR aircraft show agreement at 250-m height to within ±0.1°C. Radiation error in the tower measurements is less that 0.04°C.

Notes on Fig. 25.4

Comments from D. Martin, EERM

Temperature readings from SAM-B instrument package on carriage are higher than tower temperatures because of lack of adequate ventilation in our sensors while on the carriage. This difference in behavior proves the good ventilation on the SAM-B aircraft.

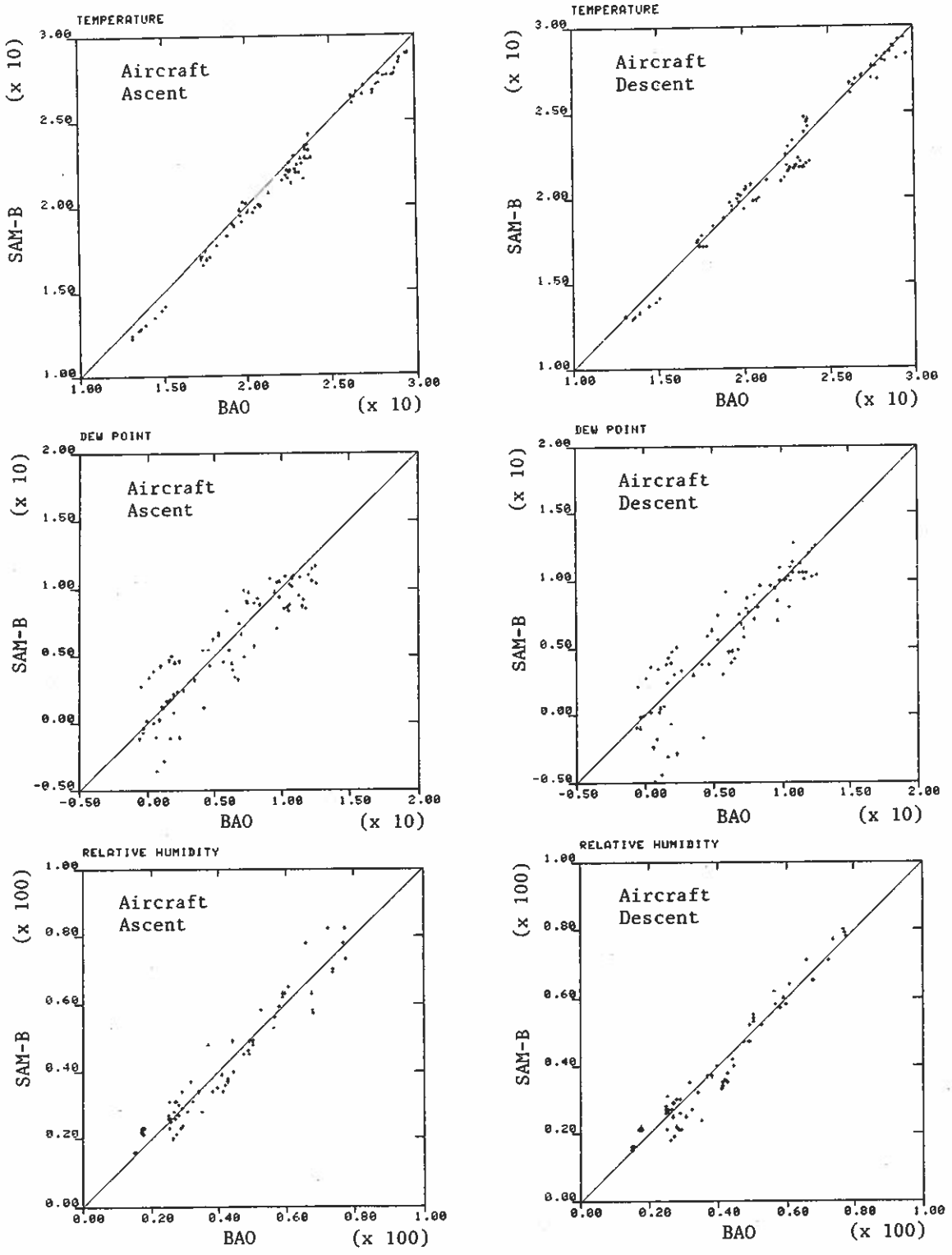

Figure 25.3. Scatter plot of data from SAM-B air-borne sensors vs. data from BAO tower sensors.

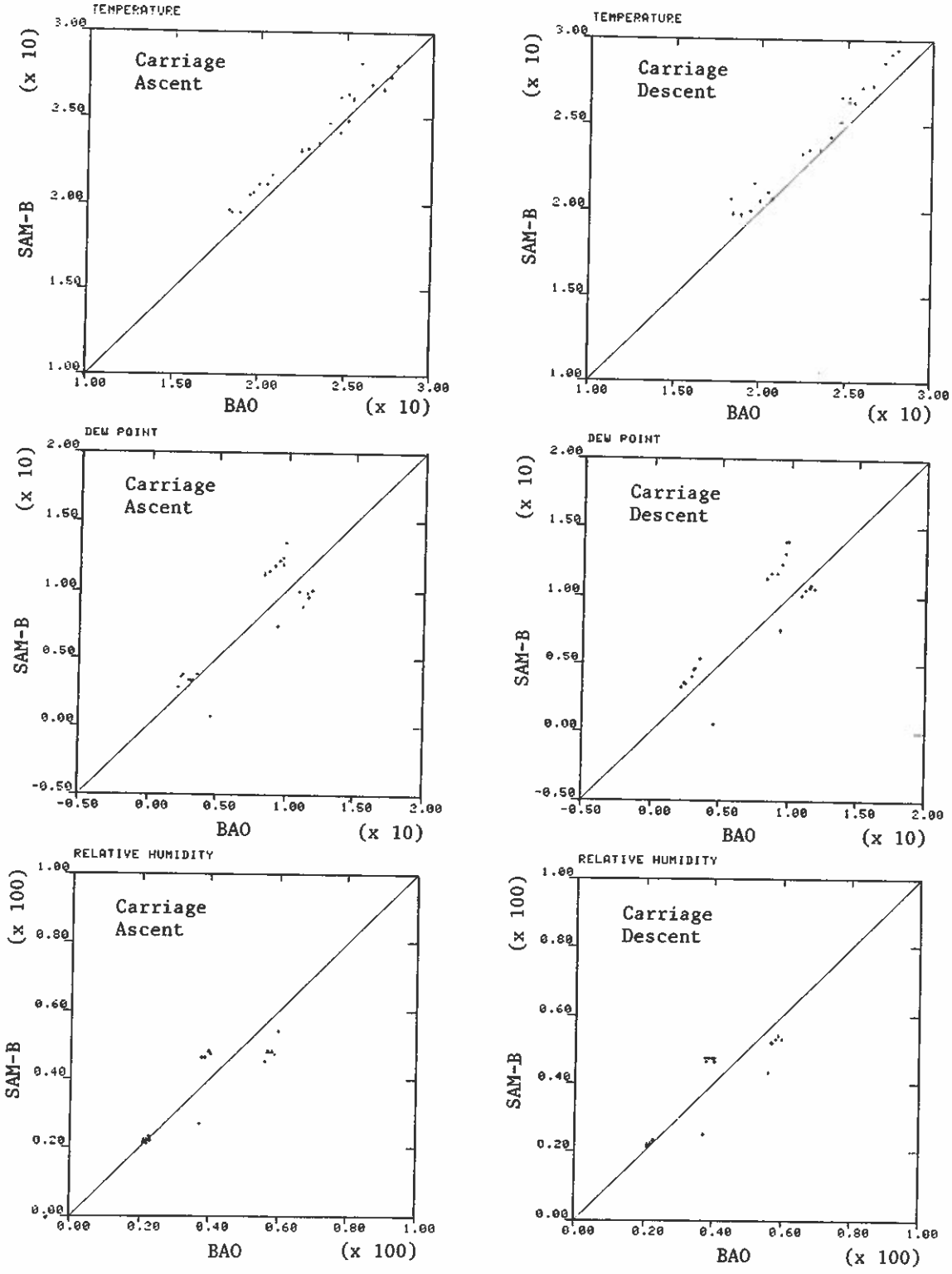

Figure 25.4. Scatter plots of data from SAM-B instrument package on carriage vs. data from BAO tower sensors.

Notes on Fig. 25.13

Comments from E. Schöllmann, Deutscher Wetterdienst

1. The TDFS data have no radiation error because the sensors are well aspirated and housed in a radiation shield. The sensors are bead thermistors with fast response.

2. Discrepancies between the sonde and the tower profiles may result because data are not compared at significant points but at fixed pressure steps.

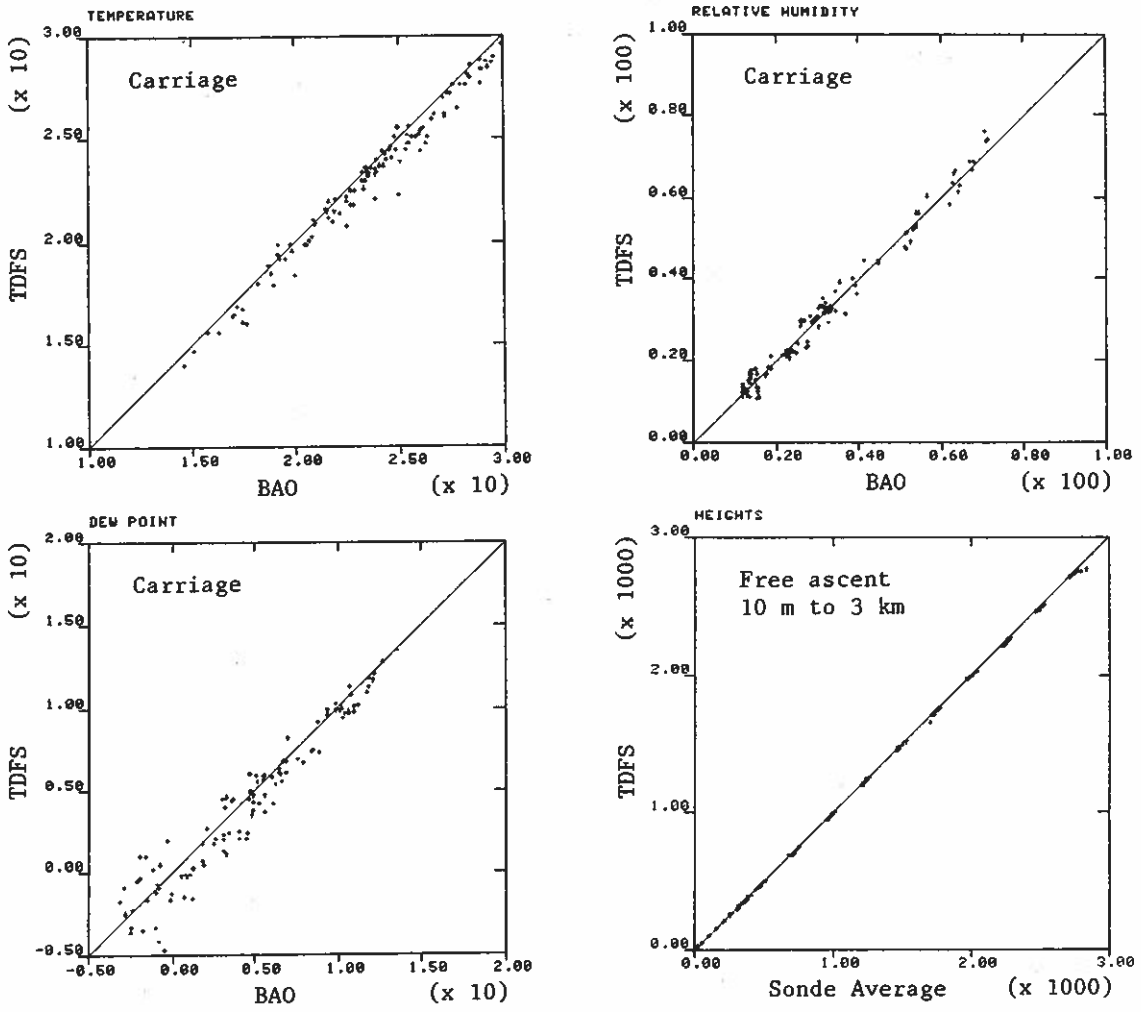

Figure 25.14. (Upper, left and right, and lower, left) Scatter plots of data from TDFS radiosondes on carriage vs. data from BAO tower sensors. (Lower, right) TDFS radiosonde computed heights vs. average heights for all balloon-borne radiosondes.

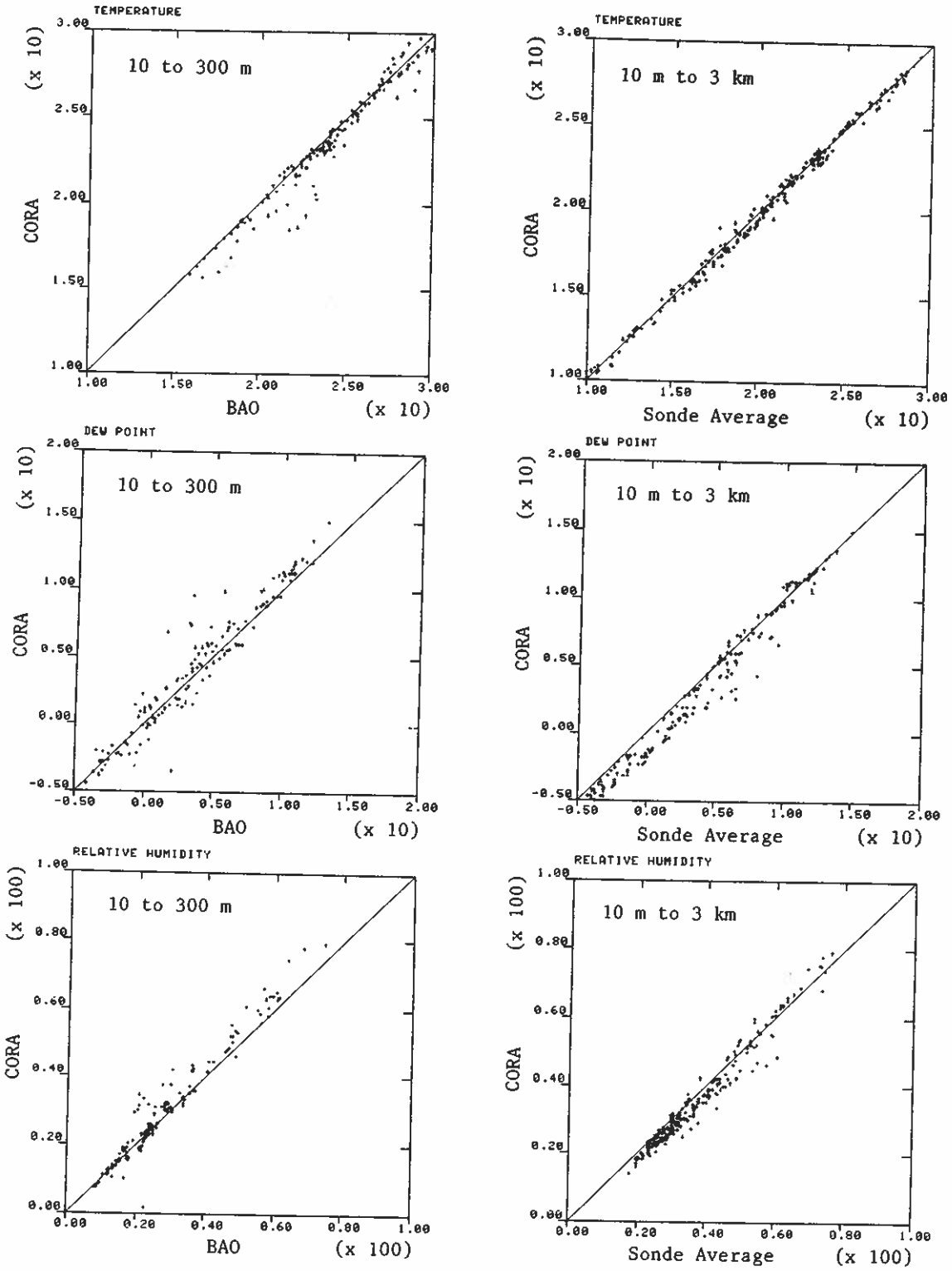

Figure 25.15. Scatter plots of balloon-borne CORA radiosonde data vs. data from BAO tower data and vs. average for all radiosondes. Data in the righthand group are restricted to periods when all four sondes were functioning satisfactorily.

Notes on Fig. 25.15

The CORA system measured relative humidity with a Humicap sensor that has a faster response than the wet-bulb systems used in the TDFS and Airsonde.

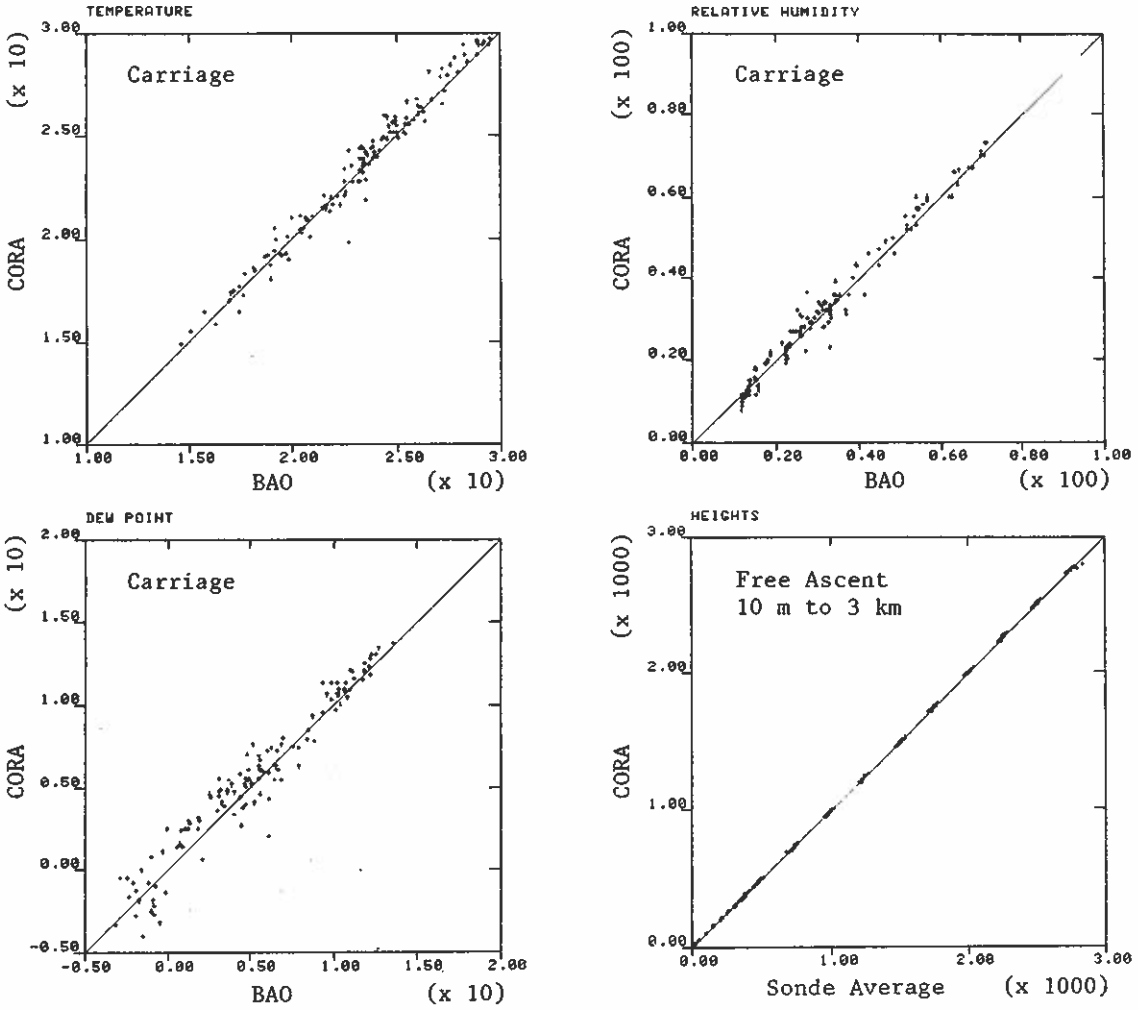

Figure 25.16. (Upper, left and right, and lower, left) Scatter plots of data from CORA radiosondes on carriage vs. data from BAO tower sensors. (Lower, right) CORA radiosonde computed heights vs. average heights for all balloon-borne radiosondes.

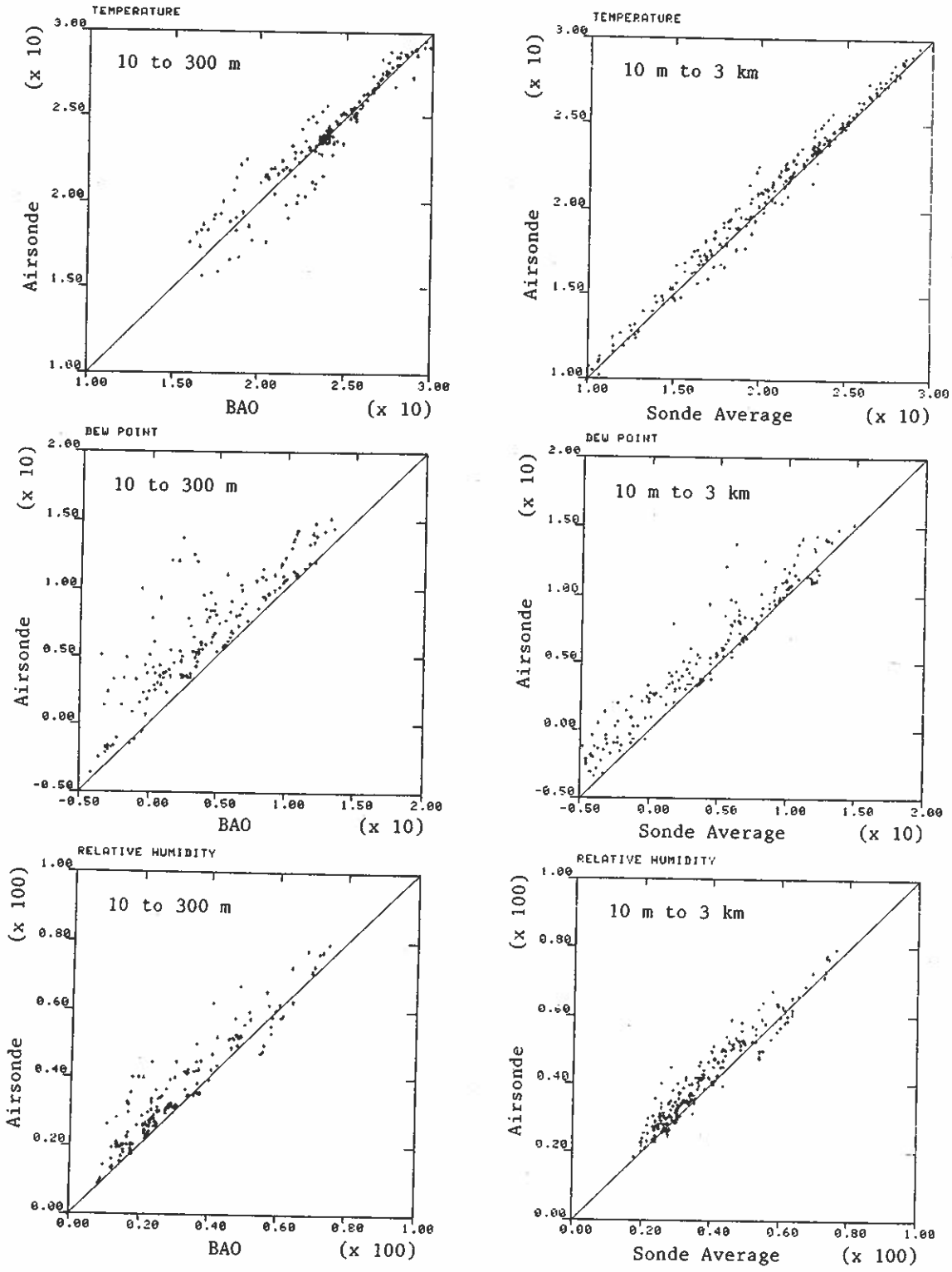

Figure 25.17. Scatter plots of balloon-borne Airsonde data vs. BAO tower data and vs. average for all radiosondes. Data in the righthand group are restricted to periods when all four sondes were functioning satisfactorily.

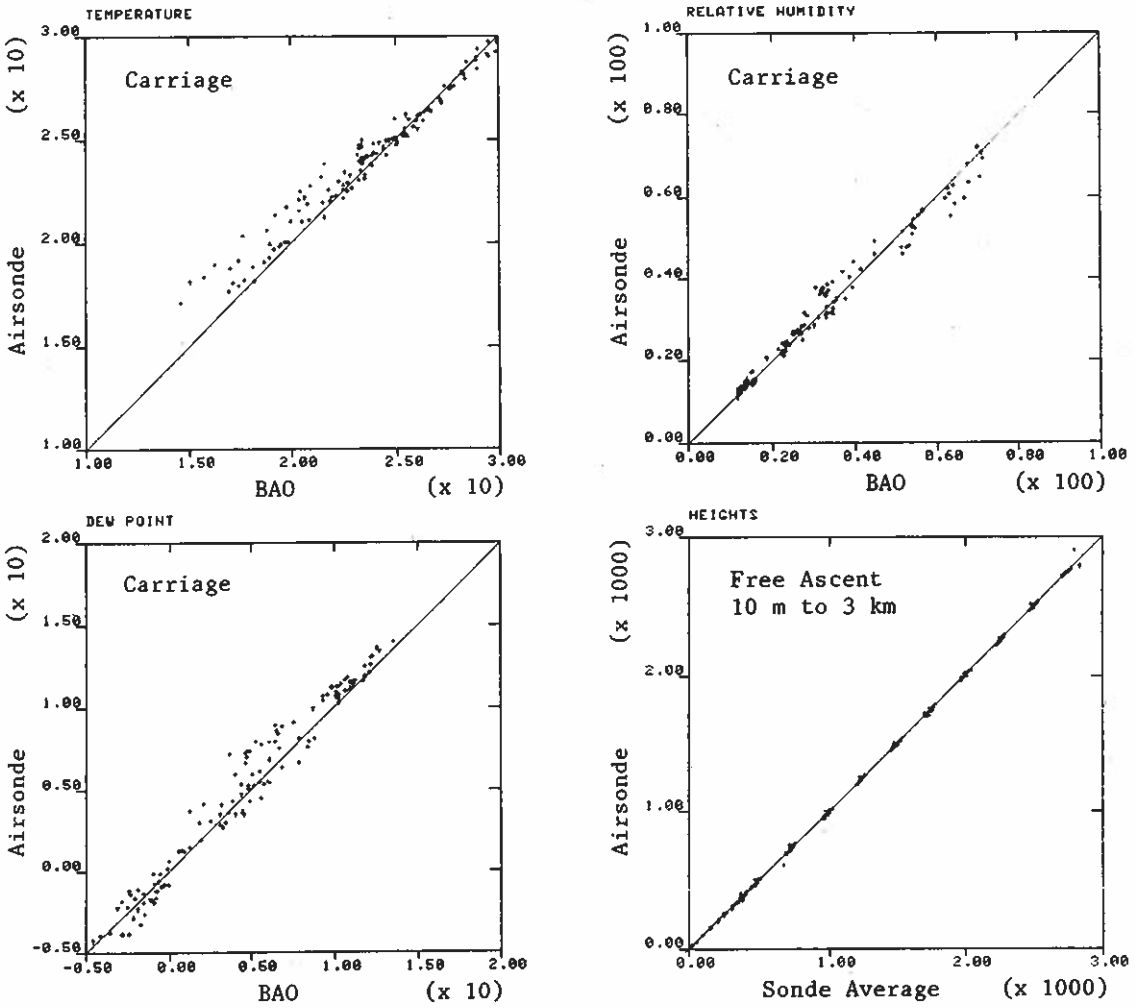

Figure 25.18. (Upper, left and right, and lower, left) Scatter plots of data from Airsondes on carriage vs. data from BAO tower sensors. (Lower, right) Airsondes computed heights vs. average heights for all balloon-borne radiosondes.

Notes on Figs. 25.17 and 25.18

Comments from D. B. Call, AIR, Inc.

1. At first, Airsonde temperatures and dew points were often 2°C or 3°C too high in full sunlight but generally accurate at dusk and after sunset. The problem, identified as radiative heating, was corrected by painting the thermistor beads white and the insides of the two ducts black (reverse of original colors). Data from modified Airsondes for 4 and 5 September show excellent agreement with tower data (see Fig. 25.19).

2. The consistent positive bias of the dew points (Fig. 25.17) is caused by absence of any aspiration of the wet thermistor until the instant of launch when the Airsonde began to rotate. The error rapidly diminishes during the first minute of flight and could be eliminated by forced aspiration of the wet thermistor while the Airsonde is on the ground. In the carriage ascents (Fig 25.18) the thermistors were aspirated before data collection, which brought the dew point readings to equilibrium.

Notes on Fig. 25.19

Comments from D. B. Call, AIR, Inc.

1. Results are restricted to data obtained with Airsondes modified to reduce radiative heating.

2. On these two days, for the carriage ascents, the wet-bulb thermistor was aspirated by a small electric fan throughout the ascent, beginning a few minutes before ascent. Thus the wet-bulb temperatures are properly depressed, and the dew point data are in good agreement with those of the tower.

3. For balloon ascents, there is little aspiration of the wet thermistor until the Airsonde begins to rotate. Since the wet thermistor requires a minute or two to cool to its proper value, the first few indicated dew points (and relative humidity) are higher than those of the tower.

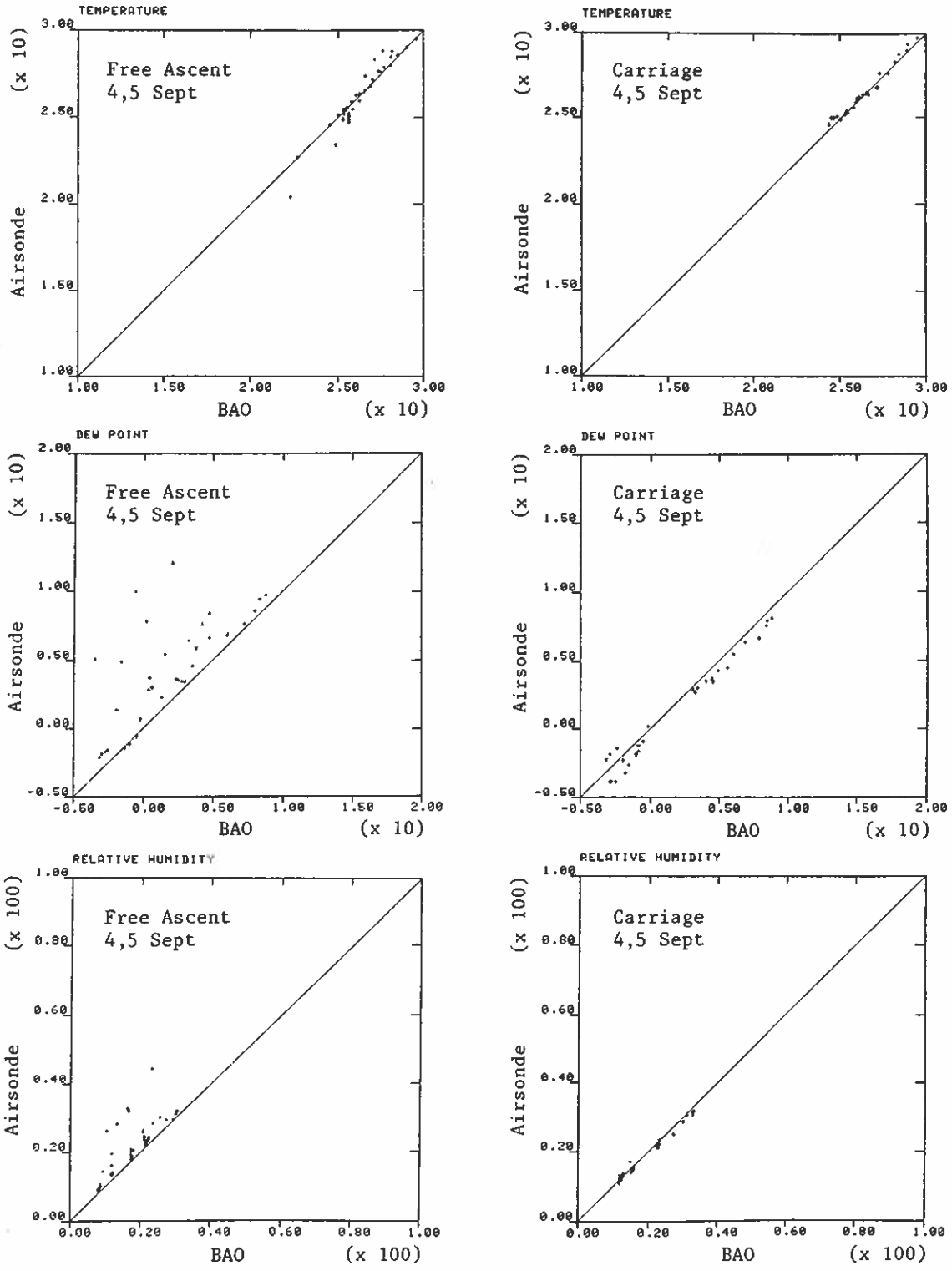

Figure 25.19. Scatter plots of data from Airsondes vs. data from BAO tower sensors for 4 and 5 September 1979.

Notes on Fig. 25.20

Comments from A. L. Morris, Ambient Analysis

1. The three plots on the left (tethered balloon ascents) show a positive bias that is absent in the plots on the right (carriage ascents). Since the balloon ascents were made at midmorning and midafternoon whereas the carriage ascents were in the evening, solar radiation undoubtedly contributed to the bias.

2. After the intercomparison experiment, the inside of the aspirated duct was painted black to reduce radiation errors.

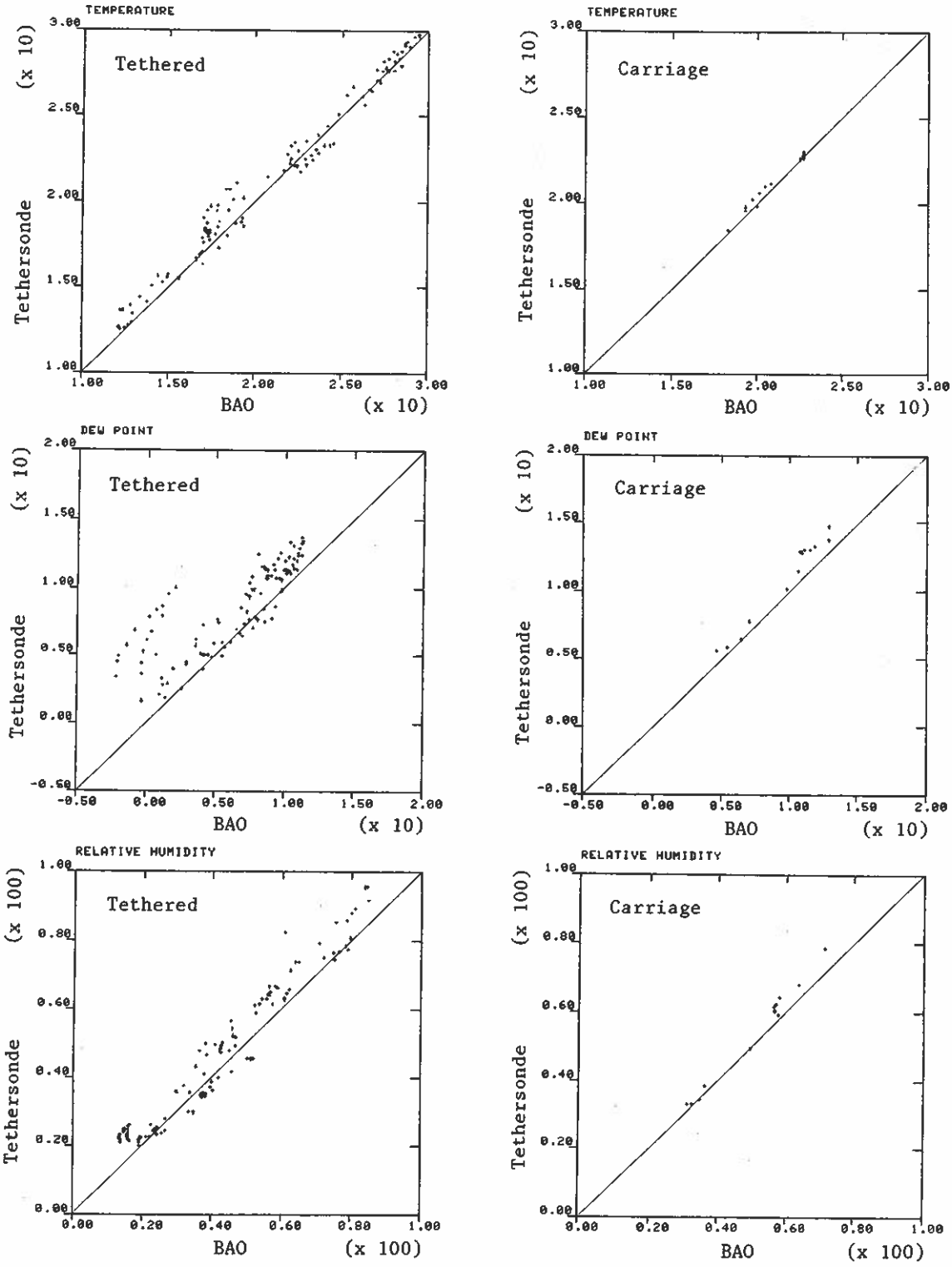

Figure 25.20. Scatter plots of data from Tethersonde vs. data from BAO tower sensors.

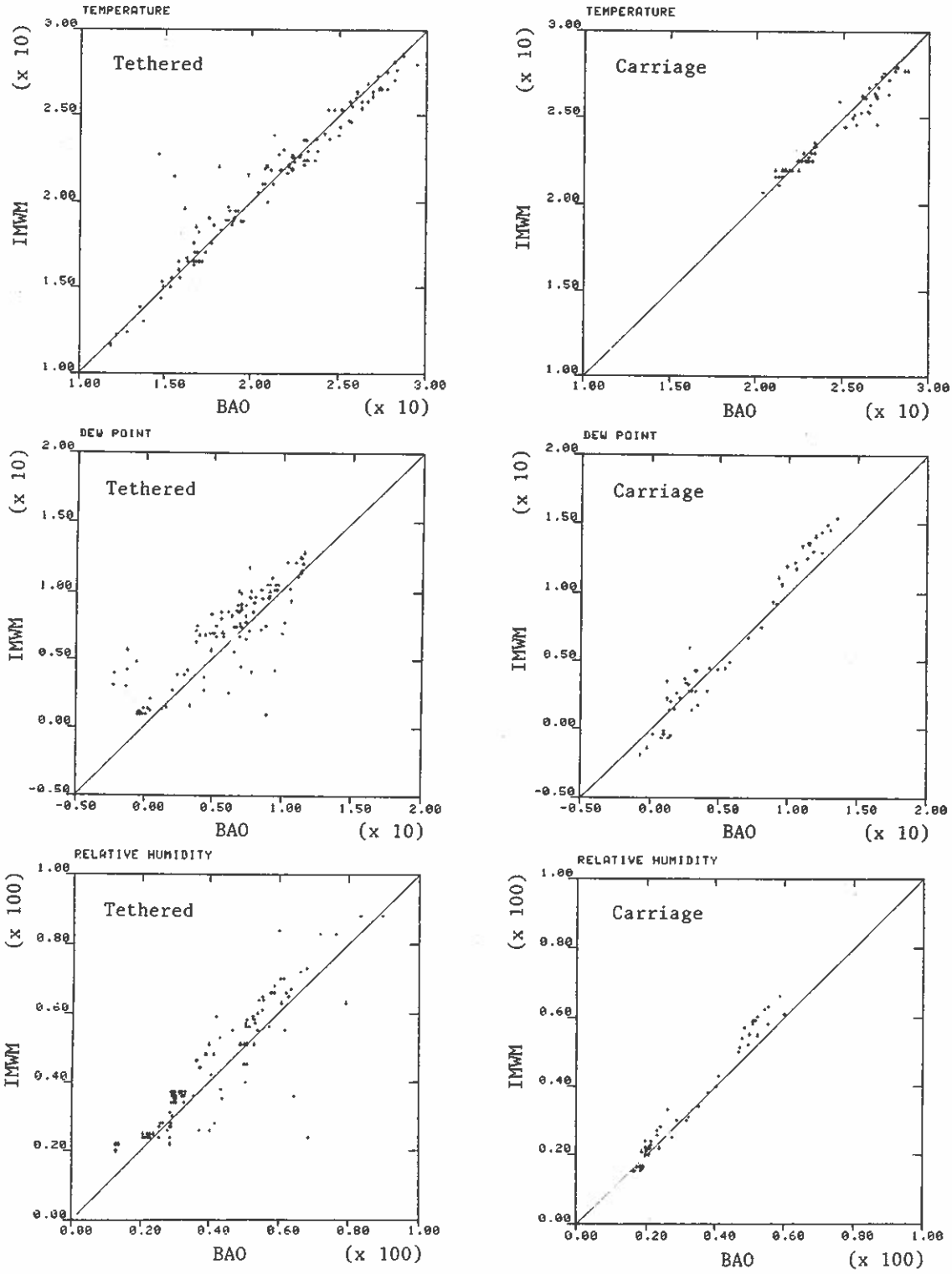

Figure 25.21. Scatter plots of data from IMWM tethered profiler vs. data from BAO tower sensors.

20.4.1.4 Voltage-controlled oscillators (VCO)

The Tethersonde transmits data on two audio channels. These channels are frequency multiplexed to modulate the RF carrier. Two VCOs are controlled by the voltage on the analog buss. One VCO oscillates at a nominal 500 Hz ± 75 Hz and is used to transmit continuous data from any individual sensor. The other VCO oscillates at 2500 Hz ± 375 Hz and is used to transmit time multiplex data on the analog bus. It carries all the information processed by the ground station microcomputer.

Output from each VCO is a square wave. The fundamental frequency is extracted from each waveform before frequency multiplexing by two low-pass active filters.

20.4.1.5 FM transmitter

A crystal-controlled RF transmitter produces 5 mW at 400-410 MHz depending on crystal selected. The transmitter is referenced to a voltage-controlled crystal oscillator (VXCO) running at a nominal 44 MHz. The ninth harmonic of the VXCO is generated through two stages of frequency conversion. The first tripler runs at about 134 MHz and the second at about 403 MHz. The final stage is a power amplifier at 403 MHz and a buffer for the monopole antenna.

20.4.2 Ground Station

The ground station is the Model TS-2A-GS, which is identical to the ground station described in Chapter 19 on the Airsonde system. The discussion of ancillary equipment such as the printing calculator and the tape recorder contained in that chapter is also pertinent here.

Table 20.1 lists typical calculator printouts. Ground station software permits every n-th data frame to be sent to the calculator whereas every frame is stored by the tape recorder. Thus, for example, a 10-s frame rate may be chosen, and every third frame may be sent to the calculator. It then has 30 s to calculate and print a data frame, time enough to produce a printout like that shown in Table 20.1 (left). Since every frame is recorded on tape, and since on playback the ground station can be programmed to send taped data to the calculator at any desired rate up to 99 s per frame, the calculator can do extensive postflight calculations with every data frame. The real-time calculations are often found to be adequate, but in any event they provide information with which to make operational decisions during flight. Then if greater vertical resolution is needed or if additional calculations are desired, the tape record can be used.

Table 20.1. Typical output from the TS-1A-PC printing calculator

Calculated printout			Not-calculated printout*		
Variable	Printout		Variable	Printout	
Time (min)	9.0505	***	Elapsed Time (min)	1.8	***
P (mb)	838.2	***	Prel (mb)	8.4	***
z (m)	121.5	***	T (°C)	25.2	***
T (°C)	23.2	***	ΔT (°C)	11.9	***
RH (%)	26.6	***	Mag Dir (deg)	321.6	***
w (g/kg)	5.7	***	U (m/s)	0.6	***
True Dir (deg)	112.1	***	BV (%)	92.7	***
U (m/s)	2.7	***			
θ(k)	311.7	***			
BV (V)	12.3	***			

*Printout without calculations, but with the order of the variables changed from the order in which they are received at the ground station.

20.5 REFERENCES

Morris, A. L., D. B. Call, and R. B. McBeth (1975): A small tethered balloon sounding system. Bull. Amer. Meteor. Soc. 56(9):964-969.

Moses, H. (1968): Meteorological instruments for use in the atomic energy industry. In Meteorology and Atomic Energy, ch. 6, David H. Slade (ed.), USAEC.

Pike, J. M., and D. W. Bargen (1976): The NCAR digital barometer. Bull. Amer. Meteor. Soc. 57(9):1106-1111.

21. TETHERED BALLOON PROFILER SYSTEM

K. Stefanicki
Institute of Meteorology and Water Management
Division of Aerology
Warsaw, Poland

21.1 INTRODUCTION

To gather more meteorological data from the boundary layer for the Institute of Meteorology and Water Management, a simple and inexpensive sounding system for heights up to about 1 km was put into operation. Figure 21.1 shows the instrumentation package used in the BLIE.

21.2 COMPONENTS OF THE SYSTEM

21.2.1 Radiosonde

Table 21.1 lists the characteristics of U.S.S.R.-made radiosonde A-22-IV with redesigned pressure element, an additional wind sensor, and automatic switch for PTU and W signals.

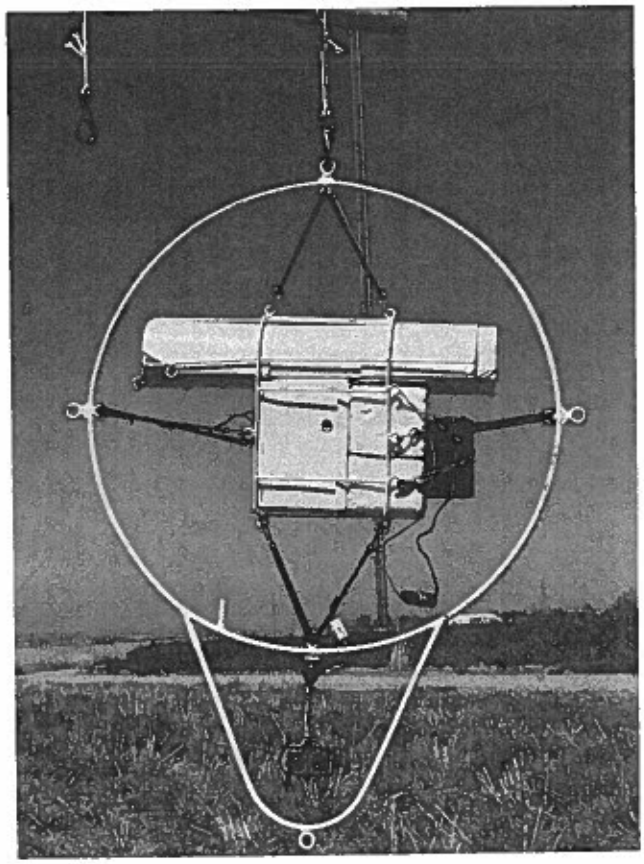

Figure 21.1. Instrumentation package used with tethered balloon in the BLIE.

Table 21.1. Radiosonde characteristics

Characteristics	Parameters			
	Pressure	Temperature	Humidity	Wind speed
Sensors	Aneroid	Bimetal	Organic	Cup anemometer
Measuring range	1050 to 700 mb	-40 to +40°C	10% to 100%	1.5 to 10 m/s
Resolution	1.5 mb	0.5°C	2%	0.1 m/s
Data rate	4/min	4/min	4/min	4/min
Coding		Morse		Pulse/10 s

Further information about the radiosonde is presented below:

Transmitter frequency: 400 ± 5 MHz.

Power supply: 4.5-, 9-, and 210-V batteries.

Ventilation: Natural if wind speed is ≥2 m/s, artificial if wind speed is <2 m/s; horizontal ventilation duct.

Fastening: Metal circular frame with shock absorbers.

Radiation shield: Two shields, metal and fiberboard.

Weight: 3.0 kg.

21.2.2 Tethered Balloons and Winch

Balloon Delacoste (made in France) has a volume of about 12 m^3 and a height limit of about 1 km and is filled with helium. This balloon may not be used when wind velocity exceeds 4 m/s at the ground and 10 m/s aloft.

Balloon Zodiac (made in France) has a volume of about 20 m^3 and a height limit of about 1.5 km and is filled with helium. This balloon may not be used when wind velocity exceeds 4 m/s at the ground and 15 m/s aloft.

The winch (our own design), which operates electrically, has two cable speeds, 1 and 2 m/s. It is equipped with a hand brake, a cable length counter, and an azimuth disc. For the BLIE the smaller 7-m^3 balloon and winch described in Chapter 20 were used.

21.2.3 Acquisition and Processing Equipment

The equipment consists of a receiver, a pulse counter, and a calculator, whose characteristics are listed below:

Power requirements: 220 V, 50(60) Hz.

Pressure, temperature, and humidity: Audio-Morse signals, recorded manually.

Wind speed: Pulse counter, recorded manually.

Processing: With the aid of a calculator, height is computed either with the barometric formula or by radar tracking; the height of the lowest levels can be determined by cable length.

21.3 SOUNDING PROCEDURE

The radiosonde is mounted on a tethered balloon. Measurements are made during balloon stops at selected levels, both during ascent and descent. Before launch and just after sounding completion, a ground check of the radiosonde is required. The measurements at each level take about 3 min.

21.4 RESULTS

The results are presented in the form of computer-generated tables and graphs (parameter vs. height). Time required to process the data is about 1 h. Data accuracies are listed below:

Height: $\pm$15 m.

Temperature: $\pm$0.5°C.

Humidity: $\pm$5%.

Wind speed: $\pm$0.2 m/s.

Wind direction: $\pm$20° (rough estimation based on determination of balloon position with respect to the north using a special attachment at the winch).

22. BOUNDARY LAYER PACKAGES FOR TETHERED BALLOON

M. Hayashi and O. Yokoyama
Nation Research Institute for Pollution and Resources
Ukima, Japan

22.1 INTRODUCTION

Three types of boundary layer packages for balloon-borne measurements were compared in the BLIE. Figure 22.1 shows the prototype, Meisei Denki, model CBS-W-5. The other two are variations of the prototype: (1) the simplest version, Makino (Fig. 22.2), and (2) the fully equipped version, Kaijo (Fig. 22.3). Although their appearances differ, the variations in sensors are minor. The packages use the same cup anemometer. Meisei uses a bi-directional vane and detects the angle of the vane by the optical method; the others have a vertical vane and detect the angle by a contactless potentiometer (see Chapter 20). Kaijo has a hot-wire anemometer and a thermocouple to measure fine fluctuations in wind speed and temperature.

22.2 SENSORS AND DATA PROCESSING

22.2.1 Cup Anemometer

Wind speed is detected by a small, three-cup anemometer. The cup is made of molded plastic. The length of the arm is 6.5 cm, the cross-section of the cup is 2.0 cm^2, and the estimated moment of inertia is 450 g cm^2. One rotation produces eight pulses on the photoelectric chopper. The pulses are shaped into square waves and mixed with other signals through subcarrier (voltage-controlled) oscillators.

22.2.2 Vane

Vertical and lateral wind direction fluctuations are detected by a bi-directional vane. It has four rectangular flat plates (8 x 9 cm) made of light wood (balsa) with plastic support. The vertical and lateral angles of the vane are detected by using an optical mechanism for reducting the friction.

22.2.3 Compass and Mean Wind Direction

The azimuth of the instrument is detected by a magnetic compass. The angle of a small rotating magnet in an oil box is detected by an optical servomechanism.

22.2.4 Thermometer

Temperature is detected by a fine platinum wire of 100 Ω. The temperature fluctuation is detected by a thermocouple of copper-constantan in the Kaijo instrument. The standard temperature is given by a transistor thermometer with a time constant of 3 min.

22.2.5 Humidity

We do not yet have a suitable humidity sensor. The gauze-covered wet-bulb thermometer yields mean humidity. A lightweight hygrometer with fast response and low electric power consumption is needed.

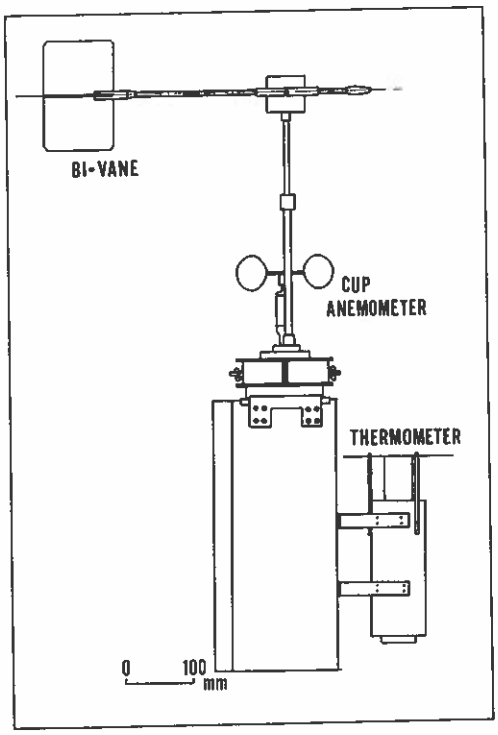

Figure 22.1. Prototype boundary layer package for balloon-borne measurements.

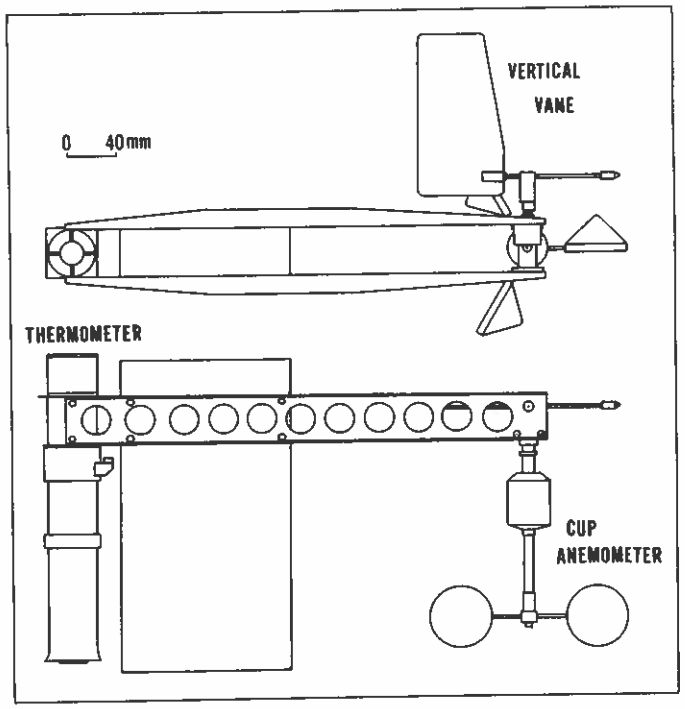

Figure 22.2. The simplest version of the prototype.

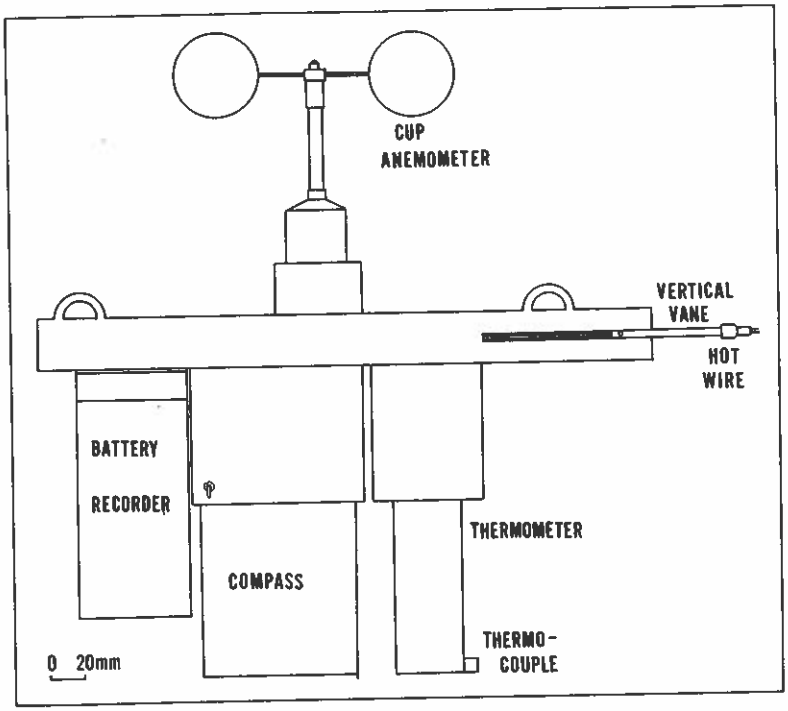

Figure 22.3. Fully equipped version of the prototype.

22.2.6 Height

The height of the instrument package is given by released line length with allowance for elevation angle to the balloon when the wind speed is high.

22.2.7 Data Processing System

The electronic data processing system in the package is diagrammed in Fig. 22.4. The signals from each sensor are converted to frequency modulated signals according to the IRIG standard and then mixed together. The mixed FM signal is transmitted by frequency-modulated UHF carrier at 404.5 MHz. However, wireless transmission of this type is permitted only for experimental tests.

22.2.8 Recording System

The mixed signal is recorded on an audio microcassette tape recorder, Sony M-200, for practical use (Hayashi et al., 1974). To avoid the wow and flutter of the tape recorder, a standard frequency (3 kHz) is recorded simultaneously. This is used as an automatic frequency controller when the signal is reproduced. The recording duration is 30 min. The recorded signal is reproduced in the laboratory, discriminated by filters, and reduced to the original signal through a frequency-voltage converter.

22.2.9 Harness

The instrument package is hung on the mooring ropes below the center of the captive balloon shown in Fig. 22.5. The balloon is tear-drop shaped, with four fins at the rear. The volume of the balloon varies from 20 to 75 m^3. The mooring rope is nylon fish line 6 mm in diameter, 0.0142 g/m, and 500 kg test. The instrument is supported by a gimbal bar so that all sensors are exposed to the wind. For the BLIE, the 7-m^3 balloon and winch described in Chapter 20 were used.

22.3 CALIBRATION

22.3.1 Cup Anemometer

The characteristics of the cup anemometer have been studied in a wind tunnel and in the field by Hayaski and Miyake (1973). The equation of motion of a cup anemometer is

$$I \frac{d\omega}{dt} + F = M,$$

where I is the moment of inertia, ω the angular velocity, F the friction, and M the torque of the rotating assembly of the cup. The torque is assumed to be given by the difference in the drag of a pair of cups:

$$M = \frac{\alpha}{2} \rho RS\{C_-(U-\omega R)^2 - C_+(U+\omega R)^2\}\frac{N}{2},$$

where U is the wind speed, R the length of the arm, ρ the air density, S the cross section of the cup, N the number of cups, C_- and C_+ the drag coefficients of the cup along and against the wind, and α the variability of the torque of the entire cup assembly during a complete revolution. If N = 2, α varies between 0 and 1, but for three- and four-cup anemometers α is nearly uniform and equal to or slightly less than 1. The drag of the rotating system is divided into static and dynamic terms as follows:

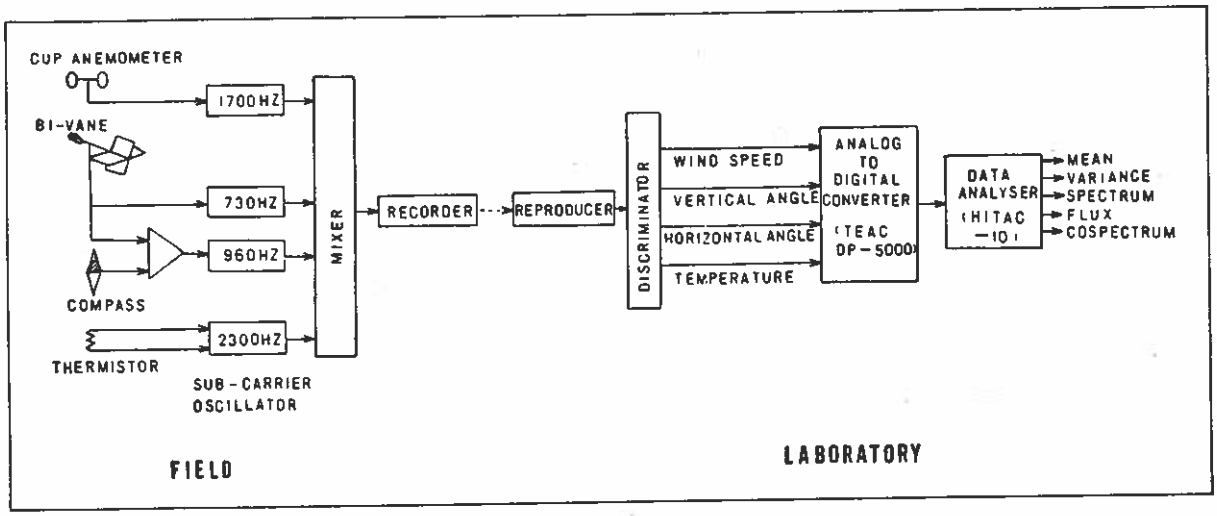

Figure 22.4. Data-processing system for the balloon package.

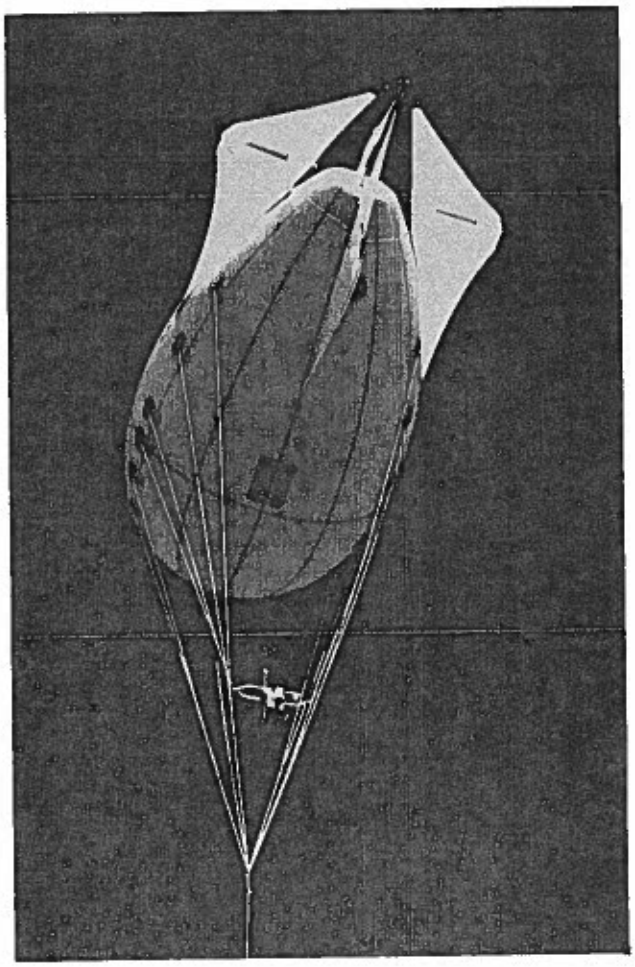

Figure 22.5. The instrument package mounted under a captive balloon.

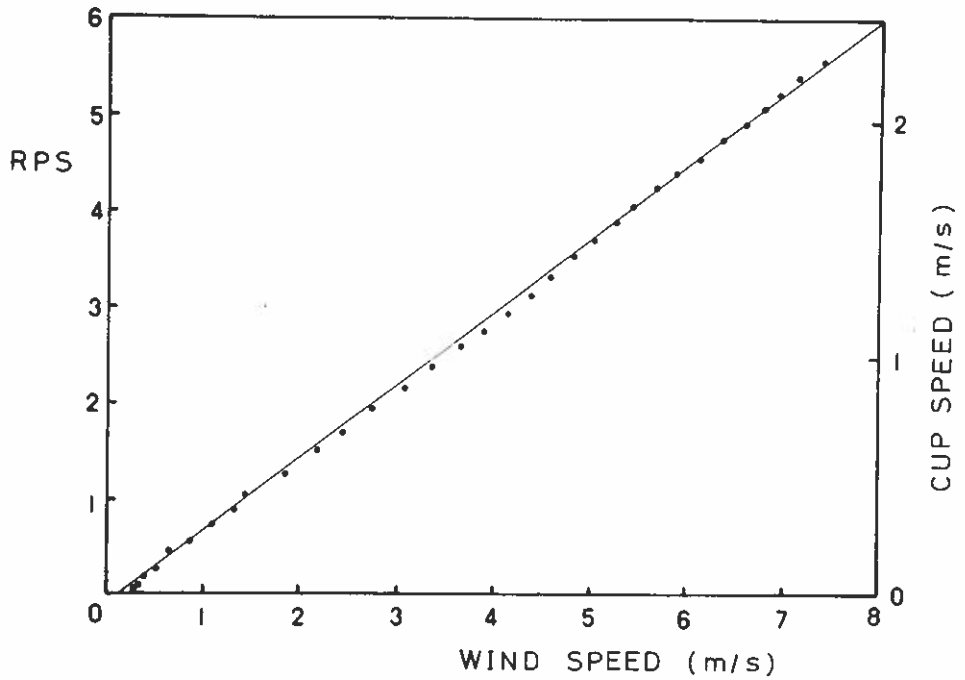

Figure 22.6. Calibration of cup anemometer in wind tunnel. Tunnel wind speeds were measured by a sonic anemometer calibrated by a Pitot tube.

$$F = B_0 + B_1\omega \ .$$

The fluctuation of wind speed, u, is smaller than the mean wind speed, $\bar{U}$:

$$U(t) = \bar{U} + \varepsilon u(t)$$

and

$$R\omega(t) = v_0 + \varepsilon v_1(t) + \varepsilon^2 v_2(t) + \ldots \ ,$$

where ε gives the order of the perturbation.

The zero-order equation gives the calibration curve of the cup anemometer. The relationship between the wind speed and the rotation of the cup assembly was tested in the wind tunnel. The Pitot tube was used as the standard instrument for measuring the flow velocity. At lower wind speeds, since the output of the Pitot tube is difficult to read, we used a sonic anemometer, Kaijo model PA-100, as our standard instrument. The result of the test is shown in Fig. 22.6. The starting wind speed is about 10 cm/s.

The transient response of the cup anemometer was tested in the wind tunnel. The first-order perturbation gives the linear response for wind speed change. The response is given by a distance constant

$$L = \frac{I}{\alpha N \rho R^2 S \sqrt{C_- C_+}}$$

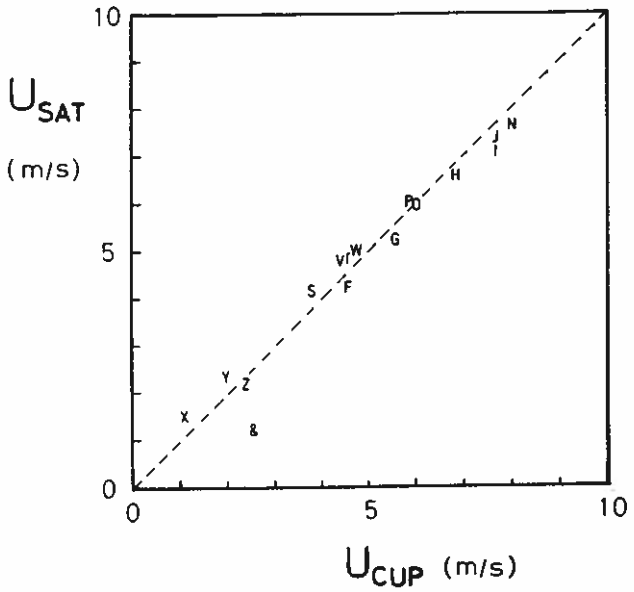

Figure 22.7. Comparison of mean wind speed measured by a cup anemometer and a sonic anemometer in turbulent atmosphere. The plotted letters identify different runs.

This response is about 4.5 m for this cup anemometer. The second-order perturbation shows the nonlinear response of the cup anemometer, i.e., the over-run (rotation) of the cup assembly. This is one of the most distinctive features of a cup anemometer, i.e., that it overestimates the mean wind speed in turbulent air flow. The cup anemometer calibrated in the wind tunnel was compared with the sonic anemometer, Kaijo model TR-32, in the real atmosphere. Both instruments were mounted on top of a 13-m tower. The overestimate of the cup anemometer amounts at most to 7%, as shown in Fig. 22.7.

The relationship between the wind speed, U, and the cut-off frequency, f_c, is obtained by comparing spectra. The cut-off frequency is $U/2\pi L$. The comparison gives the frequency response function of the cup anemometer, as shown in Fig. 22.8. The turbulent intensity measured by the cup anemometer is about 83% of that measured by the sonic anemometer, as shown in Fig. 22.9.

22.3.2 Vane

The transient response of the vane was tested by Yokoyama (1969) with a wind tunnel. Figure 22.10 shows an example of the time response of the vane to a step-function direction change. The response of the vane angle, Θ, can be represented by the following equation of simple damped oscillation:

$$\frac{d^2\Theta}{dt^2} - 2\omega_n\zeta \frac{d\Theta}{dt} - \omega_n{}^2\Theta = F(t) ,$$

where ω_n is the natural angular frequency of the vane, ζ is the damping ratio (the ratio of the actual damping to the critical damping), t is the time, and F(t) is a time-dependent forcing function. The damping ratio, ζ, and natural frequency, ω_n, are obtained from the measurements of the time response to a step-function direction change for various wind speeds by use of a solution of the equation for the case of $\zeta < 1$. The distance constant of the vane, $U/\omega_n\zeta$, is used as an index of the response characteristics and regarded as a constant for high wind speeds. It is approximately 1.6 m for this type of vane. An example of the frequency response for typical wind speeds is shown in Fig. 22.11.

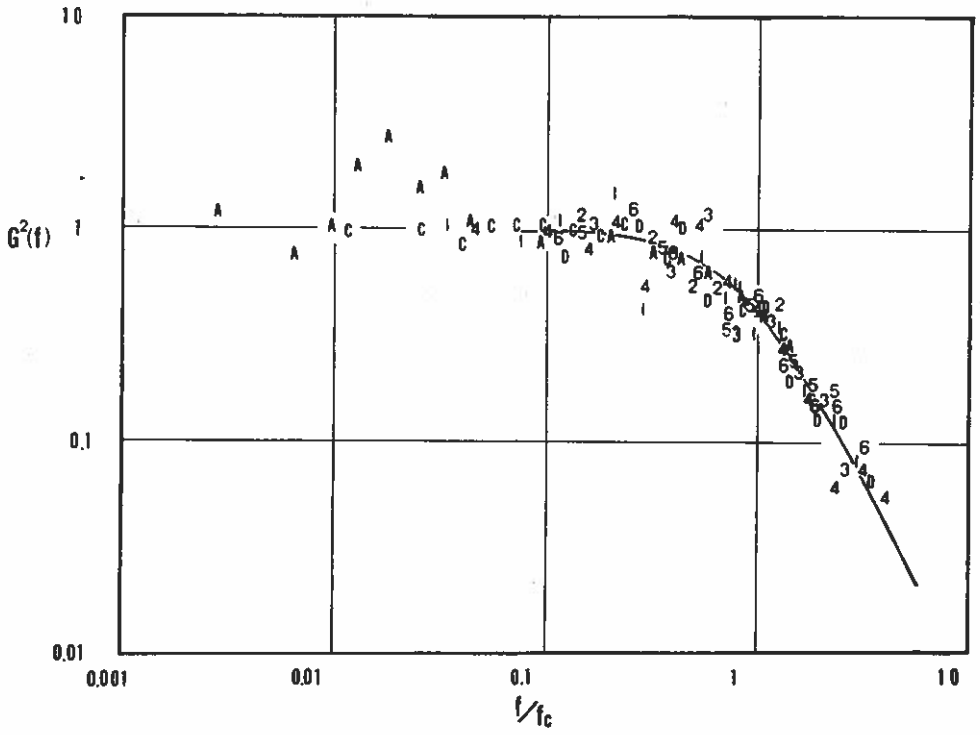

Figure 22.8. The frequency-response function as a ratio of power spectra from the cup and those of the sonic anemometer. The plotted letters and numbers identify different runs.

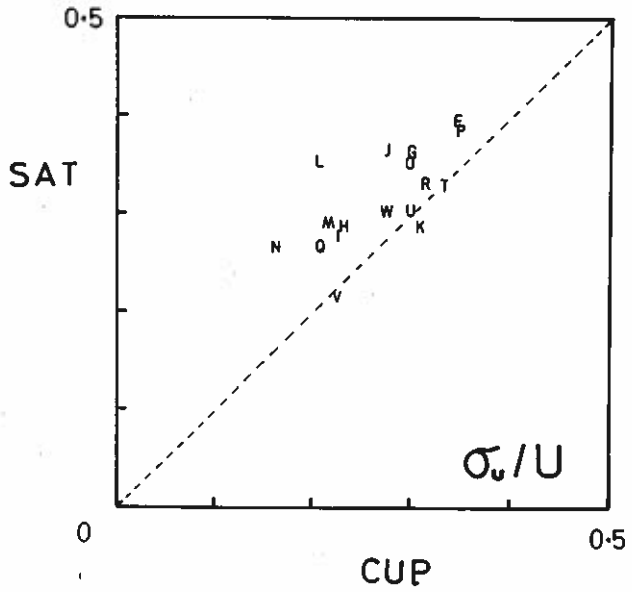

Figure 22.9. Comparison of σ_u/U as measured by cup and by sonic anemometer. The plotted letters identify different runs.

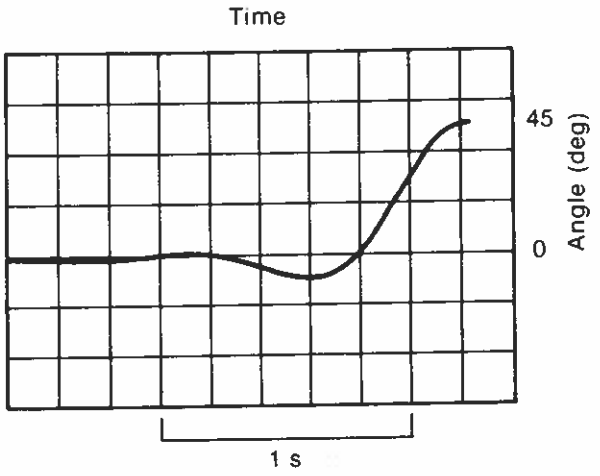

Figure 22.10. Example of the measured time response of the vane to a step-function direction change. (Mean wind speed is 3.0 m/s and angle of attack is 45.0°.)

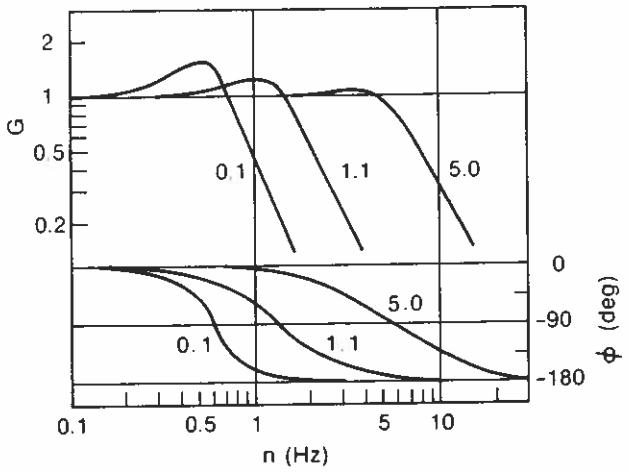

Figure 22.11. Frequency response of the vane for various wind speeds. (G is the ratio of amplitudes and ϕ is the difference of the phases. Entries are wind speed in m/s.)

22.4 OUTPUT FORMAT

The raw tape recorded data are contained within an FM multiplexed signal in the IRIG standard. The signal is separated by a discriminator into separate signals of each sensor. The output range depends on the discriminator. The discriminator used in the BLIE is for the simplest boundary layer package. It has only four channels, one each for wind speed, elevation angle, and dry- and wet-bulb temperatures. The range of the voltage is from 0.0 to 1.0 V. The corresponding outputs are 0.0 to 10.0 m/s for wind speed, -45 to +45 degrees for elevation angle, and one of the ranges -10°C to +10°C, 0°C to 20°C, 10°C to 30°C, or 20°C to 40°C, for wet- and dry-bulb temperatures. To obtain the signals from the other two sensors, hot wire and thermocouple, we need a discriminator with more channels.

22.5 REFERENCES

Hayashi, M., and M. Miyake (1973): Some characteristics of cup anemometers. Kogai (Japan) 9:53-61.

Hayaski, M., O. Yokoyama, H. Yoshikado, and K. Nemoto (1974): A boundary layer package with tape recording system inside. Tenki (Japan) 21:45-47.

Nakajima, S., (1967): On the meteorological observation in the lower atmosphere by a captive balloon. Weather Serv. Bull. (Japan) 34:1-65.

Ootsuka, S., N. Shishido, N. Honda, S. Nemoto, S. Koinuma, M. Hayashi, and M. Miyake (1975): Observations of the planetary boundary layer by tethered ballons and lower tropospheric radionsonde. Scientific Report of the Fourth AMTEX Conference, 26-29 September 1975. AMTEX Report No. 8, Tokyo, Japan, pp. 70-73.

Yokoyama, O. (1969): Measurements of wind fluctuations by a vane mounted on the captive balloon cable. J. Meteorol. Soc. Japan 47:159-166.

23. NCAR BOUNDARY PROFILER SYSTEM

Robert B. McBeth and Steven Semmer
National Center for Atmospheric Research
Boulder, Colorado, U.S.A.

23.1 INTRODUCTION

The NCAR Boundary Profiler (BP) system is a small tethered-balloon system (Morris et al., 1975) providing the user with five meteorological parameters: dry-bulb temperature, wet-bulb temperature, pressure, wind speed, and wind direction. Data information is transmitted, in a time multiplex format, to a ground station, where it is recorded on magnetic tape for later processing and on a strip chart recorder for real-time analysis. The system is portable and can be operated by one person.

23.2 DESCRIPTION

The BP system consists of a sensor package attached to an aerodynamic balloon, a tether line controlled by a winch, and a ground station.

The balloon's approximate dimensions are length, 4.8 m; maximum diameter, 1.4 m; volume, 3.25 m^3. It has a lifting capability of 1.9 kg at sea level. In calm weather the balloon has been flown to heights of 600 m. With its aerodynamic shape, the balloon acts as a wind vane and is used in computing wind direction. Because of its small size, it can be flown without a special FAA waiver.

The winch consists of a drum wheel driven by a 1/3-hp motor. The tether line, 100-lb test nylon cord, is wrapped around the drum wheel. The motor operates on 110 V a.c. An SCR controller sets the rate of ascent and descent of the package. The operator can vary the rate from 0 to 3 m/s depending on weather conditions.

The telemetry package was purchased off the shelf. A brief description of the package is given here; more detailed information can be found in the description of the Tethersonde. The package gets its power from 12 1.22-V nicad batteries, giving an average flight time of 2 h. A d.c. signal from each sensor circuit is fed into a time multiplexer. From there the signal is passed on into a voltage-controlled oscillator where it is converted to a frequency in the range of 2.6 to 3.4 kHz. The data signal is then used to modulate a 403-MHz crystal-controlled transmitter. The power output of the transmitter is about 10 mW.

The ground station is made up of three parts: a receiver, an Esterline Angus strip-chart recorder, and a digital cassette system. The receiver picks up the 403-MHz signal and passes the audio portion on to a discriminator circuit and the cassette system. The audio discriminator converts the audio tone to an electrical signal ranging from 0 to 5 V. This signal is then fed into the chart recorder to provide a real-time look at the data. The audio tone going into the cassette system is filtered and passed on into a frequency-detector circuit. The detector circuit determines when to take a sample of data and record it on tape. Between all data samples there is a down signal. The down signal has a frequency outside the range of the detector so the detector will be turned off during this signal and on during a data signal. The down frequency is at 2.3 kHz, and the data frequencies are in a range of 2.6 to 3.4 kHz. When the detector circuit is set, a short time delay takes place to allow for a clear signal, and then the data signal is passed on into a counter for 0.256 s. The lower eight bits of the counter become the digital representation of the data sample and are recorded on tape. The frequency span of 0.8 kHz represents a span of 205 counts. The cassette tape is then processed on a microcomputer system. The cassette system also contains a real-time clock, and at the beginning

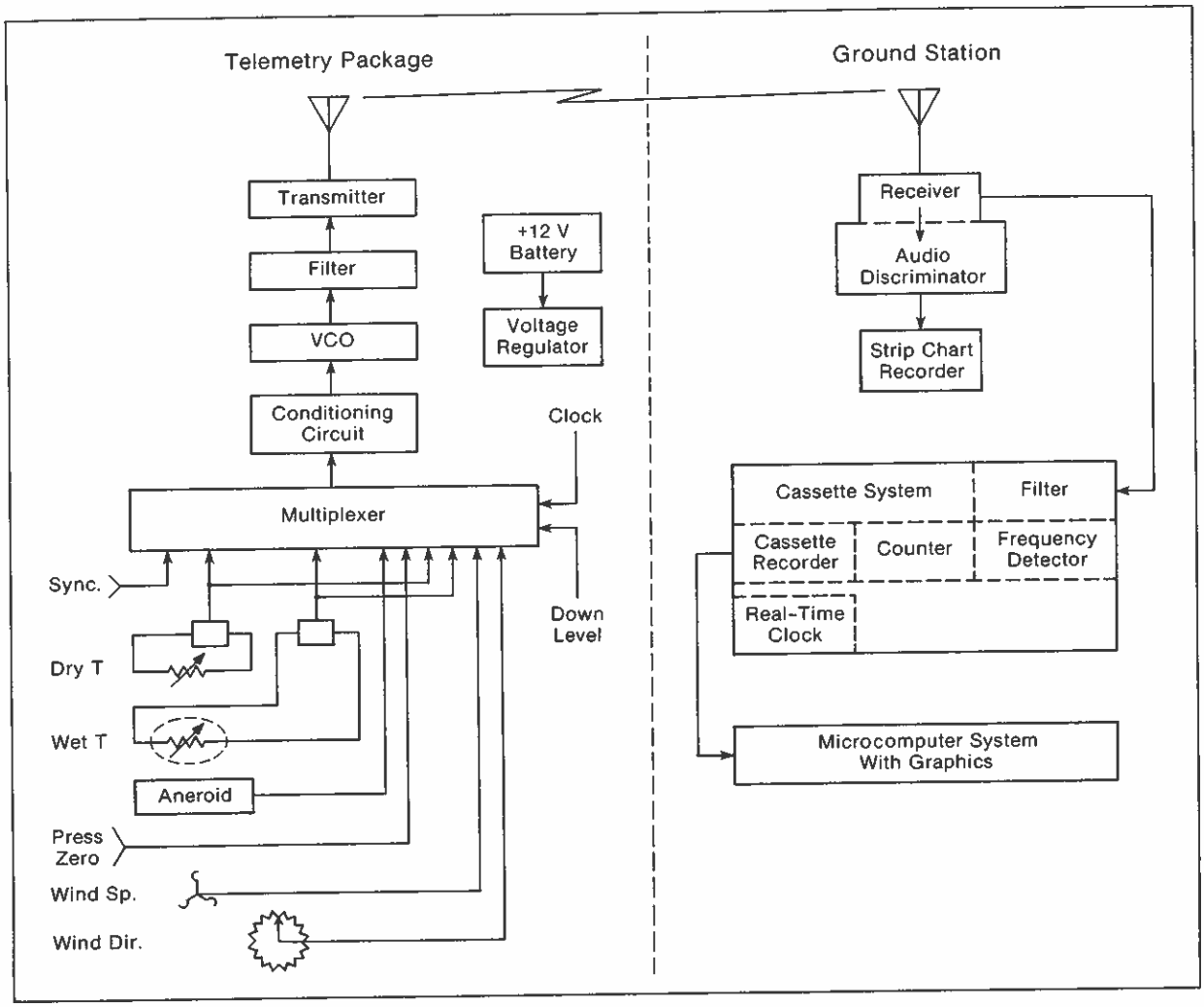

Figure 23.1. Block diagram of NCAR Boundary Profiler electronics.

of each data frame time is recorded on the magnetic tape. Figure 23.1 is a block diagram of the BP system.

23.3 SENSORS

Bead thermistors are used to measure dry- and wet-bulb temperatures. The sensors are mounted in a radiation shield tube and are aspirated by a small fan located at the end of the tube. The wet-bulb thermistor is covered by a sock, which is connected to a small reservoir.

Pressure is measured with an aneroid capsule. The pressure sensor is set up to make a relative reading, not an absolute one. The relative reading has a total differential range of 100 mb.

Wind speed is measured with a three-cup anemometer connected to a small d.c. generator. Wind direction is determined by using the balloon as a wind vane in conjunction

Table 23.1. Sensor characteristics

Sensor	Total range	Set range	Precision
Thermistor	-30° to 45°C*	25°C	±0.5°C
Aneroid capsule	Relative†	100 mb	±1 mb
Cup anemometer	0.5 to 10 m/s	0 to 10 m/s	±0.25 m/s
Magnetic compass and balloon	0° to 360°	0° to 360°	±5°

*Six switches set temperature ranges in 25°C increments.
†Pressure is set at ground level relative to launch site.

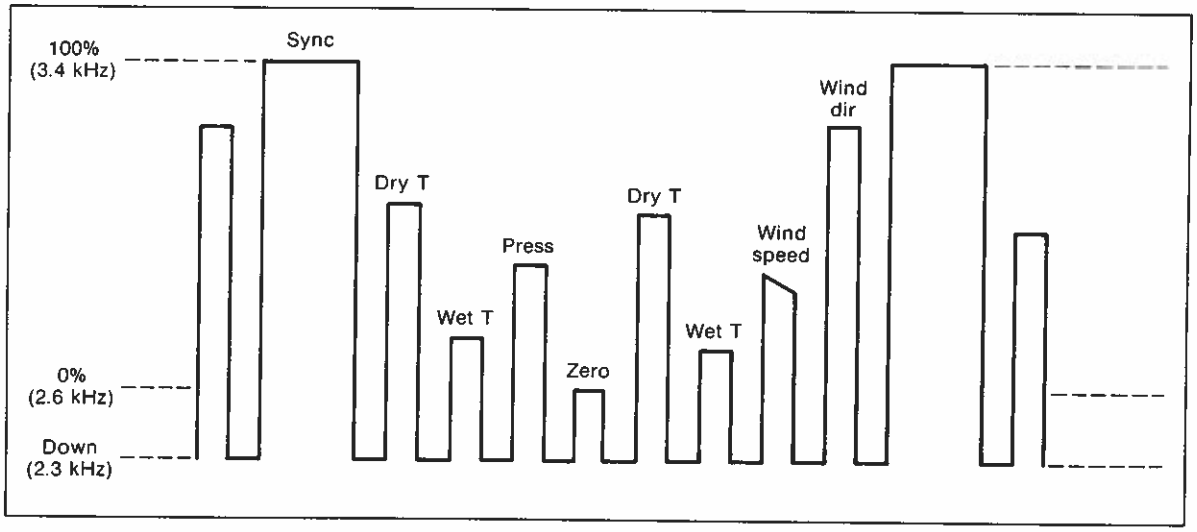

Figure 23.2. Data frame on strip chart recorder.

with a magnetic compass. The magnetic compass is a potentiometer with the compass needle acting as the arm of the pot. When it is time to sample wind direction an electric field locks the needle to the pot windings. This gives a clean reading when a sample is taken.

Table 23.1 gives more information about each sensor.

23.4 DATA FORMAT AND PROCESSING

Figure 23.2 is an example of one data frame recorded on the strip chart. The average frame duration is 30 s but can range from 20 to 40 s. The sync pulse represents 100% or 3.4 kHz, whereas the zero pulse is 0% or 2.6 kHz. Data are transmitted in the following order: (1) sync, (2) dry-bulb temperature, (3) wet-bulb temperature, (4) pressure, (5) zero, (6) dry bulb, (7) wet bulb, (8) wind speed, and (9) wind direction. The user can change this sampling order. The down signal is used to separate each channel sample from the next one. The scale ranges for each data parameter are listed in Table 23.1. The zero reference level for temperatures can be set by the user in 10°C increments

BAO/WMO

AUGUST 30,1979 FLIGHT (10)

TIME (H:M:S)	DBULB (C)	WBULB (C)	DP (C)	PRESS (MB)	WS (M/S)	WD (DG)	RH (%)	HEIGHT (M)	HT/MSL (M)
8:30:23	17.21	11.47	8.55	839.60	0.00	309	53	10.17	1587.17
8:30:45	17.24	11.49	8.58	838.50	0.00	310	53	21.36	1598.36
8:31:36	16.73	11.17	8.31	835.80	0.00	306	53	48.88	1625.88
8:33: 4	16.87	10.55	6.69	830.90	2.73	306	48	99.01	1676.01
8:34:54	17.95	10.07	4.33	826.10	4.24	332	39	148.48	1725.48
8:36:34	18.31	10.65	5.56	821.20	4.81	332	41	199.40	1776.40
8:38:35	18.55	10.22	4.16	816.40	4.32	322	37	249.63	1826.63
8:40:31	18.27	10.00	3.92	811.50	3.27	320	37	301.19	1878.19
8:43:28	19.89	10.73	4.27	804.00	2.51	325	34	380.91	1957.91
8:47:32	21.18	10.00	0.61	795.00	1.56	258	25	478.02	2055.02
9: 1:23	21.89	10.34	0.83	795.00	1.84	223	25	480.42	2057.42
9: 7:53	20.81	11.08	4.26	804.00	4.48	298	32	383.04	1960.04
9: 9:36	20.59	10.31	2.10	811.50	4.76	321	29	302.90	1879.90
9:10:56	19.83	10.11	2.33	816.40	5.11	326	31	251.03	1828.03
9:12:17	19.26	10.83	5.04	821.20	5.07	321	37	200.62	1777.62
9:13:19	18.65	11.47	7.32	826.10	4.80	320	45	149.55	1726.55
9:14:11	19.03	10.83	5.19	830.90	3.10	335	38	99.82	1676.82
9:15:12	19.46	11.80	7.28	835.80	0.55	311	42	49.29	1626.29

Figure 23.3. Example of data listing for a BLIE flight.

starting at -30°C and going up to 20°C. The user also has the ability to set a ground level reference for the pressure. Data recorded on magnetic tape have a similar format, except that no down channels are recorded and time information is placed on the tape after each sync signal.

Although the strip chart provides a real-time look at the data, the final analysis is done with the digital cassette tapes. With the use of a microcomputer graphics system, the cassette data are transferred to a digital cartridge tape. Each frame of raw data is then converted to physical units, with the sync and zero data being used for maximum and minimum levels. When all data have been converted, they are interpolated to one time point per frame, and the height, dewpoint, and relative humidity can be computed. The user can now use the graphics to obtain a listing of the flight data in tabular form or an XY plot of time versus data. Figure 23.3 is an example of a listing of flight data.

23.5 REFERENCE

Morris, A. L., D. B. Call, and R. B. McBeth (1975): A small tethered balloon sounding system. Bull. Am. Meteorol. Soc. 56: 964-969.

24. DETAILS OF THE EXPERIMENT

J. C. Kaimal and J. E. Gaynor
NOAA/ERL/Wave Propagation Laboratory
Boulder, Colorado, U.S.A.

H. W. Baynton
National Center for Atmospheric Research
Boulder, Colorado, U.S.A.

24.1 INTRODUCTION

The Boulder Low-Level Intercomparison Experiment commenced on schedule at 0800 MDT on 27 August 1979. Favorable weather conditions and the absence of major equipment problems contributed to a highly productive first week (27-31 August). As a result, no tests were run during the 3-day weekend. On 2 days during the following week (4-5 September) observations were resumed primarily for participants who needed more data. Some had made improvements in their sensors after the first week and were eager to see the effect; others simply wanted more observations.

The BAO tower instrumentation and associated data acquisition and processing systems (see Chapter 1 of this report) were operated continuously for the entire 2 wk. Functioning in a 20-min averaging mode, the data acquisition system printed out summary listings of BAO data at the end of each averaging period. The listings provided a set of common reference data for comparison of all sounding systems. Although each listing was withheld from the participants during the core observing periods until after the 24 h allowed for submission of their data, it was subsequently available for system checks and calibration.

A major problem in planning the experiment was crosstalk and interference between systems operated concurrently. Most radiosonde and tethered balloon systems used telemetering frequencies that overlapped. Balloons and kites served as reflecting targets for sodars, interfering with their Doppler measurements. The remotely piloted aircraft, besides being a reflector, generated its own acoustic noise and used radio frequency bands shared by the radiosonde and tethered balloon systems. Doppler sodars are known to interfere with one another even when their operating frequencies are far apart.

Coordinating this complex set of interactions called for optimal use of time sharing, spatial separation, and frequency tuning. The major crosstalk problems were solved before the experiment started by planning the location of sensors in the field and assigning specific observing windows for each sensor. In this chapter we describe the experiment and detail the specific problems and solutions, which should serve as background for interpreting the results in Chapter 25.

24.2 SENSORS COMPARED

Essential information on all sensors that participated in the BLIE is given in Table 24.1. The numbers indicate the order in which the papers are presented in Part 1 of this report. The sensors omitted from the list required unacceptable lead times for data processing. As mentioned in the Preface, participants in the BLIE were required either to submit data from each run within 24 h or to provide analog signals for sampling and processing in the BAO acquisition system.

Table 24.1. Sensors used in the BLIE

Sensor number	Sensor type	Parameters* measured	Country	Principal scientist	Affiliation
1	Tower system (BAO)	U,V,W,T,T_d	U.S.A.	J. C. Kaimal	Wave Propagation Laboratory, NOAA, Dept. of Commerce
2	Sonic anemometer-thermometer (Kaijo Denki)	U,V,W,T	Japan	T. Hanafusa	Meteorological Research Institute, Japan Meteorological Agency
3	Tower system (Vaisala)	S,D,T,RH	Finland	I. Ikonen	Vaisala Oy
4	Remotely piloted aircraft (SAM-B)	T,RH,P	France	D. Martin	Établissement d'Études et de Recherches Météorologiques
6	Kite anemometer (TALA)	S,D	U.S.A.	C. F. Woodhouse	Approach Fish, Inc.
7	Radio acoustic sounding system (RACES)	T	Switzerland	P. Ravussin	Federal Institute of Technology of Lausanne
8	FM-CW radar	U,V	U.S.A.	R. B. Chadwick	Wave Propagation Laboratory, NOAA, Dept. of Commerce
11	Bistatic sodar	U,V	U.S.A.	W. D. Neff	Wave Propagation Laboratory, NOAA, Dept. of Commerce
12	Monostatic sodar (AVIT)	U,V,W	U.S.A.	P. B. MacCready	AeroVironment, Inc.
13	Bistatic sodar (Echosonde)	U,V,W	U.S.A.	M. A. McAnally	Radian Corp.
14	Monostatic sodar (Sensitron)	U,V	Sweden	S. Salomonsson	University of Uppsala
15	Bistatic sodar (XONDAR)	U,V,W	U.S.A.	R. L. Peace, Jr.	Xonics, Inc.
16	GMD-1/VIZ radiosonde	S,D,T,RH,P	U.S.A.	R. B. McBeth	National Center for Atmospheric Research
17	TDFS low-level radiosonde	T,T_w,P	F.R.G	E. Schöllmann	Deutscher Wetterdienst
18	CORA radiosonde	S,D,T,RH,P	Finland	I. Ikonen	Vaisala Oy
19	Airsonde radiosonde	T,T_w,P	U.S.A.	D. B. Call	AIR, Inc.
20	Tethersonde profiler	S,D,T,T_w,P	U.S.A.	A. L. Morris	Ambient Analysis, Inc.
21	Tethered balloon profiler	S,T,RH,P	Poland	K. Stefanicki	Institute of Meteorology and Water Management
22	Tethered balloon profiler	S,E,T,T_w	Japan	M. Hayashi	National Institute for Pollution and Resources
23	Tethered balloon profiler	S,D,T,T_w,P	U.S.A.	R. B. McBeth	National Center for Atmospheric Research

*U - wind component (positive from west)
V - wind component (positive from south)
W - vertical wind component (positive up)
S - wind speed
D - wind direction
T - temperature
T_d - dew point temperature
T_w - wet-bulb temperature
RH - relative humidity
P - pressure
E - elevation angle

The variables measured by the different systems were reduced to the following common parameters for comparison:

(1) Horizontal wind component U (positive from west).
(2) Horizontal wind component V (positive from south).
(3) Vertical wind component W (positive upward).
(4) Temperature T.
(5) Dew point temperature T_d
(6) Relative humidity RH.
(7) Height above ground Z.

All measurements were reported for heights corresponding to the fixed levels on the tower. Reporting levels for radiosonde observations above tower heights were set at pressure levels corresponding to 400, 500, 750, 1,000, 1,250, 1,500, 1,750, 2,000, 2,250, 2,500, 2,750, and 3,000 m.

The unit of time for data comparison was a 20-min period coincident with the BAO averaging period. In-situ and remote sensors were expected to provide time-averaged data compatible with the BAO tower profiles. For immersion sensors, which use a single instrument package to probe the layer, a full ascent or descent had to be completed within the 20-min period. When this was not possible, the period containing the most profile points was used for comparison.

24.3 LOCATION OF SENSORS

Assignment of sensor locations (Fig. 24.1) was based on several considerations: the crosstalk problem, the availability of a.c. power, and the need for certain sensors to be far from (or close to) the tower. Groups operating in shifts or flying instruments on the same balloon train had to be close together for easy communication.

Major areas of activity centered around the tower base, anchor point B, and the temporary building. Air-conditioned office trailers were provided at each of these locations to house equipment and personnel. The circled numbers in Fig. 24.1 indicate the sensors occupying each trailer.

The electronics for the tower systems were situated in the trailer close to the tower to keep signal lines short. Radiosonde and tethered balloon activities were located near the temporary building to be far away from the tower and its guy wires. Since by arrangement the remotely piloted aircraft would not be operated when the balloons were flown, its landing strip was placed close to the balloon launch area. The installations around the building can be seen in Fig. 24.2.

The sodar antennas (see Fig. 24.3) were laid with their axes aligned E-W and N-S and their centers close to anchor point B. With this arrangement, the sampling volumes of the bistatic sodars and the lower levels of the monostatic sodars were close to each other. Their remoteness from the tower was intentional; to avoid reflections the sodars were placed at a distance from the tower equal to or greater than the expected height range of the devices.

Operating around anchor point A and sometimes around anchor point C (see Fig. 24.1), the kite anemometer was sufficiently removed from the other sensors to avoid interference. Its only potential conflict was with the remotely piloted aircraft, but this was avoided by scheduling kite and aircraft operations at different times.

24.4 OPERATING SCHEDULE

In the initial plan three observing periods with 2-h breaks for rest and refreshments were scheduled for each day:

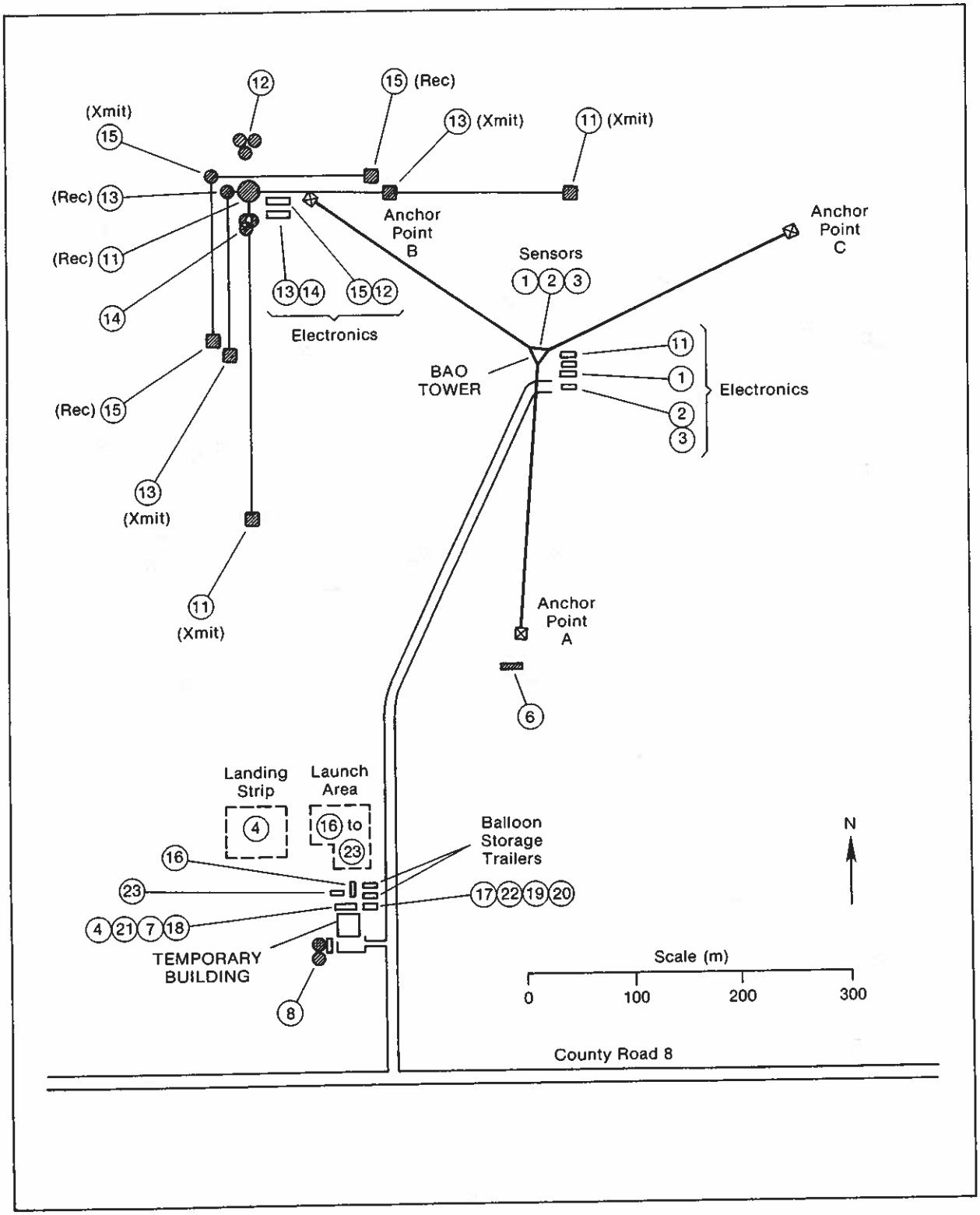

Figure 24.1. Locations of sensors operated during BLIE. Table 2.1 gives the key to number designations.

Figure 24.2. Temporary building and launch areas for balloons and aircraft.

Figure 24.3. Sodar antennas at anchor point B as seen from the BAO tower.

Period 1 (0800-1200 MDT): Period of boundary layer growth.
Period 2 (1400-1800 MDT): Period of nearly constant boundary layer depth.
Period 3 (2000-2400 MDT): Period of stable boundary layer.

As the sensors were checked out, adjustments had to be made and the observing periods extended in either direction to make room for sensors that could not be operated within the core observing periods. The basic schedule is shown in Table 24.2. The schedule and the operating procedures described in this chapter were tested in a short dry run beginning at 0800 MDT on 25 August.

According to the schedule, the sodars were assigned separate time slots. Initially AeroVironment and WPL sodars were operated concurrently; however, when interference was suspected, the AeroVironment sodar was moved to different time slots outside the core operating period during Periods 1 and 2. The remotely piloted aircraft was not operated at night because of the need for visual contact. The sodar schedules for Period 3 were rearranged to take advantage of this fact.

Tethered balloon and radiosonde operations were scheduled at different times within the observing periods. The only exception was the profiler from Poland which interfered with other telemetry systems and was assigned a period outside the core observing periods. The tethered balloon profilers were not operated at night because they required visual monitoring.

24.5 OTHER CONSIDERATIONS

24.5.1 Effect of Tower Structure on Measurements

The tower sensors are mounted on booms extending roughly 5 m SSE and NNW. The BAO sonic anemometers and the Propvanes are mounted at the ends of these booms pointing in opposite directions. Since the velocity underestimation in the shadow of the tower can be significant, this redundant velocity measurement enables the observer to select data from the upwind sensor at all times. Even with a boom length nearly 1½ times the tower width, the wind direction readings from the two sensors show the effect of flow distortion caused by the tower. The effect is most pronounced for wind directions normal to the booms. Wind direction readings from the opposite ends of the two booms appear to diverge roughly 5° in either direction for winds from the ENE and roughly 2½° for winds from the WSW. This difference can be attributed to the different aspects of the tower presented to the wind in each case; the flat WSW face in the latter case and the apex across from it in the former case.

To ensure that the anemometers compared on the tower are embedded in essentially the same flow field the Vaisala and Kaijo Denki anemometers were mounted directly behind the BAO sonic anemometors on the SSE boom (see Figs. 24.4 and 24.5). Vaisala cup and vane sensors were installed at the 22-, 100-, 200-, and 300-m levels, and the Kaijo Denki sonic anemometer-thermometer occupied the 50-m level. When the results were compared, only measurements from periods with wind directions between 64° and 244° azimuth were considered. The effect of the direction error on the intercomparison is discussed in the next chapter.

The Vaisala temperature sensors were mounted on the NNW booms at all eight levels of the tower. BAO temperature measurements were made from the opposite side, but the flow distortion from the tower did not seem to affect the temperature comparison. The Vaisala humidity sensors were housed on every other level in the same shields as their temperature sensor; thus they were close to the BAO dew point sensors.

24.5.2 Effect of Separation Between Sensors

A large spatial separation is sometimes unavoidable when sounding systems such as sodars are compared with tower sensors. Temporal averaging reduces the variability caused by separation, but no guidelines exist on how long the averaging period should be. Here we

Table 24.2. Daily operating schedule for BLIE*

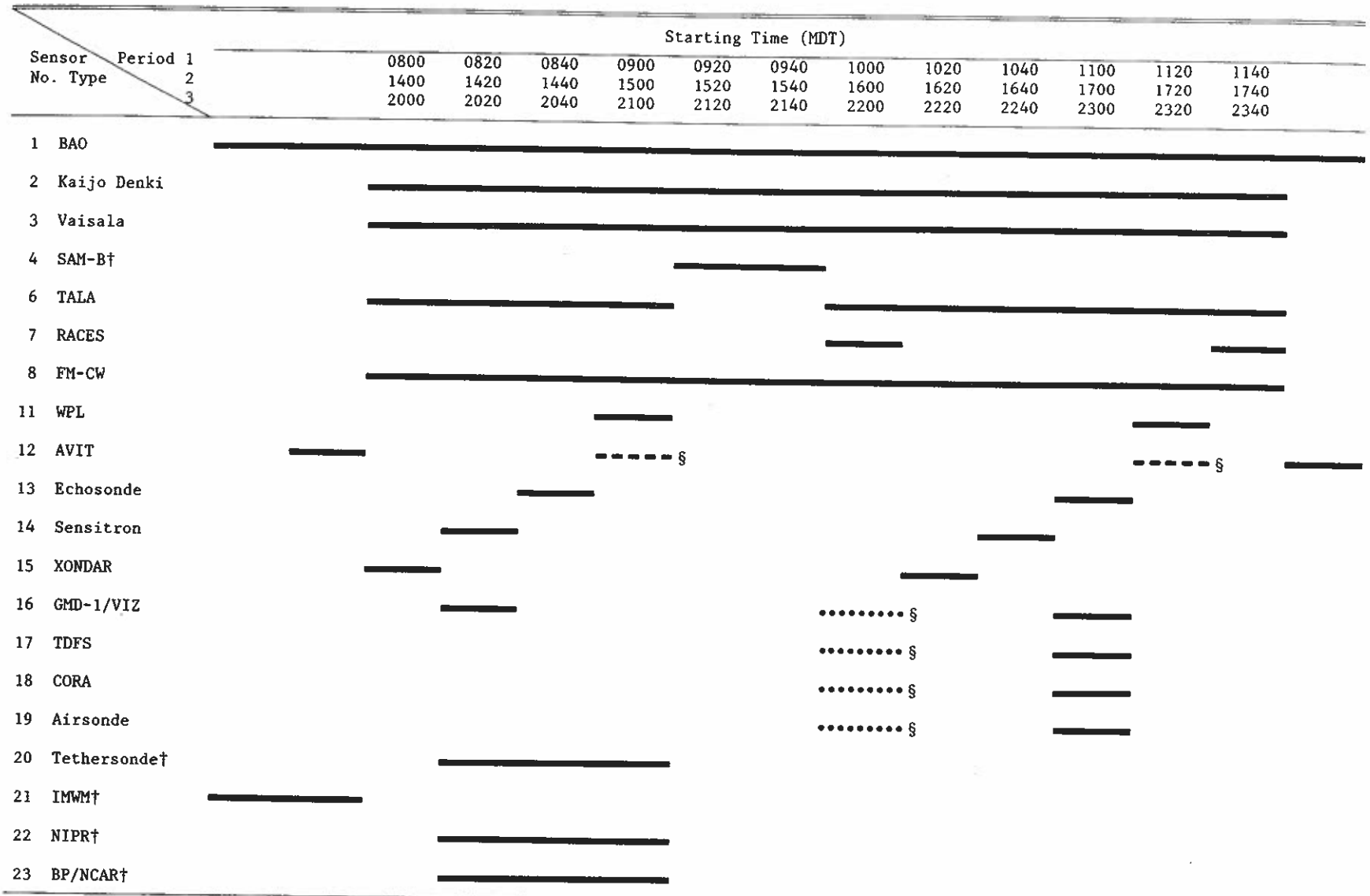

*This basic schedule was modified when participants dropped out after the first week.
†No flights of SAM-B or tethered balloons were made during Period 3 because of the need for visual contact with aircraft and balloons.
§ ▬ ▬ indicates initial measurement period that was later changed; •••• indicates carriage measurements.

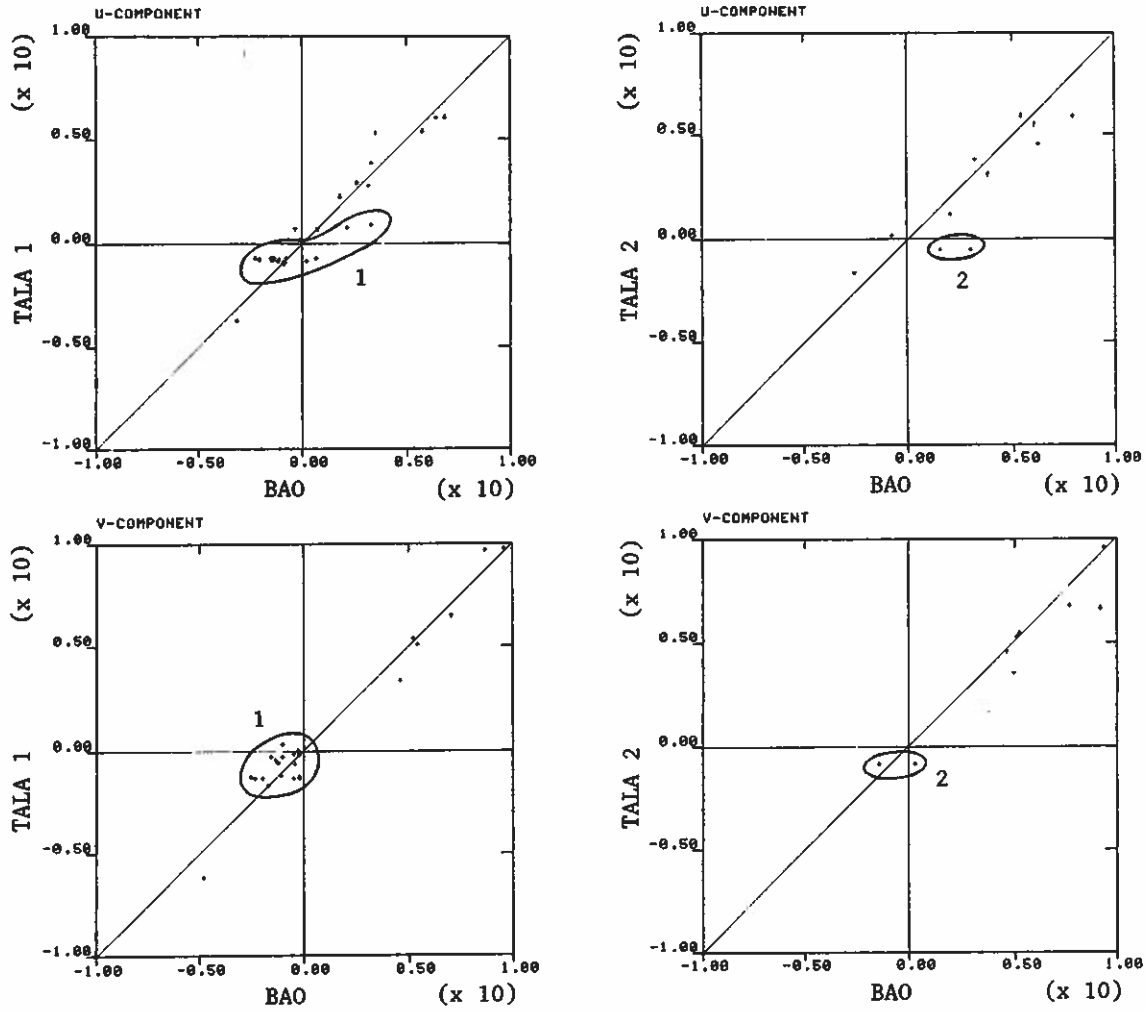

Figure 25.5. Scatter plots of data from TALA 1 and TALA 2 vs. data from BAO tower sensors. Tala 1 is the small kite flown during light winds, and TALA 2 the large kite flown during strong winds.

Notes on Fig. 25.5

Comments from C. F. Woodhouse, Approach Fish, Inc.

1. The data points in group 1 should be discounted since they were obtained from an uncalibrated lift balloon flown at 800-m altitude. The velocity points shown are only empirical estimates.

2. The data points in group 2 should be discounted because of equipment malfunction caused by an attempt to protect the electrical contacts with wet silicone in a thunderstorm.

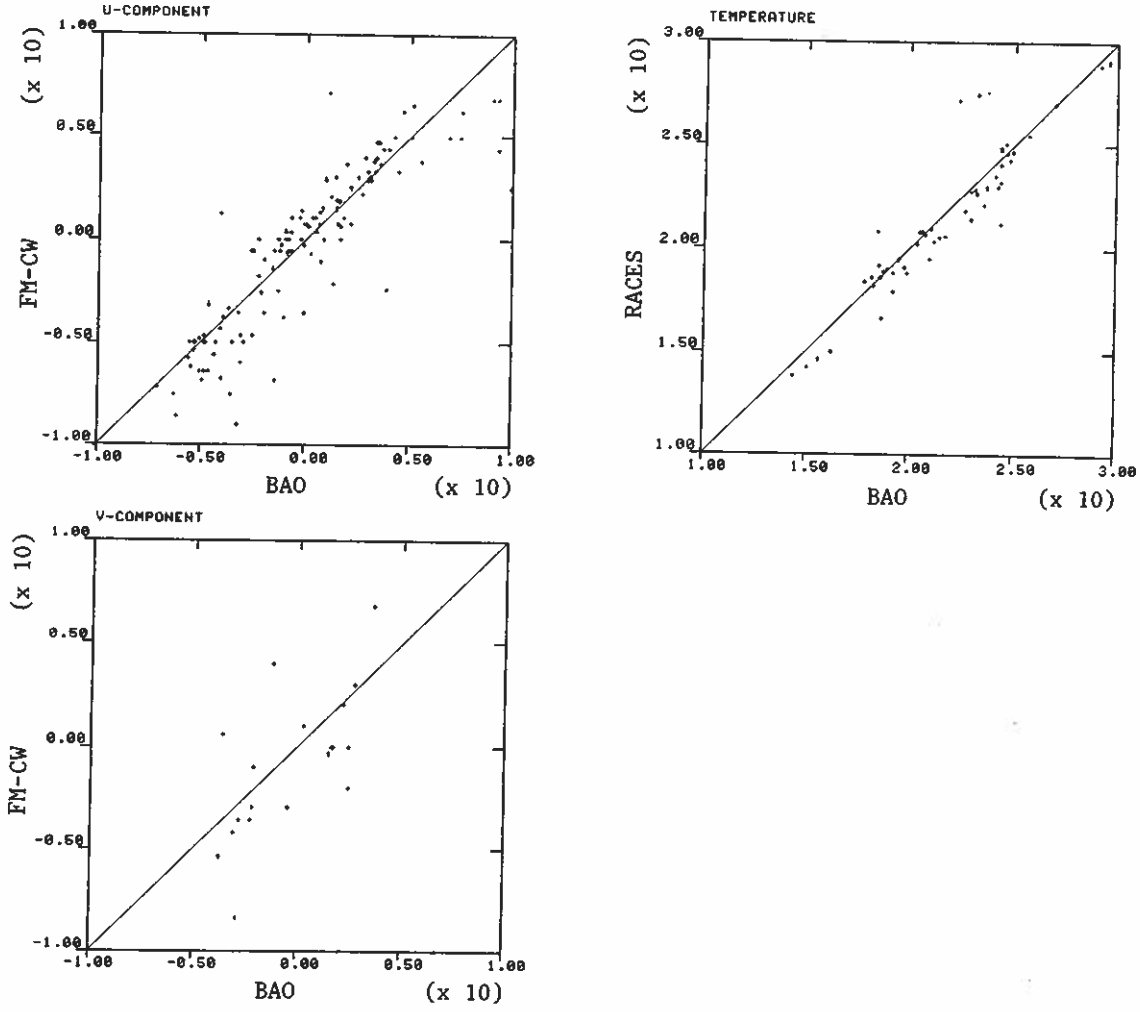

Figure 25.6. Scatter plots of data from FM-CW Doppler radar and RACES vs. data from BAO tower sensors.

Notes on Fig. 25.6

More data were collected with the FM-CW radar pointing west than pointing south, which accounts for the disparity in the number of data points along the two components.

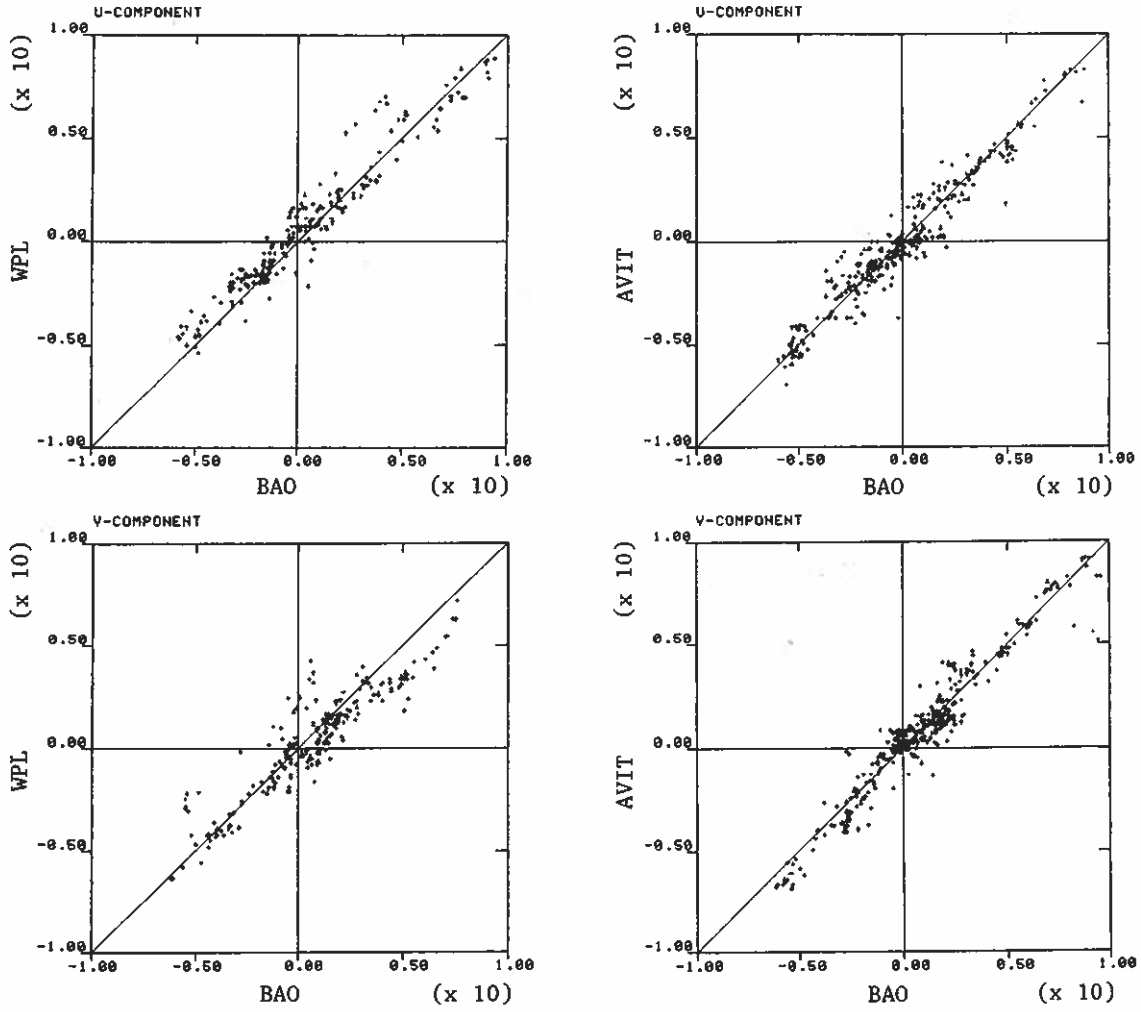

Figure 25.7. Scatter plots of data from WPL and AVIT Doppler sodars vs. data from BAO tower sensors.

Notes on Fig. 25.7

1. WPL and AVIT data were possibly affected by crosstalk when the sensors were operated concurrently for the first 3 days.

2. The 50-m WPL wind readings were raised by a factor of 2 to correct for attenuation caused by array geometry.

3. During high winds WPL Doppler measurements were contaminated by tower noise (see discussion in Chapter 11).

4. Vertical velocity correction (see section 12.3) was not applied in the wind computations of either system. For 20-min averaged U and V, this correction provided no detectable improvement.

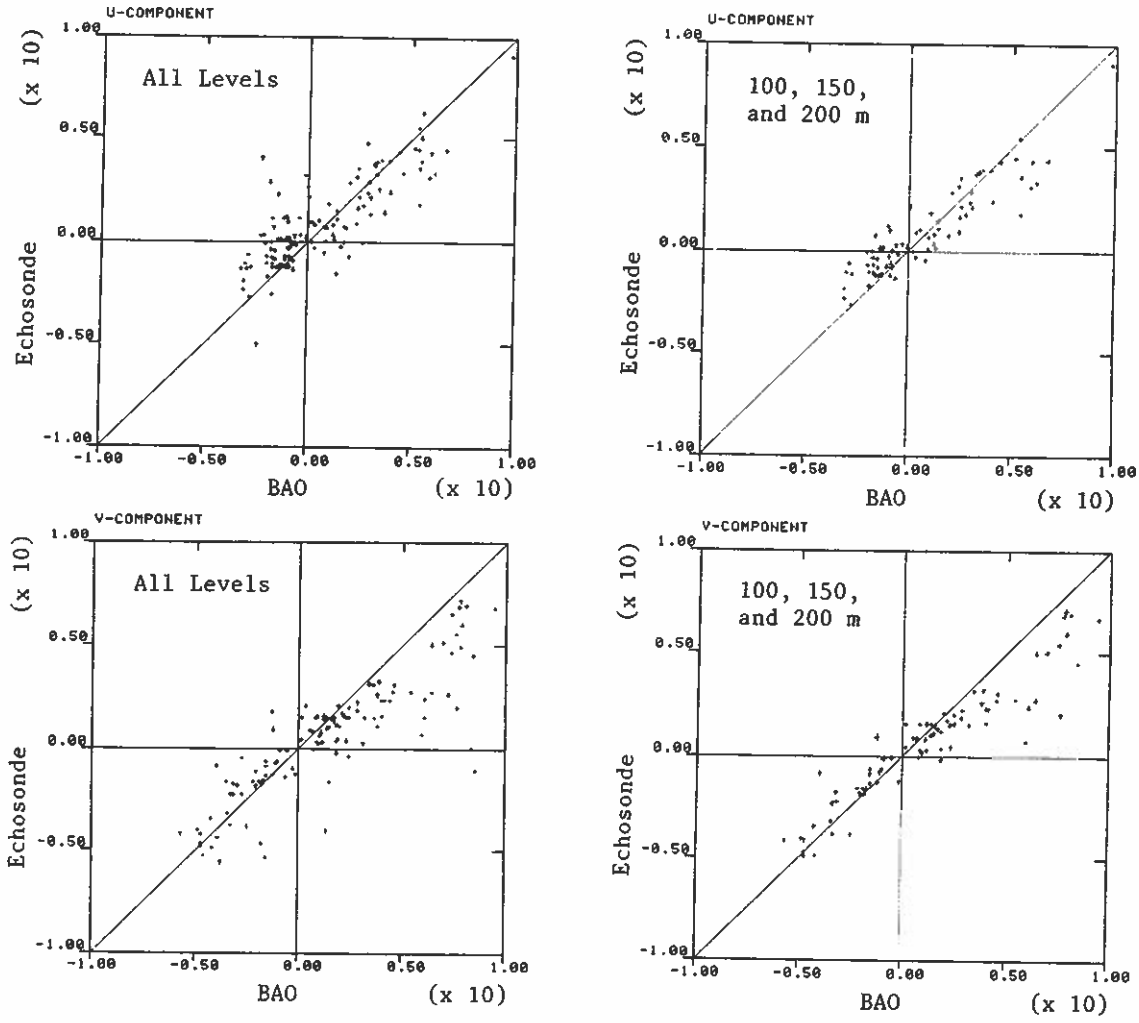

Figure 25.8. Scatter plots of data from Echosonde Doppler sodar vs. data from BAO tower sensors. Data from 100, 150, and 200 m show better agreement with BAO tower sensor data than those from levels above and below.

Notes on Fig. 25.8

Comments from M. McAnnally, Radian Corporation

1. The low bias in the Echosonde wind data is caused by an improper transmit antenna pattern resulting from an incorrect horn shape and a phasing mismatch between transducer driver pairs used with each horn. Combination of these two factors resulted in a transmit beam pattern that was much broader in azimuth than anticipated. As a result only the altitude range from 100 to 230 m received adequate acoustic energy.

2. New transmitter designs have been incorporated into the system, and subsequent testing has provided excellent agreement with observed conditions.

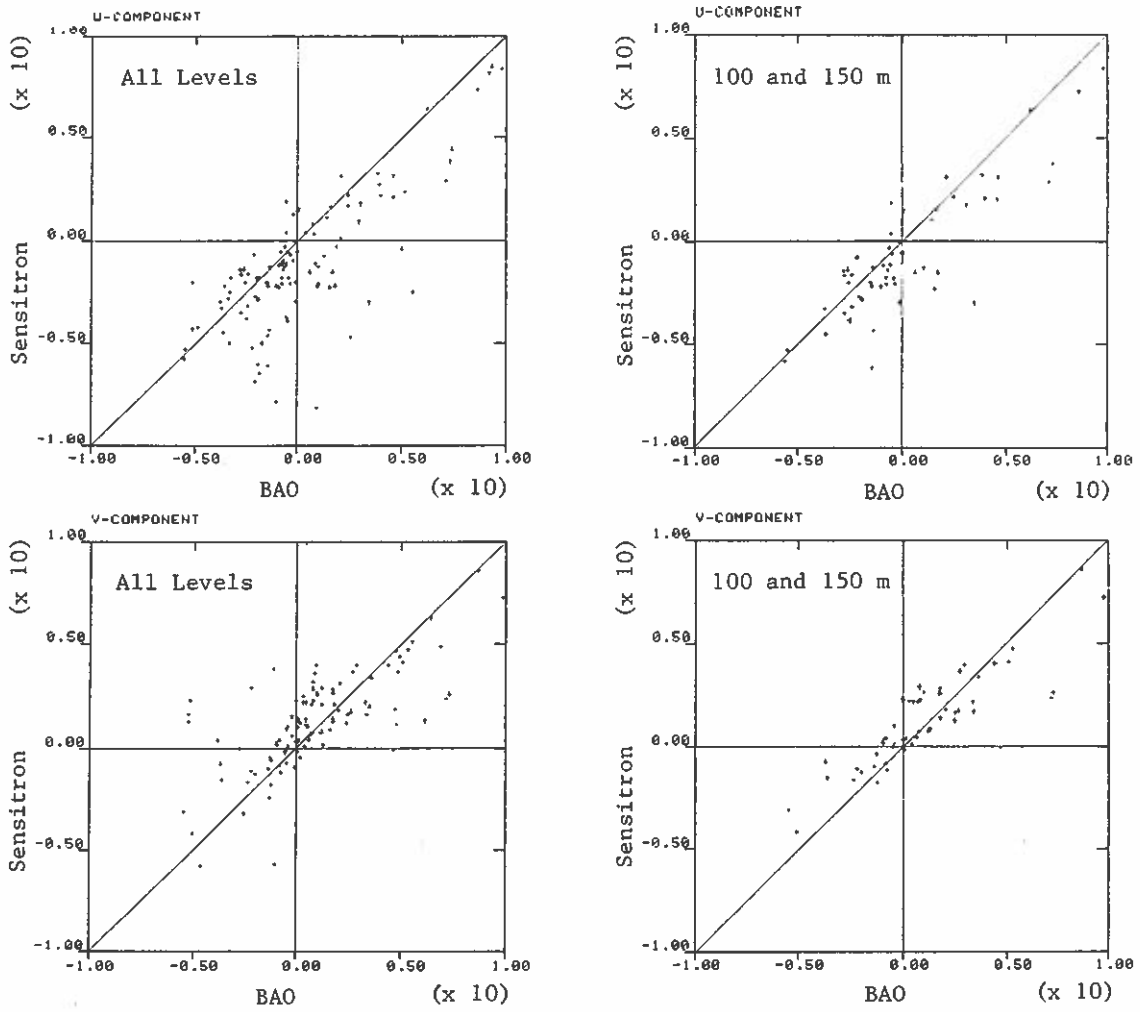

Figure 25.9. Scatter plots of data from Sensitron Doppler sodar vs. data from BAO tower sensors. Data from 100 and 150 m show much better agreement than those from levels above and below.

Notes on Fig. 25.9

Comments from S. Salomonsson, University of Uppsala

1. The large scatter in the data results from using borrowed (WPL) antennas which we could not tilt more than 22° from the vertical. The measurements may be influenced by the vertical wind component, since correction for that effect was not applied.

2. Our low pulse power (100 W) resulted in weak echo signals above 150 m, whereas a ringing in the transducer affected measurements below 100 m. Only measurements at 100 and 150 m are therefore considered appropriate for comparison with tower data.

3. Our preliminary system is not optimized for sensing at high altitudes but rather to explore the PLL technique in Doppler applications. Agreement with tower at 100 and 150 m indicates that the PLL circuit works fairly well when the echo signals are strong.

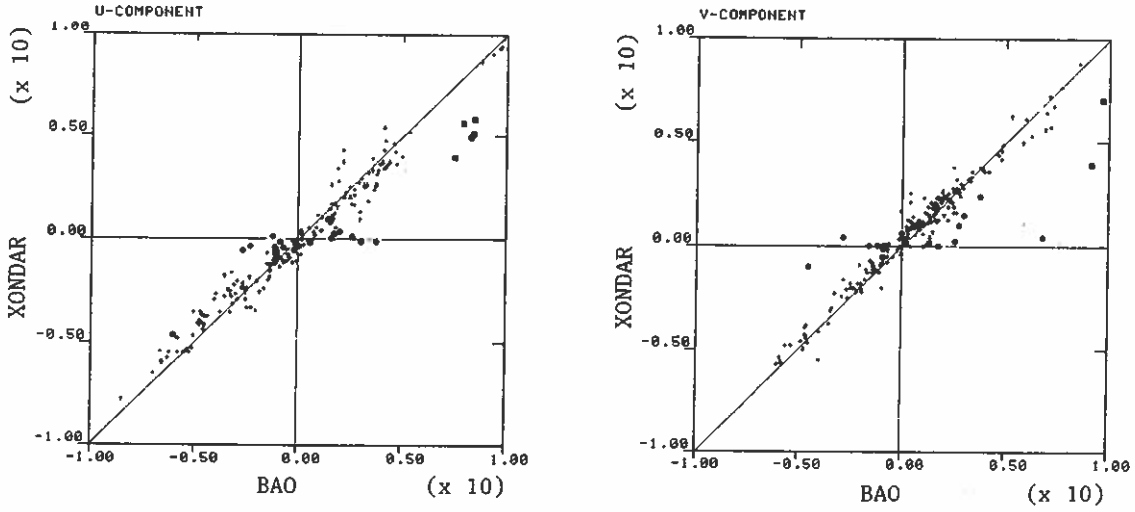

Figure 25.10. Scatter plots of data from XONDAR Doppler sodar vs. data from BAO tower sensors. ● 50-m level data; ■ data contaminated by severe tower noise.

Notes on Fig. 25.10

Comments from R. L. Peace, Jr., Xonics, Inc.

1. The plot contains data points known to be affected by tower-generated wind noise and possible crosstalk from two acoustic sounders not officially participating in BLIE. We at Xonics would like the data flagged and identified.

2. Use of 160-ms-long transmit pulse (rather than the 80-ms-long pulse used in a few soundings) resulted in a strong bias of the 50-m-level data toward zero velocity. This problem was not recognized until late in the first week.

3. We would like to point out discrepancies of the order of 0.5 to 1 m/s in the wind speed and 10° in wind direction between the BAO sonic anemometer and Propvane when the wind direction was between 20° and 120° and between 180° and 300°.

Editors' response

The unsatisfactory 50-m data and those affected by wind noise are easily identified and flagged, but points corresponding to the two periods with possible crosstalk are too close to the 1-to-1 line to benefit from flagging. Discrepancies between measurements made from opposite sides of a tower are not surprising (see discussions in section 25.1). To minimize the effect of flow distortion caused by the tower, only measurements from the upwind boom were used in the plots. Also, note that computer summaries of Propvane wind components made available to all participants were computed from the 20-min averaged speed and direction rather than from the instaneous wind components. Such averaging introduced discrepancies between the sonic anemometer and Propvane statistics for low wind speeds (when turbulence intensity is high). However, the Propvane data used in the comparisons described here are true components recomputed from the raw data.

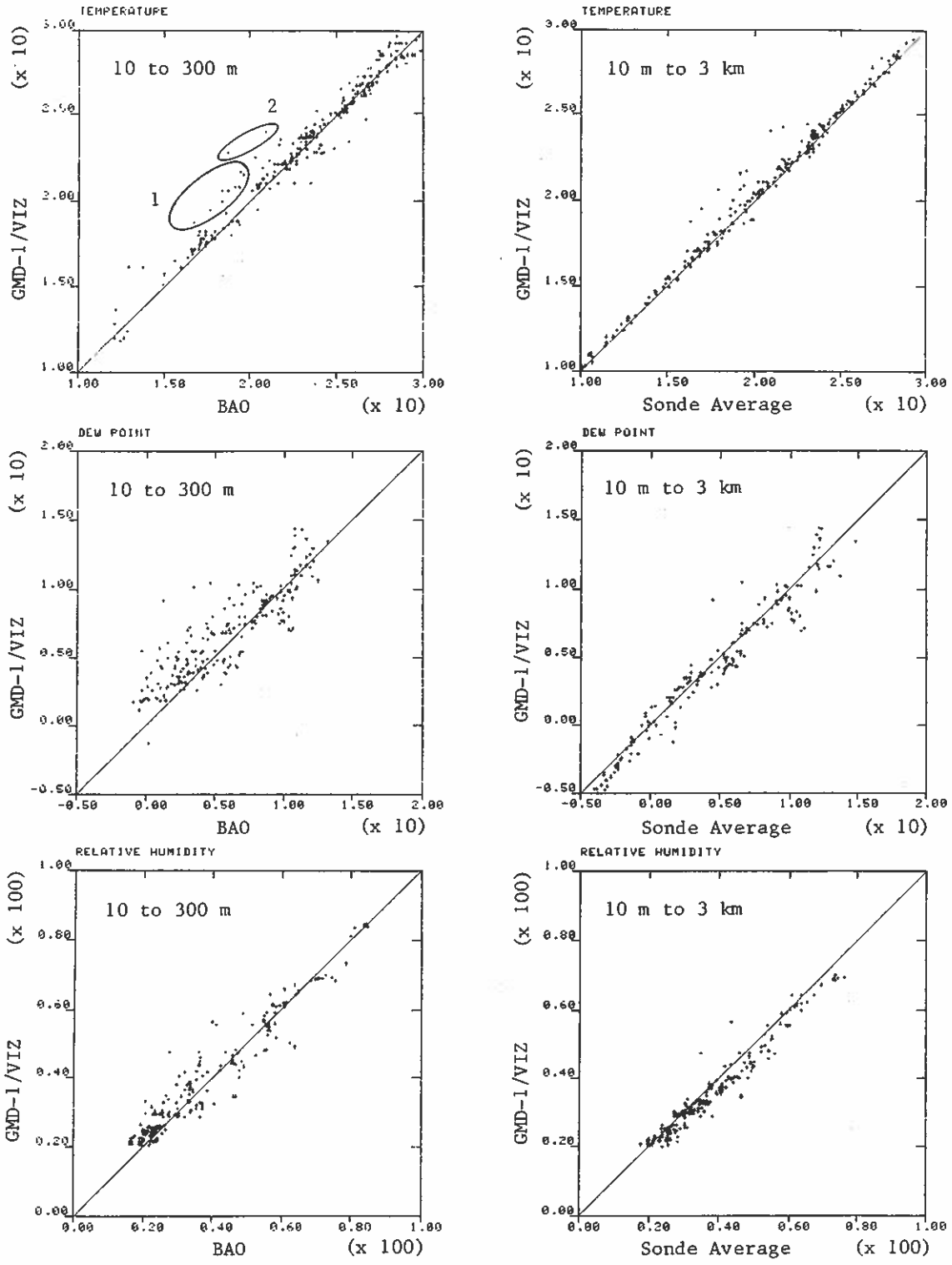

Figure 25.11. Scatter plots of balloon-borne GMD-1/VIZ radiosonde data vs. BAO tower data and vs. average for all radiosondes. Data in the righthand group are restricted to periods when all four sondes were functioning satisfactorily.

Notes on Fig. 25.11

Comments from R. B. McBeth, NCAR

1. Points in group 1 are too high because the operator failed to apply the frequency drift correction.

2. Points in group 2 are 10-m temperatures at about 2315 MDT. The sondes in these two instances were launched before they had come to thermal equilibrium with the cold outside air. Measurements from both sondes agreed within 0.4°C with the tower data during the carriage ascent that preceded the launch.

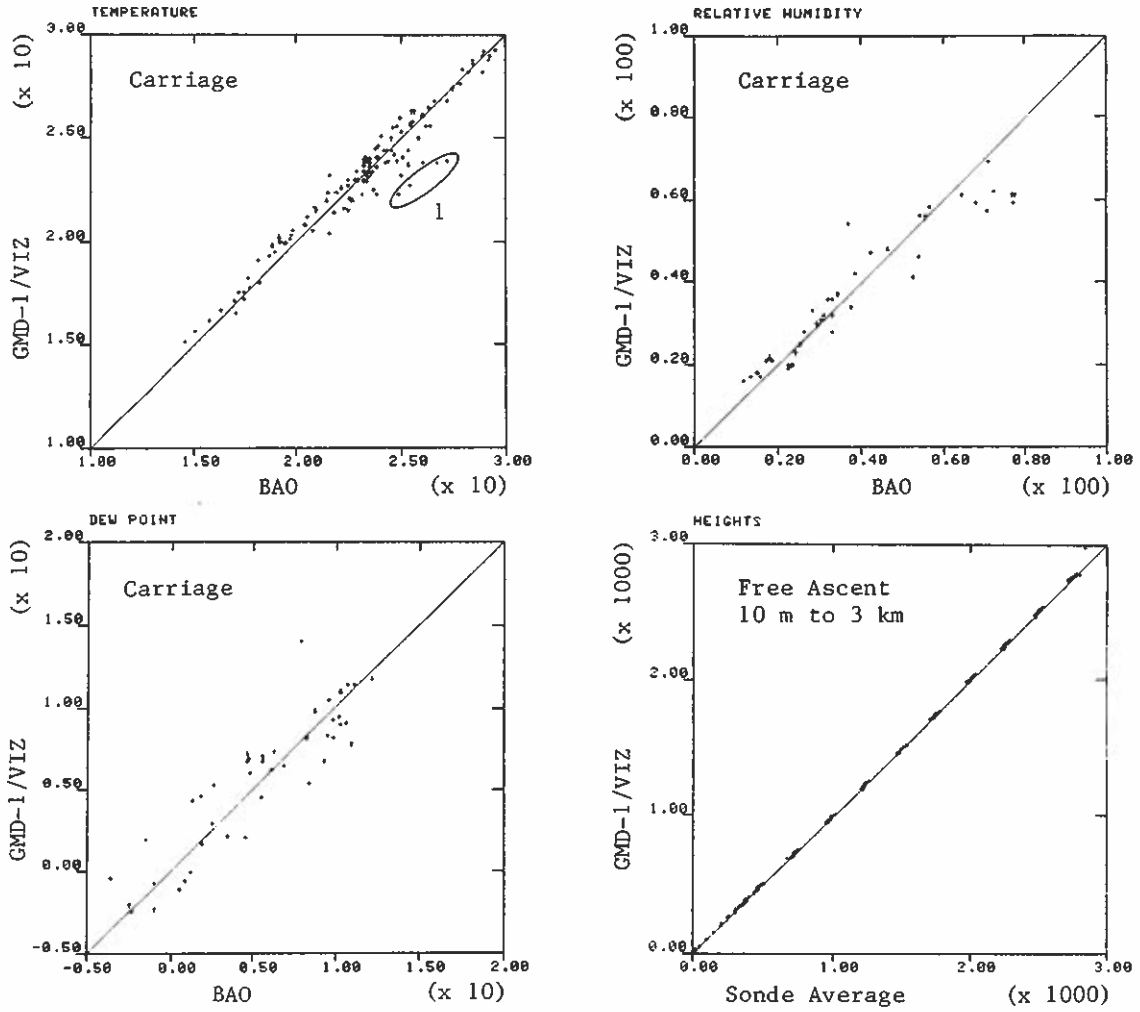

Figure 25.12. (Upper, left and right, and lower, left) Scatter plots of data from GMD-1/VIZ radiosondes on carriage vs. data from BAO tower sensors. (Lower, right) GMD-1/VIZ radiosonde computed heights vs. average heights for all balloon-borne radiosondes.

Notes on Fig. 25.12

Comments from R. B. McBeth, NCAR

The very low values in group 1 are believed to result from computational error. When the same sonde was flown from the balloon, its measurements averaged 0.13°C higher than the average data of the other three sondes and 0.19°C lower than those from the tower.

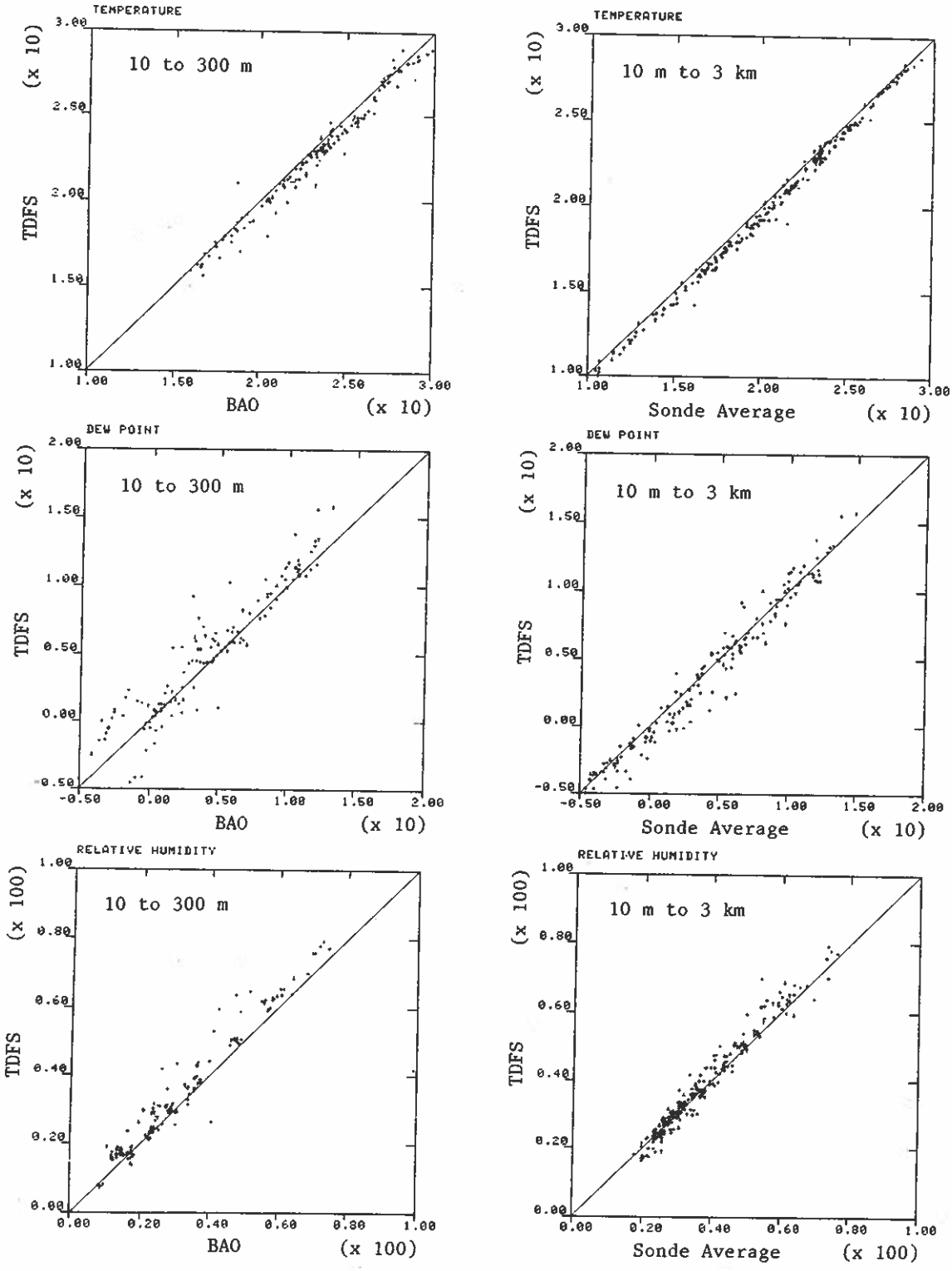

Figure 25.13. Scatter plots of balloon-borne TDFS radiosonde data vs. BAO tower data and vs. average for all radiosondes. Data in righthand group are restricted to periods when all four sondes were functioning satisfactorily.

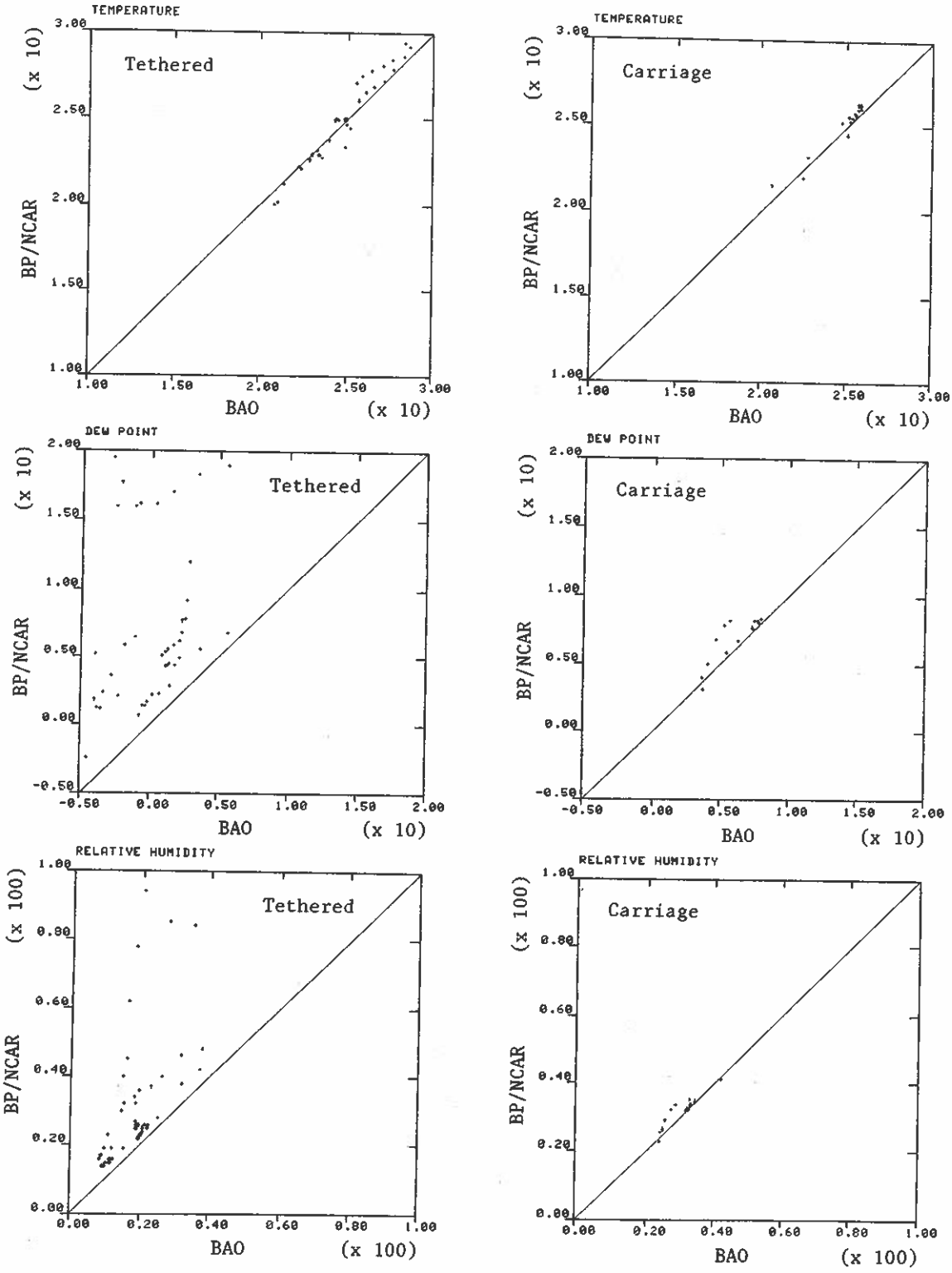

Figure 25.22. Scatter plots of data from BP/NCAR sensors vs. data from BAO tower sensors.

Notes on Fig. 25.22

Comments from R. B. McBeth, NCAR

Improper adjustment of the wet-bulb range contributed to the very large dew point scatter. At times the range was not adjusted downward promptly to accommodate sudden drops in humidity. The wet bulb was then reported equal to the lower range limit rather than the correct colder value and the computed dew point read much too high. This does not account for all the scatter; the transfer of water to the wet thermistor was probably inadequate.

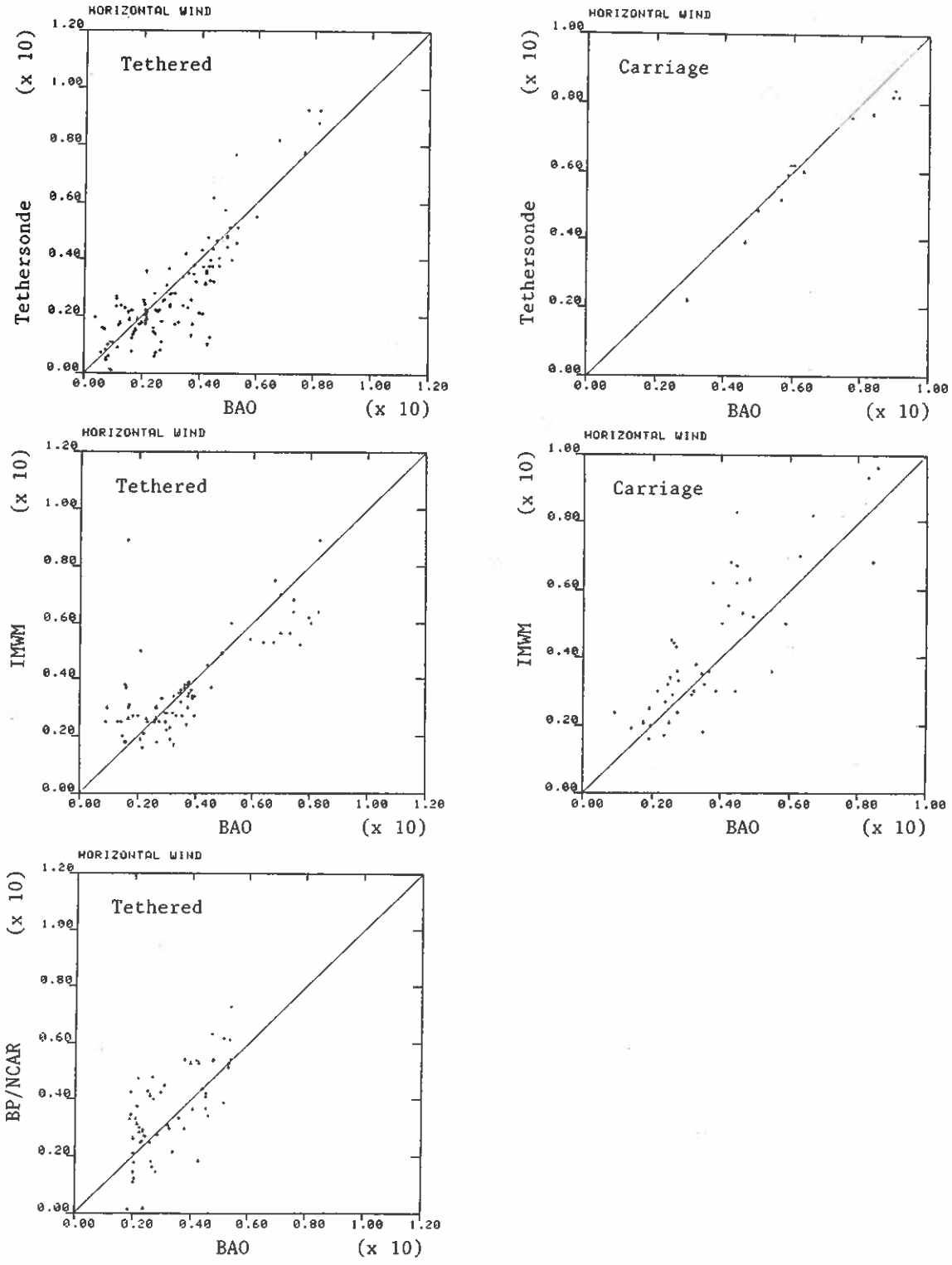

Figure 25.23. Scatter plots of horizontal wind speeds from tethered balloon sensors (balloon-borne and on carriage) vs. data from BAO tower sensors.

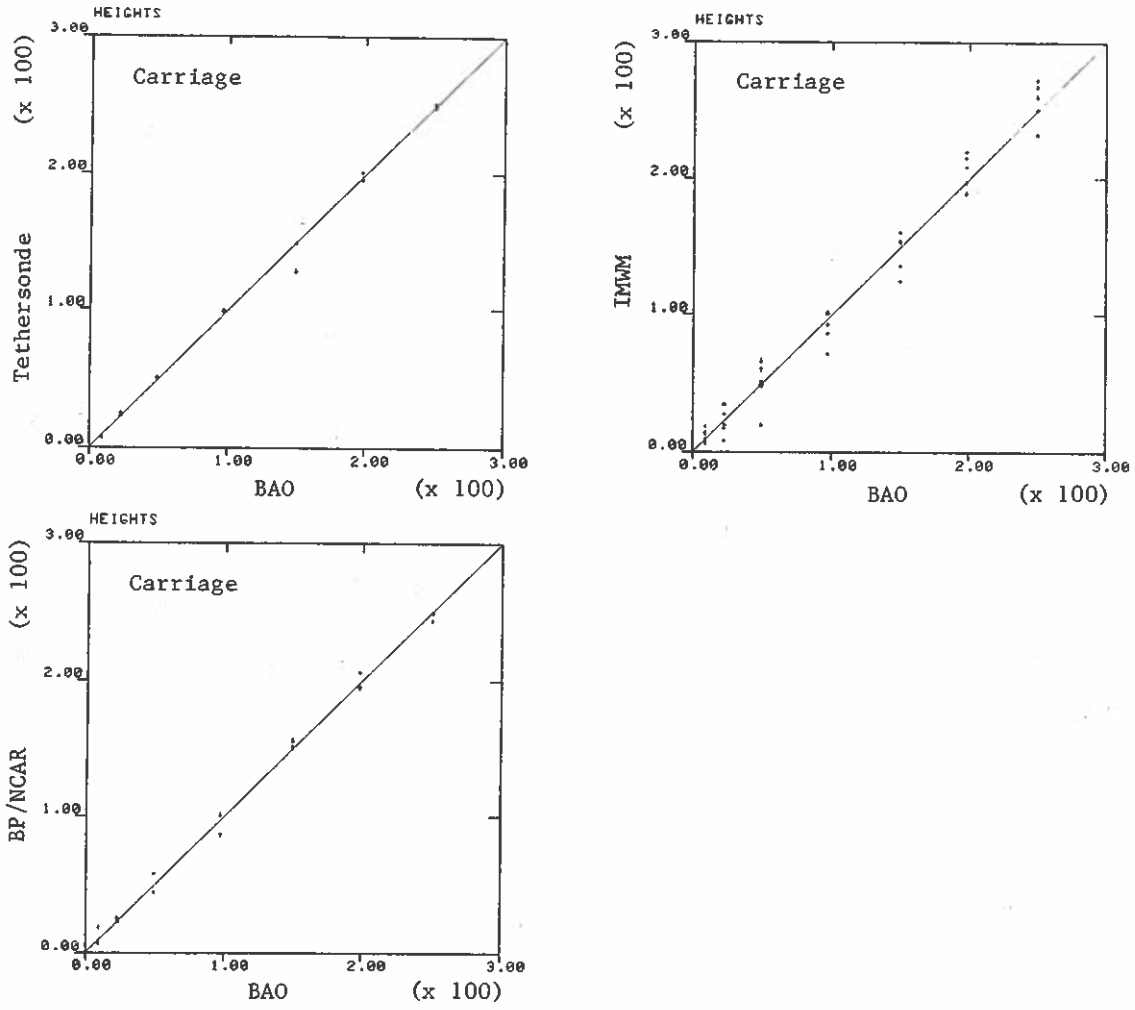

Figure 25.24. Scatter plots of heights from tethered balloon systems vs. BAO instrumentation heights.

25.4 CONCLUDING REMARKS

The results of the BLIE presented in this chapter show generally good agreement between the tested sensors and BAO sensors. The amount of agreement differs for each sensor, but differences are usually small. Where strong disagreement was found, the participant provided reasonable explanations for departures and outlined correction procedures. In one instance a participant modified his sensor midway through the experiment and got better agreement for the remaining runs (see Fig. 25.19).

The objective of this report is to present BLIE data without interpretation. In evaluating the sensors, the reader is urged to give due weight to the comments and notes accompanying the figures. Hardware and software changes made by a manufacturer after the experiment also need to be considered, since they may have solved problems experienced during BLIE.

The success of any experiment involving many different instruments depends on the cooperation between participants and experiment organizers. The authors note with gratitude the grace and generosity with which that cooperation was extended, especially in the preparation of this last chapter of the report.

☆ U.S. Government Printing Office: 1980-O-677-138/6